Primary cilia of Systemic Sclerosis dermal fibroblasts are disrupted by downregulation of Caveolin-1 and aberrant activity of Aurora A kinase, independently of Transforming Growth Factor Beta

Rebecca Ann Wells

Submitted in accordance with the requirements for the degree of

Doctor of Philosophy

The University of Leeds

School of Medicine and Health

October 2024

The candidate confirms that the work submitted is their own and that appropriate credit has been given where reference has been made to the work of others.

This copy has been supplied on the understanding that it is copyright material and that no quotation from the thesis may be published without proper acknowledgement.

The right of Rebecca Ann Wells to be identified as Author of this work has been asserted by her in accordance with the Copyright, Designs and Patents Act 1988.

© 2024 The University of Leeds and Rebecca Ann Wells

Acknowledgements

I would firstly like to thank the Medical Research Council's Discovery Medicine North (DiMeN) Doctoral Training Programme for the scholarship and funding to undertake this PhD. Next, I would like to thank my supervisors, Professor Francesco Del Galdo, Dr. Rebecca Ross, and Dr. Natalia Riobo Del Galdo, for the opportunity to carry out this research under their excellent supervision. Working with each of them has been genuinely inspiring, and I am immensely grateful for their input, wisdom, and guidance during this project.

I would also like to extend my gratitude to all members of the Del Galdo research group, past and present, for being a wonderful group of people to work with. Their support, teachings, and friendship were invaluable to this research. Additionally, I would like to thank all other colleagues in the Faculty of Medicine and Health and the Faculty of Biological Sciences who generously shared their expertise, time, and reagents during the course of my PhD.

Lastly, I would like to thank my friends, family, and loved ones for their love and support, and for keeping me sane. Special thanks to my twin Amy W, who I'm so lucky to have had as a best friend since day one; to Amy S, Sarah, and Ellie, for making sure that home always felt like home; to my incredible second family at AE (especially Emily) who have brought so much joy into my life; and to Frankie, for being amazing and never getting bored of listening to me talk about cilia for the millionth time.

Abstract

Systemic sclerosis (SSc) is a rare autoimmune disease of unknown aetiology characterised by chronic and progressive fibrosis of the skin, and of the internal organs in more advanced disease. Aberrant activation of the Transforming Growth Factor Beta (TGFβ) signalling pathway and downregulation of the cell membrane protein Caveolin-1 (CAV1) have been implicated in disease progression. Both TGFβ and CAV1 have roles at the primary cilium, a sensory organelle which forms a signalling hub for pathways involved in cellular homeostasis. Several of the pathways coordinated at the cilium, which include the TGFβ pathway itself, are dysregulated in SSc. Preliminary observations indicated that primary cilia of SSc dermal fibroblasts appeared to be abnormally short, which could hypothetically explain the dysregulation of key profibrotic pathways. This study aimed to investigate in detail cilia morphology in SSc dermal fibroblasts, the effects of TGFβ activation and Caveolin-1 downregulation on cilia length, and the mechanism by which cilia of SSc dermal fibroblasts are shortened, with the aim of identifying targets to induce cilia elongation and normalise signalling.

Dermal fibroblasts from SSc patients and from very early diagnosis of SSc (VEDOSS) patients displayed shorter cilia compared to dermal fibroblasts isolated from healthy controls (HC). Silencing of CAV1 in shCAV1 fibroblasts also resulted in shorter cilia compared to control shSCR fibroblasts, suggesting a role in establishment of the phenotype in SSc. Additionally, TGFβ treatment reduced cilium length. This effect was fully abolished by TGFβRI inhibition and partially blocked by ROCK2 inhibition, but was unaffected by inhibition of SMAD3, PI3K-AKT, or the AURKA-HDAC6 axis, a known negative regulator of

cilium length. Inhibition of the TGFβ signalling pathway did not restore SSc cilium length, but inhibition of the AURKA-HDAC6 axis restored SSc and shCAV1 cilia length to that of controls and reduced TGFβ-induced contractility. In addition to shorter cilia, we identified a loss of SPAG17 localisation at the base of the cilium in SSc, shCAV1, and TGFβ-treated dermal fibroblasts, consistent with recent findings of a role for SPAG17 in regulating cilia length, and profibrotic signalling in SSc.

This study reveals that primary cilium length is stably reduced in SSc dermal fibroblasts, even in early disease prior to clinically evident fibrosis. The results suggest that CAV1 downregulation and aberrant AURKA activity may contribute to aberrantly short cilia and profibrotic activation in SSc dermal fibroblasts. While TGFβ activation can shorten cilia in a mechanism at least partially dependent on ROCK2, TGFβ signalling is not responsible for the stably shortened cilia phenotype in SSc. These findings implicate the cilium as a potential therapeutic target for SSc, a disease for which there is currently no cure, and limited treatment options, as well as other fibrotic disorders.

Table of Contents

Acknowledgements ..... **ii**

Abstract ..... **iii**

Table of Contents ..... **v**

List of Figures ..... **x**

List of Tables ..... **xiv**

List of Abbreviations ..... **xv**

Chapter 1. Introduction **1**

1.1 The primary cilium 1

1.1.1 Structure and function of the primary cilium 1

1.1.2 Roles of the primary cilium in cellular signalling 6

1.1.3 Regulation of ciliary length 10

1.1.4 Human disease associated with the primary cilium 13

1.2 Systemic sclerosis 16

1.2.1 Fibrosis 16

1.2.2 Systemic sclerosis 18

1.2.3 TGFβ signalling in systemic sclerosis 21

1.2.4 Caveolin-1 in systemic sclerosis 24

1.3 A role for the primary cilium in systemic sclerosis 27

1.3.1 Signalling dysregulation in systemic sclerosis 27

1.3.2 The roles of TGFβ and Caveolin-1 in cilium structure and function 31

1.3.3 Fibrotic disease associated with defective cilia 35

1.4 Project rationale and aims 41

Chapter 2. Materials and Methods **44**

2.1 Cell lines 44

2.2 Cell culture 45

2.3 Treatment of fibroblasts with ligands and inhibitors 46

2.4 siRNA transfection....47
2.5 Protein extraction and quantification....47
2.6 Western Blotting....48
2.7 RNA extraction and quantification....50
2.8 cDNA synthesis....51
2.9 Quantitative polymerase chain reaction....51
2.10 Immunohistochemistry....52
2.11 Immunofluorescence....53
2.12 Confocal microscopy and image analysis....54
2.13 Cell contraction assays....54
2.14 Generation of shCAV knockdown line....55
2.15 Statistical analysis....56
Chapter 3. Characterisation of primary cilia of dermal fibroblasts in Systemic Sclerosis, and their regulation by TGFβ signalling....57
3.1 Introduction....57
3.2 Results....58
3.2.1 Primary cilia are shorter in SSc and VEDOSS dermal fibroblasts compared to healthy controls....58
3.2.2 The difference in cilia length between SSc and healthy control fibroblasts is not a consequence of immortalisation nor serum starvation....62
3.2.3 TGFβ shortens primary cilia and reduces cilia incidence in all fibroblast lines....65
3.2.4 TGFβ shortens the established primary cilium present during growth arrest, rather than inducing cell cycle-linked ciliary resorption....67
3.2.5 SSc cilia are primed for TGFβ-induced shortening....71
3.2.6 The effect of TGFβ on cilia length is lost after cells re-enter the cell cycle....74
3.3 Discussion....77
3.4 Summary....83

Chapter 4. Investigation of the mechanism of TGFβ-induced cilia shortening, and its role in the cilia phenotype of Systemic Sclerosis.....84

4.1 Introduction.....84

4.2 Results 84

4.2.1 Inhibition of the TGFβ signalling cascade does not rescue SSc cilia length.....84

4.2.2 Inhibition of canonical TGFβ signalling effector SMAD3 does not rescue SSc cilia length, nor prevent TGFβ-induced cilia shortening.....89

4.2.3 Inhibition of non-canonical TGFβ effector ROCK2 does not rescue SSc cilia length, but partially prevents TGFβ-induced cilia shortening.....93

4.2.4 Inhibition of the non-canonical TGFβ effector AKT does not rescue SSc cilia length, nor prevent TGFβ-induced cilia shortening 99

4.2.5 Inhibition of the TGFβ effector HDAC6 does not block TGFβ-induced shortening, but partially rescues SSc cilia length.....103

4.3 Discussion.....107

4.4 Summary.....111

Chapter 5. Characterisation of the role of Aurora A Kinase activity at the primary cilium in Systemic Sclerosis.....113

5.1 Introduction.....113

5.2 Results 113

5.2.1 Validation of MLN8054, a small molecule inhibitor of Aurora A Kinase 113

5.2.2 Inhibition of Aurora A Kinase rescues cilia length in SSc fibroblasts 119

5.2.3 The effect of Aurora A Kinase inhibition on the fibrotic phenotype of SSc fibroblasts at transcript level.....121

5.2.4 The effect of Aurora A Kinase inhibition on the fibrotic phenotype of SSc fibroblasts at protein level.....131

5.2.5 The effect of Aurora A Kinase inhibition on TGFβ-induced SSc fibroblast contractility 144

5.3 Discussion 148

5.4 Summary 155

Chapter 6. Characterisation of the effect of Caveolin-1 downregulation in Systemic Sclerosis on the primary cilium 156

6.1 Introduction 156

6.2 Results 157

6.2.1 Short hairpin RNA knockdown of Caveolin-1 (shCAV1) as a model for Caveolin-1 downregulation in SSc 157

6.2.2 Primary cilia are shorter in shCAV1 fibroblasts 161

6.2.3 Inhibition of Aurora A Kinase and HDAC6 rescues cilia length in shCAV1 fibroblasts 165

6.2.4 Investigation of interaction between Caveolin-1 and AURKA 168

6.2.5 The effect of Aurora A Kinase inhibition on the fibrotic phenotype of shCAV1 fibroblasts at the transcript level 170

6.2.6 The effect of Aurora A Kinase inhibition on the fibrotic phenotype of shCAV1 fibroblasts at the protein level 172

6.2.7 The effect of Aurora A Kinase inhibition on TGFβ-induced shCAV1 fibroblast contractility 176

6.3 Discussion 179

6.4 Summary 184

Chapter 7. Characterisation of SPAG17 expression and localisation at the Systemic Sclerosis primary cilium 186

7.1 Introduction 186

7.2 Results 186

7.2.1 SPAG17 expression and localisation 186

7.2.2 The effect of TGFβ on SPAG17 expression and localisation 192

7.2.3 Characterisation of SPAG17 expression and localisation in Caveolin-1 knockdown fibroblasts 194

7.3 Discussion 198

7.4 Summary 201

Chapter 8. Concluding remarks 203

Bibliography 208

List of Figures

Figure 1: Ultrastructure of the primary cilium 4

Figure 3.1: Primary cilia are shorter in dermal fibroblasts from SSc and VEDOSS patients compared to healthy controls 61

Figure 3.2: Differences in the cilia phenotype between SSc and healthy control fibroblast cilia are retained regardless of hTERT immortalisation or serum starvation 64

Figure 3.3: TGFβ decreases primary cilia incidence and length 67

Figure 3.4: TGFβ treatment under chosen experimental conditions does not affect cell cycle progression 70

Figure 3.5: Temporal analysis of the response to TGFβ in healthy vs SSc fibroblasts shows SSc cilia are primed for TGFβ-induced shortening 73

Figure 3.6: The TGFβ-induced shorter cilia phenotype is only partially stable and is lost upon cell cycle re-entry 76

Figure 4.1: Blockade of TGFβRI activity using inhibitor SD208 reduces activation of the TGFβ pathway 86

Figure 4.2: TGFβRI inhibition with SD208 blocks the effect of TGFβ on cilia but does not rescue SSc cilia length 88

Figure 4.3: Blockade of SMAD3 with siRNA-mediated knockdown 90

Figure 4.4: siRNA-mediated SMAD3 knockdown does not block the effect of TGFβ on cilia nor rescue SSc cilia length 92

Figure 4.5: Blockade of ROCK kinases using inhibitors Y27632 and KD025 reduces ROCK kinase activity 96

Figure 4.6: Inhibition of ROCK kinases using Y27632 and KD025 does not rescue SSc cilia length, but partially prevents TGFβ-induced cilia shortening 98

Figure 4.7: Blockade of PI3K with inhibitor BKM120 reduces AKT signalling activation 101

Figure 4.8: Blockade of AKT signalling using PI3K inhibitor BKM120 does not block the effect of TGFβ on cilia nor rescue SSc cilia length 102

Figure 4.9: Blockade of HDAC6 activity with inhibitor Tubacin.....104

Figure 4.10: Inhibition of HDAC6 activity with Tubacin does not block TGFβ-induced shortening, but partially rescues SSc cilia length.....106

Figure 5.1: Immunofluorescence analysis of the effect of MLN8054 to validate inhibitor activity shows reduced levels of pAURKA(Thr288) 115

Figure 5.2: Analysis of the effect of MLN8054 on protein expression supports validation of inhibitor activity.....118

Figure 5.3: AURKA inhibition with MLN8054 rescues cilia length in SSc fibroblasts.....120

Figure 5.4: Transcript levels of classic fibrotic markers vary between individual donor fibroblast lines under basal conditions.....123

Figure 5.5: The effect of inhibition of Aurora A Kinase on the fibrotic phenotype of SSc fibroblasts at transcript level is varied, with some partial rescue of basal and TGFβ-induced expression in some cell lines 130

Figure 5.6: Levels of classic fibrotic marker proteins vary between individual donor fibroblast lines under basal conditions.....133

Figure 5.7: The effect of inhibition of Aurora A Kinase for 24 h on the fibrotic phenotype of SSc fibroblasts at protein level is varied, with some partial rescue of TGFβ-induced expression in some cell lines.....138

Figure 5.8: The effect of inhibition of Aurora A Kinase for 48 h on the fibrotic phenotype of SSc fibroblasts at protein level is varied, with some partial rescue of basal and TGFβ-induced expression in some cell lines 143

Figure 5.9: Inhibition of AURKA rescues the SSc fibroblast contractile phenotype in response to stimulation with TGFβ.....147

Figure 6.1: Reduced CAV1 expression at protein and mRNA level in SSc dermal fibroblasts compared to HC 157

Figure 6.2: Generation of a stable CAV1 knockdown healthy fibroblast line using short hairpin RNA to reduce protein expression.....158

Figure 6.3: shCAV1 fibroblast lines show increased expression of classic fibrotic markers at the mRNA and protein level.....160

Figure 6.4: Primary cilia are shorter in healthy shCAV1 fibroblasts compared to shSCR controls, and are similar in length to SSc fibroblast cilia.....162

Figure 6.5: TGFβ decreases primary cilia incidence and length in shSCR and shCAV1 fibroblasts, with similar timing 164

Figure 6.6: AURKA inhibition with MLN8054 and HDAC6 inhibition with Tubacin rescues cilia length in shCAV1 fibroblasts.....167

Figure 6.7: Inhibition of AURKA has no effect on levels of CAV1, nor SSc and shCAV1-specific TGFβ-induced downregulation of CAV1.....169

Figure 6.8: Inhibition of Aurora A Kinase partially rescues the fibrotic phenotype of shCAV1 fibroblasts and response to TGFβ at transcript level 172

Figure 6.9: Inhibition of Aurora A Kinase for 24 h partially rescues the fibrotic phenotype of shCAV1 fibroblasts and their response to TGFβ...174

Figure 6.10: Inhibition of Aurora A Kinase for 48 h partially rescues the fibrotic phenotype of shCAV1 fibroblasts and response to TGFβ at protein level.....175

Figure 6.11: Inhibition of AURKA rescues the contractile phenotype of shCAV1 fibroblasts in response to stimulation with TGFβ.....178

Figure 7.1: SPAG17 expression is reduced in the SSc dermis compared to HC.....187

Figure 7.2: SPAG17 expression at the transcript and protein level vary between fibroblasts from different HC and SSc donors.....189

Figure 7.3: Ciliary base specific localisation of SPAG17 is reduced in SSc fibroblasts compared to HC.....191

Figure 7.4: Despite variable response at the protein level, TGFβ reduces *SPAG17* mRNA and ciliary base-specific localisation of SPAG17 in HC and SSc fibroblasts.....193

Figure 7.5: *SPAG17* mRNA levels, SPAG17 protein levels, and ciliary base specific localisation of SPAG17 are reduced in shCAV1 fibroblasts compared to shSCR.....196

Figure 7.6: Inhibition of AURKA partially ameliorates the reduced SPAG17 localisation at the ciliary base in shCAV1 fibroblasts 197

List of Tables

Table 1: Patient and cell line information 45

Table 2: Western Blot antibody information.....49

Table 3: qPCR primer sequence information 52

Table 4: Immunofluorescence antibody information.....53

List of Abbreviations

ACTA2	Actin Alpha 2
Ac-α-Tub	Acetylated Alpha Tubulin
AKT	RAC Serine/Threonine-protein Kinase
AURKA	Aurora A Kinase
BCA	Bicinchoninic Acid Assay
BSA	Bovine Serum Albumin
CAV1	Caveolin-1
CCA	Cholangiocarcinoma
CCN2	Cellular Communication Network Factor 2
ccRCC	Clear Cell Renal Cell Carcinoma
cDNA	Complementary DNA
COL1A1	Alpha-1 Type I Collagen
COL1A2	Alpha-2 Type I Collagen
CTGF	Connective Tissue Growth Factor
CTR	Control
DAPI	4′,6-diamidino-2-phenylindole
dcSSc	Diffuse Cutaneous Systemic Sclerosis
DMEM	Dulbecco’s Modified Eagle Medium
DMSO	Dimethyl Sulfoxide
DNA	Deoxyribonucleic Acid
dNTPs	Deoxynucleotide Triphosphates
ECM	Extracellular Matrix
FBS	Fetal Bovine Serum
FN1	Fibronectin-1

GAPDH	Glyceraldehyde 3-phosphate Dehydrogenase
HC	Healthy Control
HDAC6	Histone Deacetylase 6
HRP	Horseradish Peroxidase
hTERT	Human Telomerase Reverse Transcriptase
IFT88	Intraflagellar Transport Protein 88 Homolog
IgG	Immunoglobulin
IP	Immunoprecipitation
IPF	Idiopathic Pulmonary Fibrosis
lcSSc	Limited Cutaneous Systemic Sclerosis
mL	Millilitre
MLC2	Myosin Light Chain 2
mM	Millimole
mRNA	Messenger RNA
MRSS	Modified Rodnan Skin Score
NEDD9	Neural Precursor Cell Expressed Developmentally Down-regulated Protein 9
ng	Nanogram
nM	Nanomole
PBS	Phosphate-Buffered Saline
PI3K	Phosphoinositide 3-Kinase
qPCR	Quantitative Polymerase Chain Reaction
RIPA	Radioimmunoprecipitation Assay Buffer
RNA	Ribonucleic Acid
ROCK	Rho-associated Protein Kinase
RPE-1	Retinal Pigment Epithelial-1

SCR	Scramble
SDS-PAGE	Sodium Dodecyl Sulfate–Polyacrylamide Gel Electrophoresis
SEM	Standard Error of the Mean
SHH	Sonic Hedgehog
shRNA	Short Hairpin RNA
siRNA	Small Interfering RNA
SMAD3	Mothers Against Decapentaplegic Homolog 3
SPAG17	Sperm Associated Antigen 17
SSc	Systemic Sclerosis
STDEV	Standard Deviation of the Mean
TAO	Thyroid Associated Opthalmopathy
TBS-T	Tris-Buffered Saline Tween-20
TGFβ	Transforming Growth Factor Beta
TGFβRI	Transforming Growth Factor Beta Receptor Kinase I
TZ	Transition Zone
VEDOSS	Very Early Diagnosis of Systemic Sclerosis
Wnt	Wingless-related Integration Site
αSMA	Alpha Smooth Muscle Actin
µL	Microlitre
µM	Micromole
µm	Micrometre

Chapter 1. Introduction

1.1 The primary cilium

1.1.1 Structure and function of the primary cilium

The existence of hair-like extensions of vertebrate cell membranes was noted by scientists using light microscopy since the 17th century, and these structures were named cilia, taken from the Latin for ‘eyelash’. It was not until the advent of electron microscopy in the 1950s and 60s that the first detailed studies of these structures became possible, increasing our understanding of the structure and function of these organelles (Wheatley, 2005). Two distinct classes of cilia were identified in mammalian cells: motile cilia, which have the ability to beat and are found in varying numbers only on highly specialised cell types, and primary cilia, which are immotile and usually solitary, and are present on virtually all mammalian cells (Sorokin, 1968).

In cells which possess primary cilia, its presence is intrinsically linked to the progression of the cell cycle. After cell division, the mature mother centriole of the centrosome, an organelle which controls microtubule generation, forms attachments known as transition fibres from its distal appendages at the plasma cell surface membrane in order to initiate formation of the primary cilium during the G1-G0 phase (Sorokin, 1962). This process has since been demonstrated to be conserved throughout eukaryotic evolution, whereby ciliary sequestration of the centriole exerts negative regulation on the progression of the cell cycle (Carvalho-Santos et al., 2011).

The centriole becomes part of the basal structure of the primary cilium, called the basal body, and from it grows a central structure called the axoneme, formed by the polymerisation of α- and β- tubulin into microtubules which are stabilised by α-tubulin acetylation (Ac-α-Tub). In motile cilia, the axoneme is formed from nine microtubule doublets arranged in a symmetrical ring around two central microtubules (thus denoted as 9+2), while primary cilia lack the central pair (thus denoted as 9+0) as well as the radial spokes and dynein arms required for motility (Satir & Christensen, 2007). The axoneme is surrounded by a tapered ciliary membrane, which forms a cylindrical protrusion from the plasma cell surface membrane (Satir et al., 2010).

While the primary cilium remains present during quiescence, when a cell re-enters the cell cycle the ciliary axoneme is resorbed in the transition from G phase into S phase, releasing the centriole from the plasma cell surface membrane in order to facilitate mitosis before new cilia are formed on daughter cells (Plotnikova et al., 2009).

The primary cilium, despite being an extension of the plasma cell surface membrane, forms a highly specialised and structurally distinct organelle. The cytoplasm within the cilium, named the cilioplasm, has been shown to be markedly distinct in its contents compared to that of the cell body cytoplasm (Breslow et al., 2013). Similarly, the composition of the ciliary membrane is tightly regulated, such that its lipid and protein content differs significantly from that of the plasma cell surface membrane (Garcia et al., 2018). This specialisation is in part attributed to the tightly regulated trafficking of molecules within the cilium, with molecular cargo transported from base to tip (anterograde) and tip to base (retrograde) by motor proteins along the doublet microtubules of the axoneme by the intricate activity of the intraflagellar

transport machinery (IFT) (Malicki & Johnson, 2017). This specific composition is also determined by membrane remodelling events, with the periciliary membrane, where the cilium meets the plasma membrane, showing a characteristic invagination called the ciliary pocket region, which is generated by increased endocytic activity (Molla-Herman et al., 2010).

These activities tightly control entry and exit of components from the primary cilium and are mostly coordinated by the area at the base of the primary cilium, which is known as the ciliary gate region (Garcia et al., 2018). This gate region consists of the basal body, transition fibres formed from the distal appendages of the mother centriole after docking, and the transition zone which comprises the basal-most region of the axoneme and is defined by the presence of bifid fibres which connect the microtubules of the axoneme to the surrounding ciliary membrane. Investigation into the composition of this region has shown that the molecular components of these gate region structures are able to exhibit highly specific and controlled trafficking into and out of the primary cilium (Yang et al., 2015).

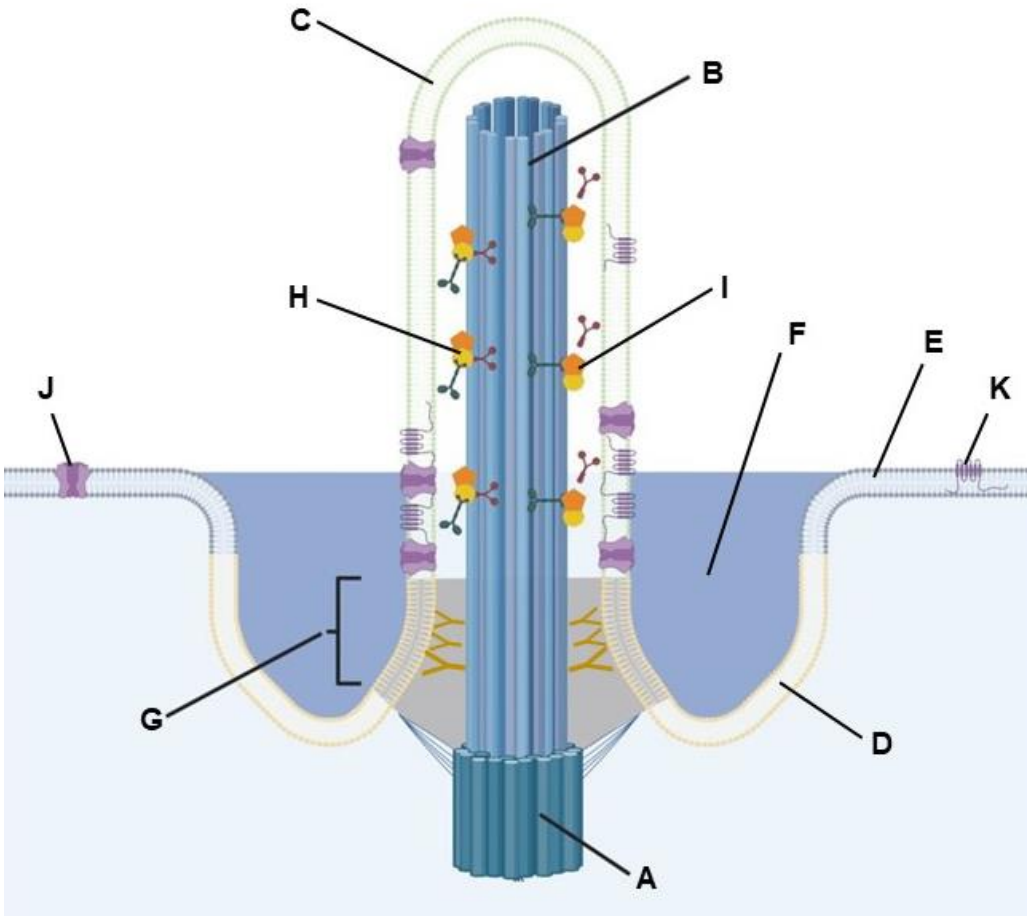

Figure 1: Ultrastructure of the primary cilium

Simplified schematic of the ultrastructure of the primary cilium (adapted from Moore, 2022). Components are not to scale. The primary cilium originates from the basal body (A), which forms when the mature mother centriole of the centrosome anchors to the cell membrane via transition fibres. The central microtubular structure of the cilium, the axoneme (B), is assembled from the basal body. The axoneme forms a protrusion from the cell surface surrounded by the ciliary membrane (C). The membrane at the base of the primary cilium, the periciliary membrane (D), separates the ciliary membrane from the plasma cell surface membrane (E). The ciliary pocket (F) is a characteristic membrane invagination at the base of the cilium. The periciliary membrane is linked to the basal-most part of the axoneme by bifid fibres, forming a region called the transition zone (G). Anterograde IFT complexes (H) transport molecular cargo from the base to the tip of the axoneme, mediated by Kinesin-II family motor proteins. Retrograde IFT complexes (I) transport cargo from the tip to the base, mediated by Dynein-II family motor proteins. The composition of the ciliary membrane is distinct from the plasma membrane, with tightly controlled regulation of ciliary entry and exit of membrane components including receptors (J) and signalling pathway components (K).

The distinct structural and compositional biology of the primary cilium allows for its function as what can be broadly defined as a sensory organelle, responsible for the detection of extracellular environmental cues, which can be physical or chemical (Mill et al., 2023). The primary cilium is often described as a cellular antenna for its role as a signalling hub which plays a crucial part in cellular development, homeostasis, and response to the environment (Anvarian et al., 2019). By housing various receptors, channels, transporters, and downstream signalling mediators, and finely controlling the spatio-temporal localisation of these, the cilium is vital in the coordination of a multitude of cellular processes (Satir & Christensen, 2007).

Advancements in imaging technologies have allowed for increasingly elegant and detailed visualisation of primary cilia, mostly led by cryo-electron tomography (Kiesel et al., 2020). While the foundational structural and functional characteristics of primary cilia outlined above are conserved in primary cilia across all cell types, research is increasingly identifying cell-type specific diversity, with variations in ciliary structure and composition which are theorised to confer different specialised roles for the primary cilium in different cellular contexts. Variations in the transition zone have been identified across different cell types, which have been suggested to lead to differences in its gating functionality (Fisch & Dupuis-Williams, 2011, Wiegering et al., 2018). The configuration of the ciliary axoneme itself, once assumed to be tightly conserved in all primary cilia, has been revealed to display heterogeneity between different cell types in recent years, though the specific influence of this is yet to be elucidated (S. Sun et al., 2019). The ciliary membrane shows distinctly adapted morphologies in cell types such as photoreceptor cells and neurons which are

suggested to contribute to the specialisation of these cilia for the specific signalling coordination mediated in these cells (Barnes et al., 2021).

Outside of ciliary architecture, extensive research into ciliary membrane and cilioplasm composition, in addition to signalling output from the primary cilium, has begun to reveal the significant adaptability of the functions of primary cilia in different cell types and contexts, and the diversity in the cellular processes that they orchestrate (Mill et al., 2023).

1.1.2 Roles of the primary cilium in cellular signalling

In mammalian cells, the primary cilium has been implicated in the coordination of a number of signal transduction pathways, including but not limited to the cellular signalling pathways activated by Sonic Hedgehog (SHH), G protein coupled receptors (GPCR), receptor tyrosine kinases (RTK), Wingless-related integration site (Wnt) family members, Transforming Growth Factor β (TGFβ), and Bone Morphogenic Protein (BMP), with multiple studies showing extensive cross-talk between many of these pathways at the primary cilium (Veland et al., 2009). Research into the association of these signalling pathways with the cilium has allowed for a greater understanding of the intricate complexity of the functions of this organelle.

The role of the primary cilium in the coordination of canonical hedgehog (HH) signalling is perhaps the most extensively studied of these examples, with the cilium long established in the literature as an organelle which is required for functional HH signalling output in numerous cellular contexts (Bangs & Anderson, 2017). Localisation of all core components of the signal transduction machinery of this pathway to the primary cilium has been identified in a plethora

of studies (Wheway et al., 2018). In the off-state of the HH pathway, the transmembrane receptor Patched (PTCH1), found on the ciliary membrane, inhibits transmembrane GCPR protein Smoothened (SMO) through modulation of the sterol composition of the ciliary membrane (Y. Zhang & Beachy, 2023). This prevents accumulation of SMO in the cilium and its activation in the absence of SHH. When SMO is inactive, the GLI transcription factors GLI2 and GLI3, also found localised in the cilium, are phosphorylated by protein kinase A (PKA) at the ciliary base, and converted into transcriptional repressors. Their trafficking from the cilium to the nucleus leads to transcriptional repression of downstream gene targets of the pathway. In the on-state, SHH binding to PTCH1 and its co-receptors alleviates its repression of SMO, leading to SMO accumulation in the cilium, where its activity blocks phosphorylation of GLI2 and GLI3 by PKA, facilitating transition of the GLIs into their active forms by phosphorylation at the ciliary tip, which are then trafficked to the nucleus and activate expression of target genes of the HH pathway. Cilium components have been demonstrated to be crucial for both the activation and repression of HH pathway transcriptional targets by GLI proteins (A. Liu et al., 2005).

While extensive research has considered the role of the primary cilium in HH signal transduction, arguably more so than any other pathway transduced there, coordination of this pathway both in and outside of the primary cilium is extremely complex, with ongoing research deciphering the exact role of the cilium in the fine-tuning of this pathway in different contexts (Hilgendorf et al., 2024). Given the complexity of pathways such as the HH pathway, crosstalk between signalling pathways, and the sensitivity and adaptability of the primary cilium, it is possible that ciliary modulation of signalling pathways may differ

depending on cell type and context to maintain the appropriate cellular balance of pathway activation and pathway repression.

In the HH pathway, PKA phosphorylates and represses GLI transcription factors specifically at the primary cilium base (Tuson et al., 2011). A recent study showed that GPCRs localised to the primary cilium differentially transduce signals compared to those localised to the plasma membrane, demonstrating that cilium-specific signalling involving ciliary PKA preferentially mediates repression of the HH pathway (Truong et al., 2021). Interestingly, the authors of this study propose a role for the primary cilium in the constraint of HH pathway activation, and postulate that this ability is dependent on the cilium's structure, with a high membrane to cilioplasm volume ratio conferring differential sensitivity to and processing of chemical cues. Using evidence from this experimental study of the HH pathway, Truong et al. theorised that the length and diameter of the primary cilium may therefore be implicated in its differential sensitivity to molecular cues and could be important in the determination of ciliary output in the context of cellular signalling pathway coordination.

The canonical Wnt signalling pathway is another primary cilium-associated pathway (Pala et al., 2017). In the off-state of the pathway, a destruction complex composed of multiple protein components, including Axin, facilitates the phosphorylation of β-catenin, causing its ubiquitinylation by JADE1 ubiquitin ligase and subsequent proteasome-mediated degradation, with this destruction demonstrated to take place at the ciliary base. Wnt ligands bind to Frizzled (FZD) transmembrane receptors, which have been found to be localised to the membrane of the primary cilium (May-Simera & Kelley, 2012). The receptor-ligand complex recruits Dishevelled (DVL), which sequesters Axin from the destruction complex, alleviating its repression of β-catenin. Components of the

ciliary transition zone have been shown to facilitate the repression of β-catenin by targeting DVL for destruction, and recruitment of JADE1 (Borgal et al., 2012). β-catenin, assisted by Abelson helper integration site 1 (AHI1), is trafficked to the nucleus and acts as a co-activator with TCF transcription factors to induce Wnt pathway target gene expression. It has been suggested that AHI1 may be sequestered by the primary cilium, restricting its ability to shuttle β-catenin to the nucleus (Lancaster et al., 2011).

Research to dissect the exact role and importance of the primary cilium in Wnt signalling coordination is ongoing, but it likely that its impact is context-specific (Pala et al., 2017). In some contexts, the cilium is proposed to exhibit Wnt pathway attenuation, with loss of cilia and several of its components shown to induce hyperactive Wnt signalling (Gerdes et al., 2007, Corbit et al., 2008, Zingg et al., 2018).

The primary cilium has also been implicated in organisation of the output of canonical TGFβ signalling, with several components of the pathway shown to localise to primary cilia by both proteomic and immunofluorescence analysis (Mick et al., 2015, Vestergaard et al., 2016). TGFβ ligands bind to serine threonine kinase receptors I and II heterocomplexes (TGFβRI and II), which have been shown to localise to the tip of the primary cilium, and the activated receptor complex induces phosphorylation of TGFβRI by TGFβRII, which stimulates clathrin-mediated endocytosis (CME) of the receptor complex at the ciliary pocket region (Clement et al., 2013). After endocytosis, receptor-regulated SMAD (R-SMAD) transcription factors SMAD2 and SMAD3 are phosphorylated and shuttled to the nucleus in a complex with SMAD4, where the SMAD3 portion of the complex induces pathway target gene expression.

SMAD3 activation has been demonstrated to occur at the ciliary base (Vestergaard et al., 2016, Labour et al., 2016).

The TGFβRs can be recycled back to the primary cilium in a process proposed to be mediated by centrosomal protein 128 (CEP128), which is localised to the ciliary basal body (Mönnich et al., 2018). Inhibitory SMADs (I-SMADs), SMAD6 and SMAD7, are induced by TGFβ pathway activation and form a feedback loop to downregulate TGFβ signalling. SMAD7, along with ubiquitin ligase SMURF1, have been identified to be localised to the base of the primary cilium (Koefoed et al., 2018). Together, in a mechanism regulated by ciliary ceramides, SMAD7 and SMURF1 limit TGFβR recycling to the cilium by targeting it for degradation, which was also shown to attenuate cross-talk with the HH pathway by limiting interaction with SMO (Gencer et al., 2017). Interestingly, experimental elongation of primary cilia of retinal pigment epithelial cells (RPE-1) with siRNA-mediated knockdown of ciliary protein Alstrom Syndrome-1 (ALSM1) was recently shown to reduce TGFβ-induced phosphorylation of SMAD2 (Álvarez-Satta et al., 2021). Further research is required to elucidate the specific role of the primary cilium in the coordination, and potential fine-tuning, of the signalling output of the TGFβ pathway in different cellular contexts.

1.1.3 Regulation of ciliary length

After the primary cilium is assembled by initial ciliogenesis in quiescent cells, and before disassembly prior to cell division, a steady state ciliary length is established, with primary cilia found on different mammalian cell types ranging in length between 2 and 10 μm. Rather than being established and simply passively maintained, cilium length is in fact dynamically regulated, with a vast

number of proteins and complex molecular processes known to participate in continuous elongation and shortening of the primary cilium, which is delicately balanced in order to maintain the length of the organelle (Avasthi & Marshall, 2012). Several of the mechanisms implicated in ciliary length modulation in quiescent and differentiated cells are also known mediators of cell-cycle linked cilia formation and resorption, which have been shown to exhibit additional ciliary length control activities in non-mitotic cells (Keeling et al., 2016).

Regulation of ciliary length is accomplished at the molecular level by the remarkably complex modulation of its microtubule-based central structure, the axoneme (Conkar & Firat-Karalar, 2021). The intricate mechanics of ciliary trafficking by IFT machinery facilitates this dynamic length modulation, through the direct addition and removal of α- and β-tubulin proteins, the axonemal building blocks (Keeling et al., 2016). Indeed, analysis of the effects of manipulation of a broad number of IFT components has demonstrated their direct involvement in functional maintenance of cilia length in quiescent cells (Wang et al., 2021). Post-translational modification of axonemal tubulin is also delicately balanced in the maintenance of cilia length, with tubulin acetylation, glutamylation, and glycylation required for axonemal microtubule stability (Pugacheva et al., 2007, Shida et al., 2010, Gadadhar et al., 2017). Conversely, tubulin ubiquitylation promotes axoneme disassembly by destabilising microtubules (Wang et al., 2019).

Cilia length maintenance by these molecular mechanisms is known to be influenced by an extensive number of complex intracellular signalling pathways. One such pathway is centred on serine/threonine kinase Aurora A (AURKA), which was initially identified as an important kinase in the regulation of the mitotic spindle in cell division (Marumoto et al., 2005). A cilium-specific role for

AURKA as a negative regulator of cilia length was subsequently identified, both as a key initiator of mitosis-linked ciliary resorption, and outside of mitosis (Pugacheva et al., 2007). At the ciliary base, interaction with scaffolding protein NEDD9 initiates AURKA autophosphorylation at Thr288, and subsequent localised phosphorylation and activation of Histone Deacetylase 6 (HDAC6) (Pugacheva et al., 2007). When active, HDAC6 induces deacetylation of axonemal tubulin, leading to resorption of the microtubules and ciliary shortening. It has since been shown that there are numerous mechanisms by which activity of AURKA is regulated at the primary cilium outside of mitosis (Korobeynikov et al., 2017).

Cilia length, once thought to be regulated independently within the organelle itself, has also been shown to be influenced more indirectly by cytoskeletal dynamics around the base of the cilium (Mirvis et al., 2018). The formation of a polymerised actin cytoskeleton has been shown to downregulate ciliary lengthening (Kim et al., 2015). It is thought that the actin cytoskeleton may partake in balancing the entry of cargo including ciliary components and IFT machinery into the cilium, which facilitate cilia elongation (Yeyati et al., 2017). Many components of cytoskeletal regulation have been implicated in negative regulation of cilia length, including the small GTPase Rho and Rho-associated kinases (ROCK) (Lake et al., 2020, Smith et al., 2020).

The PI3K-AKT signalling pathway has also been implicated in negative regulation of ciliary length associated with growth factor signalling (Nishimura et al., 2021). Phosphorylation and activation of AKT downstream of PI3K activity induces phosphorylation and inactivation of glycogen synthase kinase 3 (GSK3β) at the ciliary axoneme, promoting axonemal instability (Thoma et al., 2007, Zhang et al., 2015). It is thought that through this mechanism, cargo

trafficking to the primary cilium is directly inhibited (Walia et al., 2019). AKT acts as a mediator for a number of cellular processes which regulate cilia length, including cytoskeleton-mediated negative length regulation (Tomoshige et al., 2017).

Ciliary length maintenance in mammalian cells is remarkably complex, and research remains ongoing to unravel its mechanisms. In recent years, as well as investigating these mechanisms, research has begun to suggest that the length of the primary cilium may be integral in the determination of its signalling output (Macarelli et al., 2023, Kobayashi et al., 2024).

1.1.4 Human disease associated with the primary cilium

The significance of the primary cilium in human cell and tissue homeostasis is highlighted by the range of heterogeneous disorders, collectively named ciliopathies, which occur when cilia are dysfunctional in assembly, structure, function, signalling or trafficking (Adams et al., 2008).

Ciliopathies associated with the primary cilium are known as sensory ciliopathies, distinct from those associated with motile cilia. At least 35 ciliopathies have been identified, linked to genetic mutations in over 200 genes, leading to diverse pathologies across multiple organ systems in the human body, with diverse clinical presentation and severity (Anvarian et al., 2019). Depending on the specific ciliary defect, ciliopathies range from diseases of single organs to syndromes with multi-system involvement. The broad clinical implications of defective cilia are such that the organelle is currently the subject of intense research for its potential as a therapeutic target for many human diseases (Saito et al., 2023).

Ciliopathies are broadly classified into two types. The most well studied ciliopathies are the first-order ciliopathies, which arise from mutations in genes which encode proteins that localise within the cilium or basal body, including IFT machinery. Second-order ciliopathies are associated with mutations in genes which encode proteins that affect cilia indirectly, including transcription factors that regulate ciliary genes (Reiter & Leroux, 2017).

Many ciliopathies have been extensively researched, but it is likely that many more human diseases are linked to pathogenic ciliary defects. Recently, analysis of human genetic disorders with phenotypes reminiscent of ciliopathies identified more than 300 disorders with genetic mutations which may be linked with defective primary cilia, with these disorders described as ‘disorders with ciliary contribution’, in which the indirect contribution of their heterogeneous genetic mutations to aberrant primary cilia remain elusive (Lovera & Lüders, 2021).

Ciliopathies show heterogeneous clinical presentation, often with overlapping phenotypes which predominantly include renal, hepatic, ocular, skeletal, and central nervous system manifestations, and less frequently with additional presentation of cardiovascular, respiratory, endocrine, genital, aural, and pancreatic clinical features (Focșa et al., 2021). At the cellular and molecular level, consistent with the role of the cilium in functional signal transduction, the clinical phenotypes of many ciliopathies are associated with dysregulation of ciliary signalling pathways (Reiter & Leroux, 2017).

Meckel-Gruber syndrome (MKS), for example, is a rare and lethal ciliopathy resulting from several genetic mutations to cilia genes, characterised by severe developmental defects (Hartill et al., 2017). Clinical features of MKS are driven

in part by compromised HH signal transduction, with genetic mutations linked to the disease often resulting in defects at the ciliary transition zone which leads to the loss of SMO accumulation in the cilium (E. C. Roberson et al., 2015). Additionally, ciliary defects which lead to hyperactivation of canonical Wnt signalling have also been linked to the development of this disorder (Wheway et al., 2013, Abdelhamed et al., 2013).

While the most studied human pathogenic defects of primary cilia are the genetic ciliopathies, dysfunctional primary cilia have also been implicated in human diseases not considered classical ciliopathies. For example, a role for defective primary cilia has been proposed in the pathogenesis of Alzheimer's Disease (AD), with shortened neuronal primary cilia identified in multiple mouse models of AD (Kobayashi et al., 2022, Chakravarthy et al., 2012). The Aβ peptide known to drive AD has been shown to compromise ciliary signalling function as well as reduce cilium length (Vorobyeva & Saunders, 2018). Additionally, shortened cilia with defective ciliary trafficking have also been identified in chondrocytes from patients with rare connective tissue disorder alkaptonuria, proposed to contribute to cartilage degeneration characteristic of the disease by dysfunctional transduction of HH signalling (Thorpe et al., 2017).

As previously described, the establishment of the primary cilium exerts negative regulation on the progression of the cell cycle. As such, reduced abundance and length of primary cilia and consequent unregulated cellular progression has been identified in a plethora of human cancers, in many cases directly associated with increased activity of AURKA (Nishimura et al., 2021). Restoration of primary cilia incidence and length via modulation of a number of ciliary targets has been associated with reduced tumour growth in experimental studies of many human cancers (Yin, Wei, et al., 2022). Dysfunctional primary

cilia have also been proposed to contribute to defective cellular signalling in oncogenesis outside of their role in cell cycle regulation, and the contribution of defective primary cilia to cancer, thought to be different in specific cancer types, remains to be fully elucidated (Carotenuto et al., 2023).

1.2 Systemic sclerosis

1.2.1 Fibrosis

Fibrosis refers to the progressive formation of permanent fibrous tissue facilitated by persistent activity of activated fibroblasts known as myofibroblasts, and abnormal tissue remodelling characterised by deposition of excess extracellular matrix (ECM) which disrupts the normal architecture of the affected tissue, and is associated in some contexts with a chronic inflammatory response (Herrera et al., 2018). Fibrosis is not a disease in itself, but a condition associated with a range of heterogeneous diseases. Tissue or vascular fibrosis contributes to the pathogenesis of liver cirrhosis, cardiovascular fibrosis, nephritis, idiopathic pulmonary fibrosis (IPF), and systemic sclerosis (SSc), where organ homeostasis can become severely impaired. The contribution of fibrosis to global human ill-health is such that it was recently estimated that fibrosis is the cause of up to 45% of deaths in the industrialised world (Antar et al., 2023).

Fibrosis is driven by sustained activation of myofibroblasts: differentiated fibroblasts which, in normal physiological conditions, are essential for tissue repair and wound healing, and are active during the inflammatory repair response to injury, infection, and immune activation (Tai et al., 2021).

Myofibroblasts, once activated by cytokines and growth factors, are responsible for the secretion of autocrine and paracrine factors to coordinate the tissue repair response, and are directly responsible for the deposition of ECM components including collagen and fibronectin, and wound contraction (Younesi et al., 2024).

Myofibroblasts can originate from diverse cell types, most commonly from tissue resident fibroblasts and circulating fibrocytes. They can also originate from transition of both epithelial and endothelial precursors, in processes known and epithelial-mesenchymal transition (EMT) or endothelial-mesenchymal transition (EndoMT), or from differentiated mesenchymal stem cells (Kis et al., 2011). Once activated, myofibroblasts express distinct protein markers including α-smooth muscle actin (αSMA) and vimentin, are morphologically characterised by a web-like structure, and their contractile ability is mediated by cytoplasmic stress fibres predominantly composed of αSMA (Darby et al., 2016).

In normal physiological conditions myofibroblast activation is transient, and the tissue repair response is concluded by myofibroblast apoptosis and tissue remodelling. When the response mediated by myofibroblasts is excessive or uncontrolled, it becomes pathogenic and leads to fibrosis (Klingberg et al., 2013). Persistent environmental cues within affected tissues drive the continued activation of myofibroblasts in fibrosis, which is coupled with epigenetic alterations of gene expression to maintain the fibrotic phenotype (Neary et al., 2015).

TGFβ is a fibrogenic cytokine implicated in tissue homeostasis and regeneration. Activation of the TGFβ signalling pathway is thought to be a universal master regulator of fibrosis, responsible for driving both the initiation of

fibrosis and myofibroblast transition, and the progression of fibrosis by directly inducing fibrotic cellular processes including cellular proliferation, cell migration, profibrotic factor and ECM production, and contractility (Meng et al., 2016). TGFβ induced fibrosis is associated with remarkably complex downstream activities mediated by both canonical (SMAD-dependent) and non-canonical (SMAD-independent) TGFβ signalling, including crosstalk of the pathway with other signalling pathways including the Wnt, EGFR, and mTOR pathways, epigenetic modification of gene expression, and regulation of microRNAs and long non-coding RNAs (Budi et al., 2021). Understanding the role of the TGFβ pathway in fibrotic disease has therefore become central to research aiming to develop therapeutic strategies for the attenuation of fibrosis progression.

The molecular and cellular mechanisms which drive fibrosis are not fully elucidated, although common mechanisms driving its progression have been identified in fibrosis which occurs in diverse diseases and contexts (N. C. Henderson et al., 2020). Currently, effective clinical interventions for fibrotic diseases remain under investigation, and treatment options to improve patient outcomes are limited, highlighting the need for continued research to understand the pathogenesis of fibrosis on a cellular and molecular level for therapeutic translation (Ku et al., 2024).

1.2.2 Systemic sclerosis

Systemic sclerosis (SSc), also known as scleroderma, is a rare chronic disease characterised by tissue and vascular fibrosis affecting the skin and internal organs, driven by autoimmune activation, with an incidence of 17.6 cases per 100,000 people (Bairkdar et al., 2021).

There are two cutaneous subsets of SSc: limited cutaneous systemic sclerosis (lcSSc) and diffuse cutaneous systemic sclerosis (dcSSc) (LeRoy & Medsger, 2001) (van den Hoogen et al., 2013). lcSSc primarily affects the skin of the face, hands, and feet, and is typically diagnosed in patients following initial diagnosis of Raynaud's phenomenon, while dcSSc typically involves more extensive areas of the skin, proximal to the elbows and knees, and presents more often with internal organ involvement including fibrosis of the lung, cardiac disease, renal failure, and gastrointestinal disease (Sobolewski et al., 2019). Severe organ involvement in dcSSc often presents within the first few years of disease progression and is associated with chronic morbidity and markedly reduced survival (Steen & Medsger, 2000). Pulmonary disease in particular develops in approximately 80% of dcSSc patients and causes significant morbidity and mortality, with interstitial lung disease (ILD) the most commonly diagnosed form, associated with fibrosis of the lung (Pellar & Pope, 2017).

While diverse presentations of internal organ involvement are responsible for the high mortality in dcSSc, skin fibrosis is a hallmark characteristic of the disease, and progressive hardening and tightening of the skin is severely detrimental to patient quality of life. Skin fibrosis in SSc is associated with consequences including reduced mobility, functional impairment most commonly of the hands, facial skin tightening leading to difficulties eating and speaking, skin sensitivity, and ulceration (Herrick et al., 2022). Skin fibrosis in SSc is linked with sustained activation of myofibroblasts (Gilbane et al., 2013). Indeed, dermal fibroblasts isolated from SSc patient biopsies bear more myofibroblast-like characteristics, and the presence of these fibroblasts correlates directly with the extent and severity of skin involvement (Van Caam et al., 2018). Elucidation of the precise mechanisms which drive fibroblast-

mediated skin fibrosis remains ongoing, and single-cell studies in recent years have begun to characterise heterogeneous subsets of dermal fibroblasts which are thought to contribute differentially to skin involvement (Zhu et al., 2024).

The exact cause of SSc remains unknown, and no single factor has been identified, but the disease is believed to involve a combination of genetic and environmental risk factors (Allanore et al., 2015). The disease is more frequent in women, and onset is most common between ages 50-60. Family history confers predisposition to SSc, with implication of genes related to immune regulation including those of the major histocompatibility complex, while environmental triggers including organic solvent and silica exposure may trigger disease onset in genetically susceptible individuals (Ingegnoli et al., 2018).

There is currently no cure for SSc, and treatment focusses on symptom management, often requiring a multidisciplinary approach. Treatment options include immunosuppressive therapy and anti-inflammatory medications to mediate autoimmunity, vascular treatments including vasodilators, anti-fibrotic drugs, physical therapy and rehabilitation to maintain mobility and function, and treatment of organ-specific complications including pulmonary rehabilitation and medications which target gastrointestinal disease (Del Galdo et al., 2024).

Research for therapeutic intervention is complicated by the patient to patient variability of clinical presentation, and research remains ongoing to clarify the diverse mechanisms which contribute to the pathogenesis of the disease and its clinical manifestations (Murphy et al., 2023). This heterogeneity is such that precision medicine approaches are being considered as a means to identify optimal treatment options for individual patients (Komura et al., 2024).

Diagnosis of SSc typically involves a combination of clinical evaluation of skin thickening and hardening, blood tests for autoantibodies commonly elevated in patients including anti-nuclear and anti-centromere antibodies, imaging studies, and functional tests to determine organ involvement (Hughes et al., 2020). As skin fibrosis is a hallmark of SSc, the Modified Rodnan Skin Score (mRSS) was developed as one semi-quantitative clinical tool to assess patient skin thickness as a measure of skin involvement in the disease (Rodnan et al., 1979). Dermal thickening as a result of skin fibrosis is indicative of disease progression, with elevated mRSS found to correlate with increased risk of organ involvement and decreased survival rate (Del Galdo et al., 2020).

SSc is a disease for which early intervention strategies and biomarker identification are currently a focus of research, with the aim of treatment strategies which can be implicated before progressive and irreversible fibrosis becomes clinically challenging. As such, classification criteria have been established for the very early diagnosis of systemic sclerosis (VEDOSS), which identify the disease before the appearance of fibrosis (Avouac et al., 2011). VEDOSS allows for an insight into early disease progression, where there are detectable immunological abnormalities, but no clinically detectable fibrosis, and VEDOSS diagnosis confers predictive value for the risk of disease progression to SSc (Bellando-Randone et al., 2021).

1.2.3 TGFβ signalling in systemic sclerosis

Consistent with other fibrotic diseases, persistent activation of the TGFβ signalling pathway in SSc skin has long been considered a fundamental driving force of pathogenic skin fibrosis (Varga & Abraham, 2007, Ayers et al., 2018).

TGFβ signalling in SSc skin is implicated in the activation of profibrotic genes and proteins and myofibroblast activation, and both the deposition and preservation of ECM by both enhancing synthesis of ECM components, and reducing synthesis of matrix-degradation signals (Lafyatis, 2014). TGFβ signalling in SSc is of significant clinical relevance, with gene expression signatures classified as highly TGFβ-responsive shown to correlate with increased disease severity in dcSSc (Sargent et al., 2010).

On a molecular level, TGFβ contributes to SSc fibrosis via both canonical signalling mediated by SMAD transcription factors, and SMAD-independent non-canonical signalling associated with activation of mitogen-activated protein kinase (MAPK) pathways, Rho-kinases, and PI3K-AKT pathways (H. H. Hu et al., 2018). Collectively, this signalling leads to the expression of downstream effectors including αSMA associated with increased fibroblast contractility, ECM components including fibronectin (FN1) and alpha-1 and alpha-2 type I collagen (COL1A1 and COL1A2), and connective tissue growth factor (CTGF) (Meng et al., 2016, Mouawad & Feghali-Bostwick, 2023). CTGF is associated with fibroblast differentiation, ECM synthesis, and the further potentiation of TGFβ signalling (Biernacka et al., 2011).

Several mechanisms by which TGFβ signalling may become sustained in SSc skin have been proposed. While some studies have identified elevated circulating TGFβ levels in serum samples obtained from SSc patients, this finding has been contradicted by others (Dziadzio et al., 2005, Dantas et al., 2016, Lu et al., 2017, Lomelí-Nieto et al., 2022). Thus, is theorised that aberrantly sustained activation of autocrine TGFβ signalling in SSc skin may be mediated locally by cellular mechanisms, or that TGFβ may be preferentially sequestered by SSc-affected tissues, reducing circulating levels. Indeed,

increased expression of TGFβ, as well as its receptors (TGFβRs) has been identified in SSc skin biopsies (Lomelí-Nieto et al., 2022). In addition to multiple historic studies which also identified higher expression of TGFβRs in SSc fibroblasts, it has been suggested that SSc fibroblasts may exhibit increased sensitivity to the TGFβ ligand due to enhanced internalisation of TGFβRs (Asano et al., 2011).

Within tissues, including the skin, TGFβ is sequestered in association with the extracellular matrix through binding to latent TGFβ binding proteins (LTBPs), and this latent TGFβ can be activated by integrins on the cell surface to induce signalling. There is evidence for both increased accumulation of TGFβ in SSc skin mediated by elevated expression of LTBP4, and for increased activation of latent TGFβ mediated by increased expression of integrins in SSc dermal fibroblasts (Asano et al., 2005, Liu et al., 2009, Lu et al., 2017).

TGFβ signalling is normally subject to negative feedback regulation driven by SMAD7-SMURF1 complex-mediated receptor degradation after internalisation of the TGFβ-receptor complex and signalling activation (Gencer et al., 2017). An additional mechanism for sustained TGFβ signalling has been proposed in SSc, whereby the inhibitory effect of SMAD7-SMURF1 is impaired and TGFβR stability is increased in SSc fibroblasts, mediated by the repressive activity of SSc-specifically elevated microRNA (miRNA) miR21 on SMAD7 (Asano et al., 2004, Zhu et al., 2013).

The role of TGFβ as a central mediator of skin fibrosis in SSc is well established, and several SSc-specific mechanisms have been proposed which may contribute to aberrant activation of the pathway. Continued research to elucidate the specific mechanisms by which TGFβ signalling is mediated in SSc

are required to guide research for anti-fibrotic therapeutic targets (Györfi et al., 2018). Attempts to target TGFβ signalling for therapeutic intervention remain prospective, with studies attempting to identify targets which avoid the significant adverse implications of broad long-term inhibition of TGFβ signalling (T. Sun et al., 2024).

1.2.4 Caveolin-1 in systemic sclerosis

The integrated membrane protein Caveolin-1 (CAV1) associates with the plasma cell surface membrane and is best characterised as essential for the formation of lipid rafts at membrane invaginations called caveolae, where it plays a scaffolding role in the regulation of endocytosis in numerous signal transduction pathways by influencing receptor-mediated signalling potential (Carver & Schnitzer, 2003). Of the three Caveolin family proteins, CAV1, CAV2, and CAV3, CAV1 and CAV2 are expressed in dermal fibroblasts, with CAV1 mediating the stability, localisation, and expression of CAV2 (Schubert et al., 2007, Egger et al., 2020).

CAV1 contributes to the negative regulation of the TGFβ signalling pathway. After binding to TGFβ ligands, TGFβRs are internalised through two main cellular mechanisms, firstly in clathrin-coated pits, which leads to pathway activation mediated by SMAD2 and SMAD3, and secondly in CAV1-medaited endocytosis, which is associated with proteasomal degradation of TGFβRs mediated by SMAD7-SMURF1 and attenuation of signalling (Razani et al., 2001, Di Guglielmo et al., 2003). Additionally, it has been demonstrated that CAV1 expression leads to a reduction of TGFβR gene expression (Lee et al., 2007). In mouse models, CAV1 deficiency is associated with hyper-activation of

the TGFβ signalling pathway, and a subsequent increase in ECM deposition in response to injury (Miyasato et al., 2011). Activation of the TGFβ signalling pathway has in turn been demonstrated to reduce CAV1 expression, indicating the existence of a feedback mechanism between TGFβ signalling activation and its negative regulation by CAV1 (Del Galdo et al., 2008, Hou et al., 2017, Liakouli et al., 2018).

The demonstrated role of CAV1 in TGFβ signalling initiated significant research efforts to evaluate the implication of CAV1 in the pathogenesis of fibrosis, leading to the observed decreased expression of CAV1 in human fibroblasts associated with TGFβ-mediated fibrosis in a number of contexts, including fibrotic lung diseases, hypertrophic scarring of the skin, and systemic sclerosis (Wang et al., 2006, Del Galdo et al., 2008, Zhang et al., 2011, Kulshrestha et al., 2019, Takamura & Yamaguchi, 2022).

The murine bleomycin-induced fibrosis model is a commonly used research tool to investigate the pathogenesis of fibrosis, characterised by fibrosis of the skin and internal organs with a characteristic presentation that closely mirrors that observed in SSc (Do & Eming, 2016). In this model, reduced expression of CAV1 has been demonstrated, and restoration of CAV1 with adenovirus-mediated overexpression attenuates fibrosis (X. M. Wang et al., 2006). Caveolin scaffolding domain peptide (CSD) is a cell permeable peptide representing a 20-amino acid sequence of CAV1 which mediates CAV1-receptor interactions in signalling mediation and is used experimentally to restore CAV1 function. Treatment with CSD in the bleomycin model of fibrosis has also been shown to attenuate both skin and pulmonary fibrosis and the associated signalling pathway activation, as well as inhibiting TGFβ-inducible profibrotic gene

expression in fibroblasts obtained from the lungs of SSc patients (Tourkina et al., 2008, Reese et al., 2022).

Further understanding of the contribution of CAV1 to fibrosis has been gained through knockdown of CAV1 expression in mice, which markedly increased profibrotic characteristics overlapping with those of SSc, showing spontaneous skin fibrosis associated with increased deposition of ECM (Del Galdo et al., 2008). Additionally, CAV1 knockdown in mice has been associated with pulmonary fibrosis in addition to that of the skin, as well as impaired angiogenesis and cardiac defects (Park et al., 2003, Woodman et al., 2003, Li et al., 2013). CAV1 knockdown in mice has also been specifically linked with spontaneous initiation of both EMT and EndoMT, suggesting that loss of CAV1 primes myofibroblast activation (Li et al., 2013, Strippoli et al., 2015).

The specific contribution of CAV1 downregulation to SSc pathogenesis has been evidenced through the demonstration of a significant reduction of CAV1 expression in SSc patient skin, lungs, and explanted profibrotic SSc dermal fibroblasts by immunohistochemistry, immunofluorescence, and Western Blot in numerous studies, correlating with increased expression of TGFβ-inducible profibrotic markers (Del Galdo et al., 2008, Tourkina et al., 2008, Cipriani et al., 2014, Liakouli et al., 2018). Rescue of the profibrotic phenotype of isolated SSc fibroblasts *in vitro* has been demonstrated upon restoration of CAV1 function with CSD (Del Galdo et al., 2008, Liakouli et al., 2018). Additionally, SSc patients were found to have significantly lower levels of CAV1 in their serum and sputum compared to healthy controls, with a proposed association with SSc-associated interstitial lung disease (Yilmaz et al., 2014). Downregulation of CAV1 in fibroblasts has also been specifically associated with pathogenic

suppression of angiogenesis in SSc, by loss of its regulatory effect on PEDF secretion (Liakouli et al., 2018).

Providing further evidence that loss of CAV1 is associated with SSc pathogenesis, genome-wide analysis of SSc patients and healthy controls highlighted a specific single nucleotide polymorphism (SNP) in the *CAV1* gene which was associated with increased expression of CAV1 protein. The presence of this SNP was significantly protective in susceptibility to SSc (Manetti et al., 2012). Additionally, in a study of a population of SSc patients known to be predisposed to SSc-related interstitial lung disease, lower expression of CAV1 in this cohort was associated with this predisposition (Reese et al., 2014).

Overall, there is significant evidence for the contribution of CAV1 downregulation to fibrotic diseases, including SSc, and a demonstrable link to the association of CAV1 downregulation to activation of TGFβ signalling. Further research is required to fully elucidate the cellular and molecular mechanisms by which CAV1 downregulation mediates fibrosis in the context of SSc and other fibrotic diseases.

1.3 A role for the primary cilium in systemic sclerosis

1.3.1 Signalling dysregulation in systemic sclerosis

As previously described, the deviation from normal tissue homeostasis in the pathogenesis of SSc is characterised on a molecular level by sustained activation of the TGFβ signalling pathway, considered to be a central driving

force of fibrosis. SSc is also associated with dysregulation of both the HH and Wnt signalling pathways.

Sustained activation of HH signalling and increased expression of pathway components including the Sonic Hedgehog (SHH) ligand, HH pathway mediating GLI transcription factors GLI2 and GLI3, and HH receptor PTCH1 has been associated with fibrosis in numerous physiological contexts, including fibrosis of the skin, lungs, and kidneys (L. Hu et al., 2015). Pathway activation has been shown to contribute to the deposition of ECM, increased expression of proteins linked to profibrosis including αSMA, FN1, SNAI1 and COL1A1, and has been implicated in driving EMT (Ding et al., 2012, Bolaños et al., 2012, Hu et al., 2015).

Experimental inhibition of HH signalling pathway components including Smoothened (SMO), as well as overexpression of negative pathway regulator Suppressor of Fused (SUFU), has been demonstrated to ameliorate HH pathway-mediated fibrosis in cultured renal and dermal fibroblasts (Ding et al., 2012, Cao et al., 2016). In the bleomycin model of skin fibrosis, inhibition of SMO has been shown to ameliorate the progression of fibrosis, as well as rescuing the severity of established fibrosis (Horn, Kireva, et al., 2012, Cao et al., 2016).

In SSc specifically, it has been demonstrated that SSc patient serum, particularly that of dcSSc patients, shows elevated levels of the SHH ligand, which is associated with both vasculopathy and fibrosis (Beyer et al., 2018). SSc skin shows marked upregulation of SHH ligand, as well as GLI1 and GLI2 compared to healthy control, linked with myofibroblast activation and

heightened expression of ECM components, COL1A1 and COL1A2 (Horn, Palumbo, et al., 2012).

Ongoing research aims to understand the mechanisms by which HH signalling is dysregulated in SSc. Long range paracrine signalling mediated by palmitoylation of the SHH ligand has also been implicated in SSc pathogenesis. SSc patient dermal fibroblasts have been shown to overexpress hedgehog acetyltransferase (HHAT) which mediates SHH palmitoylation, a modification essential for its biological activity, and knockdown of HHAT led to a reduction in myofibroblast activation and ECM deposition in cultured fibroblasts, as well as attenuation skin fibrosis in two mouse models of SSc (Liang et al., 2019).

The role for GLI2 specifically as a key integration point for the crosstalk of the HH pathway with the TGFβ pathway has been highlighted in SSc, with TGFβ signalling identified as responsible for driving upregulation of GLI2 in SSc dermal fibroblasts, and GLI2 inhibition shown to be protective against fibrosis in mouse models (Liang et al., 2017). There is also evidence to suggest that GLI2 expression in SSc is meditated by crosstalk with the Notch signalling pathway, also known to be dysregulated in SSc and to contribute to myofibroblast activation (Wasson, Ross, et al., 2020). An additional mutually positive feedback crosstalk mechanism with the cJUN/AP1 pathway has been proposed to contribute to HH pathway activation and subsequent profibrosis in SSc dermal fibroblasts (Bergmann et al., 2024).

In addition to TGFβ and HH signalling activation, the canonical Wnt signalling pathway, mediated by β-catenin, has also been implicated in various fibrotic diseases, and linked to myofibroblast activation, enhanced fibroblast migration, production of ECM components, and EMT (Burgy & Königshoff, 2018).

Activation of the Wnt signalling pathway in fibrosis has been linked to crosstalk with the TGFβ signalling pathway, with several components of the Wnt signalling pathway known to be targets of TGFβ signalling (Griffin et al., 2022). Wnt signalling activation by Wnt ligand stimulation of cultured cells and β-catenin overexpression models in mice has been shown to be sufficient to induce spontaneous fibrosis, as well as the contrary, Wnt pathway inhibition has been shown to ameliorate fibrosis in several different model systems (Wei et al., 2011, Akhmetshina et al., 2012, Beyer et al., 2012, Wei et al., 2012, Svegliati et al., 2014).

The sustained activation of Wnt signalling has long been associated with the pathogenesis of SSc, although complete elucidation of the mechanisms that drive this is still under investigation. Elevated expression of several Wnt pathway ligands, particularly Wnt-1, Wnt-2, and Wnt-10b, has been identified in SSc skin compared to healthy controls, correlating with increased expression of ECM components and with patient mRSS (Wei et al., 2011, Akhmetshina et al., 2012, Koçak et al., 2020).

Additionally, significant upregulation of β-catenin has been identified in SSc skin sections and in dermal fibroblasts explanted from SSc patients, as well as upregulation of the Wnt receptor FZD2 and target transcription factor LEF1 in SSc skin (Akhmetshina et al., 2012, Beyer et al., 2012, Svegliati et al., 2014, Wei et al., 2012). Upregulation of Wnt pathway components has been linked with significant upregulation of a number of genes associated with ECM deposition in SSc, as well as other fibrotic diseases (Hamburg-Shields et al., 2015).

A marked decrease in the expression of endogenous negative regulatory components of the Wnt signalling pathway has also been reported in SSc skin sections and explanted fibroblasts compared to healthy controls, including DKK1, DKK2, and WIF1 in SSc skin, observed particularly in patients with dcSSc (Akhmetshina et al., 2012, Wei et al., 2012, Svegliati et al., 2014, Henderson et al., 2021). TGFβ signalling has been implicated specifically in downregulation of Wnt negative regulator Axin2 in SSc (Gillespie et al., 2018).

Elucidation of the mechanisms by which the TGFβ, HH, and Wnt signalling pathways are dysregulated in SSc is important to fully understand the pathogenesis of the disease, and to inform research aimed at targeting these pathways for therapeutic intervention (Riemekasten & Distler, 2022). Interestingly, as previously described, the primary cilium is well established as an important organelle for the regulation of signalling pathways in tissue homeostasis, including the TGFβ, HH, and Wnt pathways.

1.3.2 The roles of TGFβ and Caveolin-1 in cilium structure and function

As previously discussed, the molecular pathogenesis of SSc is characterised by aberrant activation of the TGFβ signalling pathway, as well as by downregulation of the expression of CAV1. Interestingly, studies have shown that both TGFβ and CAV1 have roles at the primary cilium, where they are proposed to influence both ciliary structure and function.

The primary cilium has been implicated in the coordination of TGFβ signalling, as previously outlined. However, there is also evidence to suggest that TGFβ signalling may influence the cilium itself, with studies linking TGFβ signalling to ciliary length control, structure, and function. In several cell types which possess

motile cilia, inhibition of the TGFβ effector SMAD2 led to a decreased ciliary length, as well as ablating the localisation of components of the ciliary transition zone (TZ) in the multiciliated cells of the epidermis, suggesting that TGFβ signalling is implicated in length regulation and TZ formation in motile cilia (Tözser et al., 2015). The effect of TGFβ signalling on the structure of the TZ in primary cilia has not been investigated. However, several studies in different cell types have shown that in primary cilia, activation of TGFβ signalling has the opposite effect on length than it does in motile cilia, inducing a reduction of primary cilia length, and this has been linked with alterations to functional ciliary output.

In chondrocytes, TGFβ signalling has been demonstrated to induce ciliary shortening, as well as a reduction in ciliary incidence, by suppressing the mRNA stability of IFT88, a component of the ciliary intraflagellar transport (IFT) machinery, leading to downregulation of IFT88 protein (Kawasaki et al., 2015, Stam & Clark, 2023). Kawasaki et al. showed that experimental depletion of IFT88 and ciliary shortening in chondrocytes enhanced the expression of ECM components in response to TGFβ, suggesting that functional IFT88 at the cilium plays a suppressive role in TGFβ-mediated ECM deposition.

A recent study of breast and prostate cancer identified the same mechanism of TGFβ-induced ciliary shortening in osteocytes, whereby the secretion of TGFβ by cancer cells was shown to decrease IFT88 expression leading to shortening of primary cilia (Verbruggen et al., 2024). The authors of this study demonstrated that secretion of TGFβ by cancer cells impairs a cilia-dependent ability of osteocytes to suppress the proliferation of these cancer cells by paracrine signalling.

Primary ciliary shortening and a reduction in cilia incidence in response to TGFβ was also demonstrated in osteoblasts, by a different mechanism involving TGFβ-mediated upregulation of the histone deacetylase HDAC6, and consequent deacetylation and shortening of the ciliary axoneme (Ehnert et al., 2017). Here, the authors showed that TGFβ-induced ciliary shortening led to impairments to normal osteogenic function in response to mechanical stimulus, and that experimental inhibition of HDAC6 alongside TGFβ treatment rescued both primary cilium length, and osteogenic function. The same TGFβ-HDAC6 dependent ciliary shortening mechanism has been demonstrated in tenocytes in response to mechanical loading (Rowson et al., 2018).

In a study which showed primary cilium shortening in response to TGFβ in adipocyte progenitor cells, the expression of both IFT88 and HDAC6 were shown to be unaffected by TGFβ-treatment, suggesting that TGFβ-induced shortening in these cells occurs via a different mechanism, although no other mechanism was proposed by the authors (Arrighi et al., 2017). Taken together, these studies provide evidence that while TGFβ seems to be able to induce ciliary shortening in primary cilia of numerous cell types, and that this is linked with functional changes to ciliary output, the mechanism of shortening in these cell types may be diverse.

Recent research has also begun to identify an association between CAV1 and primary cilia, although these studies are limited in number. Studies have suggested that CAV1 localisation to the base of the primary cilium may be important for signal transduction. A study of the neuronal primary cilia of the nematode model organism *C. elegans* identified CAV1 localisation at the periciliary membrane compartment at the base of the cilium (Scheidel et al., 2018). In this study, both experimental overexpression and knockdown of CAV1

led to a loss of ciliary localisation of the ciliary protein PKD2, and mutant animals showed defective mating behaviours. Thus, the authors suggest that CAV1 is important for functional localisation of ciliary components.

In human retinal pigment epithelial (RPE-1) cells, immunofluorescence experiments demonstrated marked CAV1 accumulation at the proximal end of the primary cilium, and identified two components of the ciliary TZ, kinesin family member 13B (KIF13B) and nephrocystin 4 (NPHP4), as responsible for the establishment of this CAV1-enriched microdomain (Schou et al., 2017). Schou et al. demonstrated that experimental knockdown of CAV1 in RPE-1 cells and subsequent loss of ciliary localisation of CAV1 led to decreased ciliary localisation of the HH signalling pathway component SMO in response to stimulation with exogenous SHH ligand, thus proposing a role for CAV1 microdomains at the TZ for functional signal transduction of the HH pathway. In human adipocytes, CAV1 staining was also identified, here in puncta around the base of the primary cilium, showing partial co-localisation with a lipid raft marker and with insulin receptors particularly upon stimulation with insulin, suggesting that CAV1 at primary cilia in these cells may be important for adipogenic signal transduction (Yamakawa et al., 2021).

Recent studies have also suggested that CAV1 may play a direct role in the formation and length of primary cilia. CAV1 depletion in RPE-1 cells was associated with a decrease in ciliary incidence, though non-significant, and an unquantified increase in ciliary length was described (Schou et al., 2017). In a subsequent study, experimental downregulation of CAV1 in three epithelial cell lines, RPE-1, Madin-Darby canine kidney (MDCK), and inner medullary collecting duct (IMCD3), was also shown to slightly decrease ciliary incidence, and significantly increase ciliary length (Rangel et al., 2019). Here, the authors

proposed that this was mediated by reduced Rho GTPase activity, actin cytoskeleton disorganisation, and increased vesicular trafficking observed in these CAV1 depleted epithelial cells. In another study, experimental depletion of CAV1 in foetal lung fibroblast cell lines led to an increase in ciliary incidence, and authors suggested that this may be mediated by increased degradation of Aurora A kinase (AURKA), a negative regulator of cilia length, in these CAV1 depleted cells.

Collectively, these studies demonstrate that CAV1 may be implicated both in modulation of the functional signalling output of the primary cilium, and in cilium formation and length. However, further research is required to elucidate the mechanisms by which this might occur, to explore the implications of CAV1 at primary cilia in different cell types, and its involvement in the mediation of different cellular signalling pathways.

1.3.3 Fibrotic disease associated with defective cilia

As previously described, a diverse group of human diseases collectively termed ciliopathies are known to be driven by genetic mutations to either cilia component or cilia-related genes, which lead to cilia which are aberrant in their formation, structure, or function. Interestingly, many ciliopathies present with characteristic fibrosis despite heterogeneity in genetic mutations and remarkable diversity in the specific ciliary components which are affected. Ciliopathies are commonly associated with liver fibrosis, interstitial respiratory fibrosis, pancreatic fibrosis, and interstitial renal fibrosis (Focșa et al., 2021).

For example, Joubert Syndrome (JS) is a rare ciliopathy characterised by neurodevelopmental defects and, consistent with clinical manifestations of most

known ciliopathies, presents with additional multi-system involvement in different subtypes of JS, which can include hepatic fibrosis (Spahiu et al., 2022). While the exact molecular mechanisms which drive this have not been elucidated, loss of function mutations specifically of ciliary transition zone components, MKS3, CC2DZA, RPGRIP1L, and TMEM67, have shown strong association with the manifestation of liver fibrosis in JS patients (Doherty et al., 2010, Bachmann-Gagescu et al., 2015). Interestingly, in a recent study of four cultured stem cell lines obtained from patients with JS who had genetic mutations in different genes, including *TMEM67* and *CC2DZA*, primary cilium incidence and length were significantly reduced compared to healthy controls, regardless of genotype (De Mori et al., 2024).

Mainzer Salindo Syndrome (MZSDS) is a skeletal ciliopathy which also shows diverse multi-system clinical involvement, which can include hepatic fibrosis (Focșa et al., 2021). This disorder is strongly linked to loss of function mutations of IFT140, a component of the ciliary intraflagellar transport machinery (IFT) (Perrault et al., 2012). Experimental examination of the effect of *IFT140* mutations on the primary cilia of patient-derived epithelial cells, and experimental recapitulation of these mutations in epithelial cell lines, revealed that these mutations are associated with ciliary dysfunction characterised by abnormal accumulation of IFT component IFT88 at the ciliary tip, leading to defects in normal retrograde IFT (Oud et al., 2018).

Renal fibrocystic diseases in particular are commonly associated with a number of primary ciliopathies, with renal disease being the most common clinical manifestation (Gunay-Aygun, 2009). In particular, polycystic kidney diseases (PKD) are a group of genetically and clinically heterogeneous cystic renal disorders which can present either *in utero* or with late onset in adults and are

associated with interstitial renal fibrosis, as well as hepatic fibrosis (Bergmann, 2019). Autosomal dominant PKD (ADPKD) is commonly associated with mutations to the *PKD1* and *PKD2* genes, encoding the PC1 and PC2 polycystin protein family members, which localise to the primary cilium and are proposed to play important roles in the sensory functions of the cilium (Harris & Torres, 2009, Gascue et al., 2011). Interestingly, staining of kidney sections from ADPKD patients revealed elongated primary cilia of tubule cells, which was also observed in *PKD1* and *PKD2* knockout mice, but the molecular mechanisms by which this might drive PKD cystogenesis and fibrosis remain to be elucidated (Shao et al., 2020).

Various mouse models of ciliopathies have also been employed in the study of ciliary defects in human disease and these studies have provided *in vivo* data which shows that ciliary dysfunction, driven by diverse genetic mutations, is sufficient to induce fibrosis or fibrosis associated phenotypes. For example, fibroblasts explanted from a mouse model with genetic ablation of IFT component IFT88 were shown to have reduced primary cilia incidence and length (Schneider et al., 2010). In both *in vivo* and *in vitro* studies of this model, Schneider et al. demonstrated that induced wound healing was defective, with fibroblasts showing uncontrolled migration direction and speed, which is characteristic of fibrosis. In another mouse model, kidney-specific knockdown of the small GTPase CDC42 was demonstrated to reduce ciliogenesis and induce kidney fibrosis, showing a significant increase in staining of collagen fibres in kidney sections, and in mRNA levels of type 1 collagen in explanted fibroblasts (Choi et al., 2013). Interestingly, another study of genetic ablation of IFT88 in mice was also demonstrated to induce hepatic fibrosis, which was linked to increased accumulation of infiltrating immune cells (Zimmerman et al., 2018).

Studies which have directly investigated primary cilia in disease contexts outside of known ciliopathies are limited. However, some recent studies have identified aberrant primary cilia in non-ciliopathies, which are linked with clinical fibrosis. In the progressive degenerative retinal disease age related macular degeneration (AMD), vision loss is driven by vasculopathy and subretinal fibrosis (Tenbrock et al., 2022). A recent study found that retinal pigment epithelial cells isolated from an AMD patient showed significant reduction in both cilia incidence and cilia length, and authors suggest that the cilium should be considered as a potential contributor to the pathogenesis of the disease (Ning et al., 2023).

Atrial fibrillation (AF) is a condition of abnormal heart rhythm which can present with cardiac fibrosis. In a recent study, staining of cardiac tissue sections revealed a reduced incidence of primary cilia in patients with AF compared to healthy controls, and experimental depletion of cilia in healthy human atrial fibroblasts by knockdown of IFT88 led to enhanced expression of ECM component genes, including *COL1A1* and *FN1* (Kawasaki et al., 2024). Interestingly, elevated expression of *AURKA*, a negative regulator of ciliary length, and its co-activator *NEDD9*, were also demonstrated in AF patient cardiac tissue in this study. Kawasaki et al. showed that pharmacological inhibition of AURKA in AF patient-derived atrial fibroblasts increased ciliary incidence and length, and that this was associated with a decrease in expression of ECM components, particularly in response to treatment with exogenous TGFβ ligand, leading the authors to suggest that defective primary cilia resulting from aberrant AURKA activity in atrial fibroblasts may contribute to their profibrotic phenotype.

As previously described, myofibroblast transition from various cell types including adipose progenitors, endothelial cells by EndoMT, and epithelial cells by EMT, is a cellular driving force of fibrosis, resulting in the activation of contractile myofibroblasts which mediate deposition of extracellular matrix (ECM) components. There is experimental evidence to suggest that primary cilia may be intrinsically linked with myofibroblast transition processes.

Studies have suggested that shortening or loss of the primary cilium may prime progenitor cells to undergo transition. For example, embryonic endothelial cells from IFT88 knockout mice which lacked primary cilia were demonstrated to show heightened EndoMT in response to fluid shear stress, marked by increased expression of markers including αSMA, and activation of SMAD2 signalling (Egorova et al., 2011). In canine kidney epithelial cells, experimental knockout of ciliary components ARL13B and IFT20 led to shortened primary cilia, and these cells exhibited increased expression of EMT markers under basal conditions, as well as more significantly in response to treatment with exogenous TGFβ compared to control (Han et al., 2018). This suggests that there may be positive feedback between TGFβ signalling, ciliary shortening or loss, and myofibroblast transition.

There is also evidence to suggest that primary cilia may be necessary to sense the initial signal to drive myofibroblast transition, and that cilia themselves then undergo structural transition during the myofibroblast transition process. The primary cilia of porcine kidney epithelial cells were shown to undergo a dynamic biphasic transition during EMT, with a short period of initial lengthening followed by loss of the primary cilium (Rozycki et al., 2014). In adipocyte progenitor cells from adipose tissue and skeletal muscle, myofibroblast transition induced by TGFβ was shown to be associated with shortening of the primary cilium (Arrighi

et al., 2017). In both of these studies and cell types, the authors showed through experimental inhibition of ciliogenesis that the presence of a primary cilium was required to induce myofibroblast transition (Rozycki et al., 2014, Arrighi et al., 2017).

Further elucidation of the specific role of the primary cilium during myofibroblast transition from different cell types may shed more light on the link between cilia and fibrosis, and how aberrations to primary cilia may contribute to fibrotic disease.

In the context of systemic sclerosis, the primary cilium remains to be explored. Recently, two studies have highlighted a potential link between primary cilia and the pathogenesis of SSc. Skin biopsies taken from SSc patients were subjected to RNA-sequencing analysis and a significant decrease in the expression of *SPAG17* was identified compared to healthy controls (E. D. O. Roberson et al., 2023). SPAG17 is a poorly characterised component of motile cilia which has also been implicated in the structure and function of primary cilia, with experimental knockdown of SPAG17 shown to induce ciliary shortening in chondrocytes, osteoblasts, and mouse embryonic fibroblasts (Teves et al., 2015).

In a subsequent study, SPAG17 was shown to be downregulated in SSc skin sections and cultured dermal fibroblasts explanted from SSc patients compared to healthy controls, though primary cilia were not analysed (Sapao et al., 2023). In experimental knockdown of SPAG17 in human dermal fibroblasts, Sapao et al. showed an increase in the expression of αSMA and procollagen I, as well as spontaneous skin fibrosis in a conditional SPAG17 knockout mouse model, where explanted fibroblasts were enriched in transcript levels of profibrotic

markers and had heightened nuclear accumulation of SMAD2/3, indicative of activation of the TGFβ signalling pathway. Taken together, these studies provide the first tentative evidence that defective primary cilia might be implicated in the pathogenesis of SSc.

1.4 Project rationale and aims

Primary cilia are sensory organelles which play important roles in cellular and tissue homeostasis, particularly with respect to cellular signalling regulation, including that of the Wingless-related integration site (Wnt), Hedgehog (HH), and Transforming Growth Factor Beta (TGFβ) signalling pathways. A number of human diseases are driven by ciliary dysfunction, with diverse molecular pathogenesis and clinical manifestations, including fibrosis.

Systemic sclerosis (SSc), a rare autoimmune disease of unknown aetiology, which presents with chronic progressive fibrosis and vasculopathy of the skin and internal organs, is characterised on a molecular level by dysregulated cellular signalling, particularly of the Wnt, HH, and TGFβ pathways. In particular, activation of the TGFβ signalling pathway is recognised as a fundamental driving factor of the pathogenesis of SSc fibrosis, as well as that of other human fibrotic diseases, where an aberrantly persistent activation of the tissue repair process leads to scarring, disrupting normal tissue and organ architecture.

Maintenance of the primary cilium on mammalian cells is a dynamic process, with a stable ciliary length established by an intricate balance struck between processes which elongate the cilium, and those that shorten it. As well as being implicated in the pathogenesis of SSc, and being coordinated at the primary

cilium, TGFβ signalling has been shown to directly alter primary cilium structure in a number of cellular contexts, inducing ciliary shortening through diverse molecular mechanisms.

There is also a poor understanding of the role of the membrane scaffolding protein Caveolin-1 (CAV1) in SSc pathogenesis, where CAV1 downregulation has been demonstrated to contribute to fibrosis. Additionally, at the primary cilium, it has been proposed that CAV1 localisation to the cilium may be implicated in ciliary signal transduction, as well as ciliogenesis and cilia length regulation.

The molecular and cellular driving forces of human fibrotic conditions remain to be completely elucidated. There is a growing collective body of evidence which suggests that dysfunctional primary cilia may be a hallmark of fibrotic pathogenesis, through diverse aberrations to ciliary incidence, length, structure, and function.

Primary cilia have not been investigated in the context of SSc specifically. Recent work associated loss of the ciliary component sperm associated antigen 17 (SPAG17) with SSc. Preliminary work carried out in our research group identified that dermal fibroblasts explanted from skin biopsies of two SSc patients displayed primary cilia which appeared shortened compared with those of healthy controls. Furthermore, treatment with exogenous TGFβ appeared to induce shortening of the primary cilium in dermal fibroblasts.

Consideration of these factors collectively led to the formation of the following hypotheses: first, that defective, shortened primary cilia may be found on SSc dermal fibroblasts, which could contribute to the disease phenotype through aberrant regulation of ciliary signal transduction. Second, that activation of

TGFβ signalling characteristic of SSc could lead to this shortened cilia phenotype.

To begin to address these hypotheses, this research had the following aims, using *in vitro* experimental analysis of dermal fibroblasts:

1) To characterise primary cilium length reduction in SSc patient dermal fibroblasts as well as very early diagnosis of systemic sclerosis (VEDOSS) dermal fibroblasts, compared to healthy control fibroblasts.
2) To characterise the effect of TGFβ on cilium length in dermal fibroblasts.
3) Explore the contribution of several known mediators of ciliary length modulation to both TGFβ-mediated and stable SSc ciliary shortening phenotypes, and determine if the mechanisms are shared or independent.
4) To characterise the effect of experimental CAV1 downregulation on dermal fibroblast cilium length.
5) To explore the phenotypic effects of experimental cilium length restoration, in particular on the profibrotic phenotype of dermal fibroblasts.
6) To characterise the expression of SPAG17 at the primary cilia of healthy and SSc dermal fibroblasts.

Chapter 2. Materials and Methods

2.1 Cell lines

All work in this thesis was conducted on human dermal fibroblasts in *in vitro* culture. Fibroblast lines were isolated from full thickness forearm punch biopsies from healthy control (HC) donors or from patients satisfying either the ACR-EULAR classification criteria for diffuse cutaneous SSc (dcSSc) (van den Hoogen et al., 2013), or VEDOSS classification criteria (Avouac et al., 2011). Biopsies were obtained after receiving written informed consent from participants for research use with HRE Research Ethics Committee approval (reference number 15/NE/0211). Fibroblasts were expanded out of cut biopsies, with primary cell lines established after two passages.

In cases where experiments were carried out using primary fibroblasts, experiments were performed within five passages. Primary lines were also immortalised by transduction with a retrovirus expressing human telomerase reverse transcriptase (hTERT), as previously described (Gillespie et al., 2018).

Single cell clonal lines were isolated from one heterogeneous parental hTERT SSc fibroblast cell line. A cell resuspension was serially diluted into 96-well plates to isolate single cells. Verified by light microscopy, wells which contained individual fibroblasts were subsequently expanded to generate clonal cell lines.

Patient and cell line information for all cultured lines used in this work can be found in Table 1.

Table 1: Patient and cell line information

Cell Line Name	Cell Line Code	hTERT/ Primary	Age	Sex	Disease Type	MRSS Score	Disease duration (months)
SSc 1	Strike66	hTERT	67	F	dcSSc	35	97
SSc 2	Strike262	hTERT	43	M	dcSSc	43	13
SSc 3	Strike279	hTERT	35	F	dcSSc	1	1
SSc Primary	Strike262	Primary	See Strike262				
VEDOSS 1	FDG289	Primary	33	F	VEDOSS	0	N/A
VEDOSS 2	FDG268	Primary	34	F	VEDOSS	0	N/A
VEDOSS 3	FDG189	Primary	39	M	VEDOSS	0	N/A
VEDOSS 4	FDG201	Primary	66	F	VEDOSS	0	N/A
SSc Clone 1	FDG81	hTERT	See Strike66 (parental line). See materials and methods section 2.1 for details of cell line generation.				
SSc Clone 2	FDG126	hTERT					
SSc Clone 3	FDG80	hTERT					
SSc Clone 4	FDG28	hTERT					
SSc Clone 5	FDG127	hTERT					
HC 1	FDG111	hTERT	41	M	N/A	N/A	N/A
HC 2	FDG129	hTERT	Data unavailable		N/A	N/A	N/A
HC 3	FDG300	hTERT	Data unavailable		N/A	N/A	N/A
HC Primary	FDG300	Primary	See FDG300				
HC SCR	FDG111 SCR	hTERT	See FDG111 (parental line). See materials and methods section 2.14 for details of cell line generation.				
HC shCAV	FDG111 shCAV	hTERT					

2.2 Cell culture

Cells were cultured in 1 g/L Glucose Dulbecco's Modified Eagle Medium (DMEM) (Thermo Fisher) with 10 % FBS (Thermo Fisher), 1 % Penicillin/Streptomycin (Merck), and 250 µg/mL Geneticin (Thermo Fisher) as selection for hTERT transduction. Geneticin was not included in culture medium while performing experiments. Cells were grown in adherent monolayers in

culture flasks (Corning), incubated at 37 ºC with 5 % CO2. Culture media was refreshed every 48-72 h, and cells were regularly passaged at 80-90 % confluence by aspirating media, washing with 1 X PBS (Sigma), treating with 1 X Trypsin (Merck) for 5 minutes at 37 ºC to detach cells from plastic ware, and resuspension in fresh culture medium containing 10 % FBS to deactivate Trypsin. Cells were appropriately diluted in medium and seeded into culture flasks.

For long-term storage, cell suspension aliquots were prepared in filtered complete DMEM supplemented with 10 % extra FBS and 10 % dimethylsulphoxide (DMSO) (Sigma), and frozen at -80 ºC before transfer to storage in liquid nitrogen.

For experimental work, cell seeding density was controlled by counting cells using a haemocytometer after Trypsin treatment and resuspension.

2.3 Treatment of fibroblasts with ligands and inhibitors

Unless otherwise stated, all experimental treatments were administered after fibroblasts reached confluence and were subjected to 24 h of serum starvation in DMEM (Thermo Fisher) with 0.5 % FBS (Thermo Fisher) and 1 % Penicillin/Streptomycin (Merck). Ligands or small molecule inhibitors were then added to fibroblasts at their appropriate concentrations in serum starved media for 24 h or 48 h.

To activate the Transforming Growth Factor Beta (TGFβ) pathway, fibroblasts were treated with recombinant TGFβ ligand (10 ng/mL, Merck). Small molecule inhibitors used were TGFβRI inhibitor SD208 (1 μM, Selleckchem), pan-ROCK inhibitor Y27632 (2 μM, MedChemExpress), ROCK2 inhibitor KD025 (5 μM,

Cayman Chemical), PI3K inhibitor BKM120 (2 μM, Selleckchem), HDAC6 inhibitor Tubacin (10 μM, Sigma), and AURKA inhibitor MLN8054 (10 μM, APExBIO). For controls, fibroblasts were treated with an equal volume of vehicle (DMSO, Sigma). In cases where cells were treated with both an inhibitor and with TGFβ, inhibitor treatment was introduced two hours before stimulation with TGFβ.

2.4 siRNA transfection

To inhibit the canonical TGFβ pathway, a pool of four FlexiTube GeneSolution siRNA (Qiagen) oligos specific to SMAD3 were used for post-transcriptional gene silencing. The four target sequences were as follows: AGCCTATACTTTGGCAGGTTA, AAGGAGCACCTTGACAGACTT, AAGAGATTCGAATGACGGTAA, and ATCAAGGGATTTCCTATGGAA. Oligos were combined to a total concentration of 40 nM, and transfected into fibroblasts at 70 % confluence with Lipofectamine 2000 (1 μg/mL, Thermo Fisher) before incubation for 72 h, including any additional treatments, before protein harvest or fixation for immunofluorescence. As a negative control, fibroblasts were transfected with a scrambled (SCR) siRNA oligo (Qiagen) with the following sequence: AATTCTCCGAACGTGTCACGT. Knockdown was monitored by Western Blot for SMAD3.

2.5 Protein extraction and quantification

For the harvest of protein, cells were seeded and subjected to experimental treatments in 6-well culture plates. Media was aspirated, cells were washed in ice cold 1 X PBS, then lysed in ice cold protein lysis buffer comprising of RIPA

Buffer (Merck) with 1 X Protease Inhibitor (Merck) and 1 X Phosphatase Inhibitor (Merck). Lysates were collected using a cell scraper, vortexed briefly and centrifuged for 15 minutes at 16,000 g at 4 ºC to remove cellular debris, before further analysis or storage at -20 ºC (short-term) or -80 ºC (long-term).

Protein concentration was determined by colorimetric assay using the Pierce Bicinchoninic Acid (BCA) Protein Assay kit (Thermo Fisher) as per the manufacturer's instructions. Briefly, the total protein concentration of each sample was determined by comparison of its absorbance after incubation with working reagent to a standard curve generated from the absorbance of a serial dilution of known protein concentration of Bovine Serum Albumin (BSA). Absorbance was measured at 540 nm using the Agilent BioTek Cytation 5 microplate reader (BioTek).

2.6 Western Blotting

Comparative quantification of target protein levels was carried out via Western Blotting. In each experiment, the total protein concentration loaded was normalised across each sample, with volumes adjusted based on the results of the BCA Assay. Lysates diluted in Laemmli Sample Buffer (Bio-Rad) with β-Mercaptoethanol were boiled for 5 minutes at 95 ºC, then separated by sodium dodecyl sulphate polyacrylamide gel electrophoresis (SDS-PAGE) alongside Precision Plus Protein Dual Colour Standards (Bio-Rad) using the Mini-PROTEAN Tetra electrophoresis system (Bio-Rad). Gels were run at 120 V for 10 minutes then 150 V for 45 minutes in 1 X running buffer (Thermo Fisher), then proteins were transferred to Hyperfilm™ nitrocellulose membrane

(Amersham) using the Mini-PROTEAN wet transfer apparatus (Bio-Rad) in 1 X transfer buffer (Thermo Fisher) for 2 h at 50 V.

Membranes were then blocked in 5 % milk (Applichem) or 5 % BSA (Sigma) in TBS (Thermo Fisher) 0.1 % Tween20 (Sigma) (TBS-T) for 45 minutes at room temperature with gentle shaking, before incubation with primary antibody solutions diluted in 5 % milk or BSA in TBS-T overnight at 4 ºC with gentle shaking. Membranes were then washed and incubated with HRP-linked secondary antibody solutions in 5 % milk in TBS-T for 1 hour at room temperature with gentle shaking. After washing again, membranes were developed using SuperSignal West Pico PLUS Chemiluminescent Substrate (Thermo Fisher) and visualised using the ChemiDoc™ Touch Imaging System (Bio-Rad).

Densitometry analysis was carried out using Image Lab Software (Bio-Rad), with β-Actin used for normalisation across samples. Details of primary and secondary antibodies used for Western Blotting can be found in Table 2.

Table 2: Western Blot antibody information

Antibody Target (Western Blotting)	**Antibody Manufacturer**	**Antibody Catalogue Number**
αSMA	Abcam	ab7817
β-Actin	Sigma	A5441
Acetylated-α-Tubulin	Cell Signalling	5335
AKT	Cell Signalling	9272
pAKT (Ser473)	Cell Signalling	4060
pAKT (Thr308)	Cell Signalling	4056
CAV1	Santa Cruz	sc894
CTGF	Abcam	ab20980
HEF1/NEDD9	Cell Signalling	4044
MLC2	Cell Signalling	8505

pMLC2 (Ser19)	Cell Signalling	3671
ppMLC2 (Ser19, Thr18)	Cell Signalling	3674
SMAD3	Cell Signalling	9523
pSMAD3	Abcam	ab52903
SPAG17	Bioss	bs9596
p53	Santa Cruz	sc126
Anti-Mouse IgG HRP-linked	Cell Signalling	7076
Anti-Rabbit IgG HRP-linked	Cell Signalling	7074

2.7 RNA extraction and quantification

For the harvest of RNA, cells were seeded and subjected to experimental treatments in 6-well culture plates. Media was aspirated, cells were washed in 1 X PBS, then lysed with RNA lysis buffer (Zymo Research) and collected. RNA was extracted from cell lysates using the Quick-RNA Miniprep Kit (Zymo Research) according to the manufacturer's instructions. Briefly, samples were processed by a series of filtration and washing steps to remove genomic DNA – including an incubation with DNase I – and purify RNA. RNA was eluted in DNase/RNase-Free water (Invitrogen). RNA concentration was determined using a NanoDrop 1000 Spectrophotometer (Thermo Fisher) which measures sample light absorbance to quantify genetic material. Sample quality was controlled by ensuring absorbance ratios of 260/280 nm and 260/230 nm were within the range of 1.8-2.2, indicating that the RNA is pure and clear of chemical contaminants. Compliant samples were either immediately taken to further processing or stored at -80 ºC.

2.8 cDNA synthesis

RNA was transcribed into complementary DNA (cDNA) by reverse transcription. Based on the RNA concentration determined using NanoDrop analysis, RNA concentration before cDNA synthesis was normalised across all samples by dilution with an appropriate volume of DNase/RNase-Free water (Invitrogen). cDNA synthesis was carried out using the High Capacity cDNA Reverse Transcription Kit (Applied Biosystems) according to the manufacturer's instructions. Briefly, diluted RNA samples were added to a master mix consisting of an RT buffer, random primers, Deoxynucleoside Triphosphates (dNTPs), and Multiscribe Reverse Transcriptase. The reaction was processed in the Veriti 96 Well Thermal Cycler (Applied Biosystems) with the following conditions: 25 ˚C for 10 minutes, 37 ˚C for 120 minutes, then 85 ˚C for 5 minutes. cDNA was used for further analysis or stored at -20 ºC.

2.9 Quantitative polymerase chain reaction

For the detection and quantification of cDNA, real-time quantitative polymerase chain reaction (qPCR) assays were carried out using the PowerUp™ SYBR™ Green Master Mix (Applied Biosystems) as per the manufacturer's instructions. Briefly, a master mix was prepared for each target transcript to consisting of SYBR™ Green Master Mix, a forward and reverse primer mix solution using primers specific to the target transcript, and nuclease-free water (Qiagen), to which either the cDNA sample or water control was added. Samples were run in triplicate for each primer master mix. Assays were run on the QuantStudio 7 Real-Time PCR System (Applied Biosystems) with the following conditions: 50 ˚C for 2 minutes x 1 cycle, 95 ˚C for 2 minutes x 1 cycle, 95 ˚C for 15 seconds followed by 60 ˚C for 1 minute x 40 cycles, and a dissociation step of 1.6

˚C/second to 95 ˚C for 15 seconds, 1.6 ˚C/second to 60 ˚C for 1 minute, and 0.15 ˚C/second to 95 ˚C for 15 seconds. Data was obtained and analysed using Thermo Fisher Connect software (Thermo Fisher), according to the ΔΔ Ct method, with GAPDH serving as a house-keeping gene for normalisation. Details of primer sequences used for qPCR can be found in Table 3.

Table 3: qPCR primer sequence information

Target	Forward Sequence (5'-3')	Reverse Sequence (5'-3')
ACTA2	TGT ATG TGG CTA TCC AGG CG	AGA GTC CAG CAC GAT GCC AG
CAV1	CGA CCC TAA ACA CCT CAA CGA	TCC CTT CTG GTT CTG CA
CCN2	GTG TGC ACT GCC AAA GAT GGT	TTG GAA GGA CTC ACC GCT G
COL1A1	CCT CCA GGG CTC CAA CGA G	TCT ATC ACT GTC TTG CCC CA
COL1A2	GAT GTT GAA CTT GTT GCT GAG C	TCT TTC CCC ATT CAT TTG TCT T
FN1	ACA ACA CCG AGG TGA CTG AGA C	GGA CAC ACC GAT GCT TCC TGA G
GAPDH	ACC CAC TCC TCC ACC TTT GA	CTG TTG CTG TAG CCA AAT TCG T
SPAG17	GGC CTC CAT TGC TTT TGT GG	GTT TAC GCT GAG GGA CCT GG

2.10 Immunohistochemistry

Immunohistochemistry for the visualisation of SPAG17 protein within tissue was carried out on formalin-fixed and paraffin-embedded 5 μM thickness HC and SSc skin sections mounted on slides. Sections were rehydrated in baths of xylene and serial dilutions of ethanol before boiling with 10 mM sodium citrate for 3 minutes for antigen retrieval, then BLOXALL blocking solution (Vector Laboratories) for 10 minutes to quench peroxidase activity, followed by 10 % normal horse serum (Vector Laboratories) for 20 minutes to block non-specific binding. Sections were stained with a SPAG17 primary antibody (Bioss) in an overnight incubation at 4 ºC, followed by ImmPRESS™ Polymer Anti-Rabbit

IgG Reagent (Vector Laboratories) for 30 minutes, and visualised with 3,3-diaminobenzidine (DAB) (Vector Laboratories). Slides were counterstained with haematoxylin. Images were obtained on an Olympus BX50 light microscope (Optronics) at 20 x magnification.

2.11 Immunofluorescence

For the visualisation of intracellular proteins via Immunofluorescence, cells were seeded in Nunc™ Lab-Tek™ II Chamber Slides (Thermo Fisher) and subjected to experimental treatments. Cells were fixed with 4 % paraformaldehyde in PBS for 15 minutes at room temperature while protected from light, then permeabilised with 0.2 % Triton X-100 (Sigma) in PBS for 15 minutes at room temperature. Non-specific binding was blocked with 1 % BSA (Sigma) in PBS blocking solution for 10 minutes at room temperature. Cells were then incubated overnight at 4 ºC with primary antibody solutions made up in 1 % BSA blocking solution, then incubated with secondary antibody solutions made up in 1 % BSA blocking solution for 2 hours at room temperature, protected from light. Cells were washed with 1 X PBS between all incubations. Coverslips were mounted to slides using Prolong Anti-Fade Mounting Medium with DAPI (Life Technologies) before storage at 4 ºC prior to imaging. Details of primary and secondary antibodies used for Immunofluorescence can be found in Table 4.

Table 4: Immunofluorescence antibody information

Antibody Target (Immunofluorescence)	Antibody Manufacturer	Antibody Catalogue Number
Acetylated-α-Tubulin	Cell Signalling	5335
Ki67	Proteintech	27309-1-AP
pAURKA (Thr288)	Abcam	ab83968

Phalloidin (Alexa Fluor 488)	Invitrogen	A12379
SPAG17	Bioss	bs9596
Anti-Mouse (Alexa Fluor 488)	Invitrogen	A21200
Anti-Rabbit (Alexa Fluor 594)	Invitrogen	A21442

2.12 Confocal microscopy and image analysis

Immunofluorescence was visualised and images acquired with an LSM880 upright laser scanning confocal microscope (Zeiss) (Bioimaging Facility, University of Leeds) with ZEN microscopy software, using a 40 x magnification Plan-Apochromat DIC oil immersion objective lens (Zeiss). Images were taken at 0.2 µm intervals through the entire depth of the cell monolayer, then combined into Z-stacks.

Quantitative analysis of microscopy images for the measurement of primary cilia length and incidence, quantification of Ki67-positive nuclei, and measurement of SPAG17 fluorescence intensity and incidence was conducted using ImageJ software. Results presented in this thesis based on Immunofluorescence analysis comprise of manual analysis of a minimum of 100 individual cells from a minimum of three randomly selected fields of view per experimental replicate.

2.13 Cell contraction assays

The contractile ability of fibroblasts was measured using a Cell Contraction Assay kit (Cell Biolabs) as per the manufacturer's instructions. Briefly, 200,000 fibroblasts per condition were resuspended in the kit's collagen solution, and the subsequent cell-collagen gel mixture was allowed to polymerise in a 24-well cell culture plate at 37 ˚C for 1 h in the absence of CO2. DMEM with 0.5 % FBS and

1 % Penicillin/Streptomycin containing the appropriate treatments was then added on top of the polymerised gels before incubation for 16 h at 37 ˚C with 5 % CO2. The edges of the cell-collagen gels were then released from the wells using a sterile scalpel, and images of each gel were taken at 0 h, 1 h, 2 h, 4 h, 6 h, 8 h, 24 h, and 48 h post-release. At 48 h, the weight of each gel was recorded. Images were analysed using ImageJ software to measure the area of each gel at each time point and to calculate the percentage of gel contraction relative to the 0h time point area.

2.14 Generation of shCAV knockdown line

To study the effect of Caveolin-1 (CAV1) downregulation in SSc, healthy dermal fibroblasts were transduced with short hairpin RNA (shRNA) GIPZ plasmid lentiviral vector systems (Open Biosystems) containing either scramble control shRNA (Catalogue Number RHS4348, sequence proprietary) or CAV1 sequence specific shRNA (Catalogue Number V3LHS_312897, mature antisense sequence TCGTCACAGTGAAGGTGGT) to induce long-term stable knockdown of CAV1. Constructs were introduced to fibroblasts at 60 % confluence at an initial titre of 1 x 10 ^8 TU/mL and incubated for 6 h before a 1:2 dilution of medium and incubation for a further 72 h. Stably transduced fibroblasts were selected with 1 µg/mL Puromycin (Life Technologies) for 10 days, as previously described (Liakouli et al., 2018). During culture, selection was maintained with 0.5 µg/mL Puromycin, and continuation of knockdown monitored by Western Blot for CAV1.

2.15 Statistical analysis

Results presented as continuous variables are reported as mean ± standard error or mean ± standard deviation, as noted in figure legends. Categorical variables are reported as percentages. Tests used to determine statistical significance are described in figure legends, with significance shown on data graphs as * for $P<0.05$, ** for $P<0.01$, *** for $P<0.001$, and **** for $P<0.0001$. All statistical analyses were carried out in GraphPad Prism software (version 9.2.0 332).

Chapter 3. Characterisation of primary cilia of dermal fibroblasts in Systemic Sclerosis, and their regulation by TGFβ signalling

3.1 Introduction

Preliminary data from our research group showed that the primary cilia of dermal fibroblasts isolated from two SSc patients appeared shorter than those isolated from healthy controls (HC) (unpublished data). Subsequently, based on the well-studied importance of the primary cilium as a sensory organelle and the fact that ciliary dysfunction is known to contribute to a range of human diseases, we formed the research hypothesis that an aberrant primary cilium could contribute to the pathogenesis of SSc. To investigate this hypothesis, we firstly decided to characterise primary cilia length and incidence with a comprehensive analysis including HC, SSc, VEDOSS and clonal SSc fibroblast lines obtained by single cell dilution. This characterisation included work to support the use of our chosen experimental conditions for cilia analysis. Secondly, since TGFβ has been shown to shorten cilia in a range of cell types (Kawasaki et al., 2015, Ehnert et al., 2017, Arrighi et al., 2017, Rowson et al., 2018, Han et al., 2018), we also set out to investigate the hypothesis that the chronic TGFβ signalling characteristic of SSc could be the cause of the abnormal ciliary phenotype.

3.2 Results

3.2.1 Primary cilia are shorter in SSc and VEDOSS dermal fibroblasts compared to healthy controls

To investigate the length and incidence of primary cilia in immortalised SSc and VEDOSS dermal fibroblasts compared to HC, confluent fibroblasts were cultured in 0.5 % serum-containing media for 48 h to induce cell cycle synchronization at G0/G1, to allow for complete ciliogenesis (Kasahara & Inagaki, 2021). Visualisation and analysis of cilia incidence and length was carried out by immunofluorescence of Acetylated-α-Tubulin (Ac-α-Tub) to label primary cilia, and confocal microscopy (Fig. 3.1A). Primary cilia were shorter in SSc dermal fibroblasts compared to HC, with a mean length of 2.8±0.1 μm (Mean±SEM) vs 4.4±0.2 μm ($p<0.0001$) (Fig. 3.1B, C). Surprisingly, the same phenotype was observed in dermal fibroblasts from VEDOSS patients, with a mean length of 2.5±0.1 μm, compared to HC ($P<0.0001$) (Fig. 3.1B, C). SSc cilia length was not significantly different to VEDOSS cilia length (Fig. 3.1B, C), suggesting that the shortened cilia phenotype is present even in very early stages of disease, where there is no clinically detectable skin fibrosis.

Studies have highlighted the diversity of fibroblast subsets found in the skin, including that of SSc, proposed to play different roles in tissue homeostasis (Tabib et al., 2018, Philippeos et al., 2018, Zhu et al., 2024). To assess if cilia length may differ between distinct subpopulations of heterogeneous fibroblast populations isolated from patient skin biopsies, five SSc single cell clonal lines generated from one parental line (SSc 1) were included in the analysis. These clones have different proliferation rates, and differential gene expression patterns (data not shown). However, the mean cilia lengths of all clonal lines

were similar to each other and to the parental line, all shorter than HC (parental SSc 1 = 3.1±0.9 μm (Mean±STDEV), vs Clone 1 = 3.0±0.8 μm, Clone 2 = 2.9±0.6 μm, Clone 3 = 3.1±0.7 μm, Clone 4 = 2.7±0.6 μm, Clone 5 = 2.8±0.6 μm) (Fig. 3.1B). The combined mean cilia length of the clonal lines at 2.9±0.07 μm (Mean±SEM) did not differ from that of SSc at 2.8±0.1 μm, but was significantly shorter compared to HC at 4.4±0.2 μm ($p<0.0001$) (Fig. 3.1C).

Cilia incidence was comparable between HC, SSc, VEDOSS, and clonal SSc lines (Fig. 3.1D), suggesting that the cause of the shortened cilia phenotype in SSc and VEDOSS does not also lead to an inhibition of the ability of fibroblasts to develop cilia.

Categorising cilia lengths taken from the individual HC and SSc fibroblast lines into 0.5 μm interval length ‘bins’, and calculation of the percentage of total cilia that fit into each ‘bin’, allowed for visual representation of the distribution of cilia length within each population. The distribution of SSc cilia length shows a narrower dispersion around shorter length categories compared to HC (Fig. 3.1E). Interestingly, the distribution of cilia length in the SSc Clone lines (Fig. 3.1F) was similar in appearance to that of the SSc lines (Fig. 3.1E). This suggests that cilium length variability is found at the population level even in fibroblasts that are epigenetically identical.

In addition, the distribution of cilia length in each HC and SSc fibroblast line was found to be normal (Fig. 3.1G), justifying further data analysis by combining the means of biological replicate cell lines and using parametric tests for statistical significance.

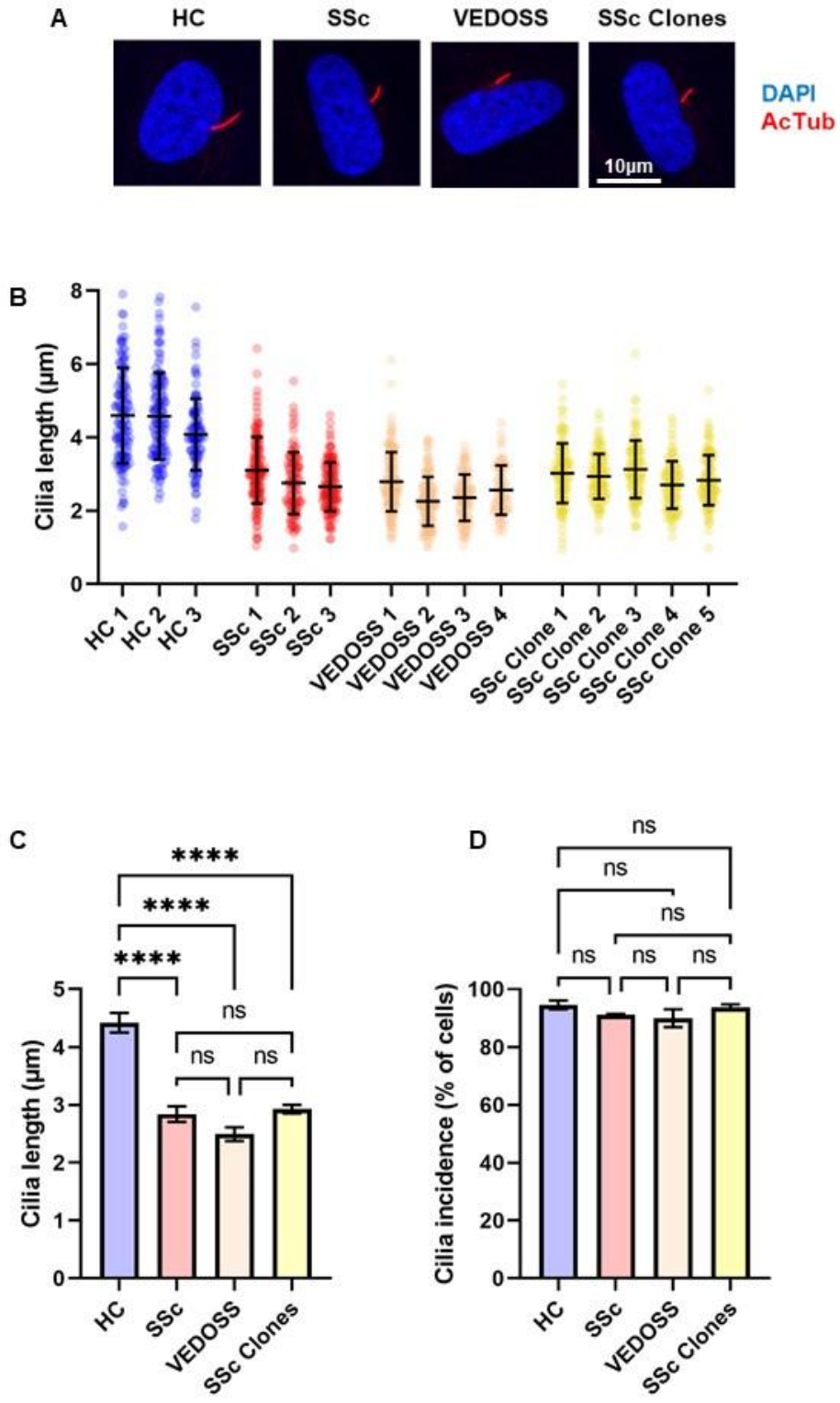
A
HC
SSc
VEDOSS
SSc Clones
DAPI
AcTub
10µm
B
Cilia length (µm)
HC 1
HC 2
HC 3
SSc 1
SSc 2
SSc 3
VEDOSS 1
VEDOSS 2
VEDOSS 3
VEDOSS 4
SSc Clone 1
SSc Clone 2
SSc Clone 3
SSc Clone 4
SSc Clone 5
C
Cilia length (µm)
****
****
****
ns
ns
ns
HC
SSc
VEDOSS
SSc Clones
D
Cilia incidence (% of cells)
ns
ns
ns
ns
ns
ns
HC
SSc
VEDOSS
SSc Clones

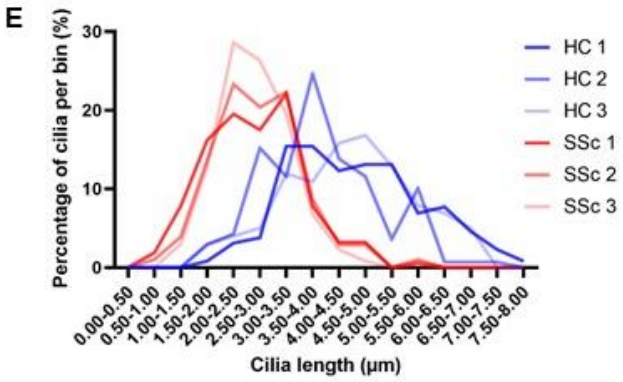

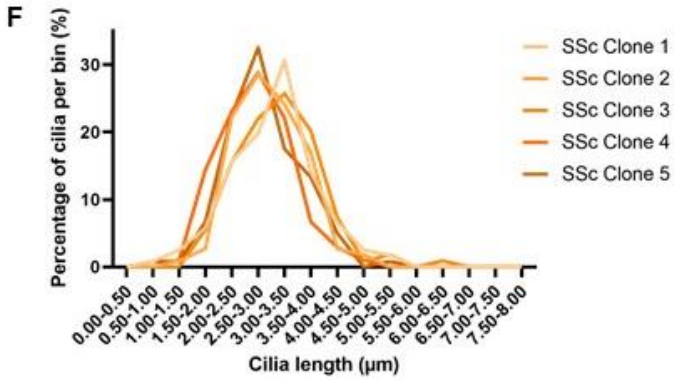

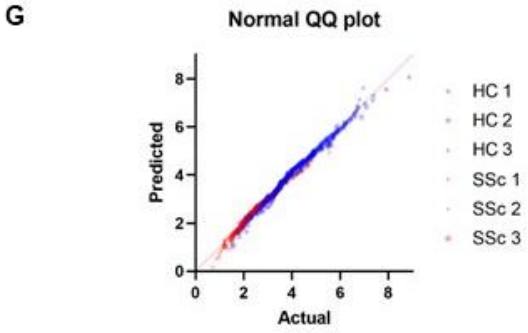

	HC 1	HC 2	HC 3	SSc 1	SSc 2	SSc 3
D'Agostino & Pearson test						
K2	4.205	3.145	1.784	3.517	5.881	2.567
P value	0.1221	0.2075	0.4099	0.1723	0.0528	0.2770
Passed normality test (alpha=0.05)?	Yes	Yes	Yes	Yes	Yes	Yes
P value summary	ns	ns	ns	ns	ns	ns

Figure 3.1: Primary cilia are shorter in dermal fibroblasts from SSc and VEDOSS patients compared to healthy controls

Confluent fibroblasts were cultured in 0.5 % serum media for 48 h, and cilia measured using immunofluorescence for Ac-α-Tub. A) Representative immunofluorescence images taken at 400 x magnification showing cilia (stained for Ac-α-Tub in red) of individual fibroblasts (DAPI nuclear staining in blue). Scale bar shown at 10 µm. B) Mean and standard deviation of cilia length in each of the

individual fibroblast lines. Each point represents a single cilium, with a minimum of 100 cilia measured per cell line, taken from a minimum of 3 independent fields of view. C) Mean cilia length observed in each group of (B). D) Mean cilia incidence, as the percentage of total fibroblasts that are ciliated in (C). HC and SSc n=3, VEDOSS n=4, SSc clones n=5. Error bars show standard error of the mean. P values were calculated by one-way ANOVA with Tukey's multiple comparisons test (****P<0.0001). E) Distribution of cilia length in each of the individual HC and SSc lines (n=3), showing the percentage of total cilia in each 0.5 μm length category. F) As for (E), but showing the distribution of cilia length in each of the SSc Clone lines. G) Normal QQ plot for the individual HC and SSc replicate lines, and results of the D'Agostino and Pearson test for normality.

Taken together, these data suggest that despite the existence of heterogeneous fibroblast subpopulations within the dermis, a shortened cilia phenotype may be a defining characteristic of all SSc dermal fibroblasts, regardless of subtype, appearing early in disease pathogenesis.

3.2.2 The difference in cilia length between SSc and healthy control fibroblasts is not a consequence of immortalisation nor serum starvation

The shorter cilia phenotype in SSc vs HC (Fig. 3.1) was observed in experiments carried out on hTERT fibroblasts, due to the ease of their maintenance and use for *in vitro* work compared to primary fibroblasts. These experiments were also carried out after 48 h of serum starvation in 0.5 % serum media at cell confluence, to induce growth arrest and cell cycle synchronisation at G0/G1 during which cells assemble a primary cilium, in order to facilitate experimental analysis of cilia length and incidence. In order to verify that experiments using immortalised serum-starved cells faithfully reflect cilia phenotype differences and that these experiments could be used for future

work, the cilia phenotype was compared in primary fibroblasts vs hTERT fibroblasts, and in hTERT fibroblasts cultured in 10 % serum vs 0.5 % serum (Fig. 3.2A), using immunofluorescence for Ac-α-Tub.

Cilia incidence was unaffected by hTERT-mediated immortalisation of HC and SSc fibroblasts and was similar in all tested conditions (Fig. 3.2B). As for cilia length, there was no significant difference in mean cilia length when comparing primary fibroblasts to hTERT, while the significant reduction in cilia length in SSc compared to HC was observed in both primary and hTERT fibroblasts ($p<0.0001$) (Fig. 3.2C).

Due to the intrinsic link between cilia and the cell cycle, in which ciliogenesis occurs during G0/G1 and cilia resorption occurs prior to cell division, asynchronous cell cycling means that fewer cells in a population will possess a fully established primary cilium, and will instead be either unciliated, or partway through either ciliogenesis or cilia resorption (Plotnikova et al., 2009). Therefore, as expected, cilia incidence in fibroblast populations that were asynchronous was significantly lower in both HC and SSc fibroblasts, when cultured in 10 % serum compared to 0.5 % serum ($p<0.05$). There was no difference in cilia incidence between HC and SSc in either serum percentage (Fig. 3.2D). Also as expected, mean cilia length was significantly lower in both HC ($p<0.001$) and SSc ($p<0.05$) when cultured in 10 % serum media compared to 0.5 % (Fig. 3.2E). Despite this, SSc cilia length was still significantly shorter than HC even when cells were cultured in 10 % serum ($p<0.05$) (Fig. 3.2E).

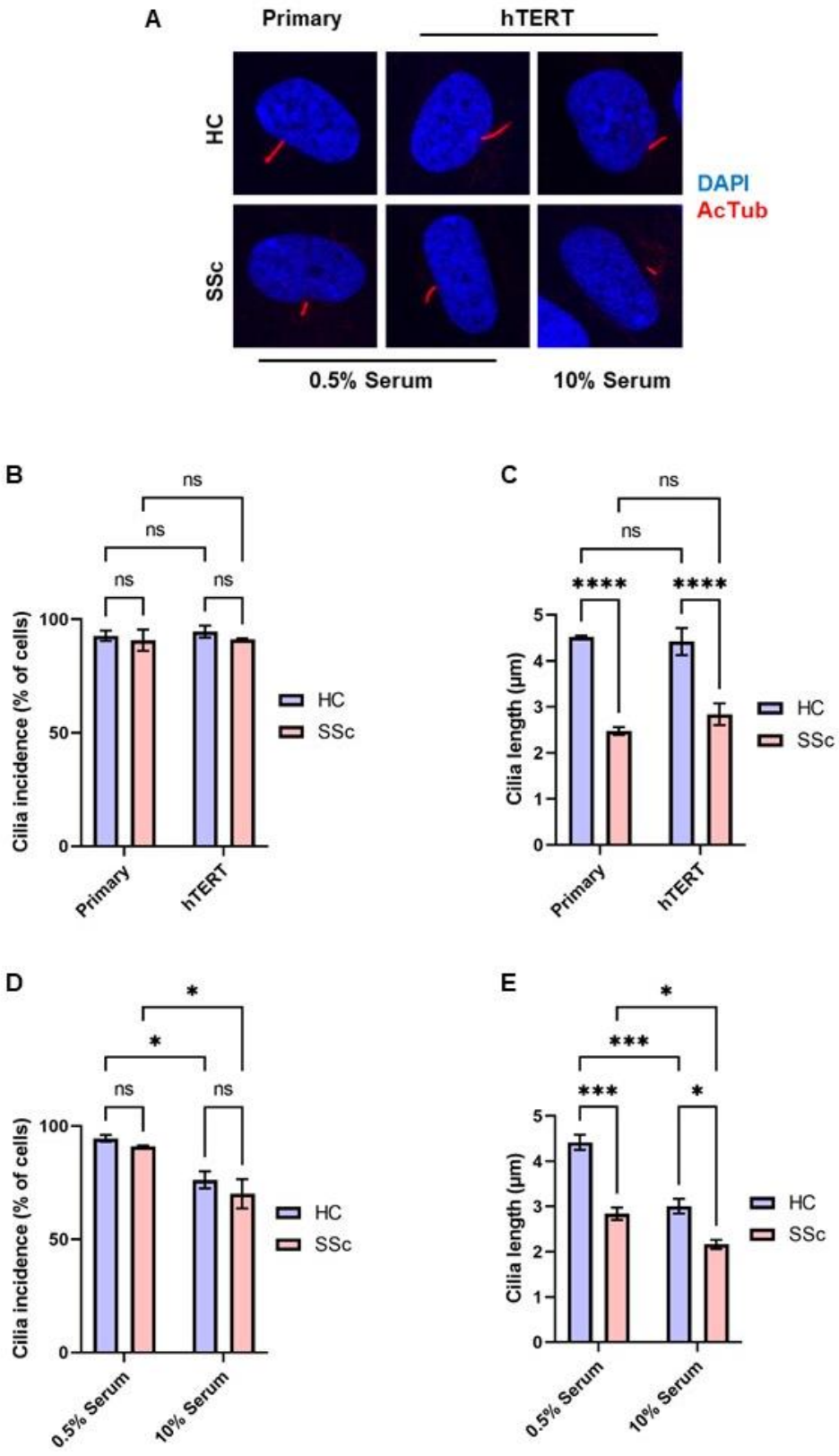

Figure 3.2: Differences in the cilia phenotype between SSc and healthy control fibroblast cilia are retained regardless of hTERT immortalisation or serum starvation

Confluent primary and hTERT fibroblasts were cultured in 0.5 % or 10 % serum media for 48 h. Cilia were measured using immunofluorescence for Ac-α-Tub in each

experimental condition. A) Representative immunofluorescence images taken at 400 x magnification showing cilia (stained for Ac-α-Tub in red) of individual fibroblasts (DAPI nuclear staining in blue) in each cell type and serum percentage. Scale bar shown at 10 μm. B) Cilia incidence in primary vs hTERT HC and SSc fibroblasts. C) Cilia length in primary vs hTERT HC and SSc fibroblasts. D) Cilia incidence in hTERT HC and SSc fibroblasts cultured in 0.5 % serum vs 10 % serum media. E) Cilia length in hTERT HC and SSc fibroblasts cultured in 0.5 % serum vs 10 % serum media. For all data shown, HC and SSc n=3, with bars showing the mean and error bars showing standard error of the mean. P values were calculated by two-way ANOVA with Tukey's multiple comparisons test (*P<0.05, ***P<0.001, ****P<0.0001).

From this data, it can be concluded that the shortened cilia phenotype found in hTERT SSc fibroblasts is not a consequence of hTERT immortalisation, and mirrors the phenotype of primary fibroblasts, justifying the use of hTERT fibroblast lines for this research. Additionally, the shortened cilia phenotype seen in SSc is evident regardless of serum starvation, although more obvious in starved conditions. This justified the use of serum starvation for this research, in order to better examine the cilia phenotype in a population of fibroblasts that are expressing a mature primary cilium.

3.2.3 TGFβ shortens primary cilia and reduces cilia incidence in all fibroblast lines

In order to investigate the effect of TGFβ on the cilia phenotype, fibroblasts were treated with TGFβ for 24 h and cilia examined by immunofluorescence (Fig. 3.3A). Both primary and hTERT immortalised HC and SSc fibroblasts were included in the analysis in order to determine if any effect of TGFβ on cilia was affected by immortalisation. TGFβ treatment caused a small but significant reduction in the incidence of ciliated cells in all lines ($p<0.05$ for all except SSc

hTERT at p<0.01) (Fig. 3.3B). TGFβ treatment also significantly shortened cilia in all lines (p<0.0001) (Fig. 3.3C). Cilia length was reduced from 4.5±0.02 μm to 1.9±0.01 μm in HC primary, 4.2±0.1 μm to 1.6±0.02 μm in HC hTERT, 2.5±0.05 μm to 1.8±0.08 μm in SSc primary, from 2.6±0.07 μm to 1.6±0.1 μm in SSc hTERT, and from 2.4±0.1 μm to 1.6±0.07 μm in VEDOSS. None of the post-TGFβ treatment lengths were significantly different from each other between any cell lines (Fig. 3.3C). The effect of TGFβ on cilia incidence and length was determined not to be affected by fibroblast immortalisation, as significant reductions in both parameters were observed regardless of whether cells were primary or immortalised (Fig. 3.3B, C), justifying the continued use of hTERT immortalised fibroblasts in work further exploring this phenotype.

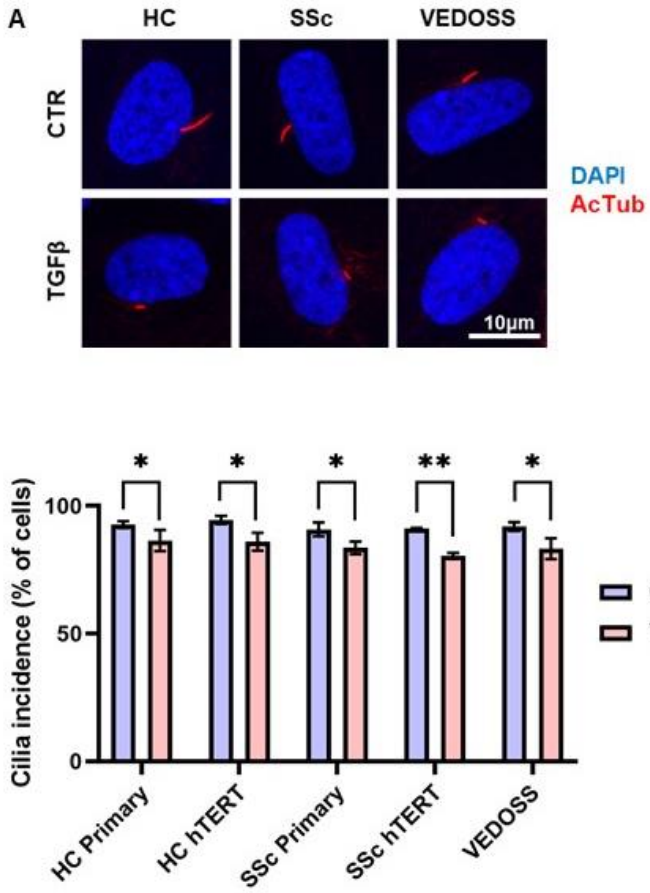

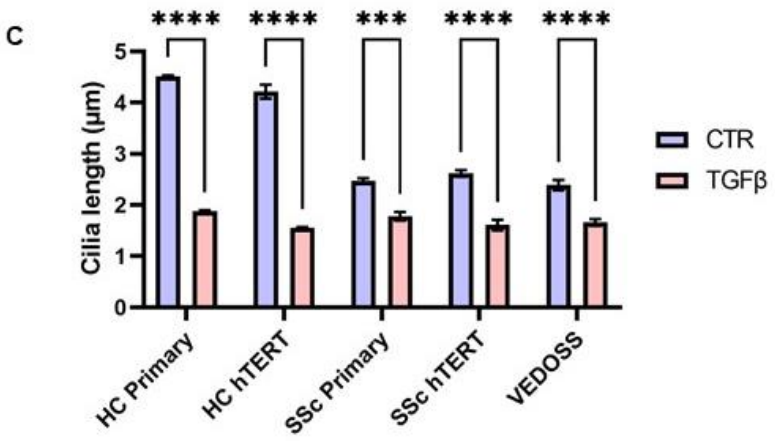

Figure 3.3: TGFβ decreases primary cilia incidence and length
Confluent primary HC and SSc, hTERT HC and SSc, and primary VEDOSS fibroblasts were cultured in 0.5 % serum media for 24 h, followed by 24 h in the presence or absence of 10 ng/mL TGFβ. Cilia were measured using immunofluorescence for Ac-α-Tub. A) Representative immunofluorescence images taken at 400 x magnification showing cilia (stained for Ac-α-Tub in red) of individual fibroblasts (DAPI nuclear staining in blue) with and without TGFβ. Scale bar shown at 10 µm. B) Cilia incidence changes in each cell type with and without TGFβ. C) Cilia length changes in each cell type with and without TGFβ. For all data shown, primary and hTERT HC and SSc n=3, VEDOSS n=4. Bars show the mean and error bars show standard error of the mean. P values were calculated by two-way ANOVA with Tukey's multiple comparisons test (*P<0.05, **P<0.01, ***P<0.001, ****P<0.0001).

These data show that TGFβ is able to reduce both cilia incidence and length in all dermal fibroblasts analysed, regardless of cell line origin. Interestingly, cilia length was reduced to a similar final length in all fibroblast lines.

3.2.4 TGFβ shortens the established primary cilium present during growth arrest, rather than inducing cell cycle-linked ciliary resorption

Cells possess fully established mature primary cilia only during growth arrest, in the G0/G1 phase of the cell cycle. When cells proliferate and enter S phase, ciliary disassembly is initiated, and the cilium is completely lost during G2 and M

phases when the basal body duplicates to form two centrioles for formation of the mitotic spindle (Fabbri et al., 2019) (Fig. 3.4A). TGFβ is known to be able to induce fibroblast proliferation. Our data showing that TGFβ treatment reduces the incidence and length of primary cilia (Fig.3.3) were obtained from fibroblasts that were serum starved (cultured in 0.5 % serum media) in order to synchronise the cell cycle of all cells in the population at interphase, as previously discussed, but it is a possibility that the addition of TGFβ could cause cells to re-enter the cell cycle. It was therefore pertinent to this study to determine whether the effects of TGFβ on cilia incidence and length observed previously were due to the potential proliferative effect of TGFβ inducing cell-cycle linked ciliary disassembly, or if TGFβ is able to alter the phenotype of fully established mature primary cilia, without inducing proliferation.

In order to do this, cellular proliferation was investigated by immunofluorescence for Ki67. Ki67 is a cellular proliferation marker which is not expressed during quiescence (G0) but is upregulated during the active phases of the cell cycle (G1, S, G2, and M) (Fig. 3.4A), enabling experimental determination of the proportion of cells in the active phases. This was done by counting the number of cells that were positive for Ki67 expression, and comparing to the total number of cells based on DAPI staining. Fibroblasts were cultured using the same experimental parameters as the experiments presented in Fig. 3.3 with 0.5 % serum media and TGFβ at 10 ng/mL, in order to determine whether this concentration of TGFβ could ‘override’ the cell cycle synchronisation effect of serum starvation and induce proliferation. For comparison, fibroblasts cultured in 10 % serum media, which facilitates normal and asynchronous cell cycling in a population, and in which we would expect to

see a higher proportion of cells in the active phases of the cell cycle, were included in the analysis.

In fibroblasts cultured in 10 % serum media, 23.2 % of cells imaged were Ki67-positive, whereas as expected far fewer (2.1 %) were Ki67-positive in 0.5 % serum media (Fig. 3.4B). TGFβ treatment in 10 % serum media increased the proportion of Ki67-positive cells to 29.8 % ($p<0.01$) (Fig. 3.4B), suggesting that TGFβ is able to promote cellular proliferation in this condition. However, this effect was not observed in serum starved conditions, where the proportion of Ki67-positive cells after TGFβ treatment at 10ng/mL was 1.7 % vs 2.1 % in control fibroblasts (Fig. 3.4B). This indicates that in serum starved conditions, TGFβ at the chosen experimental concentration is not able to induce proliferation, confirming that 10 ng/mL TGFβ can be used in further experiments to explore its effect on the mature primary cilium.

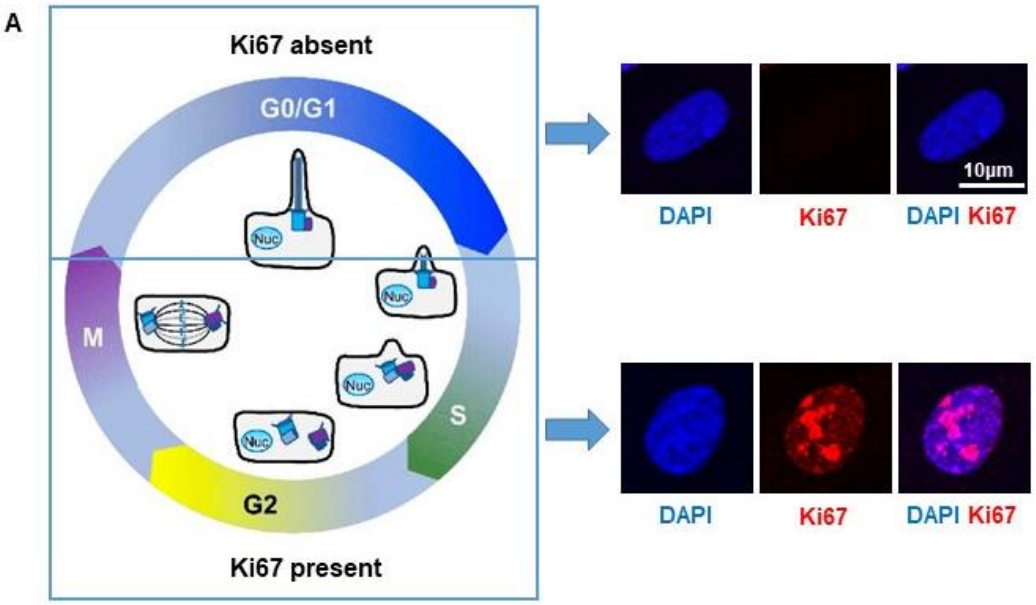

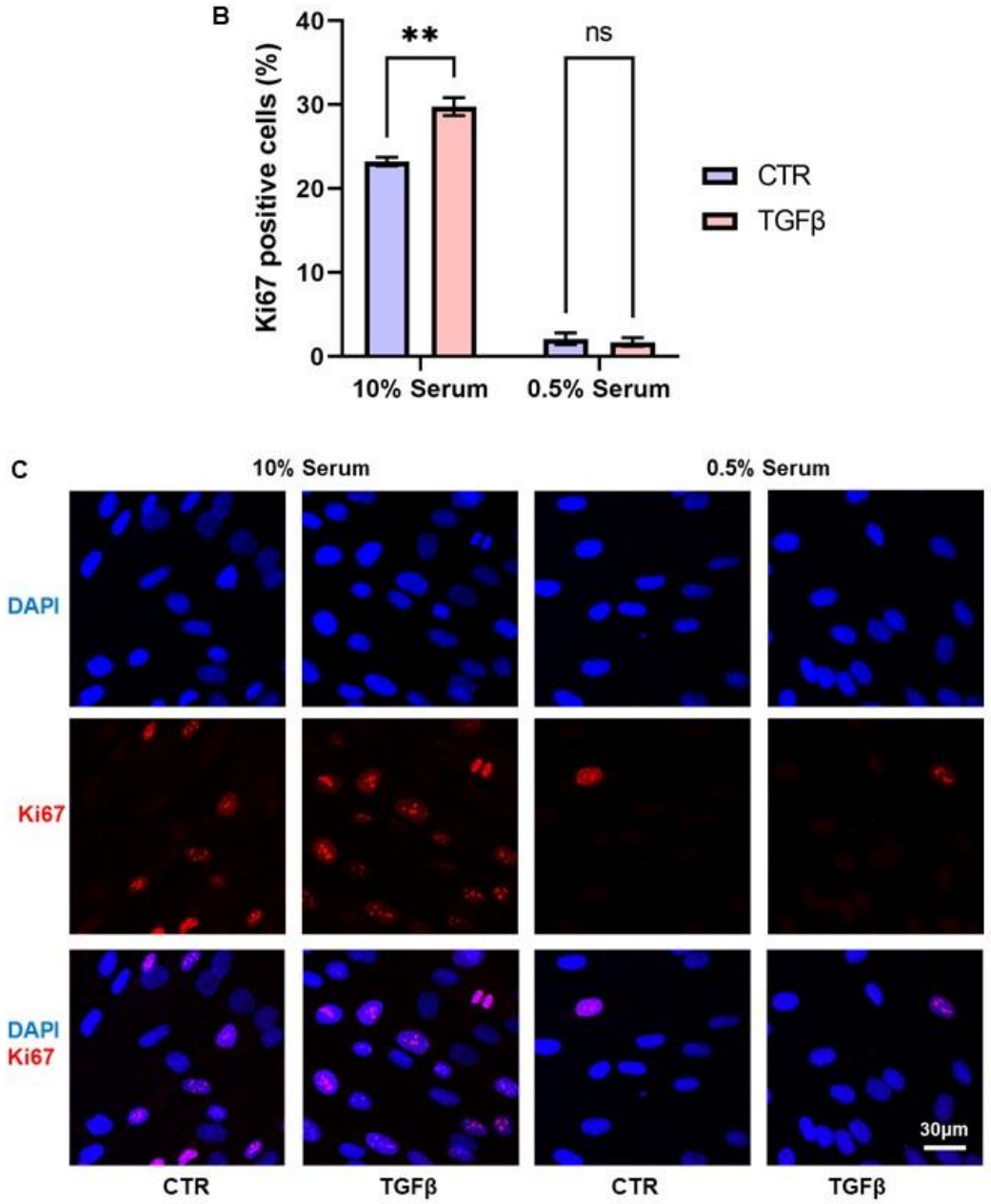

Figure 3.4: TGFβ treatment under chosen experimental conditions does not affect cell cycle progression

Confluent healthy dermal fibroblasts were cultured in either 10 % or 0.5 % serum media for 24 h, followed by 24 h with or without 10 ng/mL TGFβ. The percentage of cells expressing Ki67 was measured by immunofluorescence, measuring a minimum of 100 cells per experimental condition. A) Cell cycle schematic (adapted from Fabbri et al., 2019) showing the link between ciliogenesis, cilia resorption, and the cell cycle. Schematic also shows the presence and absence of Ki67 expression at different stages of the cell cycle, with representative immunofluorescence images of the appearances of each of those states in individual fibroblast nuclei (DAPI nuclear staining in blue, Ki67 stained in red). Scale bar shown at 10 μm. B) Percentage of total cells that were Ki67 positive in each condition, quantified by manual counting of

the number of Ki67 positive cells against the total number of cells. N=3 for each condition. Bars show the mean and error bars show standard error of the mean. P values were calculated by two-way ANOVA with Tukey's multiple comparisons test (**P<0.01). C) Representative immunofluorescence images taken at 200 x magnification showing Ki67 expression (stained in red) of individual fibroblasts (DAPI nuclear staining in blue) with and without TGFβ at the two serum percentages. Scale bar shown at 30 μm.

Taken together, these data suggest that the observed effect of TGFβ on the cilia phenotype is not a consequence of ciliary resorption caused by re-entry into the cell cycle, but that TGFβ is able to affect the established primary cilium present during growth arrest.

3.2.5 SSc cilia are primed for TGFβ-induced shortening

After 24 h treatment with TGFβ, cilia incidence and length were reduced in both HC and SSc dermal fibroblasts, with length reduced to a similar length in all fibroblast lines (Fig. 3.3). In order to investigate the kinetics of TGFβ-induced ciliary shortening in HC and SSc dermal fibroblasts, TGFβ time course experiments were conducted over a 24 h period. Cilia were measured using immunofluorescence for Ac-α-Tub. Protein was also harvested at each time point, and the levels of pSMAD3, total SMAD3, and αSMA were assessed by Western Blotting (Fig 3.5A), as a positive control to confirm a TGFβ response. Indeed, as expected, there was a sharp initial increase in pSMAD3 levels relative to total SMAD3 at 2 h post-TGFβ, followed by a gradual increase up to 24 h (Fig. 3.5A, B), and an induction of αSMA expression evident by 18 h and 24 h post-TGFβ (Fig. 3.5A, C).

In both HC and SSc fibroblasts, TGFβ treatment significantly reduced cilia incidence by the 18 h time point ($p<0.05$ for both) (Fig. 3.5D). TGFβ treatment shortened cilia in both HC and SSc gradually over the time course but, notably, ciliary shortening occurred as early as 4 h in SSc fibroblasts ($p<0.01$), compared to 18 h of TGFβ treatment in HC cells ($p<0.0001$) (Fig. 3.5E).

It is interesting to note that the abundance of phosphorylated SMAD3 relative to total SMAD3 over the TGFβ time course follows a similar pattern in both HC and SSc, with a sharp increase at 2 h followed by similar fluctuations between 2 h-4 h and 4 h-6 h, and higher levels by 18 h and 24 h (Fig. 3.5B). This does not align with the difference in the temporal response of cilium length between SSc and HC, with SSc cilia shortening reaching statistical significance at 4 h vs 18 h in HC (Fig. 3.5E). This could suggest that TGFβ-induced cilia shortening might not be a canonical TGFβ response dependent on SMAD3 phosphorylation.

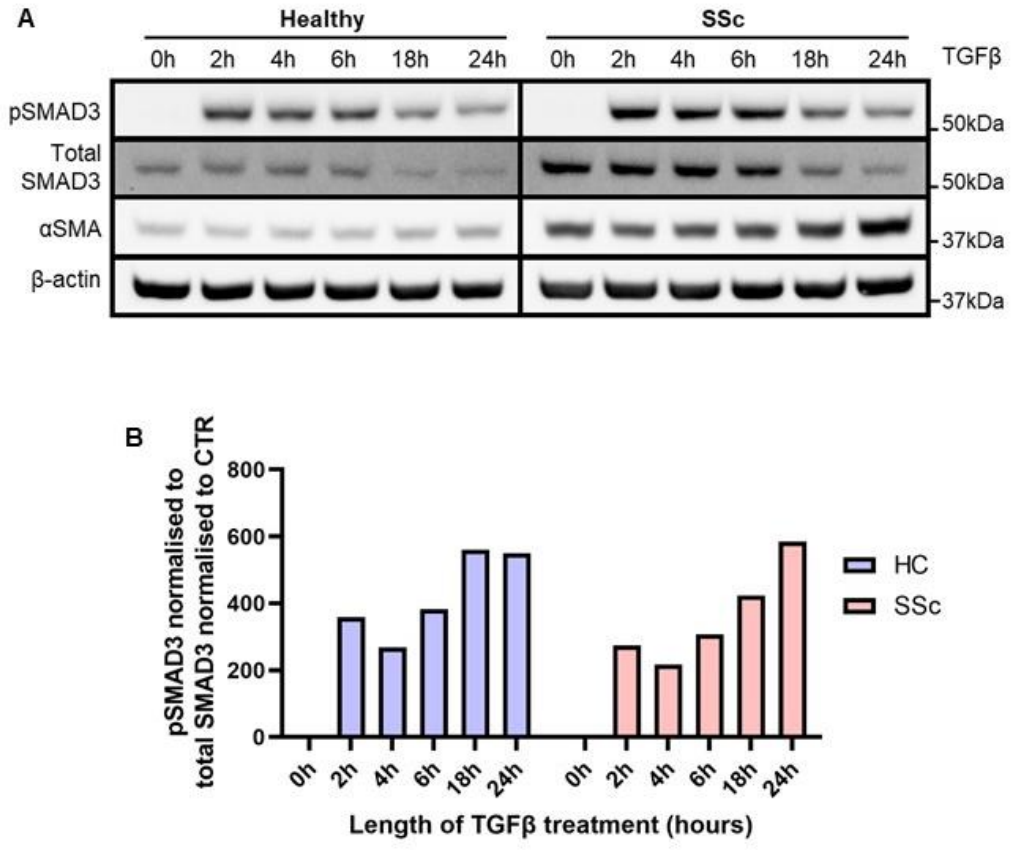

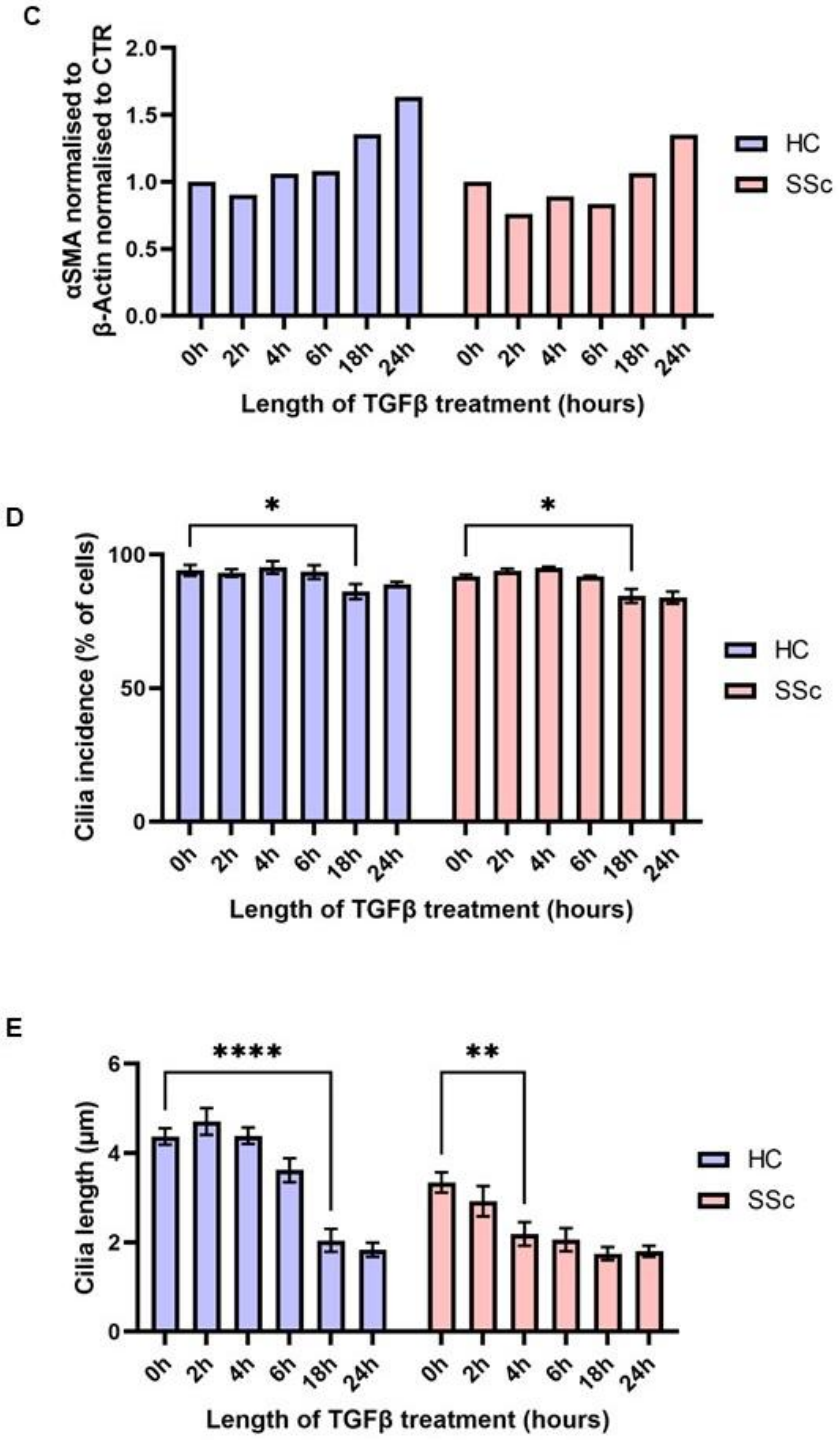

Figure 3.5: Temporal analysis of the response to TGFβ in healthy vs SSc fibroblasts shows SSc cilia are primed for TGFβ-induced shortening

Confluent HC and SSc fibroblasts were cultured in 0.5 % serum media for a total of 48 h, with 10 ng/mL TGFβ added for indicated periods of time before cilia measurement using immunofluorescence for Ac-α-Tub, and protein harvest for quantification by Western Blot. A) Western Blots showing response to TGFβ over time, determined by activation of pSMAD3 and αSMA induction. β-Actin included as a loading control. B) pSMAD3/total SMAD3 densitometry of (A). C) αSMA

densitometry of (A). For protein data, HC and SSc n=1. D) Time course reduction of cilia incidence in response to TGFβ. E) Length of cilia observed in (D). For cilia data, HC and SSc n=3. Bars show the mean and error bars show standard error of the mean. P values were calculated by two-way ANOVA with Dunnet's multiple comparisons test (*P<0.05, **P<0.01, ****P<0.0001).

Taken together, these data suggest that although TGFβ shortens cilia in dermal fibroblasts in both SSc and HC fibroblasts to a similar final length, SSc fibroblasts behave as if they are 'primed' for TGFβ-induced ciliary shortening, as cilia length reduction is initiated more quickly following stimulation compared to HC.

3.2.6 The effect of TGFβ on cilia length is lost after cells re-enter the cell cycle

In order to investigate the stability of the TGFβ-induced cilia phenotype in fibroblasts, cilia were examined after 24 h of TGFβ treatment followed by either media change to eliminate TGFβ from culture medium (Fig. 3.6A), or by passaging cells in regular growth medium to resume cell cycling (Fig. 3.6D).

After TGFβ is removed from culture medium (Fig. 3.6A), the TGFβ-induced reduced cilia incidence phenotype (Fig. 3.6B) and shortened cilia phenotype (Fig. 3.6C) both persist. There was no significant difference in cilia incidence or length regardless of whether cilia were measured immediately after 24 h of TGFβ treatment and 24 h or 48 h post-removal of TGFβ, in neither HC nor SSc fibroblasts.

However, when cells are allowed to resume the cell cycle by a return to 10 % serum media and two passages following TGFβ treatment (Fig. 3.6D), both the

TGFβ-induced reduced cilia incidence phenotype (Fig. 3.6E) and the shortened cilia phenotype (Fig. 3.6F) are lost, with no significant difference between these fibroblasts and their respective controls which were never exposed to TGFβ stimulation. This is true in both HC and SSc fibroblasts.

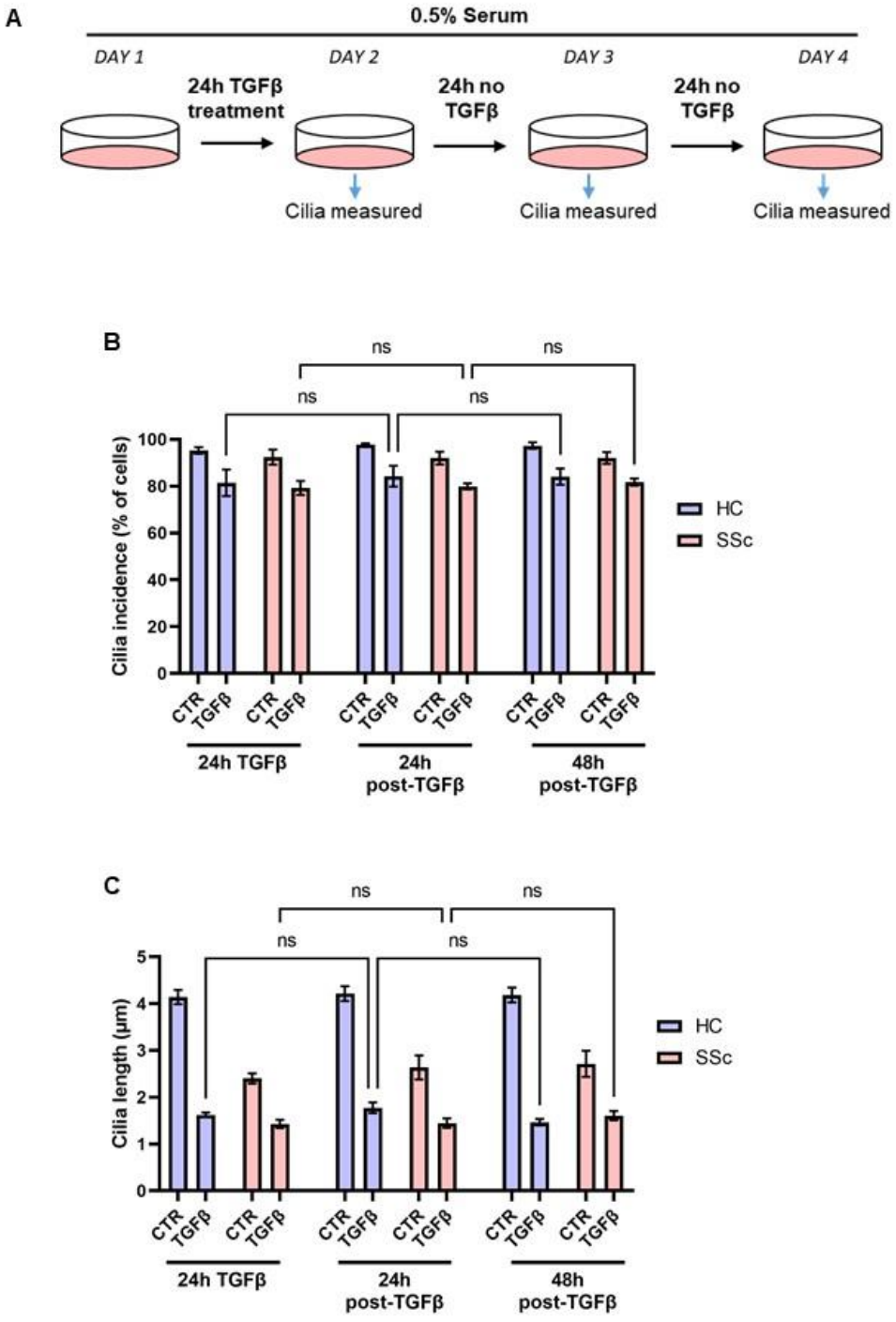

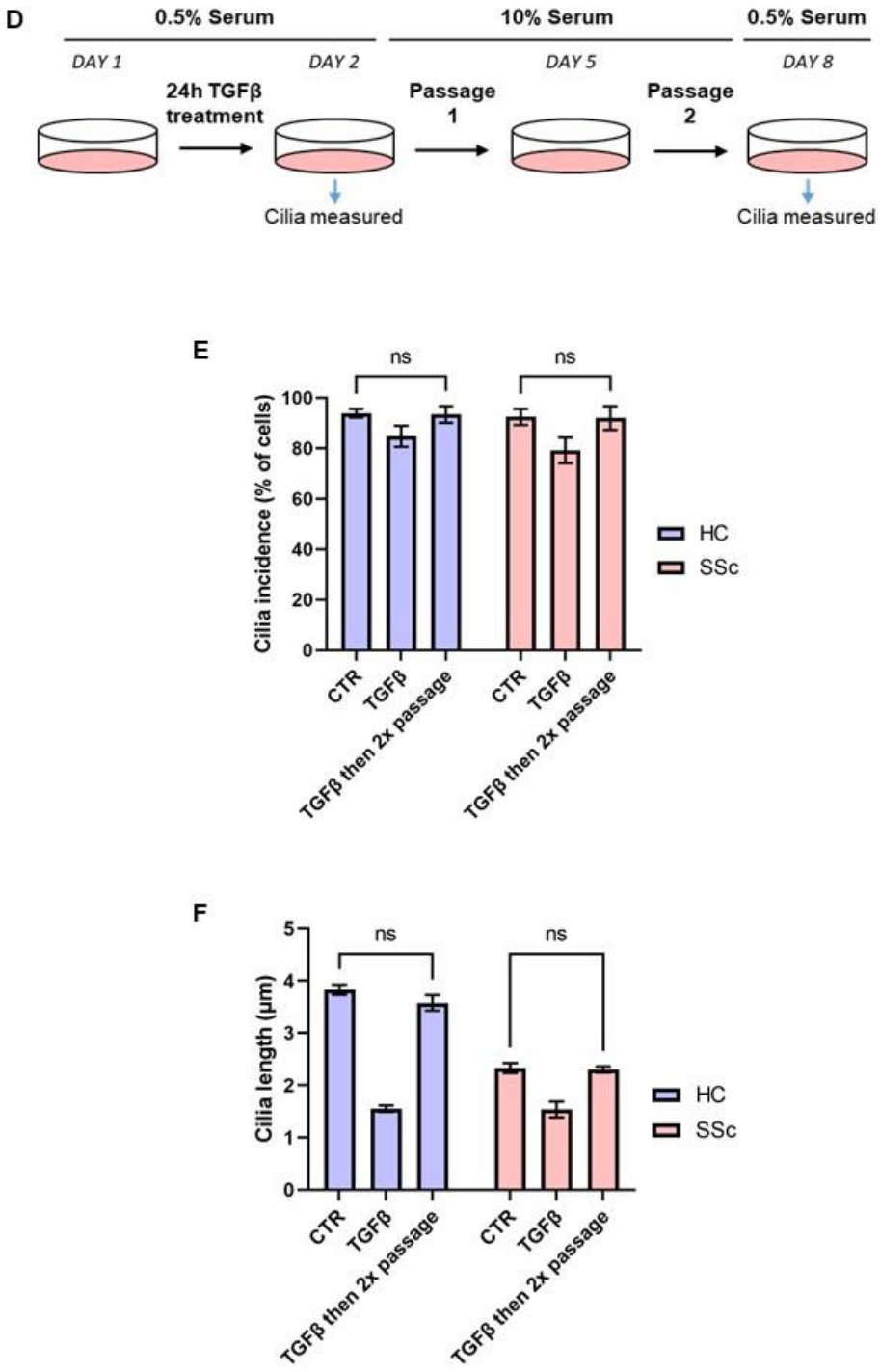

Figure 3.6: The TGFβ-induced shorter cilia phenotype is only partially stable and is lost upon cell cycle re-entry

Confluent HC and SSc fibroblasts were cultured in 0.5 % serum media for 24 h followed by 24 h treatment with 10 ng/mL TGFβ in 0.5 % serum media. Cells were then either returned to 0.5 % serum media with no TGFβ for a further 24 h or 48 h, or they were returned to 10 % serum media and passaged twice over the following 6 days. Cilia were measured by immunofluorescence for Ac-α-Tub in each experimental condition. A) Experimental schematic demonstrating that cells were

treated with TGFβ, then TGFβ removed from culture medium for 24 h or 48 h. 0.5 % serum starvation was maintained throughout this experiment. B) Cilia incidence changes after treatment with TGFβ followed by removal of TGFβ. C) Cilia length changes after treatment with TGFβ followed by removal of TGFβ. D) Experimental schematic demonstrating that cells were treated with TGFβ in 0.5 % serum starvation, then returned to regular cell cycling in 10 % serum media with no additional TGFβ, before an additional 24 h of starvation to induce ciliogenesis before cilia measurement. E) Cilia incidence changes after treatment with TGFβ followed by return to cell cycle. F) Cilia length changes after treatment with TGFβ followed by return to the cell cycle. HC and SSc n=3. Bars show the mean and error bars show standard error of the mean. P values were calculated by two-way ANOVA with Tukey's multiple comparisons test (ns = non-significant).

These data suggest that as long as fibroblasts remain in growth arrest, a single 'hit' of TGFβ stimulation is sufficient to trigger a decrease in both cilia incidence and length that remains stable even once the TGFβ ligand is no longer physically present. However, the effect is transient in cells that undergo proliferation, and it can be inferred that no long-term epigenetic changes passed to daughter cells that affect the cilia phenotype are induced by TGFβ.

3.3 Discussion

This study found that primary cilia are shorter in SSc dermal fibroblasts than HC dermal fibroblasts, a characteristic that was observable even in VEDOSS fibroblasts. This suggests a potential association between ciliary shortening and the pathogenesis of the disease possibly from its onset, prior to clinically detectable fibrosis. While an extensive body of research, reviewed in the introduction to this thesis, suggests a link between aberrant primary cilia and various fibrotic diseases, collaboration between our group and other researchers has now produced the first manuscript to show that shortened

primary cilia are characteristic of not only SSc fibroblasts, but also of fibroblasts in two other diseases with characteristic fibrosis: idiopathic pulmonary fibrosis (IPF) and thyroid-associated ophthalmopathy (TAO) (Verma et al., 2024). This supports the hypothesis that the primary cilium should be considered as an organelle which may play a key role in the cellular mechanisms which drive fibrotic activation regardless of disease context, and one for which further research is certainly warranted to elucidate the cellular and molecular mechanisms underpinning fibrosis further. This growing evidence also warrants consideration of the primary cilium as a potential therapeutic target for disease intervention, both in SSc and in other fibrotic diseases.

The observation that shortened primary cilia were present in all SSc single-cell derived clonal fibroblast lines analysed also provides a notable insight into the phenotype. Single cell studies revealing the extent of dermal fibroblast heterogeneity within the skin have highlighted the diversity of fibroblast subsets, proposed to play differing roles in tissue homeostasis (Tabib et al., 2018, Philippeos et al., 2018). Indeed, in explanted SSc dermal fibroblasts, marked variability in expression levels of markers such as αSMA between individual cells has been demonstrated, and single cell studies have confirmed distinct subpopulations of dermal fibroblasts in SSc patient skin (Wasson, Abignano, et al., 2020, Zhu et al., 2024). In accordance with this, the clonal lines used in this study were isolated from one patient biopsy but show notable differences in gene and protein expression profiles, and functional characteristics (data not shown). Despite this, all clonal lines were found to possess shortened primary cilium of a very similar length, suggesting that a shortened primary cilium may be characteristic of all SSc dermal fibroblasts regardless of subset, and may therefore be intrinsically linked with pathogenesis of the disease.

The discrepancy in cilium length between HC and SSc fibroblasts in this study was mostly examined in hTERT immortalised dermal fibroblast lines, but was also found in primary fibroblast lines, which adds strength to the validity of the observation. Additionally, despite most of the work in this study being carried out in serum starved cells to facilitate ciliary examination, the finding was also validated in cells grown in full serum culture media, which suggests that the observation is not simply a consequence of experimental parameters. However, it is important to note that all work in this study was carried out *in vitro* in cultured cells. Despite cultured cells providing a commonly used, simple, and accessible system in which to study primary cilia, it would be interesting to also examine primary cilia length and morphology in the context of the skin itself. Cilia can be examined using immunofluorescence in fixed and embedded tissue sections, a technique which could be applied to SSc patient skin sections in order to observe primary cilia *in situ* (Deane et al., 2013). While visualisation of primary cilia *in vivo* is challenging, the development of novel imaging techniques such as a window chamber-based methodology developed and utilised recently to observe cilia in live mouse kidneys could facilitate *in vivo* characterisation of cilia in animal models of SSc (Revell & Yoder, 2019).

While this study focussed on the skin, all of these techniques could also be applied to cells or tissues from other organs which also develop fibrosis during SSc pathogenesis, such as the lungs, kidneys, and gastrointestinal tract. This would provide interesting insight into the role of the primary cilium in fibrosis in diverse organ contexts.

It is also important to note that cultured fibroblasts used in this study were initially isolated using standard explant culture of skin biopsies. Recent work has highlighted that this method favours the isolation of ‘migratory’ fibroblast

populations, while ‘resident’ fibroblasts require additional collagenase digestion to be extracted from biopsies (Clark et al., 2023). Clark et al. suggest that these two populations of SSc fibroblasts have distinct phenotypes with differential gene expression patterns and functional behaviours, and hypothesise that they may contribute to disease pathogenesis in different ways. Therefore, it would be pertinent to apply the same ‘resident’ fibroblast extraction methodology to SSc skin biopsies and examine the primary cilia to ascertain whether a shortened primary cilium is characteristic of both ‘migratory’ and ‘resident’ fibroblast populations.

Changes to primary ciliary length alone, in the absence of aberrations to its ultrastructure, have been reported to be able to modify its ability to sense and coordinate extracellular signals, altering ciliary function (Macarelli et al., 2023). Therefore, it could be proposed that the discrepancy in primary cilium length between HC and SSc observed in this study could be sufficient to contribute to the dysregulated signalling coordination and subsequent fibrotic activation characteristic of SSc. However, it would be interesting to assess the ultrastructure of SSc primary cilia to see if their shorter length correlates with any structural defects in ciliary organisation, for example at the ciliary gate region at the base of the cilium, or whether they are defective in length only. The ciliary gate plays key roles in proper ciliary function (Garcia-Gonzalo & Reiter, 2017). Electron microscopy (EM) and super-resolution microscopy provide high resolution methods for visualisation of ciliary ultrastructure. These techniques have even been elegantly combined, by overlapping coordinate-defined super-resolution images and EM images of the ciliary gate region (Yang et al., 2015). Such methodology could be employed to assess the structural integrity of shortened SSc primary cilia at high resolution.

High resolution microscopy could also be used to investigate the localisation of signalling pathway components in shortened SSc primary cilia. The primary cilium is able to contribute to the coordination of a number of signalling pathways due to specific spatio-temporal mechanisms of signal detection and transduction, during which pathway components localise to specific regions of the ciliary membrane and cilioplasm (Anvarian et al., 2019). Therefore, immunofluorescence experiments to assess any discrepancies in spatio-temporal localisation of signalling components upon pathway stimulation between HC and SSc fibroblast cilia could further our understanding of the specific mechanisms by which shortened SSc cilia may contribute to the dysregulated signalling observed in the disease.

While TGFβ-induced ciliary shortening has been previously demonstrated in various cell types including chondrocytes (Kawasaki et al., 2015), osteoblasts (Ehnert et al., 2017), adipocyte progenitors from adipose tissue and skeletal muscle (Arrighi et al., 2017), tenocytes (Rowson et al., 2018), and MDCK cells (Han et al., 2018), this study is the first to confirm that the effect is also observed in dermal fibroblasts, with cilia shortening to a similar final length in all fibroblasts analysed regardless of disease state. Importantly, experimental analysis of cell cycle progression confirmed that TGFβ acts to alter the length of the established and mature post-mitotic primary cilium, rather than the effect being a consequence of cell-cycle linked ciliary resorption.

Interestingly, SSc primary cilia were ‘primed’ to TGFβ-induced shortening compared to HC in time course experiments. This aligns with the previously described notion that SSc fibroblasts may be hyper-responsive to TGFβ signalling (Asano et al., 2004, Asano et al., 2011, Lu et al., 2017, Lomelí-Nieto et al., 2022). It would be interesting to assess if the shortened primary cilia

found on SSc fibroblasts may contribute to this phenomenon, as TGFβ signalling is known to be coordinated at the primary cilium (Clement et al., 2013, Mönnich et al., 2018, Koefoed et al., 2018). It is clear that TGFβ signalling leads to ciliary shortening, but could this mechanism also exist in reverse, with shorter cilia leading to an increase in TGFβ signalling? Indeed, it has been hypothesised that normally functioning and normal length cilia may exhibit a 'dampening' effect on certain signalling pathways (Truong et al., 2021), and thus it could be hypothesised that shortened primary cilia could be defective in this ability in its regulation of TGFβ signalling. Comparative investigation of the spatio-temporal dynamics of ciliary TGFβ pathway coordination in healthy and SSc primary cilia could also shed light on this hypothesis. For example, TGFβ stimulation immediately followed by live imaging of fluorescently labelled TGFβ receptor has been successful in visualising intracellular dynamics downstream of TGFβ (He et al., 2015), and a similar method could be employed to see if the ligand-receptor complex is perhaps internalised at a different speed, or is less or more susceptible to degradation at the SSc primary cilium. Or, any aberrations to the normal localisation of the TGFβ receptor at the ciliary tip (Clement et al., 2013) could be investigated using super-resolution microscopy.

One initial hypothesis of this work was that TGFβ-induced ciliary shortening could be the reason for the shorter cilia of SSc dermal fibroblasts, due to the heightened TGFβ pathway activation characteristic of the disease (Varga & Abraham, 2007, Ayers et al., 2018). However, this study showed that while fibroblast cilia remain shortened after TGFβ ligand is removed from experimental culture medium, the phenotype is lost after cells re-enter the cell cycle. This provides evidence against this hypothesis, as the shortening effect of TGFβ on primary cilia appears not to be a stable phenotype, suggesting that

SSc fibroblasts may possess shortened primary cilia via a TGFβ-independent mechanism. It would, however, be interesting to stimulate a population of actively cycling fibroblasts with TGFβ for longer durations than the 24 h time point used in this study, in order to fully rule out the notion that TGFβ is able to induce any stable ciliary re-programming.

3.4 Summary

SSc dermal fibroblasts show shortened primary cilia compared to HC *in vitro*. This observation is consistent even at the VEDOSS stage of disease, before clinically detectable fibrosis, suggesting that cilium shortening may be linked to the onset of disease. Activation of the TGFβ signalling pathway shortens the established cilium, present during growth arrest, of dermal fibroblasts. SSc fibroblasts appear to be ‘primed’ for TGFβ-induced ciliary shortening compared to HC. However, the TGFβ-induced shortened cilia phenotype is only partially stable, suggesting that the stable shorter cilia phenotype observed in SSc may be independent of TGFβ signalling.

Chapter 4. Investigation of the mechanism of TGFβ-induced cilia shortening, and its role in the cilia phenotype of Systemic Sclerosis

4.1 Introduction

The experimental results discussed so far showed that SSc dermal fibroblasts have shorter primary cilia compared to HC. They also showed that in dermal fibroblasts, activation of the TGFβ signalling pathway leads to a partially stably induced reduction in the incidence and length of mature primary cilia, in a response that SSc fibroblasts appear primed to in comparison to HC. Therefore, we next decided to address the two following research aims. Firstly, to examine the specific downstream mechanism by which TGFβ pathway activation alters the ciliary phenotype in dermal fibroblasts. And secondly, to continue to examine the hypothesis that endogenous TGFβ signalling pathway activation and the activities of its downstream effectors in SSc could be the reason that SSc fibroblasts have shorter primary cilia than HC.

4.2 Results

4.2.1 Inhibition of the TGFβ signalling cascade does not rescue SSc cilia length

To begin to investigate these research questions, the entire TGFβ signalling pathway was blocked by inhibition of TGFβRI with small molecule inhibitor SD208 (Uhl et al., 2004) (Fig. 4.1A). Treatment with TGFβ for 24 h led to an increase in phosphorylation of SMAD3 and increased αSMA levels, which was

lessened when cells were treated with SD208 in combination with TGFβ, confirming the action of the inhibitor in blocking the activation of TGFβRI (Fig. 4.1B-D).

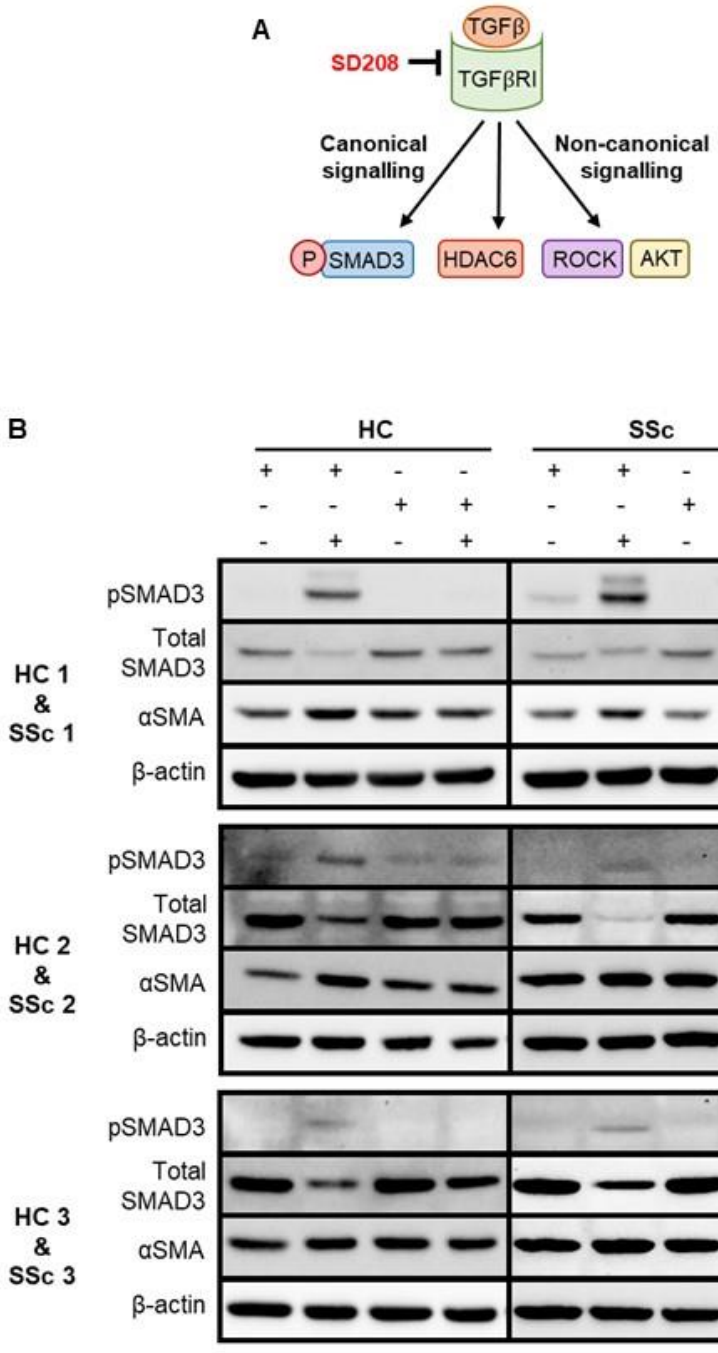

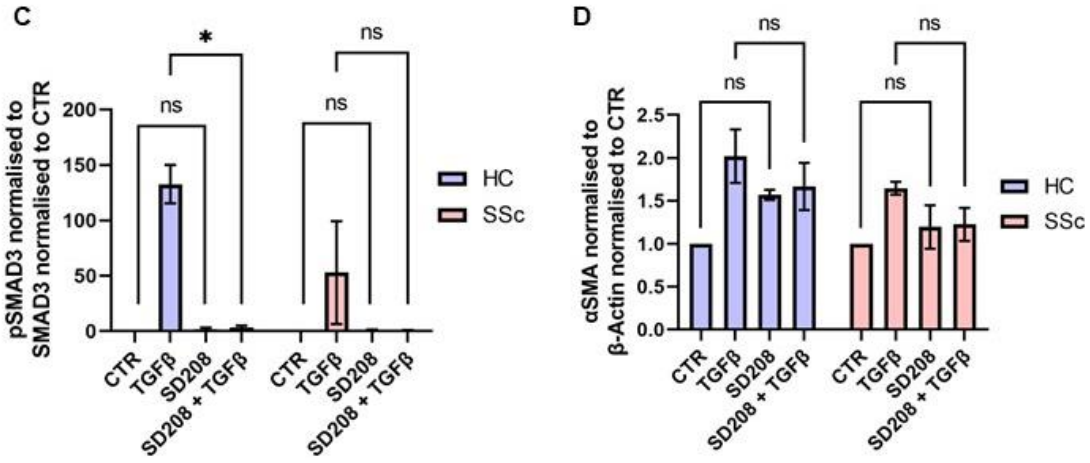

Figure 4.1: Blockade of TGFβRI activity using inhibitor SD208 reduces activation of the TGFβ pathway

Confluent HC and SSc fibroblasts were cultured in 0.5 % serum media for 24 h followed by 24 h treatment with 10 ng/mL TGFβ and/or 1 μM SD208 or DMSO control in 0.5 % serum media. Protein was harvested for quantification by Western Blot to validate inhibitor activity. A) Schematic showing the components of the TGFβ signalling pathway relevant to this study, and the inhibition of TGFβRI by SD208. B) Western Blots showing pSMAD3, total SMAD3, and αSMA protein expression in response to treatments comprising of TGFβ and/or SD208 or DMSO control in three HC donor and three SSc donor fibroblast lines. β-Actin included as a loading control, and values normalised to each group's CTR. C) pSMAD3/total SMAD3 densitometry of (B). D) αSMA protein densitometry of (B). HC and SSc n=3. Bars show the mean and error bars show standard error of the mean. P values were calculated with paired two-tailed t-tests (ns = non-significant, *P<0.05).

Inhibition of TGFβRI alongside stimulation with TGFβ was sufficient to block the TGFβ-induced reduction in cilia incidence in both HC (TGFβ at 86.0 % vs SD208 + TGFβ at 94.3 %, p<0.05) and SSc (TGFβ at 80.4 % vs SD208 + TGFβ at 93.9 %, p<0.001) (Fig. 4.2A), and to abolish TGFβ-induced ciliary shortening in both HC (TGFβ at 1.8±0.1 μm (Mean±SEM) vs SD208 + TGFβ at 4.5±0.2 μm, p<0.0001) and SSc (TGFβ at 1.8±0.1 μm vs SD208 + TGFβ at 3.0±0.2 μm, p<0.001) (Fig. 4.2B). This provides further experimental evidence to the previous observations that activation of the TGFβ signalling pathway leads to a

reduction in the incidence and length of primary cilia, as blockade of the pathway is sufficient to prevent the effect. As for the mechanism by which TGFβ alters the ciliary phenotype, this data confirms that this mechanism depends upon activation of its receptor kinase.

This data also provides evidence against the hypothesis that SSc cilia are shorter in length than HC because of TGFβ pathway activation. Blockade of the TGFβRI-dependent signalling pathway does not rescue SSc cilium length – there was no significant difference in length between SSc CTR at 2.8±0.1 μm and SSc SD208 at 3.1±0.2 μm, and the difference in length between HC and SSc cilia was maintained whether cells were treated with SD208 or not (HC CTR at 4.4±0.2 μm vs SSc CTR at 2.8±0.1 μm, $p<0.0001$; HC SD208 at 4.5±0.2 μm vs SSc SD208 at 3.1±0.2 μm, $p<0.0001$) (Fig. 4.2B). The same result was observed even when TGFβRI was continuously inhibited with SD208 over two passages for five days in 10 % serum media, which did not affect cilia length nor incidence in HC or SSc (Fig. 4.2C, D). Thus, even over an extended period of time in a population of proliferating cells, inhibition of the TGFβ pathway was not able to rescue SSc cilia length.

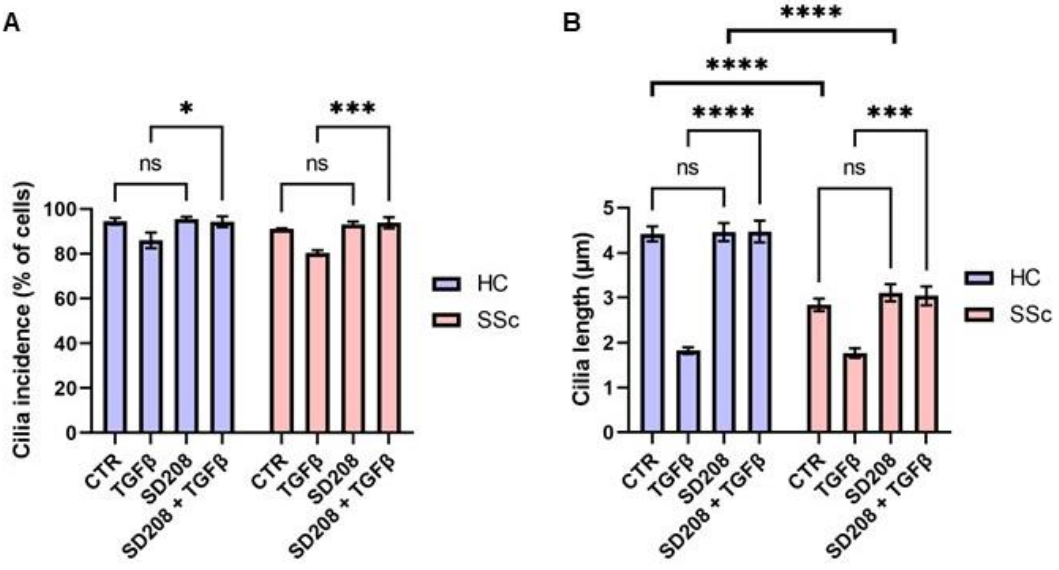

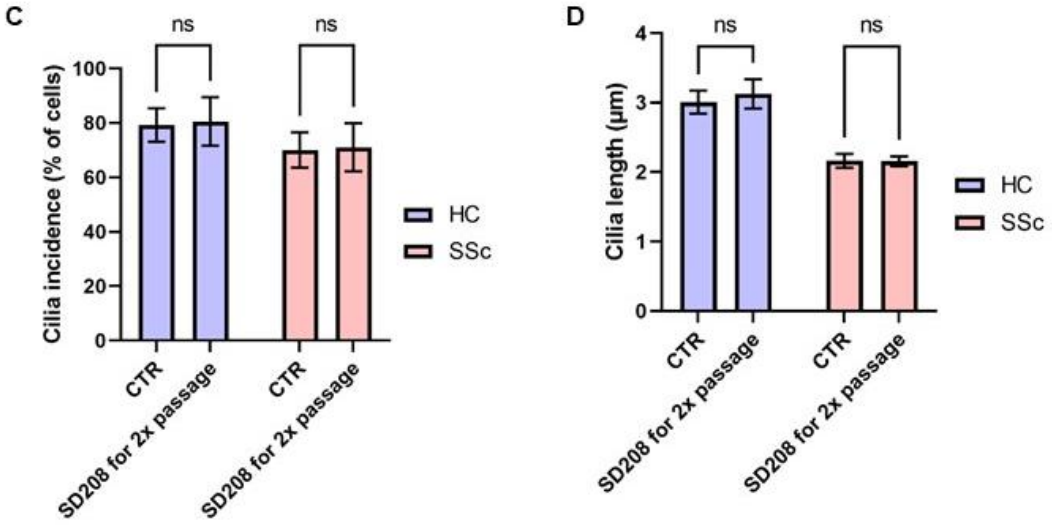

Figure 4.2: TGFβRI inhibition with SD208 blocks the effect of TGFβ on cilia but does not rescue SSc cilia length

Confluent HC and SSc fibroblasts were cultured in 0.5 % serum media for 24 h followed by 24 h treatment with 10 ng/mL TGFβ and/or 1 µM SD208 or DMSO control in 0.5 % serum media. Fibroblasts were also cultured in the presence of SD208 in 10 % serum media for two passages over the course of 5 days. Cilia were measured using immunofluorescence for Ac-α-Tub. A) Cilia incidence changes in response to TGFβ/SD208 treatment. B) Cilia length changes in response to TGFβ/SD208 treatment. C) Cilia incidence changes in response to SD208 treatment over two passages. D) Cilia length changes in response to SD208 treatment over two passages. HC and SSc n=3. Bars show the mean and error bars show standard error of the mean. P values were calculated by two-way ANOVA with Tukey's multiple comparisons test (ns = non-significant, *P<0.05, ***P<0.001, ****P<0.0001).

Taken together, these data imply that the biological mechanism by which SSc dermal fibroblasts possess shorter cilia may be independent of TGFβ activation, despite the ability of TGFβ to shorten cilia.

4.2.2 Inhibition of canonical TGFβ signalling effector SMAD3 does not rescue SSc cilia length, nor prevent TGFβ-induced cilia shortening

In order to further investigate the downstream mechanism by which TGFβ signalling activation alters the ciliary phenotype, we next aimed to ascertain whether the mechanism is part of the canonical or non-canonical arm of the TGFβ signalling pathway. Firstly, the canonical TGFβ signalling pathway, which depends upon phosphorylation of SMAD3, was inhibited by siRNA-mediated post-transcriptional gene silencing of SMAD3 (Fig. 4.3A). The success of this knockdown was evident in the significantly reduced protein levels of total SMAD3 in fibroblasts transfected with siSMAD3 vs siSCR control ($p<0.001$ for HC, $p<0.0001$ for SSc) (Fig. 4.3B, C). Treatment with TGFβ stimulated an increase in pSMAD3 abundance in both siSCR and siSMAD3-treated cells; however, the total TGFβ-induced pSMAD3 level was reduced by siSMAD3 (Fig. 4.3B, D).

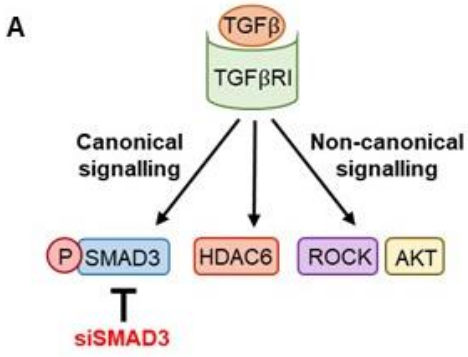

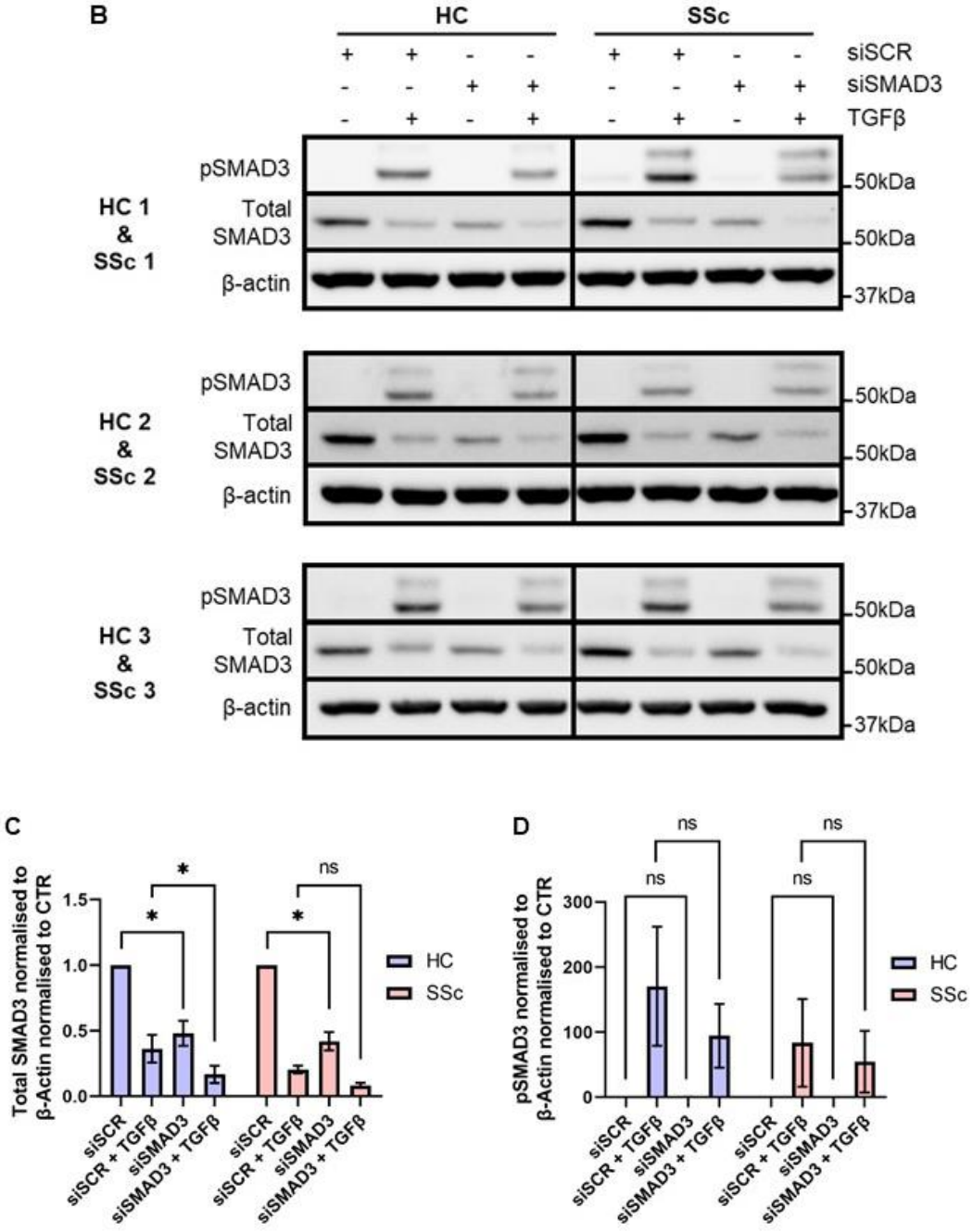

Figure 4.3: Blockade of SMAD3 with siRNA-mediated knockdown

HC and SSc fibroblasts treated with siRNA oligos to knockdown SMAD3 expression (siSMAD3), or SCR control siRNA (siSCR), were cultured in 0.5 % serum media for 24 h followed by treatment with 10 ng/mL TGFβ in 0.5 % serum media for a further 24 h. Protein was harvested for quantification by Western Blot to validate siRNA knockdown. A) Schematic showing the components of the TGFβ signalling pathway relevant to this study, and the inhibition of SMAD3 by siRNA-mediated post-transcriptional gene silencing. B) Western Blots showing pSMAD3 and total SMAD3 protein expression in response to treatments comprising of TGFβ and/or siSMAD3/siSCR in three HC donor and three SSc donor fibroblast lines. β-Actin

included as a loading control, and values normalised to each group's CTR. C) Total SMAD3 densitometry of (B). D) pSMAD3 densitometry of (B). HC and SSc n=3. Bars show the mean and error bars show standard error of the mean. P values were calculated with paired two-tailed t-tests (ns = non-significant, *P<0.05).

Partial reduction of pSMAD3 abundance via siSMAD3 alongside stimulation with TGFβ had no preventative effect on the ability of TGFβ to induce a reduction in cilia incidence in both HC (siSCR + TGFβ at 83.0 % vs siSMAD3 + TGFβ at 87.3 %) and SSc (siSCR + TGFβ at 79.8 % vs siSMAD3 + TGFβ at 83.8 %) (Fig. 4.4A), and also had no preventative effect on the ability of TGFβ to induce ciliary shortening in both HC (siSCR + TGFβ at 1.4±0.04 μm vs siSMAD3 + TGFβ at 1.5±0.07 μm) and SSc (siSCR + TGFβ at 1.5±0.02 μm vs siSMAD3 + TGFβ at 1.5±0.1 μm) (Fig. 4.4B). This suggests that the downstream mechanism by which TGFβ reduces cilia incidence and length may not rely on canonical, pSMAD3-mediated TGFβ signalling, and instead the mechanism may be part of the non-canonical TGFβ signalling pathway.

Additionally, partial reduction of pSMAD3 abundance with siSMAD3 did not rescue SSc cilium length. There was no significant difference in length between SSc siSCR at 2.4±0.1 μm and SSc siSMAD3 at 2.5±0.1 μm, and the difference in length between HC and SSc cilia was maintained whether cells were treated with siSMAD3 or siSCR (HC siSCR at 3.8±0.2 μm vs SSc siSCR at 2.4±0.1 μm, $p<0.0001$; HC siSMAD3 at 3.7±0.2 μm vs SSc siSMAD3 at 2.5±0.1 μm, $p<0.0001$) (Fig. 4.4B).

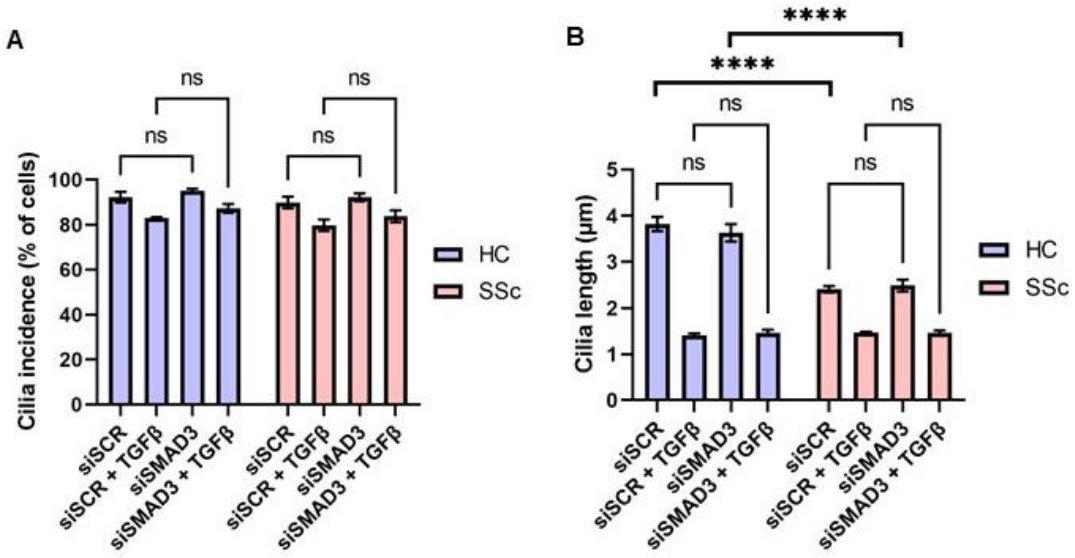

Figure 4.4: siRNA-mediated SMAD3 knockdown does not block the effect of TGFβ on cilia nor rescue SSc cilia length

HC and SSc fibroblasts treated with siRNA oligos to knockdown SMAD3 expression (siSMAD3), or SCR control siRNA (siSCR), were cultured in 0.5 % serum media for 24 h followed by 24 h treatment with 10 ng/mL TGFβ in 0.5 % serum media. Cilia were measured using immunofluorescence for Ac-α-Tub. A) Cilia incidence changes in response to TGFβ /siSMAD3/siSCR treatment. B) Cilia length changes in response to TGFβ /siSMAD3/siSCR treatment. HC and SSc n=3. Bars show the mean and error bars show standard error of the mean. P values were calculated by two-way ANOVA with Tukey's multiple comparisons test (ns = non-significant, ***P<0.001, ****P<0.0001).

These data imply that the mechanism by which TGFβ alters the ciliary phenotype may not be dependent on pSMAD3-mediated canonical signalling, and support the notion that the biological mechanism by which SSc dermal fibroblasts possess shorter cilia may be independent of TGFβ activation. However, it is important to note that there was variable silencing efficiency of SMAD3 between fibroblast lines and the reduction of TGFβ-induced pSMAD3 in siSMAD3 vs siSCR was not significant. Therefore, an additional approach would be needed in order to reach these conclusions confidently to rule out

canonical TGFβ signalling. We next set out to investigate the effect of non-canonical mediators of TGFβ signalling in TGFβ-induced ciliary shortening.

4.2.3 Inhibition of non-canonical TGFβ effector ROCK2 does not rescue SSc cilia length, but partially prevents TGFβ-induced cilia shortening

Next, the ROCK kinases, which are known to be activated by TGFβ including in SSc (Korol et al., 2016, Mendoza & Jimenez, 2022), were investigated as potential downstream effectors of non-canonical TGFβ-induced alterations to the ciliary phenotype. While both ROCK1 and ROCK2 have been implicated in negative regulation of cilia length through alterations to the cytoskeleton (Smith et al., 2020), there is evidence to suggest that the two kinases have distinct molecular targets (Newell-Litwa et al., 2015), and that ROCK2 is more heavily involved in cilia length regulation than ROCK1 (Lake et al., 2020).

Two small molecule inhibitors were used, one pan-ROCK inhibitor (Y27632) to inhibit both ROCK1 and ROCK2 (Ishizaki et al., 2000), and one ROCK2-specific inhibitor (KD025) (Boerma et al., 2008) (Fig. 4.5A). ROCK kinases, when active, facilitate Myosin Light Chain 2 (MLC2) mono-phosphorylation at Ser19 (pMLC2), and di-phosphorylation at Thr18 in addition to Ser19 (ppMLC2) (Kimura et al., 1996) (Fig. 4.5A). This readout was utilised to validate the activity of the ROCK inhibitors by Western Blot using two antibodies specific to the two differentially phosphorylated forms of MLC2. ROCK inhibitor efficacy was evident in the reduced MLC2 phosphorylation levels of pMLC2 and ppMLC2 when cells were treated with the inhibitors in combination with TGFβ, compared to treatment with TGFβ alone (Fig. 4.5B-D). As expected, this effect was more obvious in fibroblasts treated with the pan-ROCK inhibitor Y27632 in

comparison to those treated with the ROCK2-specific inhibitor KD025. Also of note was an observed reduction in the protein levels of CTGF and αSMA in some of the fibroblast lines when treated with ROCK inhibitors and TGFβ, compared to TGFβ alone, which suggests that inhibition of ROCK kinases lessens the profibrotic response to TGFβ, providing experimental evidence to support the previously described role of ROCK kinases as downstream effectors of TGFβ signalling in dermal fibroblasts (Fig. 4.5B, E, F).

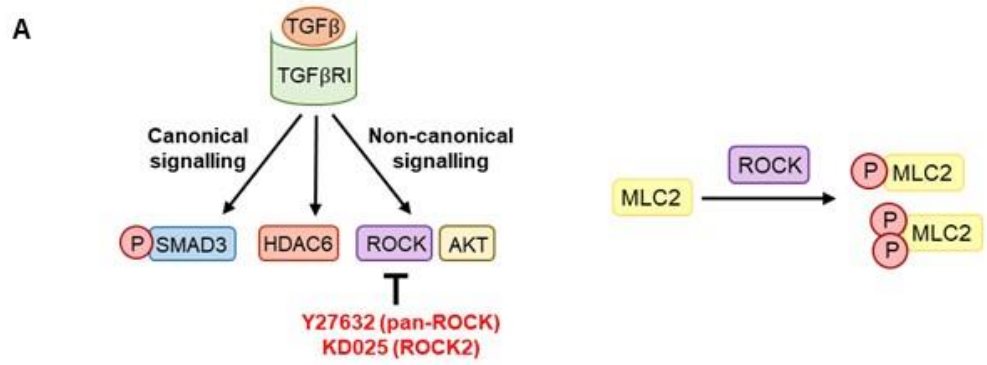

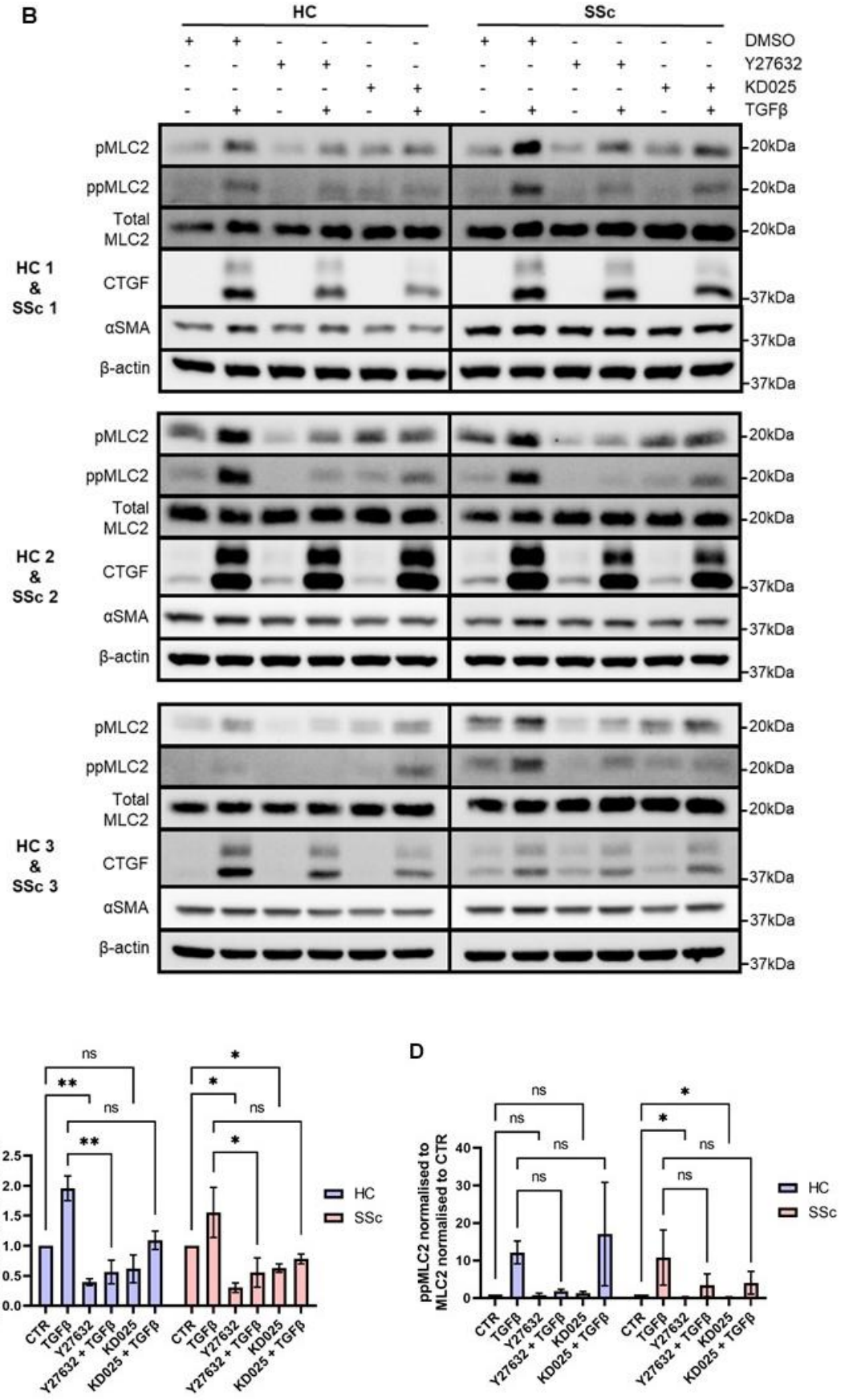
B
HC
SSc
DMSO
Y27632
KD025
TGFβ
HC 1 & SSc 1
HC 2 & SSc 2
HC 3 & SSc 3
pMLC2
ppMLC2
Total MLC2
CTGF
αSMA
β-actin
20kDa
37kDa
C
pMLC2 normalised to MLC2 normalised to CTR
CTR
TGFβ
Y27632
Y27632 + TGFβ
KD025
KD025 + TGFβ
HC
SSc
ns
*
**
D
ppMLC2 normalised to MLC2 normalised to CTR

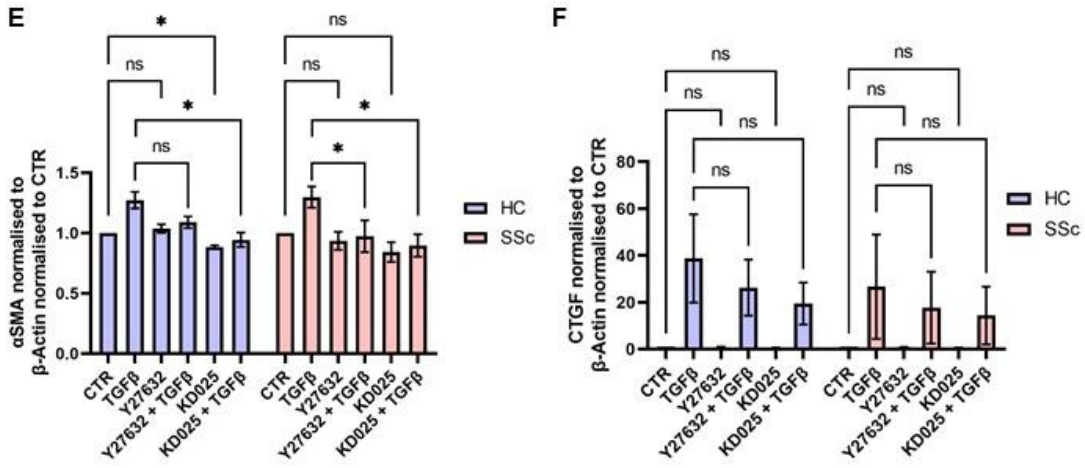

Figure 4.5: Blockade of ROCK kinases using inhibitors Y27632 and KD025 reduces ROCK kinase activity

Confluent HC and SSc fibroblasts were cultured in 0.5 % serum media for 24 h followed by 24 h treatment with 10 ng/mL TGFβ and/or 2 μM Y27632, 5 μM KD025 or DMSO control in 0.5 % serum media. Protein was harvested for quantification by Western Blot to validate inhibitor activity. A) Schematic showing the components of the TGFβ signalling pathway relevant to this study, and the inhibition of ROCK kinases by Y27632 and KD025. Also shown is the mechanism of MLC phosphorylation by ROCK kinases. B) Western Blots showing pMLC2, ppMLC2, total MLC2, CTGF, and αSMA protein expression in response to treatments comprising of TGFβ and/or Y27632, KD025 or DMSO control in three HC donor and three SSc donor fibroblast lines. β-Actin included as a loading control, and values normalised to each group's CTR. C) pMLC2/total MLC2 densitometry of (B). D) ppMLC2/total MLC2 densitometry of (B). E) αSMA protein densitometry of (B). F) CTGF protein densitometry of (B). HC and SSc n=3. Bars show the mean and error bars show standard error of the mean. P values were calculated with paired two-tailed t-tests (ns = non-significant, *P<0.05, **P<0.01).

Treatment with the pan-ROCK inhibitor Y27632 alongside stimulation with TGFβ had no preventative effect on the ability of TGFβ to reduce cilia incidence in both HC (CTR + TGFβ at 85.2 % vs Y27632 + TGFβ at 88.9 %) and SSc (CTR + TGFβ at 86.0 % vs Y27632 + TGFβ at 89.7 %) (Fig. 4.6A). There was a mild preventative effect on the ability of TGFβ to induce ciliary shortening in both HC (CTR + TGFβ at 1.3±0.1 μm vs Y27632 + TGFβ at 1.9±0.1 μm) and

SSc (CTR + TGFβ at 1.3±0.1 μm vs Y27632 + TGFβ at 1.9±0.1 μm), although this did not reach statistical significance (Fig. 4.6B). Treatment with ROCK2-specific inhibitor KD025 alongside stimulation with TGFβ similarly did not prevent the ability of TGFβ to reduce cilia incidence in both HC (CTR + TGFβ at 83.4 % vs KD025 + TGFβ at 85.6 %) and SSc (CTR + TGFβ at 80.1 % vs KD025 + TGFβ at 75.6 %) (Fig. 4.6C). Remarkably, KD025 treatment alongside TGFβ was able to partially prevent ciliary shortening by TGFβ in both HC (CTR + TGFβ at 1.3±0.04 μm vs KD025 + TGFβ at 2.1±0.1 μm, $p<0.0001$) and SSc (CTR + TGFβ at 1.3±0.1 μm vs KD025 + TGFβ at 2.2±0.2 μm, $p<0.0001$) (Fig. 4.6D). Taken together, these data suggest that the downstream mechanism by which TGFβ reduces cilia length may be at least partially dependent on ROCK2-mediated non-canonical TGFβ signalling.

Pan-ROCK inhibition with Y27632 did not rescue SSc cilium length – there was no significant difference in length between SSc CTR at 2.8±0.1 μm and SSc Y27632 at 3.0±0.2 μm, and the difference in length between HC and SSc cilia was maintained whether cells were treated with Y27632 or not (HC CTR at 4.1±0.3 μm vs SSc CTR at 2.8±0.1 μm, $p<0.001$; HC Y27632 at 4.0±0.2 μm vs SSc Y27632 at 3.0±0.2 μm, $p<0.001$) (Fig. 4.6B).

ROCK2 inhibition with KD025 did increase SSc cilium length from 2.7±0.1 μm to 3.2±0.04 μm ($p<0.05$) (Fig. 4.6D). However, the same effect was observed in HC where KD025 increased cilium length from 4.0±0.1 μm to 4.4±0.03 μm ($p<0.05$) (Fig. 4.6D). Furthermore, the difference in length between HC and SSc cilia was maintained whether cells were treated with KD025 or not (HC CTR at 4.0±0.1 μm vs SSc CTR at 2.7±0.1 μm, $p<0.0001$; HC KD025 at 4.4±0.03 μm vs SSc KD025 at 3.2±0.04 μm, $p<0.0001$) (Fig. 4.6D). Therefore, the increase in cilia length in response to ROCK2 inhibition was not an SSc-specific ‘rescue’

of cilia phenotype, but a reflection of ROCK2's involvement in the shortening function of ciliary homeostasis in dermal fibroblasts, unrelated to disease status.

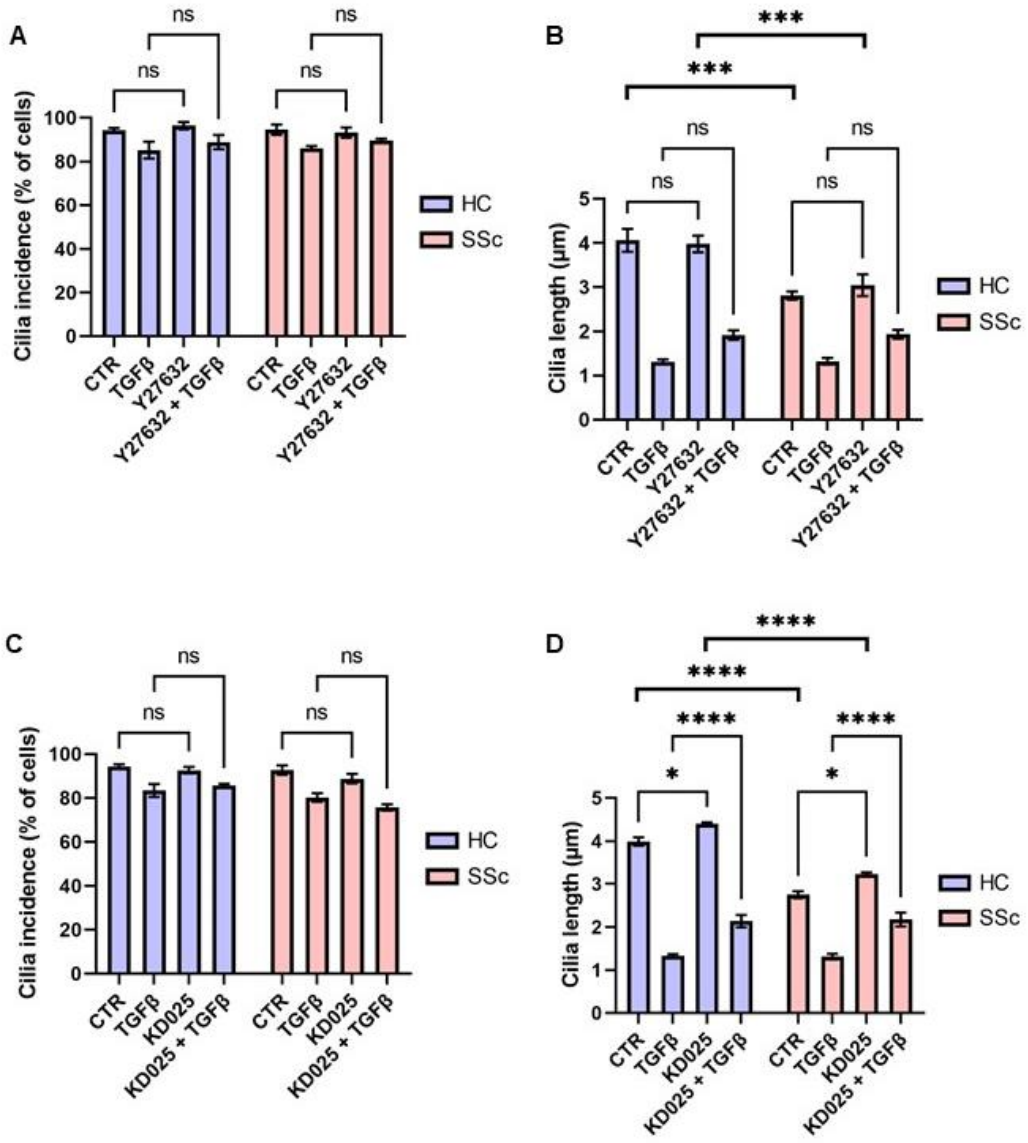

Figure 4.6: Inhibition of ROCK kinases using Y27632 and KD025 does not rescue SSc cilia length, but partially prevents TGFβ-induced cilia shortening
Confluent HC and SSc fibroblasts were cultured in 0.5 % serum media for 24 h followed by 24 h treatment with 10 ng/mL TGFβ and/or 2 µM Y27632, 5 µM KD025 or DMSO control in 0.5 % serum media. Cilia were measured using immunofluorescence for Ac-α-Tub. A) Cilia incidence changes in response to TGFβ/Y27632 treatment. B) Cilia length changes in response to TGFβ/Y27632 treatment. C) Cilia incidence changes in response to TGFβ/KD025 treatment. D)

Cilia length changes in response to TGFβ/KD025 treatment. HC and SSc n=3. Bars show the mean and error bars show standard error of the mean. P values were calculated by two-way ANOVA with Tukey's multiple comparisons test (*P<0.05, ***P<0.001, ****P<0.0001).

These data suggest that although ROCK2 may have a role as a downstream effector of TGFβ in TGFβ-induced ciliary shortening, and under basal conditions ROCK2 also influences ciliary length homeostasis, this is independent of the mechanism by which SSc dermal fibroblasts possess shorter cilia than HC. It is unlikely that SSc cilia are shorter due to aberrant activity of ROCK2 in SSc dermal fibroblasts.

Additionally, the observation that the pan-ROCK inhibitor was not able to alter ciliary phenotype in these experiments to the same degree as the ROCK2-specific inhibitor corroborates the notion that ROCK2 plays a more prevalent role in ciliary length homeostasis than ROCK1 (Lake et al., 2020).

4.2.4 Inhibition of the non-canonical TGFβ effector AKT does not rescue SSc cilia length, nor prevent TGFβ-induced cilia shortening

PI3K-AKT signalling, which is also known to be activated by TGFβ (H. Liu & Chen, 2022) and to be implicated in shortening of primary cilia (Nishimura et al., 2021), was investigated as an alternative potential downstream effector of the non-canonical TGFβ signalling pathway in the TGFβ-induced alterations to the ciliary phenotype. Small molecule inhibitor BKM120 was used to inhibit PI3K and subsequently reduce its ability to activate AKT (Brachmann et al., 2012) (Fig. 4.7A). The efficacy of BKM120 to prevent AKT activation was validated by monitoring levels of pAKT(Ser473) and pAKT(Thr308) – key phosphorylation

sites for AKT activity (Alessi et al., 1996). Indeed, levels of pAKT(Ser473) were significantly reduced when cells were treated with BKM120 compared to control, and with BKM120 in combination with TGFβ compared to TGFβ alone (Fig. 4.7B, C), confirming the action of BKM120 in reducing AKT activation. Reduction in the level of pAKT(Thr308) with BKM120 treatment was also observed (Fig 4.7B), but this did not reach statistical significance (Fig 4.7D).

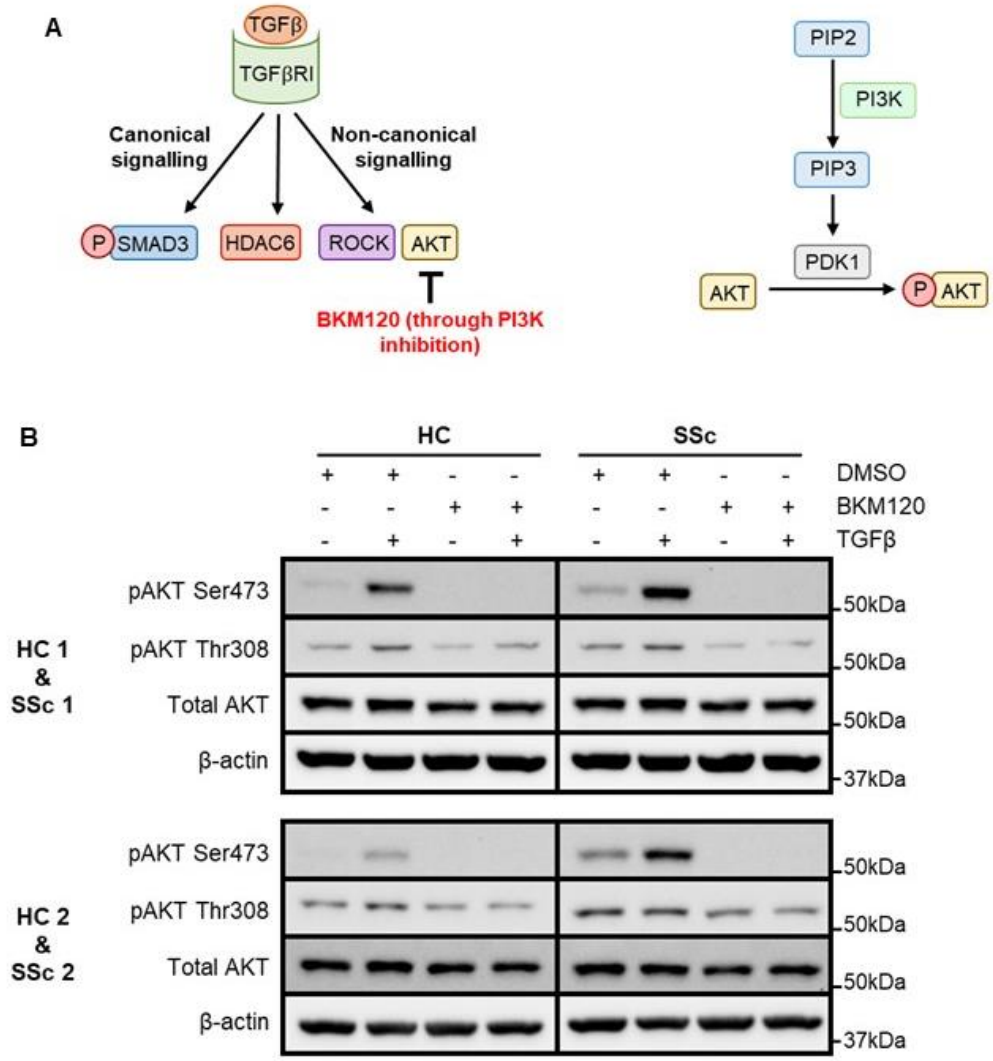

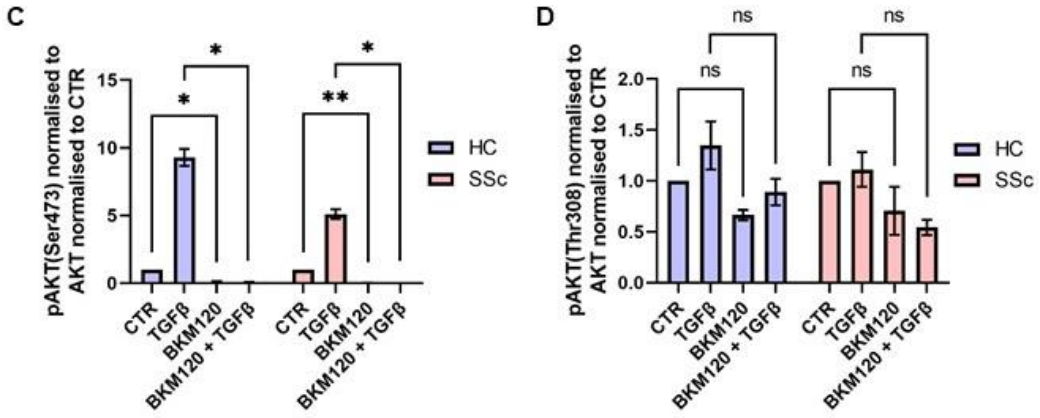

Figure 4.7: Blockade of PI3K with inhibitor BKM120 reduces AKT signalling activation

Confluent HC and SSc fibroblasts were cultured in 0.5 % serum media for 24 h followed by 24 h treatment with 10 ng/mL TGFβ and/or 2 μM BKM120 or DMSO control in 0.5 % serum media. Protein was harvested for quantification by Western Blot to validate inhibitor activity. A) Schematic showing the components of the TGFβ signalling pathway relevant to this study, and the blockade of AKT activation via PI3K inhibitor BKM120. Also shown is the role of PI3K in the AKT phosphorylation mechanism. B) Western Blots showing pAKT (Ser473), pAKT (Thr308), and total AKT protein expression in response to treatments comprising of TGFβ and/or BKM120 or DMSO control in two HC donor and two SSc donor fibroblast lines. β-Actin included as a loading control, and values normalised to each group's CTR. C) pAKT(Ser473)/total AKT densitometry of (B). D) pAKT(Thr308)/total AKT densitometry of (B). HC and SSc n=2. Bars show the mean and error bars show standard error of the mean. P values were calculated with paired two-tailed t-tests (ns = non-significant, *P<0.05, **P<0.01).

Inhibition of the PI3K-AKT pathway did not prevent the ability of TGFβ to reduce cilia incidence in both HC (CTR + TGFβ at 83.3 % vs BKM120 + TGFβ at 81.0 %) and SSc (CTR + TGFβ at 80.9 % vs BKM120 + TGFβ at 72.9 %) (Fig. 4.8A), and also had no preventative effect on the ability of TGFβ to induce ciliary shortening in both HC (CTR + TGFβ at 1.5±0.1 μm vs BKM120 + TGFβ at 1.5±0.2 μm) and SSc (CTR + TGFβ at 1.5±0.1 μm vs BKM120 + TGFβ at 1.5±0.1 μm) (Fig. 4.8B). This implies that the downstream non-canonical

mechanism by which TGFβ signalling reduces cilia incidence and length does not depend on PI3K-AKT pathway activation.

PI3K-AKT inhibition with BKM120 did increase SSc cilium length from 2.6±0.1 µm to 3.4±0.1 µm ($p<0.05$) (Fig. 4.8B). However, the same effect was observed in HC where BKM120 increased cilium length from CTR (from 3.9±0.3 µm to 4.9±0.4 µm, $p<0.01$) (Fig. 4.8B). Additionally, the statistically significant difference in cilia length between HC and SSc was maintained under BKM120 treatment (HC CTR at 3.9±0.3 µm vs SSc CTR at 2.6±0.1 µm, $p<0.001$; HC BKM120 at 4.9±0.4 µm vs SSc BKM120 at 3.4±0.1 µm, $p<0.001$) (Fig. 4.8B). Therefore, the increase in cilia length in response to PI3K-AKT inhibition was not a disease-specific 'rescue' of cilia phenotype, but a reflection of the involvement of PI3K-AKT signalling in ciliary length regulation in dermal fibroblasts.

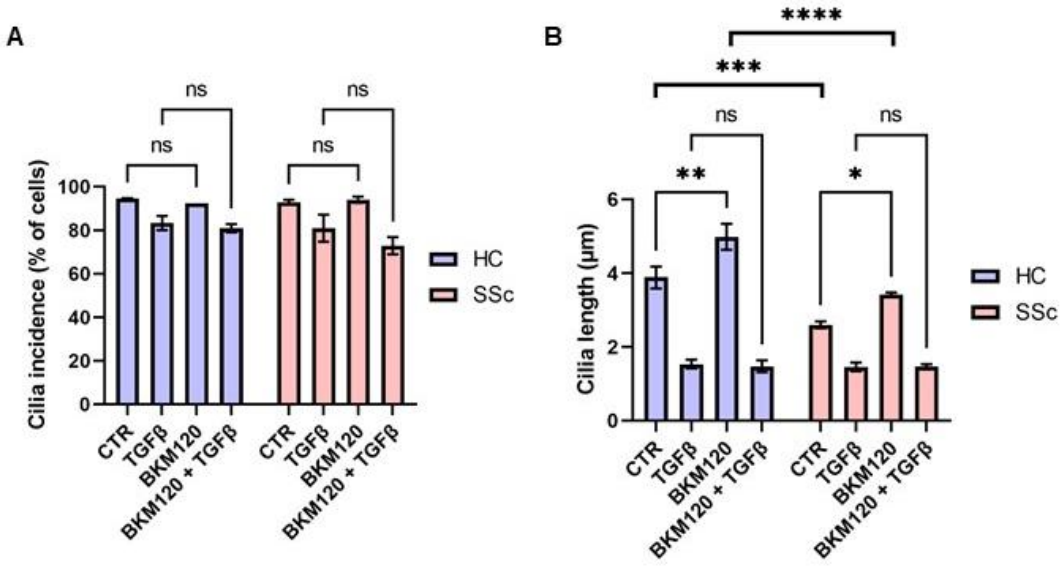

Figure 4.8: Blockade of AKT signalling using PI3K inhibitor BKM120 does not block the effect of TGFβ on cilia nor rescue SSc cilia length

Confluent HC and SSc fibroblasts were cultured in 0.5 % serum media for 24 h followed by 24 h treatment with 10 ng/mL TGFβ and/or 2 µM BKM120 or DMSO control in 0.5 % serum media. Cilia were measured using immunofluorescence for

Ac-α-Tub. A) Cilia incidence changes in response to TGFβ/BKM120 treatment. B) Cilia length changes in response to TGFβ/BKM120 treatment. HC and SSc n=3. Bars show the mean and error bars show standard error of the mean. P values were calculated by two-way ANOVA with Tukey's multiple comparisons test (*P<0.05, **P<0.01, ***P<0.001, ****P<0.0001).

Thus, although under basal conditions PI3K-AKT activity influences ciliary length homeostasis, this does not explain why SSc dermal fibroblasts possess shorter cilia than HC, and it is unlikely that SSc cilia are shorter due to aberrant activity of PI3K-AKT in SSc.

4.2.5 Inhibition of the TGFβ effector HDAC6 does not block TGFβ-induced shortening, but partially rescues SSc cilia length

HDAC6 is another known contributor to ciliary length reduction (Pugacheva et al., 2007) and has been shown to mediate TGFβ-induced ciliary shortening in other human cell types (Ehnert et al., 2017, Rowson et al., 2018), although it is not known whether the activation of HDAC6 by TGFβ is via the canonical or non-canonical pathway. HDAC6 was therefore investigated as an alternative potential downstream effector of TGFβ-induced alterations to the ciliary phenotype in dermal fibroblasts. Small molecule inhibitor Tubacin (Haggarty et al., 2003) was used to inhibit HDAC6 and subsequently reduce its ability to deacetylate Acetylated-α-Tubulin (Ac-α-Tub) (Fig. 4.9A). The functionality of this inhibitor was validated by monitoring levels of Ac-α-Tub. Treatment with Tubacin led to increased levels of Ac-α-Tub, with stronger increases observed at higher Tubacin concentrations (Fig. 4.9B, C), confirming the efficacy of Tubacin in reducing Ac-α-Tub deacetylation by HDAC6.

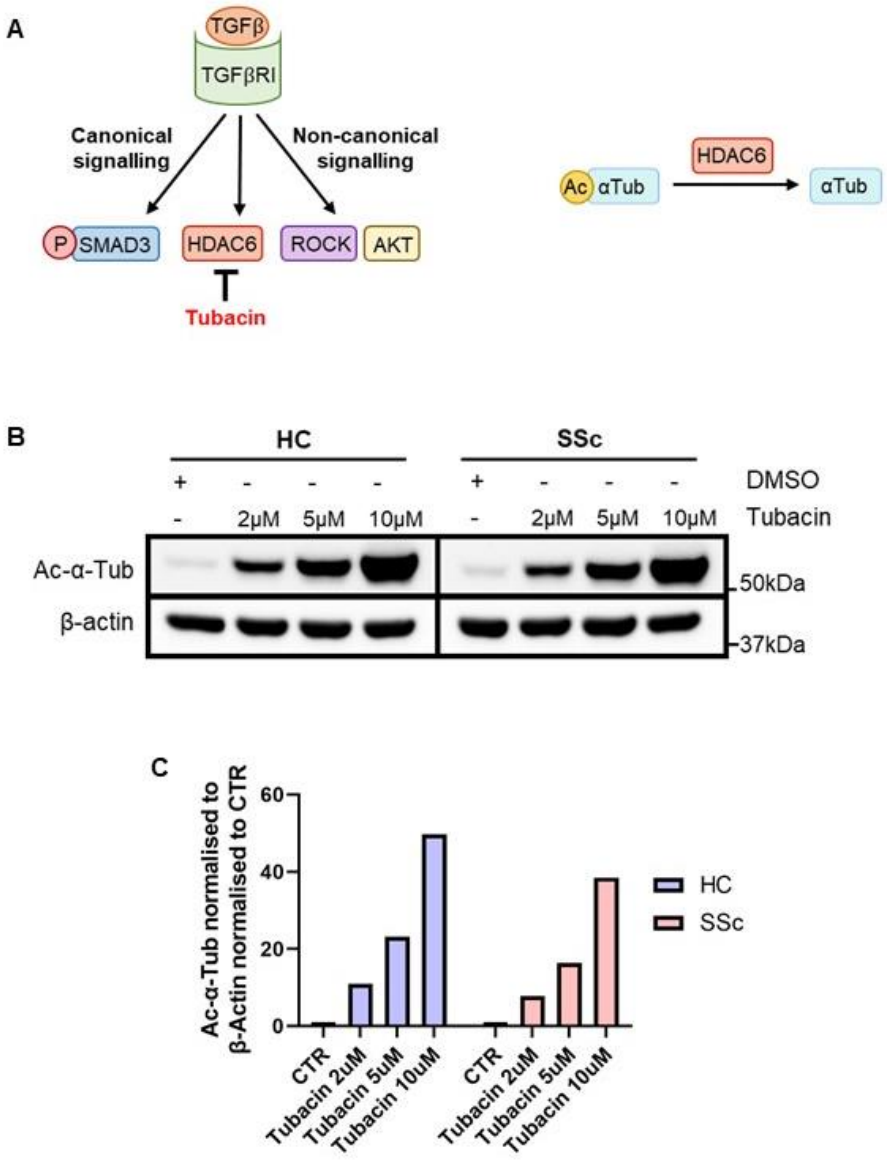

Figure 4.9: Blockade of HDAC6 activity with inhibitor Tubacin

Confluent HC and SSc fibroblasts were cultured in 0.5 % serum media for 24 h followed by 24 h treatment with 2, 5 or 10 μM Tubacin or DMSO control in 0.5 % serum media. Protein was harvested for quantification by Western Blot. A) Schematic showing the components of the TGFβ signalling pathway relevant to this study, and the inhibition of HDAC6 via Tubacin. Also shown is the mechanism of Ac-α-Tub deacetylation by HDAC6. B) Western Blots showing Ac-α-Tub levels in response to treatment with 2, 5 or 10 μM Tubacin or DMSO control in an HC and SSc fibroblast line. β-Actin included as a loading control, and values normalised to each group's CTR. C) Ac-α-Tub densitometry of (B) in response to Tubacin treatment.

Inhibition of HDAC6 had no preventative effect on the ability of TGFβ to induce a reduction in cilia incidence in both HC (CTR + TGFβ at 85.2 % vs Tubacin + TGFβ at 89.6 %) and SSc (CTR + TGFβ at 83.6 % vs Tubacin + TGFβ at 86.5 %) (Fig. 4.10A), and also had no preventative effect on TGFβ-induced ciliary shortening in both HC (CTR + TGFβ at 1.6±0.02 μm vs Tubacin + TGFβ at 1.6±0.1 μm) and SSc (CTR + TGFβ at 1.6±0.1 μm vs Tubacin + TGFβ at 1.5±0.1 μm) (Fig. 4.10B). This suggests that TGFβ does not reduce ciliary incidence or length in dermal fibroblasts via a mechanism which is dependent upon activation of HDAC6.

Interestingly, HDAC6 inhibition with Tubacin increased SSc cilium length from 2.6±0.1 μm to 3.3±0.03 μm ($p<0.01$), while HC cilia length was unaffected (4.2±0.1 μm vs 3.9±0.2 μm) (Fig. 4.10B). Thus, the difference in length between HC and SSc cilia was reduced after Tubacin treatment (HC CTR at 4.2±0.1 μm vs SSc CTR at 2.6±0.1 μm, $p<0.0001$; HC Tubacin at 3.9±0.2 μm vs SSc Tubacin at 3.3±0.03 μm, $p<0.05$) (Fig. 4.10B). Visual representation of the distribution of cilia lengths within each population shows a shift to the right towards higher lengths in SSc cilia upon treatment with Tubacin, but no change in HC cilia length distribution (Fig. 4.10C).

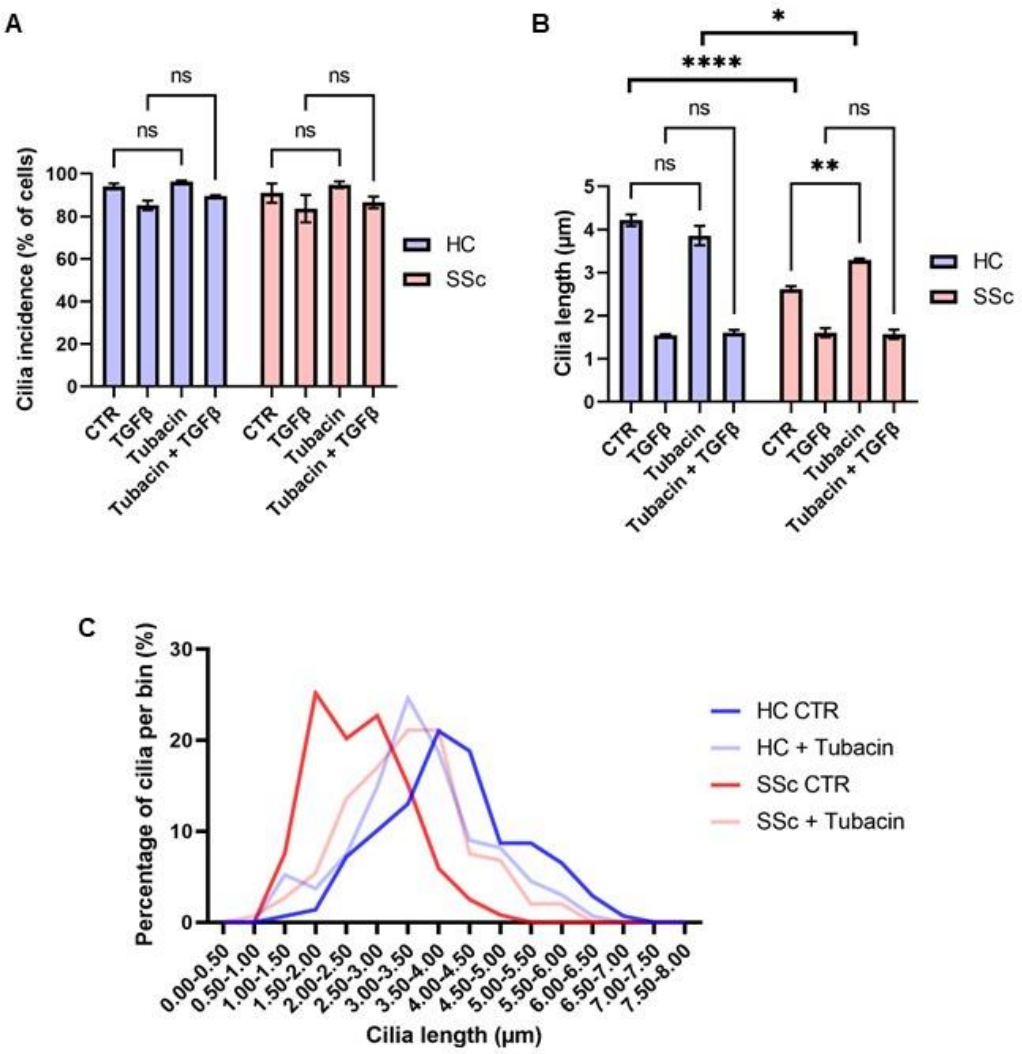

Figure 4.10: Inhibition of HDAC6 activity with Tubacin does not block TGFβ-induced shortening, but partially rescues SSc cilia length

Confluent HC and SSc fibroblasts were cultured in 0.5 % serum media for 24 h followed by 24 h treatment with 10 ng/mL TGFβ and/or 10 μM Tubacin or DMSO control in 0.5 % serum media, and cilia were measured using immunofluorescence for Ac-α-Tub. A) Cilia incidence changes in response to TGFβ/Tubacin treatment. B) Cilia length changes in response to TGFβ/Tubacin treatment. C) Distribution of cilia length in HC and SSc with and without Tubacin treatment, showing the percentage of total cilia in each 0.5 μm length category. HC and SSc n=3. Bars show the mean and error bars show standard error of the mean. P values were calculated by two-way ANOVA with Tukey's multiple comparisons test (*P<0.05, **P<0.01, ****P<0.0001).

These data show an SSc-specific 'rescue' of cilia phenotype in response to HDAC6 inhibition. Thus, the mechanism by which SSc dermal fibroblasts

possess shorter cilia than HC may be at least partially due to aberrant activity of HDAC6 in SSc.

4.3 Discussion

Importantly, this work demonstrated that inhibition of the TGFβ signalling pathway, even over the course of several passages, was not sufficient to increase primary cilium length to normal levels in SSc dermal fibroblasts. Therefore, it can be concluded that SSc fibroblast cilia are not shorter than HC cilia due to hyperactivation of the TGFβ signalling pathway as originally hypothesised. Instead, this work shows that the mechanism by which TGFβ signalling shortens primary cilia, and the mechanism by which SSc fibroblasts possess stably shortened cilia, are independent. This sheds further light on the mechanistic understanding of the SSc shorter cilia phenotype, necessary to inform future research into how therapeutic targeting of aberrant SSc cilia may be possible.

Although TGFβ signalling is not responsible for the shortened primary cilia phenotype of SSc, TGFβ is a known driver of fibrotic activation, and coordination of its downstream signalling is known to be influenced by the primary cilium (Clement et al., 2013, Mönnich et al., 2018, Koefoed et al., 2018). This work provides important insight into the relationship between TGFβ and the dermal fibroblast primary cilium by showing that TGFβ is able to alter ciliary length, but does not provide direct evidence that a shortened primary cilium in turn may lead to an aberrant response to the TGFβ signal. Interestingly, such a relationship has been suggested. Experimental knockdown of ciliary component SPAG17 was shown to shorten cilia in multiple cell types, including mouse

embryonic fibroblasts (Teves et al., 2015). SPAG17 was shown to be downregulated in SSc skin, and explanted dermal fibroblasts from mice with experimental knockdown of SPAG17 showed increased nuclear accumulation of SMAD2/3 and heightened expression of profibrotic markers (Sapao et al., 2023). Together, these data suggest that shortened primary cilia may induce aberrant activation of the TGFβ signalling pathway. Further investigation to elucidate this relationship will lead to a greater understanding of the regulation of the TGFβ pathway in fibrosis, and any ciliary involvement. It would be interesting, for example, to experimentally shorten the primary cilia of HC dermal fibroblasts, and investigate any differences in the way that these fibroblasts respond to TGFβ signalling.

TGFβ-induced ciliary shortening has been previously demonstrated in various cell types, with different downstream mechanisms proposed. In chondrocytes, TGFβ was shown to shorten primary cilia by decreasing mRNA stability of *IFT88* (Kawasaki et al., 2015). In osteoblasts, TGFβ-induced ciliary shortening was attributed to HDAC6 activation (Ehnert et al., 2017), with the same mechanism proposed in tenocytes (Rowson et al., 2018). Despite no mechanism being proposed in a study which showed that adipocyte progenitor cells undergo ciliary shortening in response to TGFβ, the study did suggest that the mechanism did not involve IFT88 or HDAC6, and must be via an alternative mechanism (Arrighi et al., 2017). The current study is the first to provide evidence to suggest that in dermal fibroblasts, the mechanism by which TGFβ shortens cilia is likely at least partially due to the activation of non-canonical TGFβ effector ROCK2 – differing from the downstream TGFβ effectors implicated in ciliary shortening in other cell types. This addition to the field of

research adds evidence to the notion that the effect of TGFβ signalling on primary cilia may occur via cell-type specific mechanisms.

The implication of ROCK2 in TGFβ-induced ciliary shortening aligns with published data which has shown that ROCK2 activation impedes ciliary assembly, shifting the balance of ciliary length homeostasis to favour disassembly, leading to ciliary shortening (Smith et al., 2020, Lake et al., 2020). In order to validate this finding, an additional method of ROCK2 inhibition could be employed in further experiments, such as siRNA-mediated knockdown. Ciliary shortening has been shown to occur with two morphologically distinct appearances – either taking place gradually via ciliary resorption, or rapidly via ciliary 'decapitation' (Mirvis et al., 2019). With ROCK2 activation proposed to shift ciliary length homeostasis to favour disassembly rather than induce ciliary 'decapitation', it would be expected that ROCK2-mediated ciliary shortening should appear to be gradual. Indeed, the TGFβ time course experimental data presented in the previous chapter demonstrating a gradual reduction in ciliary length over a 24 h time period following TGFβ stimulation are concordant with TGFβ-ROCK2 induced shortening. It could also be interesting to visualise primary cilia of TGFβ-treated fibroblasts in real time to observe disassembly. Live-cell imaging of fluorescently labelled cilia has been used to observe ciliary loss (Mirvis et al., 2019), and such techniques could be employed to gain an even more informative insight into the dynamics of this mechanism in dermal fibroblasts.

It is important to note, however, that inhibition of ROCK2 was only able to partially prevent TGFβ-induced ciliary shortening. This could be due to incomplete experimental inhibition of ROCK2 by the inhibitor used in this study, KD025. Additional optimisation of experimental application of KD025 to confer

greater inhibition efficiency, as well as the inclusion of an additional method of ROCK2 inhibition as mentioned above, would be required in order to assess whether ROCK2 inhibition alone is sufficient to prevent TGFβ-induced ciliary shortening in dermal fibroblasts. Such work would be important to determine whether additional downstream TGFβ effectors work in tandem with ROCK2 in this process.

Successful inhibition of PI3K-AKT activation with BKM120 and of HDAC6 with Tubacin did not affect TGFβ-induced ciliary shortening, ruling out involvement of either of these downstream effectors of TGFβ in the ciliary shortening mechanism in dermal fibroblasts. As TGFβ has also been shown to shorten chondrocyte cilia by decreasing *IFT88* mRNA stability (Kawasaki et al., 2015), it would be interesting to investigate *IFT88* expression after TGFβ treatment in dermal fibroblasts, in order to rule out involvement of IFT88 in the TGFβ-induced ciliary shortening mechanism in this cell type.

While the data presented in this study showed that siRNA mediated inhibition of SMAD3 did not prevent TGFβ-induced ciliary shortening, suggesting that TGFβ-induced ciliary shortening is dependent only on non-canonical downstream effectors rather than canonical signalling, it is important to note that siRNA knockdown of SMAD3 had variable efficiency in different experimental repeats, and in none of them was it sufficient to completely banish phosphorylation of SMAD3 in response to TGFβ stimulation. Therefore, in order to prove that the mechanism is entirely independent of canonical signalling, these experiments should be optimised for greater knockdown efficiency and repeated, or alternative methods of pSMAD3 inhibition employed, such as with small molecule pSMAD3 inhibitor SIS3 (Jinnin et al., 2006).

In this study, there was a notable variability of response to inhibitors used experimentally between dermal fibroblast lines obtained from different donors, at the level of the proteins assessed during inhibitor validation, likely reflective of the patient-to-patient heterogeneity of the disease (Allanore et al., 2015). However, despite the heterogeneity in signalling response, differences in cilia length were minimal between the different fibroblast lines within HC and SSc. Additionally, the ciliary shortening response to TGFβ was very similar between all HC and all SSc fibroblast lines. This suggests that cilia length – both basal and post-stimulation – is subject to the same tight regulation regardless of fibroblast heterogeneity. This adds strength to the argument that cilium length may be a key aspect in the control of its functionality.

A crucial observation from this work was that while TGFβ does not shorten dermal fibroblast primary cilia via HDAC6 activation, inhibition of HDAC6 with Tubacin led to a partial increase of SSc primary cilium length, while not affecting HC cilium length. This provides novel evidence that the mechanism by which SSc fibroblasts possess stably shortened primary cilia is at least partially dependent on the activity of HDAC6, a known negative regulator of ciliary length, predominantly as part of the AURKA-HDAC6 axis (Pugacheva et al., 2007). This observation informed the next step of our investigation.

4.4 Summary

The data in this chapter suggest that TGFβ shortens primary cilia in dermal fibroblasts through a non-canonical mechanism which is at least partially dependent on the activation of ROCK2. However, while TGFβ is able to shorten cilia, inhibition of the TGFβ signalling cascade did not rescue cilia length in SSc

fibroblasts, strengthening the notion that the SSc-specific short cilia phenotype is independent of TGFβ signalling. Inhibition of HDAC6, however, was able to partially rescue cilium length in SSc fibroblasts without altering HC cilium length, suggesting that the mechanism by which SSc cilia are shorter may involve an aberrant activation of HDAC6.

Chapter 5. Characterisation of the role of Aurora A Kinase activity at the primary cilium in Systemic Sclerosis

5.1 Introduction

The experimental results discussed so far suggest that the shortened primary cilia phenotype observed in SSc dermal fibroblasts compared to HC is at least partially dependent on HDAC6 activity. HDAC6 is known to facilitate ciliary shortening in mammalian cells by deacetylation of microtubules leading to resorption of the ciliary axoneme (Pugacheva et al., 2007). In this ciliary disassembly mechanism, HDAC6 is directly activated by upstream serine/threonine kinase, Aurora A Kinase (AURKA). Aberrant activation of this AURKA-dependent ciliary shortening pathway has been implicated in pathogenic primary cilia defects in other human diseases, including von Hippel-Lindau disease (Dere et al., 2015, Hasanov et al., 2017). Therefore, we set out to investigate the hypothesis that aberrant HDAC6 activity in SSc and the resulting shortened cilia phenotype could be associated with AURKA. To do this, we inhibited AURKA and studied the effect on primary cilia, and on the fibrotic phenotype of the fibroblasts.

5.2 Results

5.2.1 Validation of MLN8054, a small molecule inhibitor of Aurora A Kinase

To begin to investigate this hypothesis, we set out to validate the activity of MLN8054, a selective small molecule AURKA inhibitor, in dermal fibroblasts. MLN8054 prevents autophosphorylation of the Thr288 residue in the activation

loop of AURKA, required for its kinase activity (Manfredi et al., 2007). Due to the difficulty of assessing phosphorylated AURKA via Western Blot due to low protein abundance (data not shown) and antibody suitability to this assay, we instead stained HC and SSc fibroblasts treated with MLN8054 by immunofluorescence with an antibody specific to AURKA phosphorylated at its Thr288 residue (pAURKA(Thr288)). Cells were co-stained with DAPI to stain the nucleus and Phalloidin to stain actin fibres, to confirm that observed nuclei belong to intact cells and are not simply cellular debris. Initial attempts to observe pAURKA(Thr288) localising specifically to the ciliary basal body were not successful (data not shown), and so we opted to study pAURKA(Thr288) in the nuclei of dividing cells, where it is known to localise to mitotic spindle poles. Staining at these poles was clearly identifiable in dividing nuclei, and fluorescence intensity was visibly reduced in cells treated with MLN8054 compared to DMSO control, suggesting that the inhibitor is able to reduce the abundance of pAURKA(Thr288) in dermal fibroblasts (Fig. 5.1A, B).

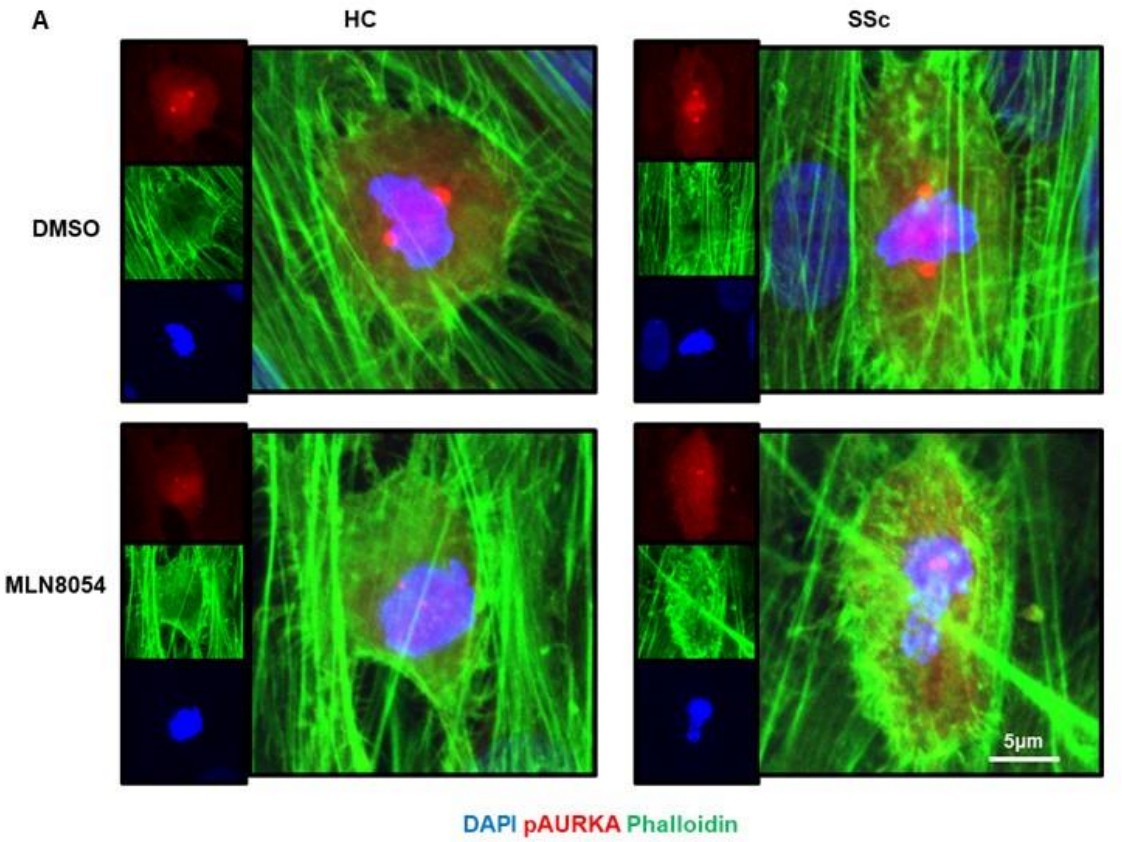

Figure 5.1: Immunofluorescence analysis of the effect of MLN8054 to validate inhibitor activity shows reduced levels of pAURKA(Thr288)

HC and SSc fibroblasts at confluence were cultured in 10 % serum media for 24 h with 10 μM MLN8054 or DMSO control. Immunofluorescence was used to visualise pAURKA(Thr288) (stained red), Phalloidin (stained green) and nuclei (DAPI staining in blue). Cells were imaged at 400 x magnification. A) Representative immunofluorescence images showing individual colour channels and combined red-blue-green colour channels of images of individual healthy and SSc fibroblasts treated with MLN8054 or DMSO control. Scale bar shown at 5 μm. B) Representative red-blue colour channel images of three further individual fibroblasts per experimental condition. Scale bar shown at 10 μm.

We also investigated other indirect readouts of AURKA activity (Fig. 5.2A) after MLN8054 treatment at the protein level, to give further insight into the efficacy of the inhibitor in dermal fibroblasts. In a preliminary investigation, we observed increased protein levels of total AURKA upon MLN8054 treatment (Fig. 5.2B). There is some evidence that AURKA phosphorylated at Thr288 becomes a preferential target for degradation (Walter et al., 2000) (Fig. 5.2A). Increased AURKA protein levels following inhibition of AURKA kinase activity with MLN8054 could be consistent with reduced phosphorylation-mediated degradation. AURKA is also known to induce ubiquitination and consequent destruction of p53 (Katayama et al., 2004) (Fig. 5.2A). Consistent with this, inhibition of AURKA with MLN8054 led to an increase in p53 protein levels (Fig. 5.2B). Interestingly, treatment with MLN8054 also led to reduced levels of NEDD9 protein (Fig. 5.2B). NEDD9 is an important co-activator of AURKA and the two interact when AURKA is phosphorylated, with NEDD9 impeding proteasomal degradation of AURKA (Shagisultanova et al., 2015). It has not been shown that this mechanism exists in reverse and that binding confers mutual stability to NEDD9, but it is an interesting observation nonetheless that inhibition of AURKA phosphorylation with MLN8054 leads to a reduction in NEDD9, suggesting that such an interaction could be occurring in fibroblasts.

Finally, we assessed the effect of MLN8054 on Acetylated-α-Tubulin (Ac-α-Tub) levels. AURKA phosphorylates HDAC6 leading to its activation and deacetylation of Ac-α-Tub (Pugacheva et al., 2007) (Fig. 5.2A). In both HC and SSc dermal fibroblasts, treatment with MLN8054 led to a significant increase in Ac-α-Tub levels compared to control as expected ($p<0.05$) (Fig. 5.2C, D), suggesting that the inhibitor is able to reduce AURKA-dependent activation of HDAC6. TGFβ signalling is also known to induce HDAC6 expression in an

AURKA-independent manner (Ehnert et al., 2017). As expected, treatment with recombinant TGFβ reduced Ac-α-Tub levels in HC and SSc fibroblasts. Consistent with the independence of TGFβ-mediated HDAC6 upregulation from AURKA-mediated HDAC6 activation, this reduction was only mildly ameliorated when TGFβ treatment was delivered in the presence of MLN8054 (Fig. 5.2C, D).

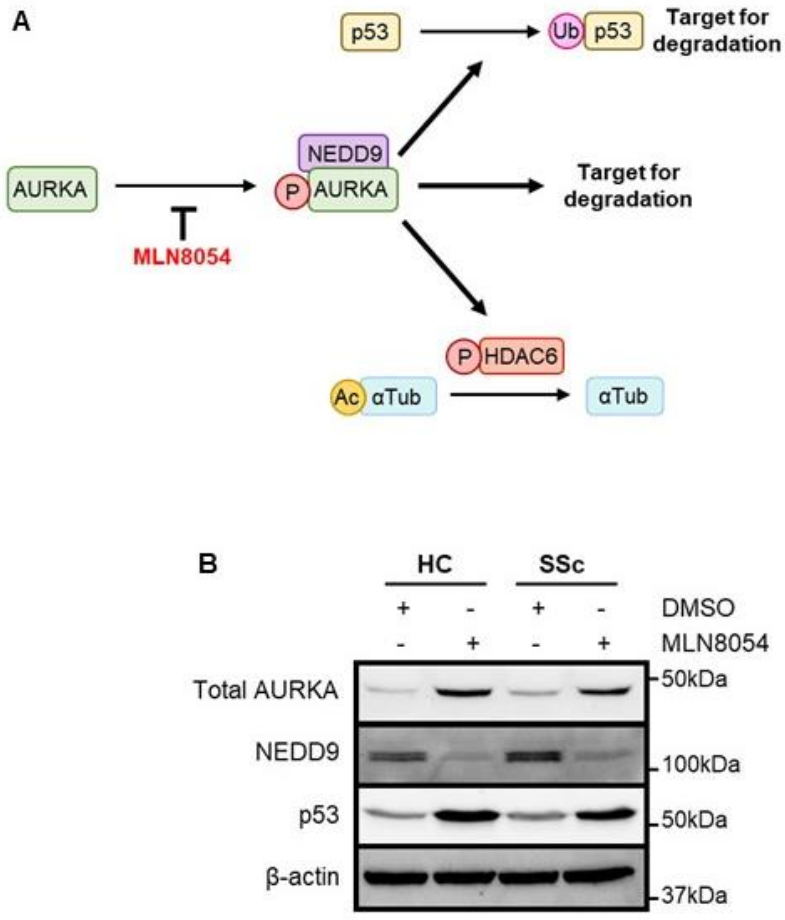

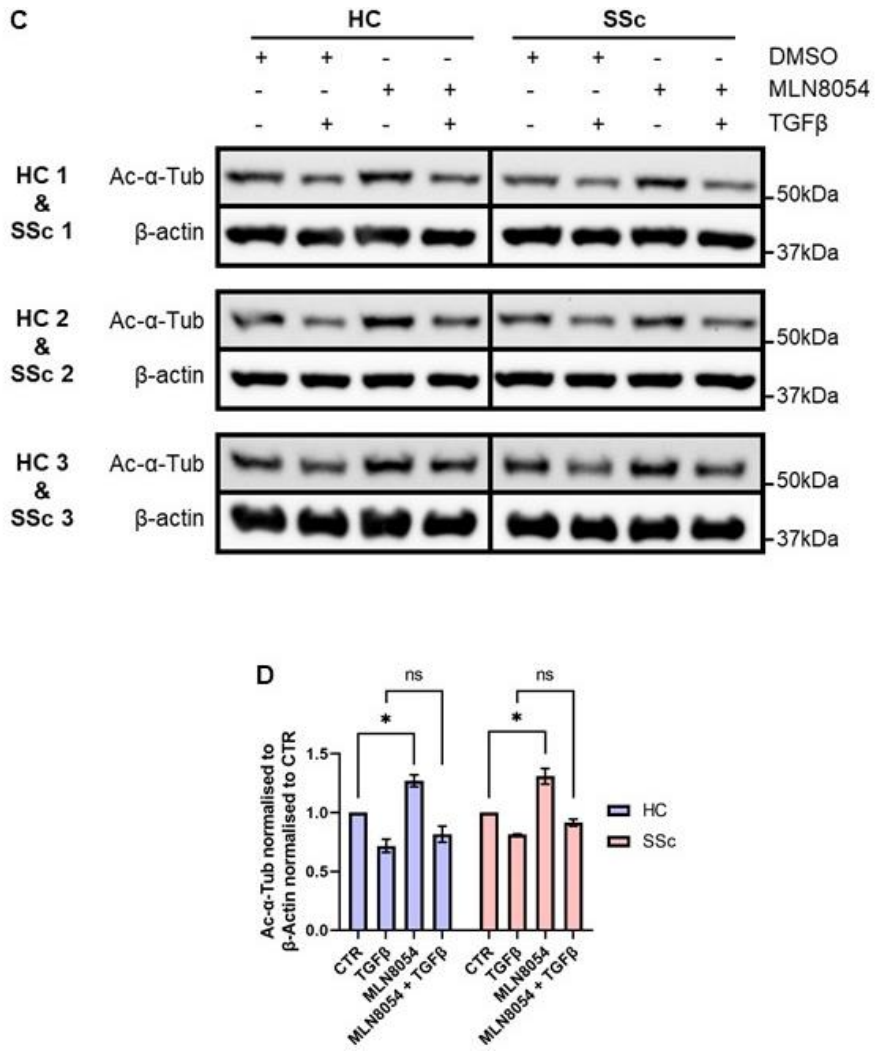

Figure 5.2: Analysis of the effect of MLN8054 on protein expression supports validation of inhibitor activity

HC and SSc fibroblasts at confluence were cultured in 0.5 % serum media for 24 h followed by 24 h treatment with 10 μM MLN8054 or DMSO control in 0.5 % serum media. In a second experiment, fibroblasts were treated with the same conditions with or without the addition of 10 ng/mL TGFβ for the final 24 h. Protein was harvested for quantification by Western Blot. A) Schematic showing the molecular interactions of AURKA relevant to this study, and the inhibition of AURKA autophosphorylation by MLN8054. B) Western Blots showing total AURKA, NEDD9, and p53 protein expression in response to treatments comprising of MLN8054 or DMSO control in one HC and one SSc fibroblast line. β-Actin included as a loading control. C) Western Blots showing Ac-α-Tub levels in response to treatments comprising of MLN8054 or DMSO control with or without TGFβ in three HC and SSc fibroblast lines. β-Actin included as a loading control. D) Ac-α-Tub densitometry of (C), normalised to each group's CTR. HC and SSc n=3. Bars show the mean of three

donor lines with error bars showing the standard error of the mean. P values were calculated with paired two-tailed t-tests (ns = non-significant, *P<0.05).

These data provide indirect evidence to support the notion that MLN8054 treatment efficiently inhibits AURKA kinase activity in dermal fibroblasts, justifying the continued use of MLN8054 for further research to investigate the potential role of AURKA in the short cilia phenotype of SSc fibroblasts.

5.2.2 Inhibition of Aurora A Kinase rescues cilia length in SSc fibroblasts

In order to determine whether AURKA activity is involved in an HDAC6-mediated ciliary shortening phenotype in SSc, AURKA was inhibited in HC and SSc dermal fibroblasts with MLN8054 and primary cilia were studied by immunofluorescence for Ac-α-Tub (Fig. 5.3A). AURKA inhibition had no effect on primary cilia incidence (Fig. 5.3B), but increased SSc cilium length from 2.8±0.2 μm (Mean±SEM) to 3.9±0.3 μm ($p<0.01$), while having no effect on cilium length in HC (4.2±0.2 μm vs 4.1±0.2 μm, not significant) (Fig 5.3C). The difference in length between HC and SSc cilia in control conditions (4.2±0.2 μm vs 2.8±0.2 μm, $p<0.0001$) was nullified upon treatment with MLN8054 (4.1±0.2 μm vs 3.9±0.3 μm, not significant) (Fig 5.3C). Visual representation of the distribution of cilia lengths within each population shows a shift in the length distribution of SSc cilia towards longer lengths upon treatment with MLN8054, but no change in HC cilia length distribution (Fig. 5.3D).

Inhibition of AURKA had no preventative effect on TGFβ-induced ciliary shortening in neither HC (TGFβ at 1.5±0.1 μm vs Tubacin + TGFβ at 1.7±0.1 μm) nor SSc (TGFβ at 1.5±0.1 μm vs Tubacin + TGFβ at 1.5±0.1 μm) (Fig.

5.3C). This suggests that TGFβ does not reduce ciliary length in dermal fibroblasts via an AURKA-dependent mechanism.

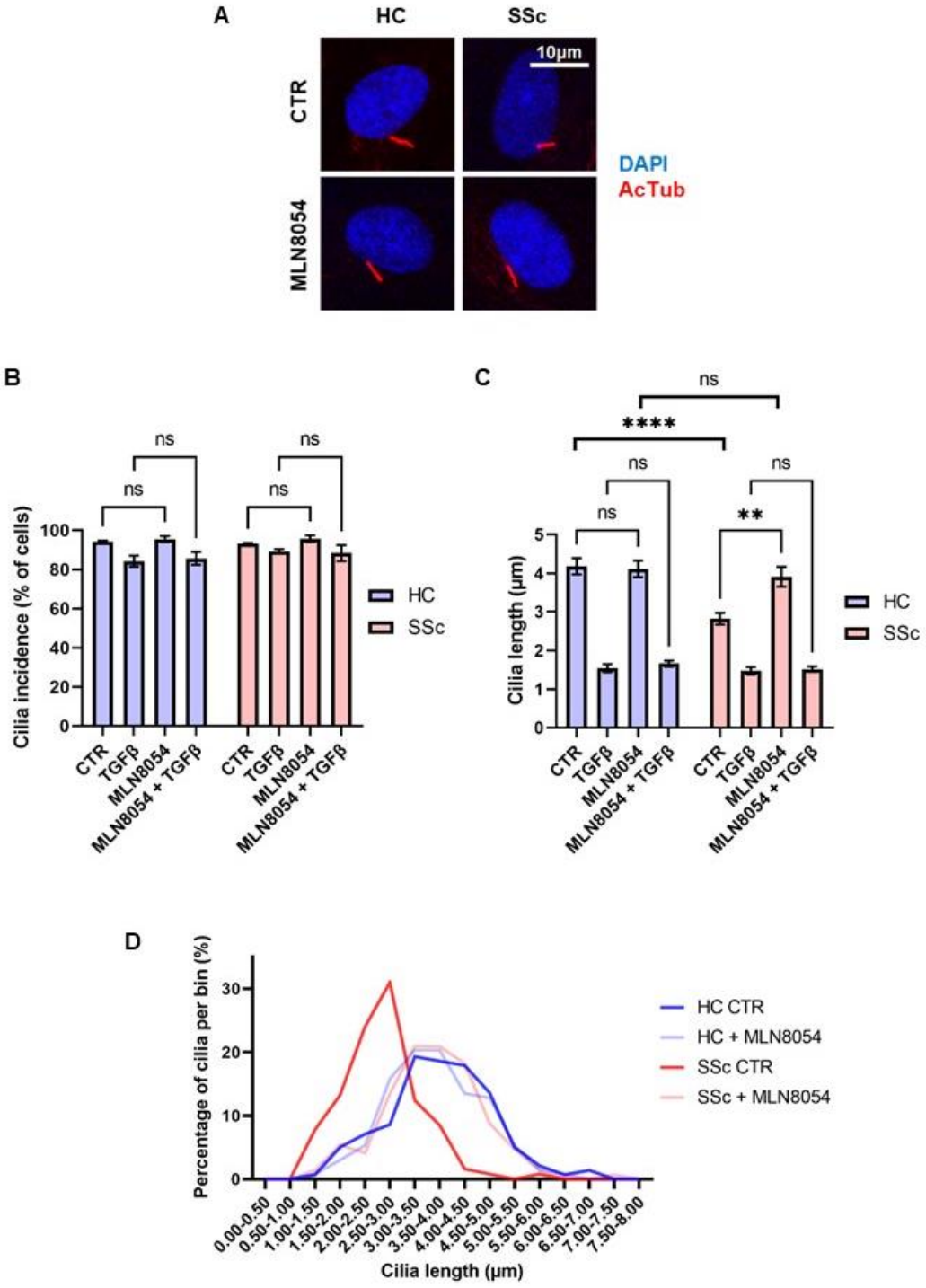

Figure 5.3: AURKA inhibition with MLN8054 rescues cilia length in SSc fibroblasts

HC and SSc fibroblasts at confluence were cultured in 0.5 % serum media for 24 h followed by 24 h treatment with 10 µM MLN8054 or DMSO control with or without 10 ng/mL TGFβ in 0.5 % serum media. Cilia were measured using immunofluorescence

for Ac-α-Tub. A) Representative immunofluorescence images taken at 400 x magnification showing cilia (stained for Ac-α-Tub in red) of individual fibroblasts (DAPI nuclear staining in blue). Scale bar shown at 10 μm. B) Cilia incidence changes in response to MLN8054/TGFβ treatment. C) Cilia length changes in response to MLN8054/TGFβ treatment. D) Distribution of cilia length in HC and SSc with and without MLN8054 treatment, showing the percentage of total cilia in each 0.5 μm length category. HC and SSc n=3. Bars show the mean and error bars show standard error of the mean. P values were calculated by two-way ANOVA with Tukey's multiple comparisons test (ns = non-significant, **P<0.01, ****P<0.0001).

These data, consistent with the observations upon HDAC6 inhibition, show an SSc-specific 'rescue' of cilia phenotype in response to AURKA inhibition, and suggest that aberrant activity of AURKA and subsequent activation of HDAC6 may be responsible for the shorter cilia phenotype of SSc dermal fibroblasts. They also support the notion that this stable ciliary phenotype may be independent of the influence of TGFβ on ciliary length.

5.2.3 The effect of Aurora A Kinase inhibition on the fibrotic phenotype of SSc fibroblasts at transcript level

In order to study the pathological relevance of AURKA-dependent ciliary shortening in SSc dermal fibroblasts, we first investigated the effect of AURKA inhibition with MLN8054 on gene expression by quantifying the expression of transcripts recognised in the literature as characteristic of SSc fibroblasts, and known to be induced by TGFβ during myofibroblast activation in SSc (Mouawad & Feghali-Bostwick, 2023). We selected a panel of genes comprising of *ACTA2*, *CCN2*, *FN1*, *COL1A1*, and *COL1A2*, and quantified expression using qPCR.

We first characterised basal expression levels of these transcripts in three HC and three SSc fibroblast cell lines from different donors. When results from these triplicate lines were combined, expression of all transcripts was higher in SSc compared to HC as expected, but not to statistical significance (Fig. 5.4A-E), due to high variability between donor lines. Basal expression levels of all five transcripts studied was higher in two of the three SSc fibroblast lines compared to all three of the HC lines. However, in one SSc fibroblast line (SSc 1), the expression of these transcripts was similar to HC (Fig. 5.4A-E). These results show variability between fibroblast cell lines obtained from different donors, with gene expression profiles which do not consistently align with the classical differences in transcript expression that might be expected in SSc vs HC but do reflect the heterogeneity of SSc in different patients (Sargent & Whitfield, 2011).

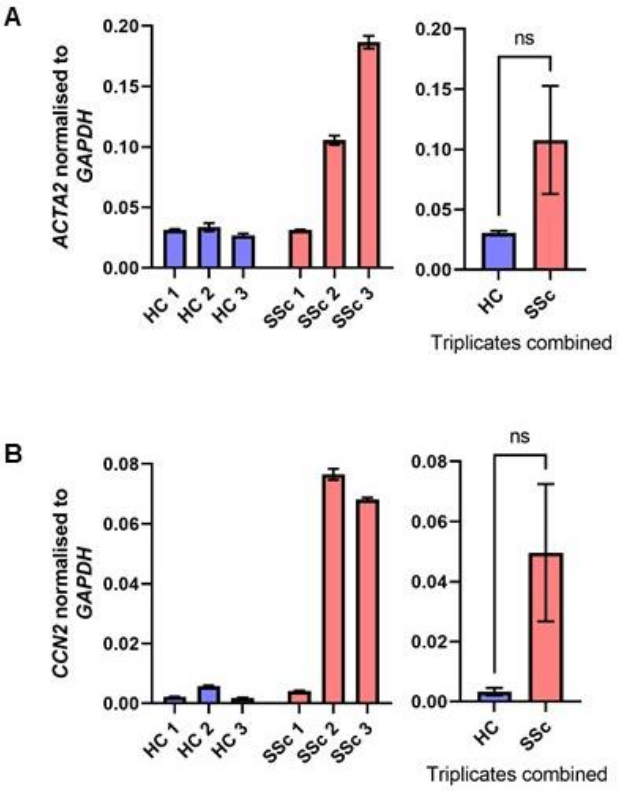

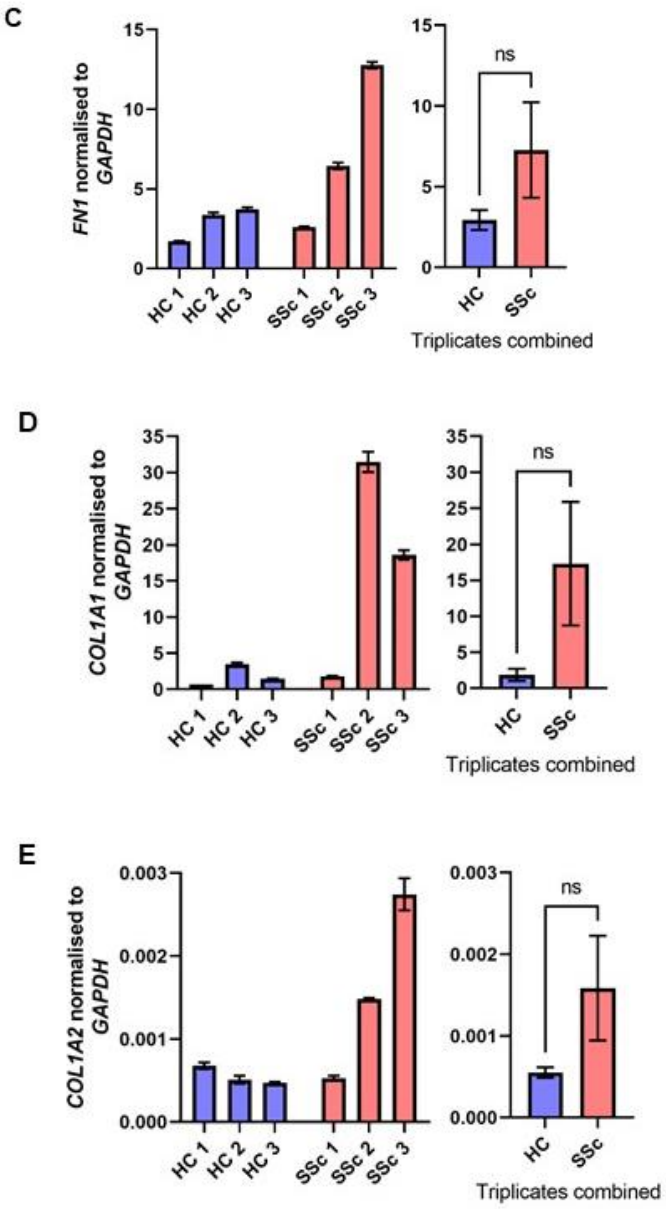

Figure 5.4: Transcript levels of classic fibrotic markers vary between individual donor fibroblast lines under basal conditions

HC and SSc fibroblasts at confluence were cultured in 0.5 % serum media for 48 h. RNA was harvested for quantification by qPCR, with normalisation to housekeeping gene *GAPDH*. A) Transcript levels of *ACTA2*. B) Transcript levels of *CCN2*. C) Transcript levels of *FN1*. D) Transcript levels of *COL1A1*. E) Transcript levels of *COL1A2*. HC and SSc n=3. Bars show the mean of triplicate well results for each transcript analysed in each donor line, or the mean of the three donor lines in combined triplicate graphs. Error bars show standard error of the mean. P values were calculated with unpaired two-tailed t-tests (ns = non-significant).

We next studied the effect on expression of these genes upon AURKA inhibition with MLN8054 compared to control in each donor cell line. As previously mentioned, these genes are not only myofibroblast-associated, but also known to be TGFβ-inducible. Numerous studies have suggested that the primary cilium plays a role in the fine-tuning of TGFβ signalling (Christensen et al., 2017). Therefore, we also quantified gene expression upon fibroblast stimulation with TGFβ alone, as well as TGFβ in combination with MLN8054, to investigate the possibility that inhibition of AURKA and subsequent rescue of SSc cilia length may change the way that fibroblasts respond to TGFβ.

For *ACTA2*, the response was varied between the cell lines (Fig. 5.5A). In SSc 2 and SSc 3, MLN8054 alone and in combination with TGFβ reduced *ACTA2* transcript levels compared to their respective controls. The same was not observed in SSc 1, interestingly the cell line with the lowest basal expression of all the SSc cell lines (Fig. 5.4A). MLN8054 treatment had little effect in HC cell lines, except for a reduction of *ACTA2* transcript levels with MLN8054 and TGFβ compared to TGFβ alone, in HC 2 alone.

Basal levels of *CCN2* transcript were reduced by MLN8054 treatment in all HC and SSc cell lines, while TGFβ-induced expression was reduced slightly by co-treatment with MLN8054 in all three SSc lines vs two of the three HC lines (Fig. 5.5B).

There was very little change observed in *FN1* transcript levels in any individual HC line, and a variable response between individual SSc lines, with MLN8054 causing a slight reduction of basal expression and TGFβ-induced expression in SSc 3, but a slight increase of TGFβ-induced expression in SSc 1 (Fig. 5.5C).

For *COL1A1*, we observed a slight and variable decrease in basal transcript expression in all HC and SSc lines with MLN8054, and a variable response to TGFβ plus MLN8054, with all lines showing a slight decrease in *COL1A1* transcript levels compared to TGFβ alone except for SSc 3 which remained roughly the same, and SSc 1 which showed a slight increase (Fig. 5.5D).

Changes in *COL1A2* transcript levels were highly variable between individual cell lines (Fig 5.5E). Basal expression compared to expression after treatment with MLN8054 stayed roughly the same in HC 3, SSc 1, and SSc 3, while decreasing in HC 1 and more obviously in SSc 2, and increasing in HC 2. Expression upon stimulation with TGFβ alone compared to TGFβ with MLN8054 was similarly variable, remaining roughly the same in HC 1, HC 2, and SSc 3, but increasing in HC 3 and SSc 1, and decreasing in SSc 2.

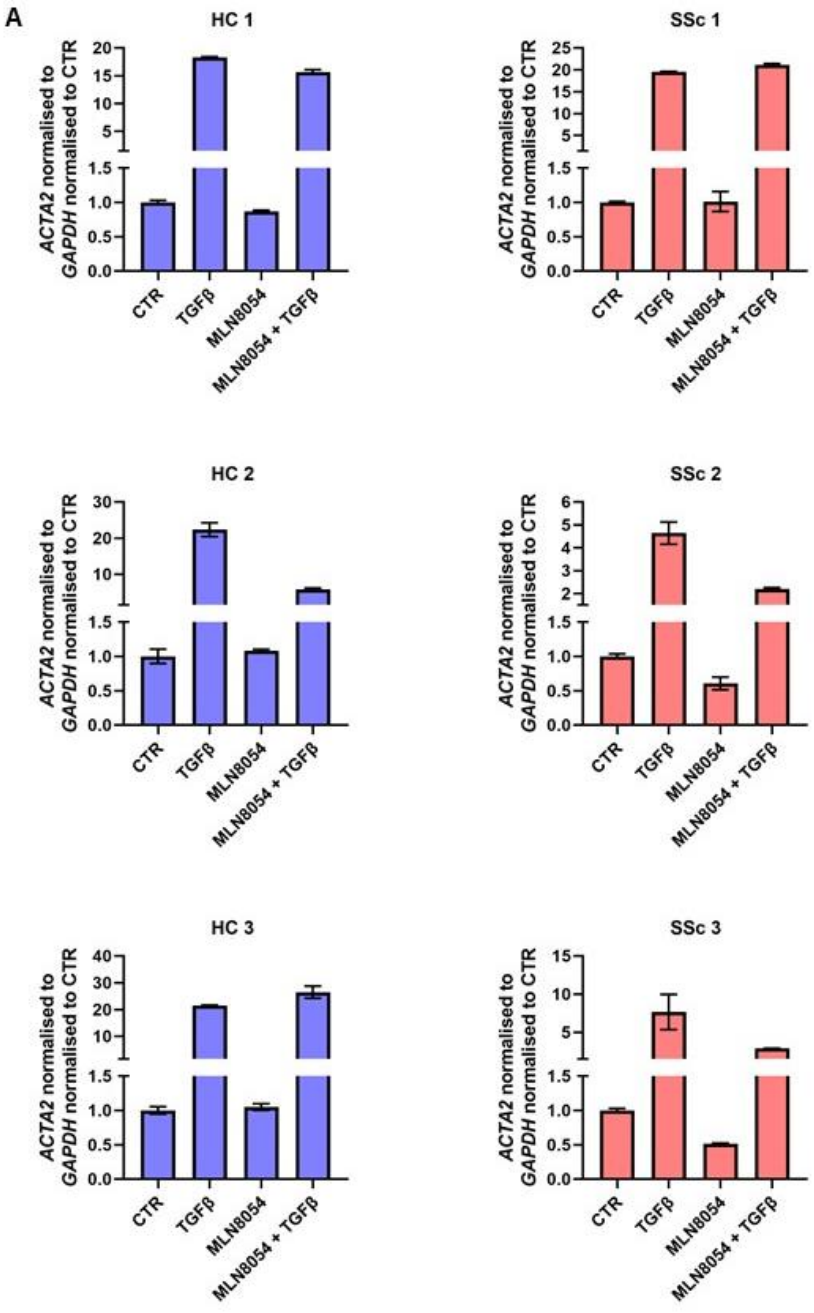
A
HC 1
SSc 1
HC 2
SSc 2
HC 3
SSc 3
ACTA2 normalised to GAPDH normalised to CTR
CTR
TGFβ
MLN8054
MLN8054 + TGFβ

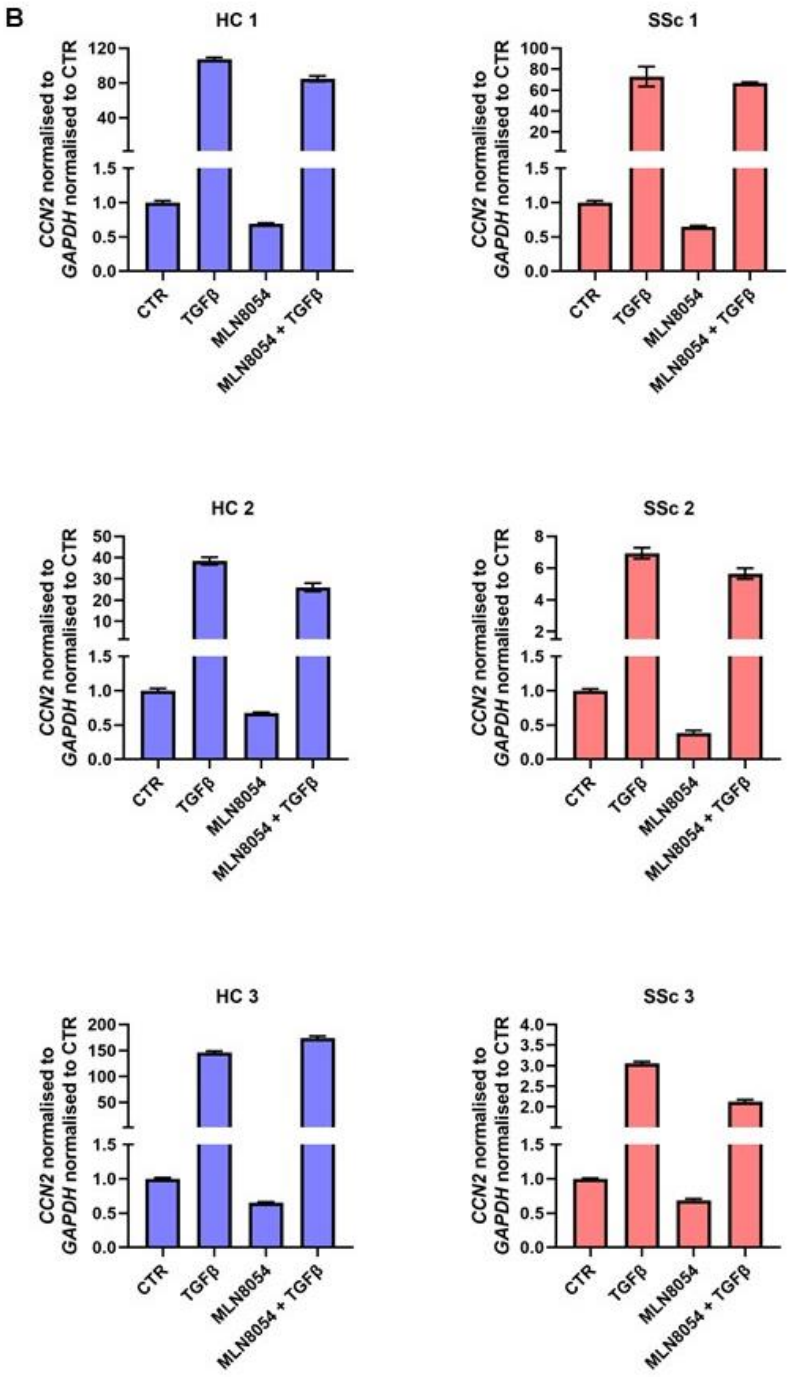
B
HC 1
SSc 1
HC 2
SSc 2
HC 3
SSc 3
CCN2 normalised to GAPDH normalised to CTR
CTR
TGFβ
MLN8054
MLN8054 + TGFβ

C

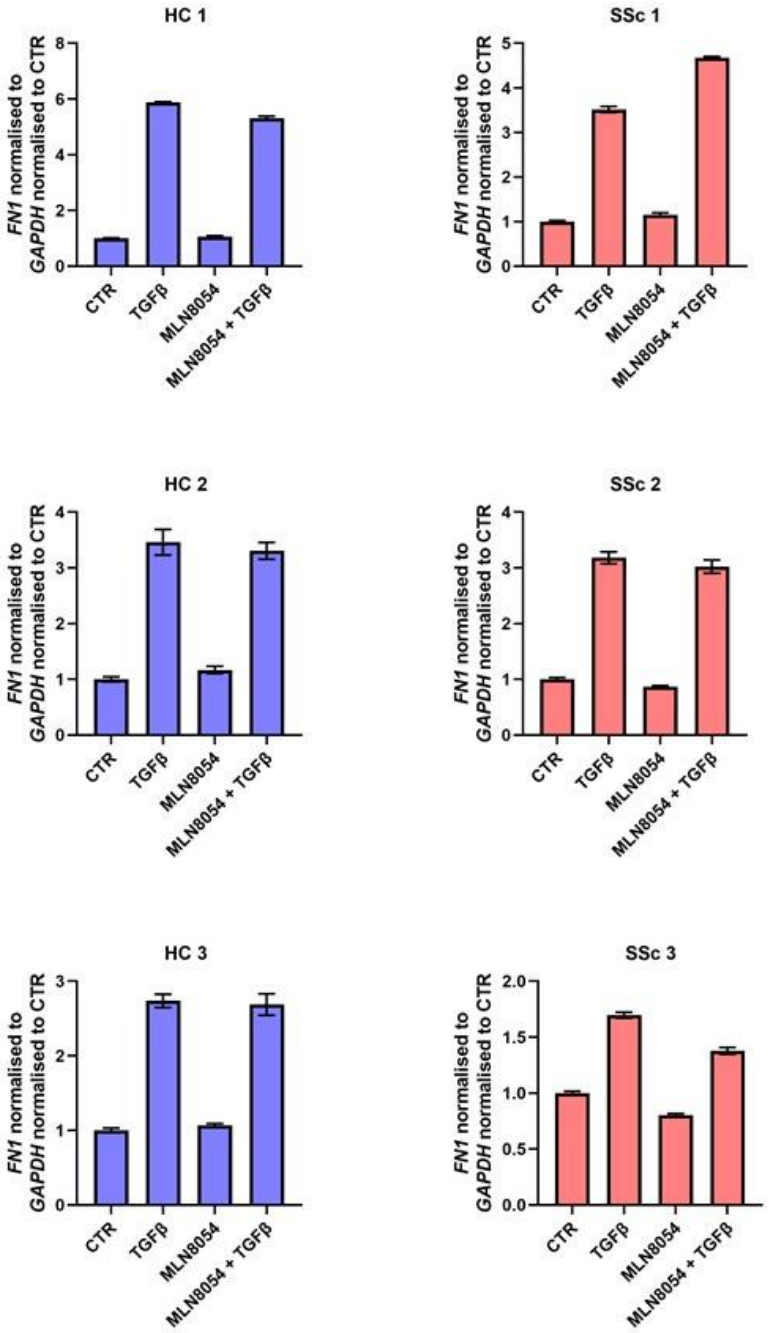
HC 1
SSc 1
HC 2
SSc 2
HC 3
SSc 3
FN1 normalised to GAPDH normalised to CTR
CTR
TGFβ
MLN8054
MLN8054 + TGFβ

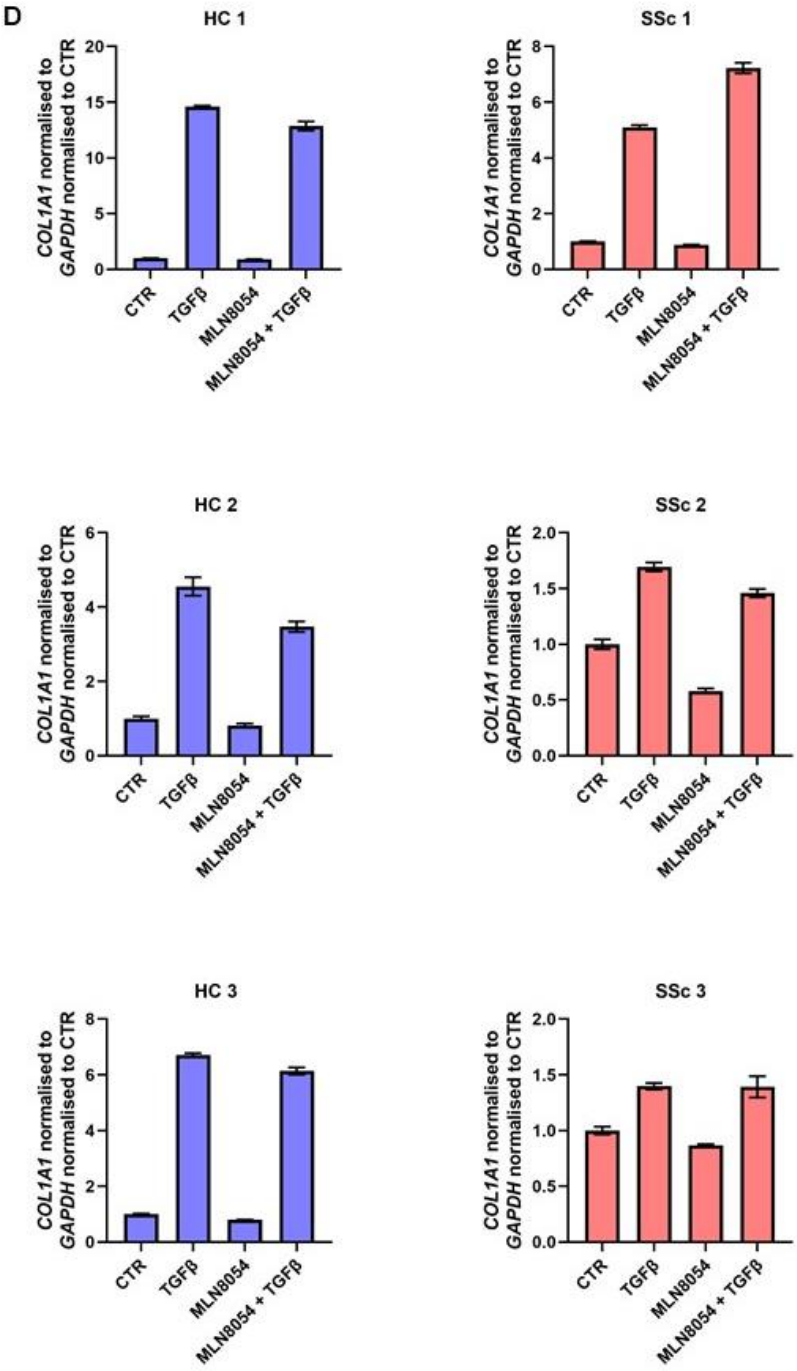
D
HC 1
SSc 1
HC 2
SSc 2
HC 3
SSc 3
COL1A1 normalised to GAPDH normalised to CTR
CTR
TGFβ
MLN8054
MLN8054 + TGFβ

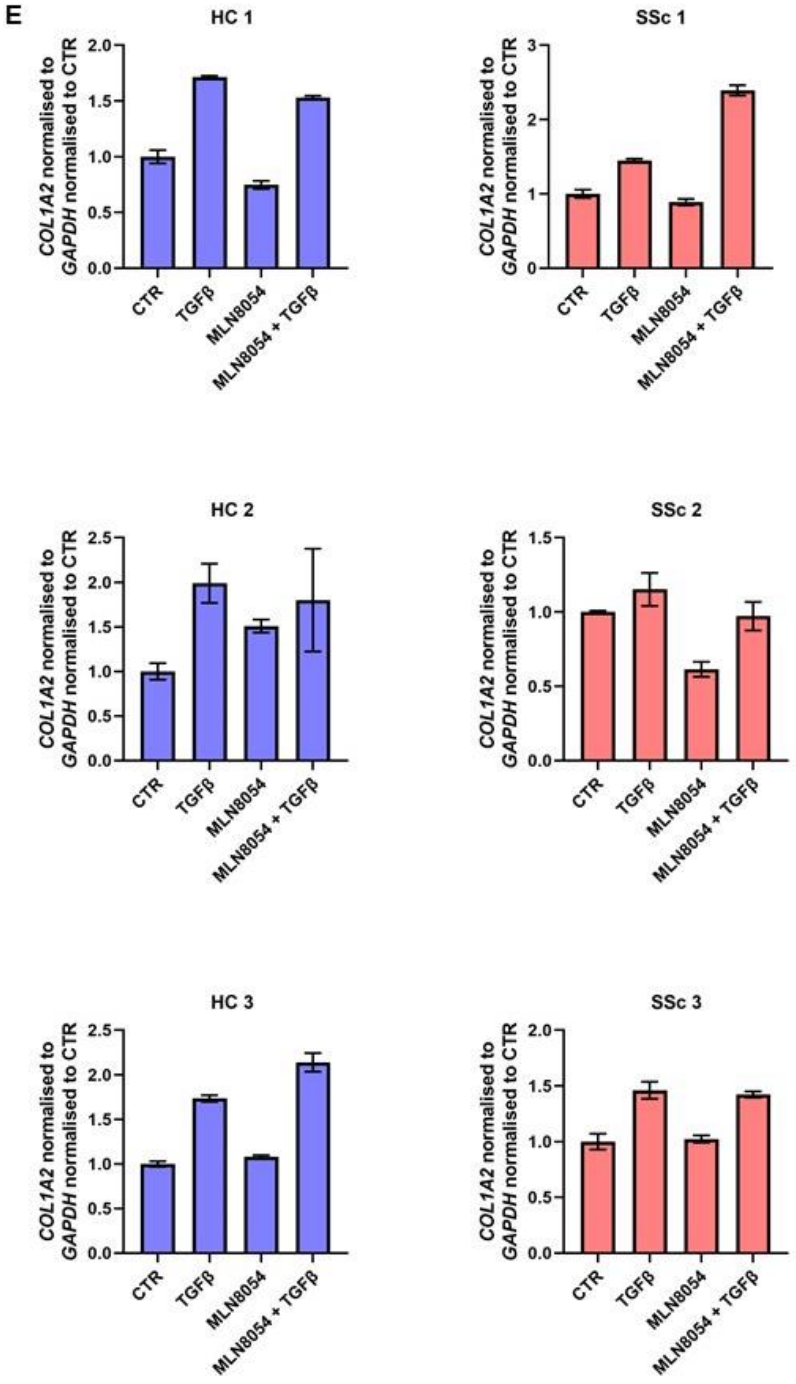

Figure 5.5: The effect of inhibition of Aurora A Kinase on the fibrotic phenotype of SSc fibroblasts at transcript level is varied, with some partial rescue of basal and TGFβ-induced expression in some cell lines

HC and SSc fibroblasts at confluence were cultured in 0.5 % serum media for 24 h followed by 24 h treatment with 10 μM MLN8054 or DMSO control in 0.5 % serum media, with or without the addition of 10 ng/mL TGFβ. RNA was harvested for quantification by qPCR, with normalisation to housekeeping gene *GAPDH*. A) Transcript levels of *ACTA2*. B) Transcript levels of *CCN2*. C) Transcript levels of *FN1*. D) Transcript levels of *COL1A1*. E) Transcript levels of *COL1A2*. HC and SSc n=3

donor lines. Bars show the mean of triplicate well results for each transcript analysed per condition in each cell line. Error bars show standard error of the mean.

Overall, inhibition of AURKA with MLN8054 did lead to partial reduction of both basal and TGFβ-induced expression of typical fibrosis-associated transcripts in SSc cell lines. However, this was variable between cell lines, with a lesser effect observed in general in the SSc 1 cell line, which showed basal expression more similar to HC cell lines than the other two SSc lines studied. Additionally, rescue was also not always SSc-specific. Therefore, it cannot be clearly demonstrated that inhibition of AURKA with MLN8054 is able to rescue the SSc phenotype at the level of gene expression, despite some data supporting this notion.

5.2.4 The effect of Aurora A Kinase inhibition on the fibrotic phenotype of SSc fibroblasts at protein level

Next, we studied the effect of AURKA inhibition with MLN8054 on the level of proteins well established in the literature as characteristic of SSc fibroblasts, and known to be induced in SSc by TGFβ during myofibroblast activation (Mouawad & Feghali-Bostwick, 2023). We selected a panel of these proteins comprising of αSMA, encoded by the *ACTA2* gene, CTGF, encoded by the *CCN2* gene, and the phosphorylated form of SMAD3 (pSMAD3), and quantified expression via Western Blot (Fig. 5.6A).

We first characterised basal levels of these proteins in three HC and three SSc fibroblast cell lines from different donors. When results from these triplicate lines were combined, expression of CTGF and abundance of pSMAD3 was higher in SSc compared to HC as expected, but not to statistical significance due to

variability between donor lines, while expression of αSMA was higher in HC than SSc (Fig. 5.6A-D).

Consistent with transcript expression analysis and reflective of the heterogeneity of SSc in different patients (Sargent & Whitfield, 2011), basal levels of all three proteins were highly variable between fibroblast cell lines obtained from different donors, and did not consistently align with the classical differences in protein levels that may be expected in SSc vs HC. CTGF protein expression was highest in SSc 3, with SSc 2 and HC 2 showing similar basal levels. SSc 1 basal levels were lower than HC 2, with the lowest levels in HC 3 and HC 1 (Fig. 5.6A, B). αSMA protein expression was highly variable, similar between HC 2, HC 3, and SSc 3. The next highest expression was in SSc 1, followed by HC 1 and SSc 2 (Fig. 5.6A, C). Levels of phosphorylated SMAD3 were higher in SSc 2 and 3 than in all HC lines, but lowest in SSc 1 (Fig. 5.6A, D).

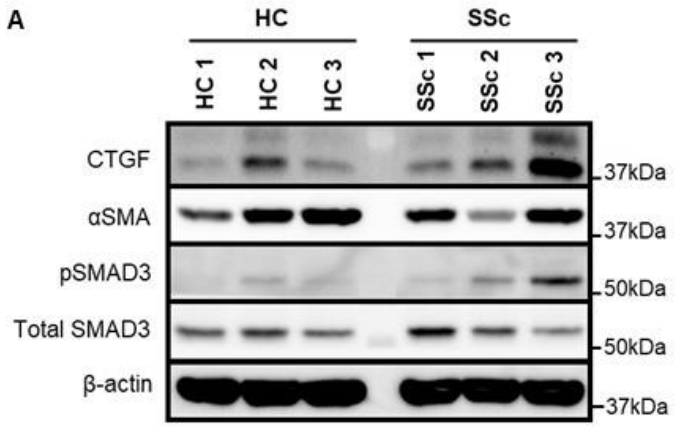

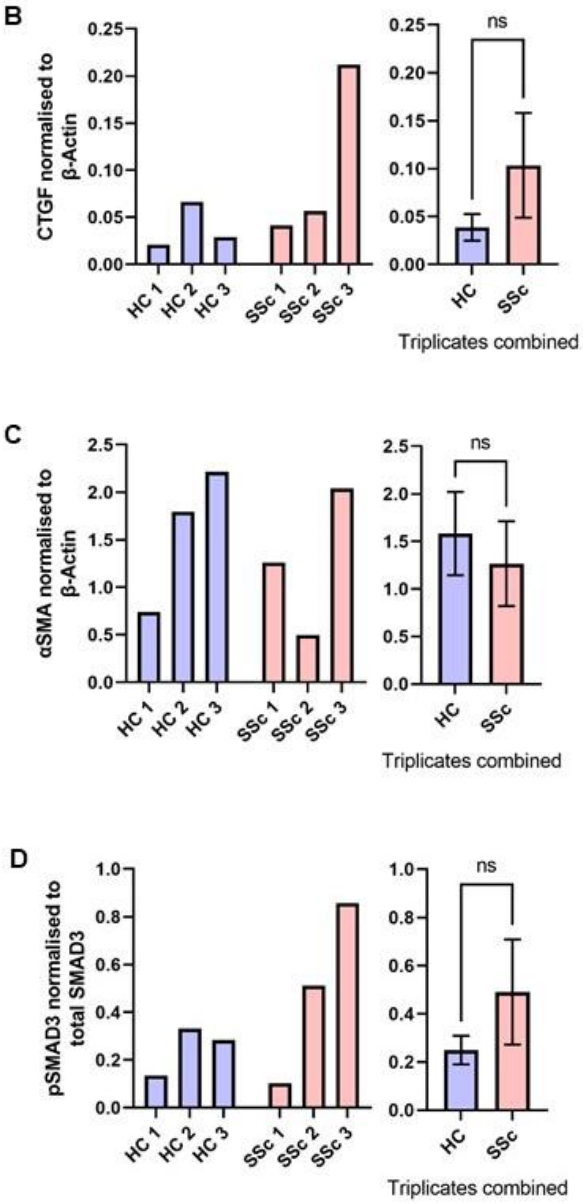

Figure 5.6: Levels of classic fibrotic marker proteins vary between individual donor fibroblast lines under basal conditions

HC and SSc fibroblasts at confluence were cultured in 0.5 % serum media for 48 h. Protein was harvested for quantification by Western Blot. A) Western Blots showing CTGF, αSMA, pSMAD3 and total SMAD3 protein in three HC and SSc fibroblast lines. β-Actin included as a loading control. B) CTGF densitometry of (A). C) αSMA densitometry of (A). D) pSMAD3/total SMAD3 densitometry of (A). HC and SSc n=3. Bars show the quantified protein levels from each individual donor line, or the mean of the three donor lines in combined triplicate graphs. Error bars show standard error of the mean. P values were calculated with unpaired two-tailed t-tests (ns = non-significant).

With this variability considered, we next studied the effect of MLN8054 treatment over 24 h and 48 h in each individual donor fibroblast line. Fibroblasts were also treated with TGFβ alone or in combination with MLN8054, to study any effect that AURKA inhibition and subsequent cilia length rescue may have on cellular response to TGFβ stimulation.

MLN8054 treatment for 24 h caused no real change to protein levels of αSMA under basal conditions in any individual cell line, but did reduce αSMA protein levels induced by TGFβ in HC 1 and HC 2, as well as in all three SSc lines (Fig. 5.7A, B).

CTGF protein levels after 24 h showed a similar trend to αSMA, with expression largely unchanged between CTR and MLN8054 conditions. A small reduction in CTGF when TGFβ stimulation was coupled with MLN8054 treatment compared to TGFβ alone was observed in HC 1 and HC 2, and in all three SSc lines (Fig. 5.7A, C).

Levels of phosphorylated SMAD3 (pSMAD3) after 24 h were varied in CTR vs MLN8054 conditions in different cell lines, with pSMAD3 levels increasing slightly in HC 1 and SSc 1, decreasing slightly in HC 2 and SSc 2, and staying roughly the same in HC 3 and SSc 3. Comparing co-treatment with TGFβ plus MLN8054 vs TGFβ alone, there was very little difference in any of the HC fibroblast lines, but there was a small reduction of pSMAD3 in all three SSc cell lines, of varying degrees (Fig. 5.7A, D).

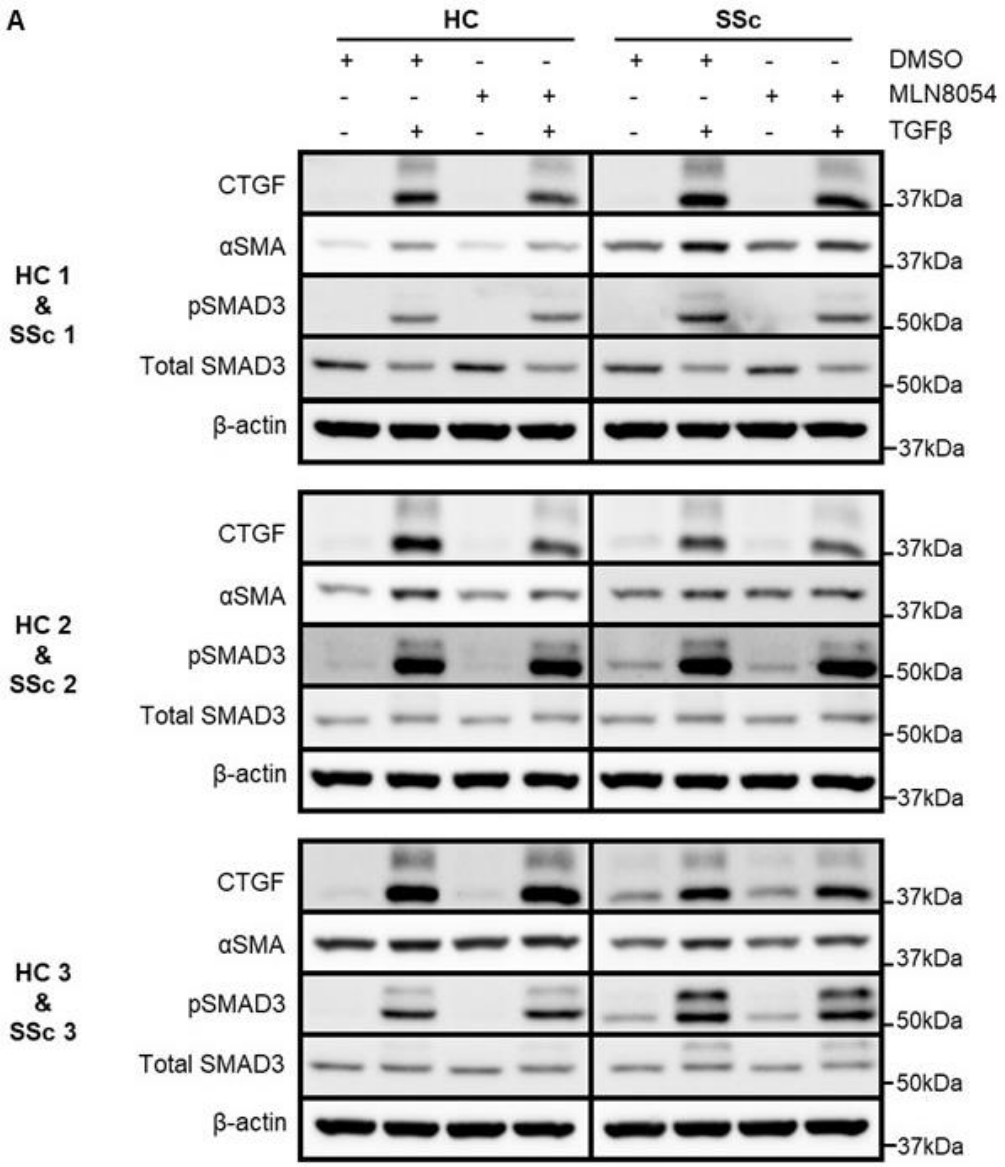
A
HC
SSc
DMSO
MLN8054
TGFβ
HC 1 & SSc 1
HC 2 & SSc 2
HC 3 & SSc 3
CTGF
αSMA
pSMAD3
Total SMAD3
β-actin
37kDa
50kDa

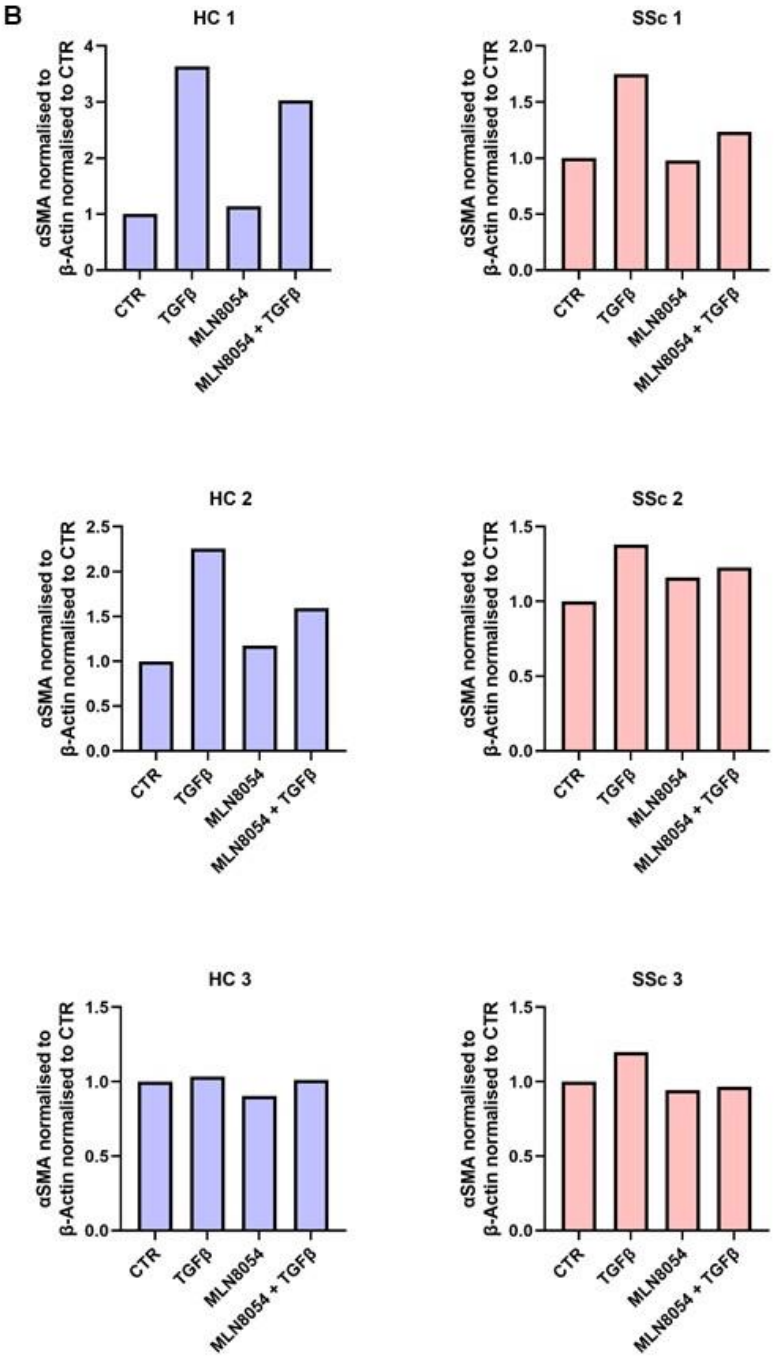
B
HC 1
SSc 1
HC 2
SSc 2
HC 3
SSc 3
αSMA normalised to β-Actin normalised to CTR
CTR
TGFβ
MLN8054
MLN8054 + TGFβ

C

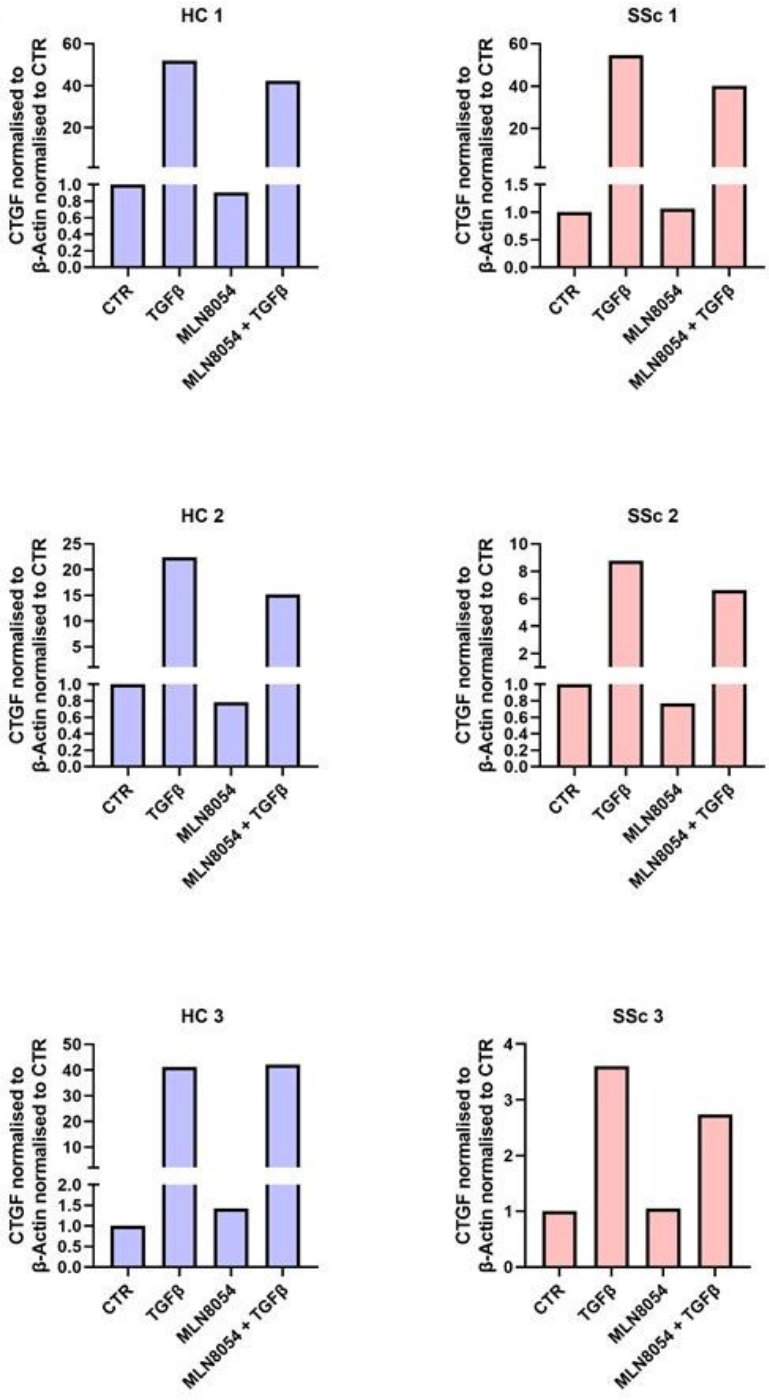
HC 1
SSc 1
HC 2
SSc 2
HC 3
SSc 3
CTGF normalised to β-Actin normalised to CTR
CTR
TGFβ
MLN8054
MLN8054 + TGFβ

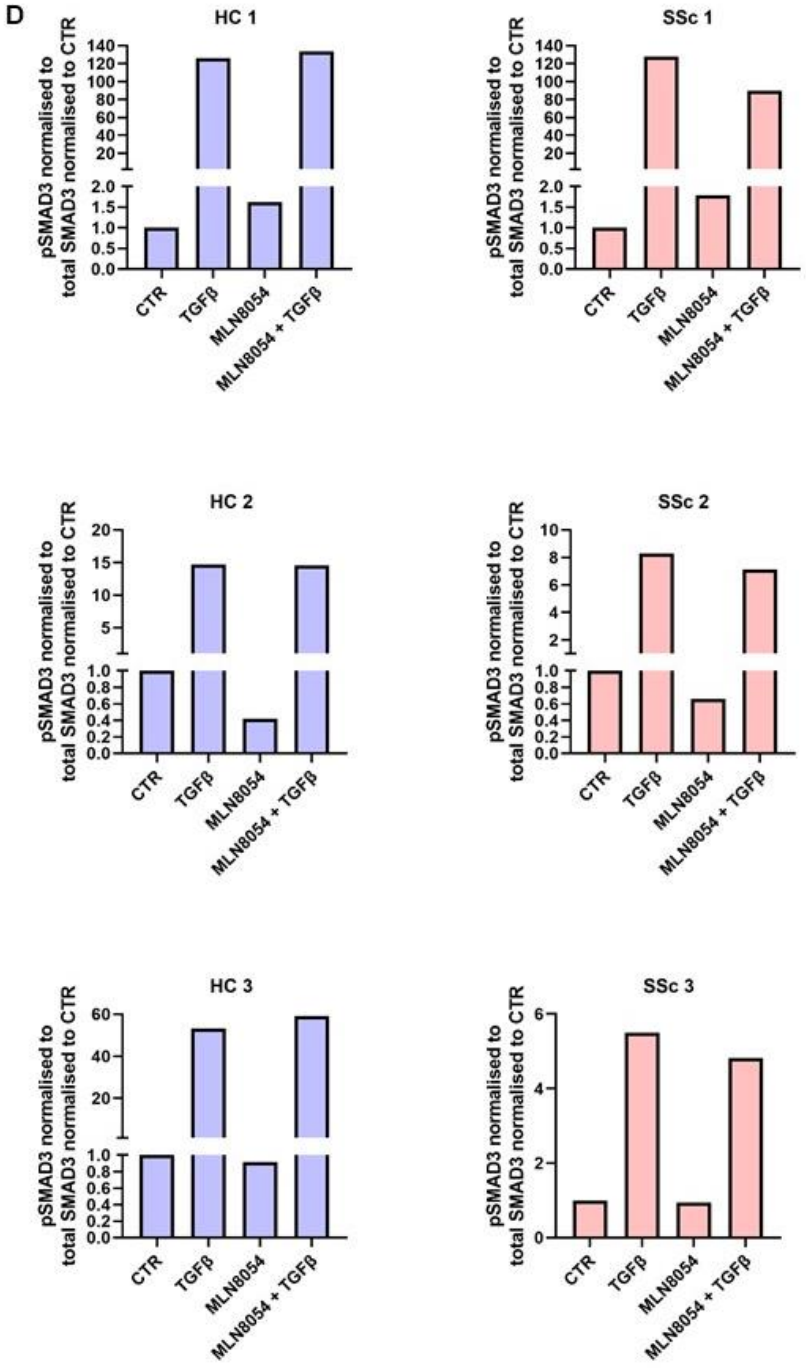

Figure 5.7: The effect of inhibition of Aurora A Kinase for 24 h on the fibrotic phenotype of SSc fibroblasts at protein level is varied, with some partial rescue of TGFβ-induced expression in some cell lines

HC and SSc fibroblasts at confluence were cultured in 0.5 % serum media for 24 h followed by 24 h treatment with 10 μM MLN8054 or DMSO control in 0.5 % serum media, with or without the addition of 10 ng/mL TGFβ. Protein was harvested for quantification by Western Blot. A) Western Blots showing CTGF, αSMA, pSMAD3 and total SMAD3 protein expression in response to treatments comprising of MLN8054 or DMSO control with or without TGFβ in three HC and SSc fibroblast

lines. β-Actin included as a loading control. B) αSMA densitometry of (A). C) CTGF densitometry of (A). D) pSMAD3/total SMAD3 densitometry of (A). HC and SSc n=3 donor lines. Bars show the levels of each protein analysed per condition in each cell line.

The effects of MLN8054 treatment on protein levels were more evident after 48 h. For αSMA, while there was no real difference in any individual cell line under basal conditions, there was a reduction in TGFβ-induced αSMA expression with MLN8054 co-treatment in all cell lines except for SSc 1, with the most dramatic reduction evident in SSc 2 and SSc 3 (Fig. 5.8A, B).

CTGF protein expression differences after 48 h MLN8054 treatment under basal conditions were minor but highly variable between donor lines, while a reduction in TGFβ-induced CTGF expression was observed in all six cell lines (Fig. 5.8A, C).

There was little change in TGFβ-induced pSMAD3 levels in any cell line after 48 h MLN8054 treatment, except for a slight reduction in HC 2 and SSc 2. For all HC lines, pSMAD3 level changes after 48 h MLN8054 treatment under basal conditions were varied, with a decrease in HC 1, an increase in HC 2, and HC 3 remaining roughly the same, while a reduction in pSMAD3 levels was observed in all three SSc lines (Fig. 5.8A, D).

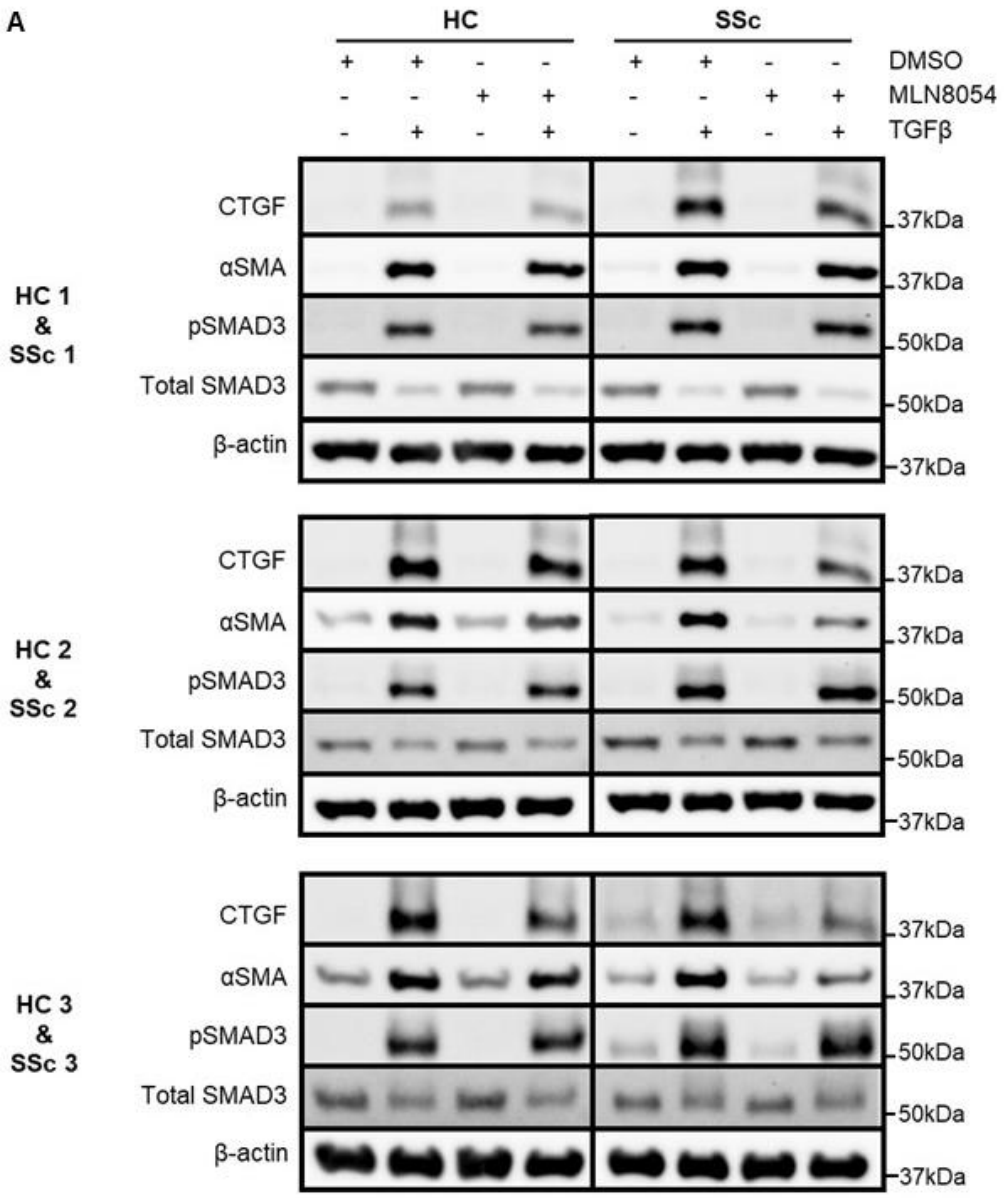
A
HC
SSc
+ + - - + + - - DMSO
- - + + - - + + MLN8054
- + - + - + - + TGFβ
HC 1 & SSc 1
CTGF
αSMA
pSMAD3
Total SMAD3
β-actin
37kDa
37kDa
50kDa
50kDa
37kDa
HC 2 & SSc 2
CTGF
αSMA
pSMAD3
Total SMAD3
β-actin
37kDa
37kDa
50kDa
50kDa
37kDa
HC 3 & SSc 3
CTGF
αSMA
pSMAD3
Total SMAD3
β-actin
37kDa
37kDa
50kDa
50kDa
37kDa

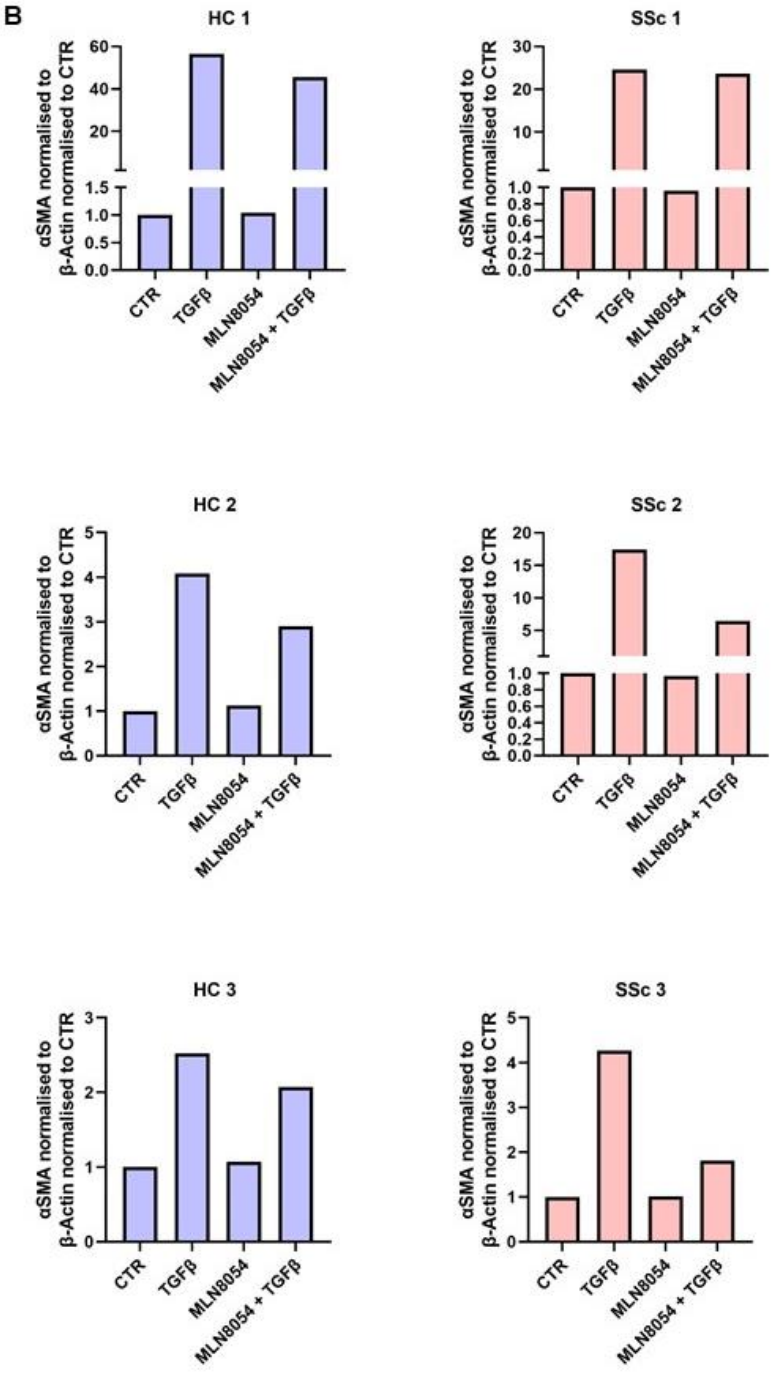
B
HC 1
SSc 1
HC 2
SSc 2
HC 3
SSc 3
αSMA normalised to β-Actin normalised to CTR
CTR
TGFβ
MLN8054
MLN8054 + TGFβ

C

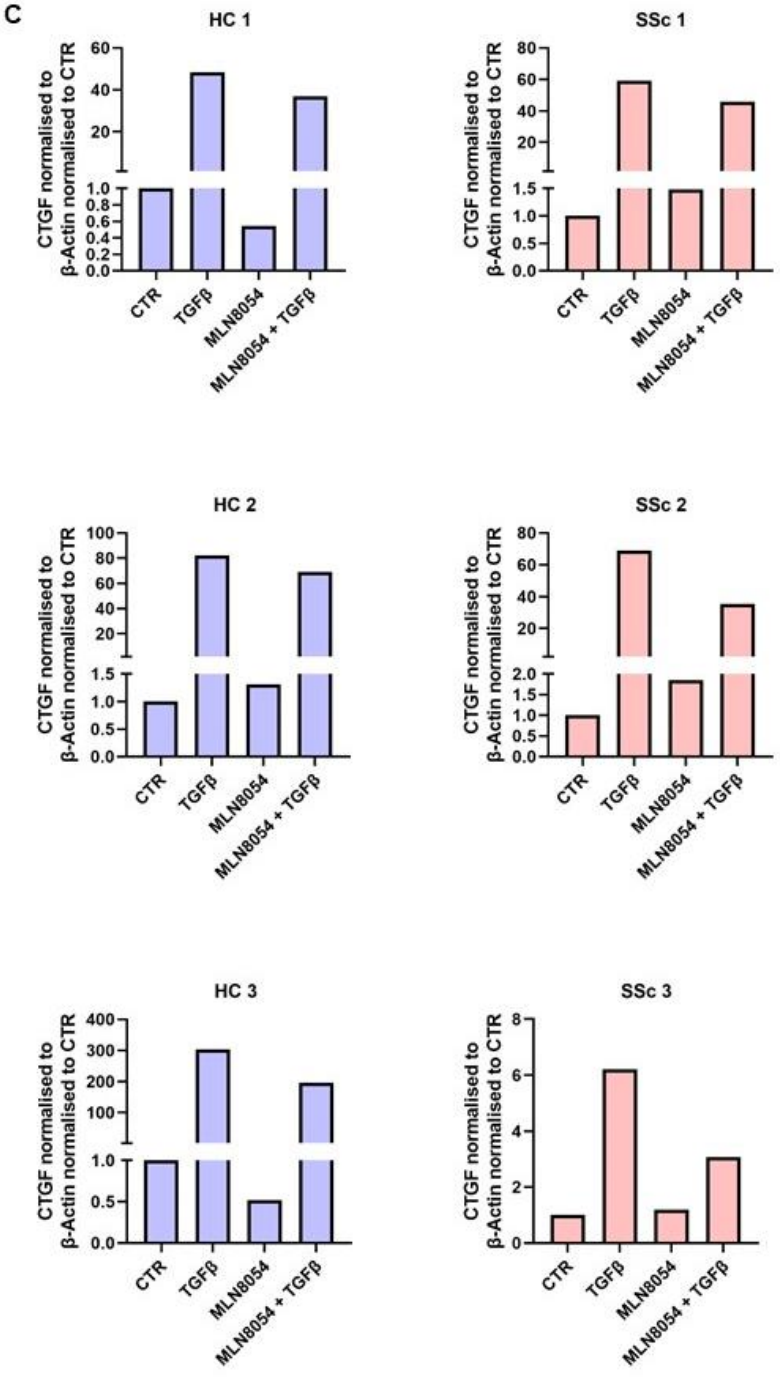
HC 1
SSc 1
HC 2
SSc 2
HC 3
SSc 3
CTGF normalised to β-Actin normalised to CTR
CTR
TGFβ
MLN8054
MLN8054 + TGFβ

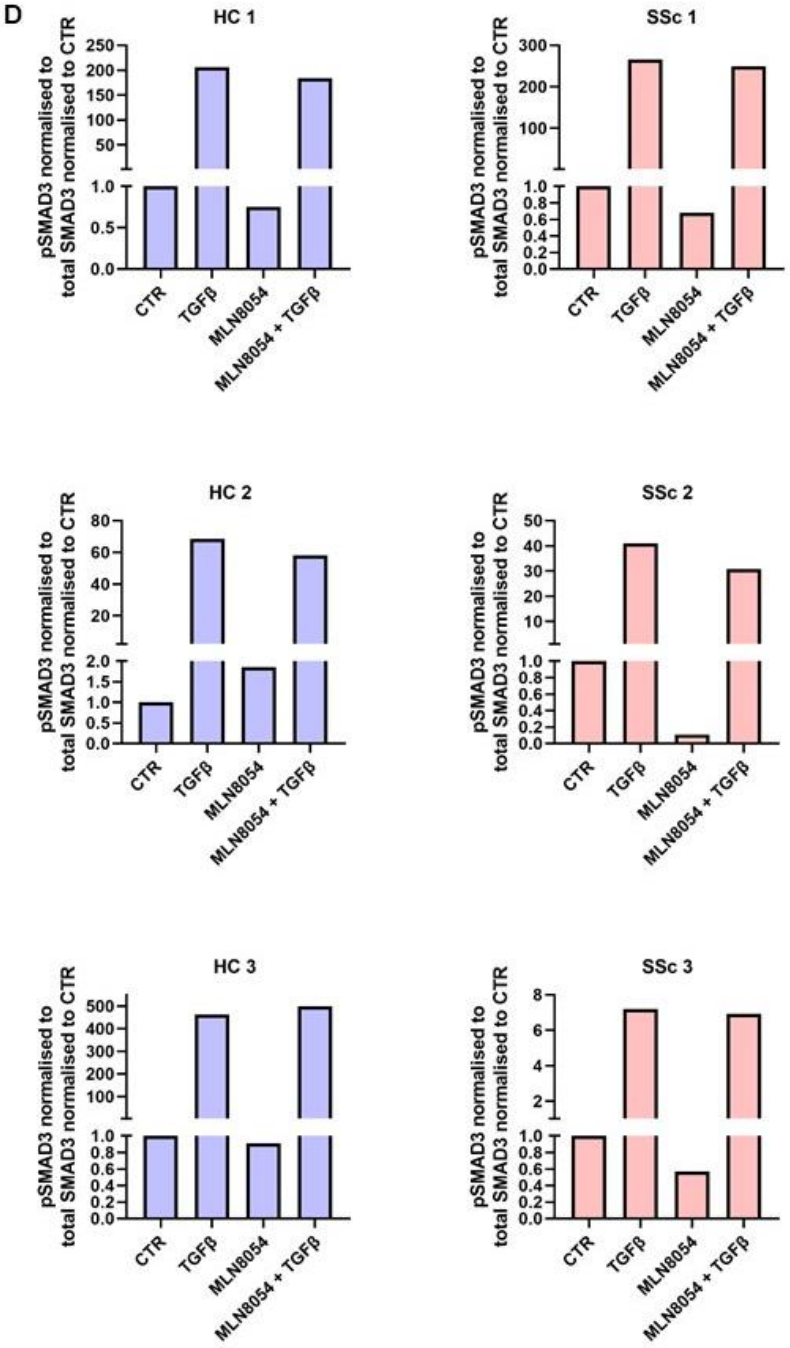

Figure 5.8: The effect of inhibition of Aurora A Kinase for 48 h on the fibrotic phenotype of SSc fibroblasts at protein level is varied, with some partial rescue of basal and TGFβ-induced expression in some cell lines

HC and SSc fibroblasts at confluence were cultured in 0.5 % serum media for 24 h followed by 48 h treatment with 10 μM MLN8054 or DMSO control in 0.5 % serum media, with or without the addition of 10 ng/mL TGFβ. Protein was harvested for quantification by Western Blot. A) Western Blots showing CTGF, αSMA, pSMAD3 and total SMAD3 protein expression in response to treatments comprising of MLN8054 or DMSO control with or without TGFβ in three HC and SSc fibroblast lines. B-Actin included as a loading control. B) αSMA densitometry of (A). C) CTGF

densitometry of (A). D) pSMAD3/total SMAD3 densitometry of (A). HC and SSc n=3 donor lines. Bars show the levels of each protein analysed per condition in each cell line.

In summary, these results confirm that inhibition of AURKA with MLN8054 leads to partial reduction of typical fibrosis-associated markers at the protein and transcript level under basal conditions and after TGFβ-stimulation in SSc cell lines. However, this effect varied among different donor cell lines, and rescue was not consistently SSc-specific. Therefore, these results do not provide conclusive evidence that AURKA inhibition with MLN8054 is able to rescue the SSc profibrotic phenotype at the protein and transcript level.

5.2.5 The effect of Aurora A Kinase inhibition on TGFβ-induced SSc fibroblast contractility

Although the effect of AURKA inhibition at the level of transcript and protein expression did not show a clearly consistent SSc-specific ‘rescue’ of fibrotic markers, the genes and proteins investigated were a selected panel that do not give a full and comprehensive representation of the fibrotic phenotype of these fibroblasts, especially considering the high variability of baseline marker expression between different donor cell lines. Therefore, we next carried out a functional collagen-cell contraction assay as a way to investigate the effect of AURKA inhibition on fibrotic phenotype at the functional level. In this assay, fibroblasts are cultured in a three-dimensional collagen matrix (Fig. 5.9A), which mimics tissue conditions, and in which fibroblast-mediated contraction can be studied by measuring the decrease in area of the gels over time. This gives a readout of contractile ability (Dallon & Ehrlich, 2008), reported as the gel area

(%) compared to the 0 h time point. In these experiments, stimulation with TGFβ was used to induce cell contraction mimicking the pathological TGFβ-induced fibrotic contraction of myofibroblasts in SSc skin. In this setting, stimulation with TGFβ treatment in the presence of MLN8054 was included to determine whether AURKA inhibition and subsequent cilia length rescue could reduce cell contractility.

While unstimulated SSc fibroblasts in basal, starved conditions (CTR) contracted only slightly more than HC after 48 h culture (Fig. 5.9B, C), and AURKA inhibition via MLN8054 in basal conditions gave rise to little change in the contraction of HC or SSc fibroblasts (Fig. 5.9C), upon stimulation with exogenous TGFβ, SSc fibroblasts contracted significantly more than HC (78.2±1.9 % vs 87.1±0.8 %, $p<0.01$) (Fig. 5.9B, C). Treatment with MLN8054 in combination with TGFβ had no effect in HC fibroblasts (85.9 ±1.5 %, not significantly different from TGFβ alone), but led to a significant amelioration of contraction in SSc fibroblasts (87.5±1.9 %, $p<0.0001$ compared to TGFβ alone). The increased contraction of SSc fibroblasts compared to HC fibroblasts in response to TGFβ was effectively rescued by co-treatment with MLN8054 (85.9 ±1.5 % for HC vs 87.5±1.9 % for SSc, not significantly different) (Fig. 5.9B, C).

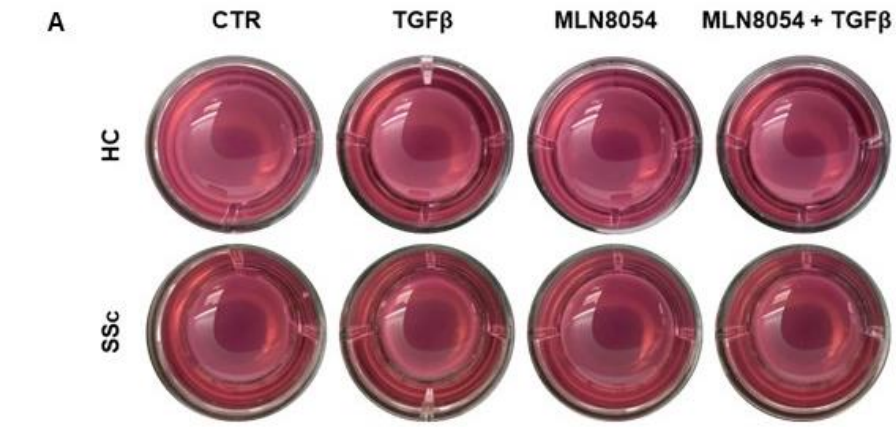
A
CTR
TGFβ
MLN8054
MLN8054 + TGFβ
HC
SSc

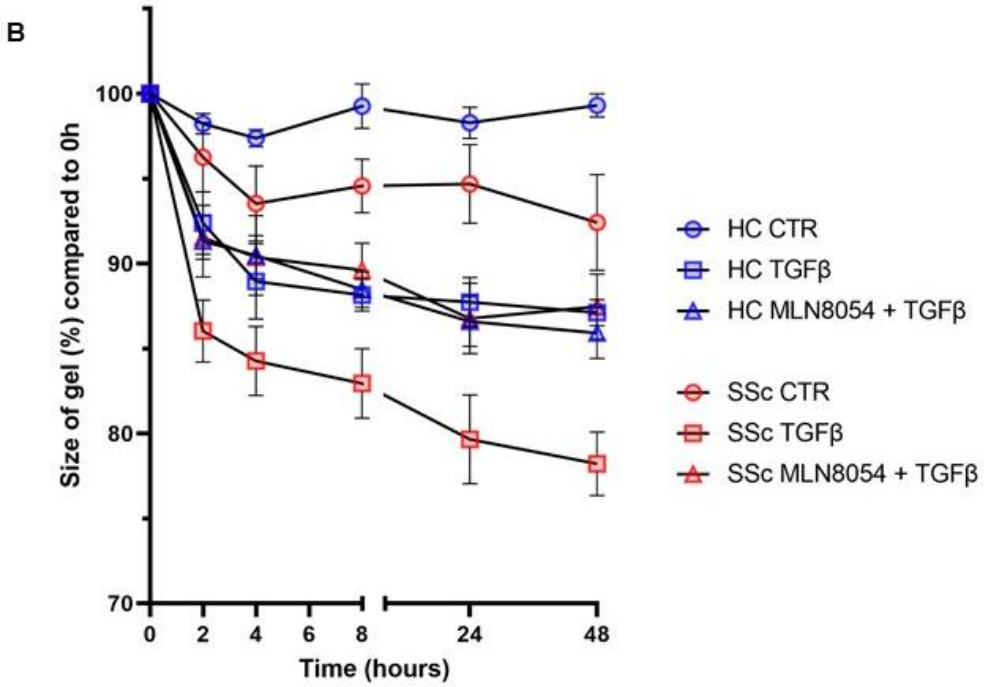
B
Size of gel (%) compared to 0h
100
90
80
70
0
2
4
6
8
24
48
Time (hours)
HC CTR
HC TGFβ
HC MLN8054 + TGFβ
SSc CTR
SSc TGFβ
SSc MLN8054 + TGFβ

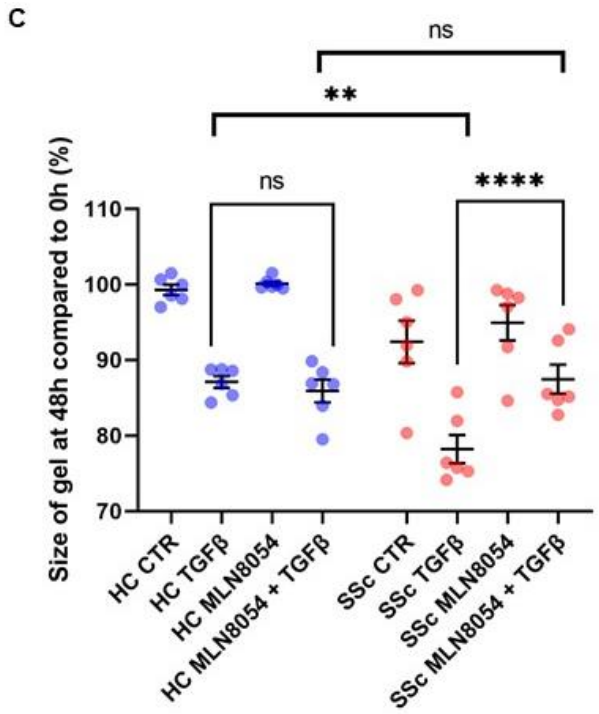

Figure 5.9: Inhibition of AURKA rescues the SSc fibroblast contractile phenotype in response to stimulation with TGFβ

HC and SSc fibroblasts at confluence were cultured in 0.5 % serum media for 24 h followed by 2 h pre-treatment with 10 μM MLN8054 or DMSO control in 0.5 % serum media. Fibroblasts were seeded into cell-collagen gels which were allowed to set, then incubated for 16 h in 10 μM MLN8054 or DMSO control in 0.5 % serum media, with or without the addition of 10 ng/mL TGFβ. Gels were released from the wells, and gel area measured at the indicated time points over a time course of 48 h. A) Representative images of cell-collagen gels taken at 48 h. B) Cell-collagen gel contraction in each of the experimental conditions, shown as the area of the gel at each time point, as a percentage of the gel area at 0 h. Each point plotted shows the mean and bars show standard error of the mean (HC and SSc n=3, carried out in duplicate). C) Gel areas of the 48 h time point of (B), with each replicate shown as an individual point. Box and whisker plots show the mean and standard error of the mean. P values were calculated with paired or unpaired two-tailed t-tests (ns = non-significant, **P<0.01, ****P<0.0001).

These data suggest that inhibition of AURKA reduces the contractile phenotype of SSc fibroblasts stimulated with TGFβ, in an *in vitro* model of the functional fibrotic capacity of fibroblasts in SSc patient skin.

5.3 Discussion

The results presented in this chapter suggest that the shortened primary cilia characteristic of SSc dermal fibroblasts are likely a consequence of hyperactivation of the AURKA-HDAC6 axis, which promotes ciliary disassembly. Additionally, as inhibition of either AURKA or HDAC6 activity (Chapter 4) did not interfere with the ability of TGFβ to shorten primary cilia, this work also adds evidence to support the notion explored in the previous chapter that the mechanism by which cilia are shortened in SSc is independent to the mechanism of TGFβ-induced shortening. It is, of course, important to note that all of the findings presented in this chapter are from experimental application of a single AURKA inhibitor. To validate these findings, it will be important to employ an additional method of inhibition of AURKA, such as with other commercially available inhibitors including MLN8237 (Görgün et al., 2010).

The proposed link between AURKA and primary cilia in SSc in this work is novel. In a genome-wide gene expression study across three independent cohorts of SSc patients, AURKA was found in a set of upregulated genes identified as a conserved core expression signature (Mahoney et al., 2015). Beyond this, however, no previous research has directly linked AURKA to the pathogenesis of SSc. Therefore, the current study is the first to demonstrate a potential role for AURKA in SSc, and to implicate the kinase in an aberrant primary cilia phenotype.

The suggestion that AURKA-HDAC6 dysregulation can cause pathogenic ciliary defects is human disease is not novel. Such a mechanism has been explored most extensively in von Hippel-Lindau syndrome (VHL) in recent years. VHL is a hereditary condition resulting from loss-of-function mutations in the VHL tumour suppressor gene, and is marked by the development of both benign and

malignant cysts and tumours in various organs, including clear cell renal cell carcinoma (ccRCC) (Varshney et al., 2017). Immunohistochemistry of ccRCC tissue first identified a correlation between loss of VHL and overexpression of AURKA (Ferchichi et al., 2012). Soon after, an investigation into primary cilia frequency – but not length – in renal epithelia from patients with VHL-associated ccRCC identified primary cilia loss as characteristic in these tissues (Basten et al., 2013). A follow-up study investigated the mechanism by which loss of VHL leads to ciliary loss in VHL-deficient ccRCC cell lines (Dere et al., 2015). It was found that VHL deficiency leads to activation of the transcription factor β-catenin, and that β-catenin transcriptionally induced AURKA expression, leading to a reduced frequency of primary cilia as well as reduction of cilium length by around 50-60 %. Additionally, inhibition of β-catenin was demonstrated to reduce AURKA and HDAC6 levels and restore normal cilia frequency and length in VHL-knockdown cells. Several subsequent studies expanded on these findings, showing that VHL deficiency also reduces proteasomal degradation of AURKA, leading to reduction in ciliary frequency and length, which was prevented by inhibition of both AURKA and HDAC6 (Hasanov et al., 2017). Since then, a screening of small molecule compounds which rescued cilia defects in VHL-deficient cells identified Bexarotene (Chowdhury et al., 2018). Crucially, here the authors demonstrated that treatment with Bexarotene rescued cilia defects by decreasing AURKA phosphorylation, and that this correlated with reduced malignancy in a mouse model of RCC. Similar results were again obtained in a study utilising an alternative compound to modulate AURKA expression and restore defective cilia in VHL-deficient cells (Chowdhury et al., 2021). Application of some of these findings to the evaluation of primary cilia in SSc, for example with inhibition of β-catenin, which is a known

mediator of SSc fibrosis (Beyer et al., 2012), or with compounds identified in these studies, would be extremely interesting.

A role for AURKA-HDAC6 in pathogenic ciliary defects has also been proposed in cancers other than those associated with VHL. Cholangiocarcinoma (CCA), has been associated with defective primary cilia, and a recent study showed that inhibition of HDAC6 lengthened primary cilia in the CCA cell line HuCCT1, which correlated with decreased cell proliferation and invasion (Peixoto et al., 2020). A reduction in cilia incidence was also recently demonstrated in oral squamous cell carcinoma (OSCC) tissues, along with abnormal activation of AURKA by EGFR (Yin, Chen, et al., 2022). In this study, lentiviral silencing of AURKA restored primary cilia and decreased tumour growth *in vivo*. Interestingly, the length of primary cilia in OSCC was not different from control, only the incidence, and thus Yin et al. proposed that HDAC6 was not involved in this particular mechanism in OSCC. This suggests that the involvement of AURKA in pathogenic ciliary defects may be varied in both presentation and mechanism in different disease contexts. Analysis of primary cilia-deficient cells in bladder cancer also recently implicated AURKA as a mediator of cilia disassembly induced by SCL/TAL1 interrupting locus (STIL) (J. Li et al., 2023). Li et al. suggest that this contributes to dysfunctional cilia, malignancy, and interestingly to aberrant SHH signalling activation – a morphogen signalling pathway also dysregulated in SSc (Horn, Palumbo, et al., 2012).

Recently, reduced ciliary incidence was demonstrated in cardiac tissue from patients with the cardiac condition atrial fibrillation (AF), which can present with cardiac fibrosis, compared to healthy controls, along with elevated expression of *AURKA* and its coactivator *NEDD9* (Kawasaki et al., 2024). Pharmacological inhibition of AURKA in atrial fibroblasts isolated from AF patients increased

ciliary incidence and length, and reduced expression of fibrotic markers, leading Kawasaki et al. to suggest that aberrant AURKA hyperactivity in AF may contribute to its fibrotic pathogenesis in a cilia-dependent manner. The shared implication of aberrant activation of AURKA and subsequent ciliary aberrations in AF by Kawasaki et al, and in SSc in this study, warrants its investigation in other fibrotic diseases.

Collectively, this research demonstrates that aberrant AURKA activity can be associated with pathogenic ciliary defects in human diseases including cancer and the cardiac condition AF. The current study is the first to suggest that SSc may be one such disease, and highlights the need for more extensive research to elucidate the role that AURKA may play in the shortened primary cilia phenotype in SSc and importantly, what pathogenic relevance this may have. Therefore, in addition to investigating the effect of AURKA inhibition on cilia length, this study also assessed its effect on the fibrotic phenotype of SSc dermal fibroblasts, by investigating expression of fibrosis-associated genes and proteins, and fibroblast contractility.

At the gene and protein level, inhibition of AURKA and/or rescue of cilia length correlated with a small reduction in the expression and abundance of some typical fibrosis-associated transcripts and proteins in some donor lines. In particular, the induction of these in response to TGFβ-treatment was reduced in some experimental data. These findings may, in part, be reflective of the experimental conditions. While cilia rescue was evident after 24 h of inhibition of AURKA in 0.5 % serum culture media, the knock-on effect on gene and protein expression may not be evident until later and, perhaps, would require re-entry into the cell cycle. It is possible that ciliary length rescue for longer time periods or in cells in complete media which are actively cycling may give a more

informative insight into the consequences of AURKA inhibition-mediated ciliary length rescue. While long-term inhibition of AURKA in cultured cells presents experimental challenges due to its central role in facilitating mitosis (Nikonova et al., 2013), as well as additional non-mitotic functions (Bertolin & Tramier, 2020), long-term HDAC6 inhibition could present an alternative approach. To gain clarity on the effect of AURKA inhibition on gene and protein expression, it would also be useful to increase the number of donor fibroblast lines subjected to these analyses.

It is also important to note that the transcripts and proteins assessed in this study represent a narrow selection of the vast number that have been implicated in fibrosis. Comprehensive analysis using techniques such as RNA-Sequencing or proteomics after AURKA inhibition would give greater insight into the consequences on gene and protein expression at a more global scale.

Despite the limited reduction of fibrosis-associated genes and proteins, inhibition of AURKA and rescue of cilium length did correlate with a reduction of the increased contractile response of SSc dermal fibroblasts to TGFβ, to the same level as healthy controls. It is therefore pertinent to consider that shortened SSc dermal fibroblast primary cilia associated with AURKA activity may contribute to their heightened fibrotic response to TGFβ. It would be interesting to use similar experiments to those described in this chapter to explore any effect of AURKA inhibition on other signalling pathways, which are known to be dysregulated in SSc and coordinated by the primary cilium, such as the Sonic Hedgehog and Wnt pathways (Horn et al., 2012, Dees & Distler, 2013).

While it is possible that our findings upon inhibition of AURKA could be associated with inhibition of cilia-independent functions of AURKA (Nikonova et al., 2013, Bertolin & Tramier, 2020), the fact that HDAC6 inhibition with Tubacin also lengthened SSc primary cilia without affecting HC cilia supports the notion that hyperactivation of the AURKA-HDAC6 axis is implicated in the ciliary phenotype of SSc. Furthermore, data from our collaborators showed that both lithium chloride-mediated and Tubacin-mediated elongation of primary cilia in SSc dermal fibroblasts correlated with reduced expression of αSMA (Verma et al., 2024). Additionally, AF patient-derived fibroblasts treated with PHA-680632, a selective AURKA inhibitor, showed reduced expression of fibrotic markers including *FN1*, *CTGF*, and *COL1A1*, particularly that which was induced by exogenous TGFβ treatment (Kawasaki et al., 2024). Together, these data provide independent corroboration to suggest that the AURKA-HDAC6-fibrotic phenotype link is cilia-dependent, and that it may also be implicated in fibrotic conditions other than SSc. To prove that reduced cilium length is implicated in increased fibrotic gene expression and function, specific modulation of structural or functional components of primary cilia independent of AURKA could be explored as experimental means to artificially lengthen cilia, followed by assessment of functional ‘rescue’. For example, inhibition of a negative regulator of cilia length, ciliogenesis-associated kinase 1 (CILK1), has recently been demonstrated to experimentally increase cilia length (E. X. Wang et al., 2022).

While it will be important to fully understand whether the phenotypic effects of AURKA inhibition which ameliorate the fibrotic phenotype are indeed a direct result of ciliary length rescue, further research to understand the role of AURKA

in fibrosis independently of its role in cilia regulation may provide important insight to inform our understanding of the disease.

It is interesting that ciliary length in SSc fibroblasts is consistently similar between the different donor cell lines utilised in this study, despite the heterogeneity of their gene and protein expression phenotypes typical of patient heterogeneity within SSc (Allanore et al., 2015), and that the cilia length of all SSc lines was restored to normal levels by AURKA inhibition. This could indicate that AURKA-HDAC6 mediated ciliary shortening may be intrinsically linked to SSc pathogenesis. Recently, elegant single-cell studies have begun to establish that in SSc pathogenesis distinct roles are carried out by heterogeneous dermal fibroblast subpopulations, with some proposed to be more profibrotic, others proposed to be more proinflammatory, and others proposed to regulate vascular processes (Zhu et al., 2024). It is therefore interesting to consider whether a shorter cilium may correspond with other functional characteristics of SSc, outside of the profibrotic phenotype which was the focus of this study. Therefore, an interesting future direction for this research could be to evaluate the effect of AURKA inhibition and ciliary length rescue in functionally distinct single-cell derived clonal lines, such as those for which cilium length was analysed in this study (Chapter 3).

The work presented in this chapter provides evidence that SSc dermal fibroblast primary cilia may be shortened due to aberrant AURKA activity, and suggests that this phenotype could have a potential contribution to pathological fibrosis. Further research is required to elucidate this finding, and to begin to explore the potential benefits of making primary cilia a candidate for therapeutic intervention. The AURKA-specific inhibitor Alisertib, deemed the safest available AURKA inhibitor for clinical use, is currently in several Phase 2 and 3

clinical trials in different types of cancer, but these studies have been impeded by off-target side effects in patients (Liewer & Huddleston, 2018, Haddad et al., 2023). While AURKA itself may therefore not be an ideal candidate for therapeutic intervention, furthering our understanding of how its activity in SSc may be dysregulated could reveal other, more appropriate candidate targets for intervention.

5.4 Summary

Taken together, these data show that inhibition of AURKA activity rescues the shortened cilia phenotype of SSc dermal fibroblasts. Although study of the effect of AURKA inhibition on SSc dermal fibroblasts at the level of gene and protein expression did not provide consistent evidence of SSc-specific rescue of ‘classical’ SSc expression profiles, AURKA inhibition reduced TGFβ-induced fibroblast contractility in SSc-derived fibroblasts. This provides evidence that further supports a potential pathogenic contribution of the short cilia phenotype in SSc, which warrants further investigation.

Chapter 6. Characterisation of the effect of Caveolin-1 downregulation in Systemic Sclerosis on the primary cilium

6.1 Introduction

Caveolin-1 (CAV1) downregulation in SSc dermal fibroblasts has been shown to contribute to pathogenesis (Del Galdo et al., 2008). While the most prominent localisation of CAV1 is in caveolae, it has also been shown to localise to the primary cilium of mammalian cells, where it is proposed to be important for the regulation of ciliary membrane composition and ciliary function (Schou et al., 2017, Yamakawa et al., 2021). These factors led to the formulation of the hypothesis that CAV1 downregulation in SSc could lead to aberrations of primary cilium composition and function, which could contribute to SSc fibroblast pathogenesis. Despite two previous studies demonstrating that experimental depletion of CAV1 led to increased cilia length (Schou et al., 2017, Rangel et al., 2019) – the opposite of the cilia phenotype observed in SSc dermal fibroblasts – these studies were carried out in epithelial cells, and ciliary dynamics are complicated and varied in different cellular settings (Mill et al., 2023). Therefore, we aimed to investigate any contribution of CAV1 downregulation to the SSc dermal fibroblast cilia phenotype. The experimental results discussed so far suggest that the shortened primary cilia phenotype in SSc dermal fibroblasts is likely AURKA-HDAC6 dependent. Therefore, we also aimed to investigate any link between CAV1 downregulation and AURKA-HDAC6 dependent ciliary disassembly in dermal fibroblasts.

6.2 Results

6.2.1 Short hairpin RNA knockdown of Caveolin-1 (shCAV1) as a model for Caveolin-1 downregulation in SSc

To begin to investigate the hypothesis that CAV1 downregulation in SSc could contribute to the shorter cilia phenotype, we first set out to confirm that the fibroblast lines assessed for cilia length did indeed have reduced CAV1 expression. CAV1 was found to be downregulated at both the protein (Fig. 6.1A, B) and mRNA level (Fig. 6.1C) in SSc compared to HC.

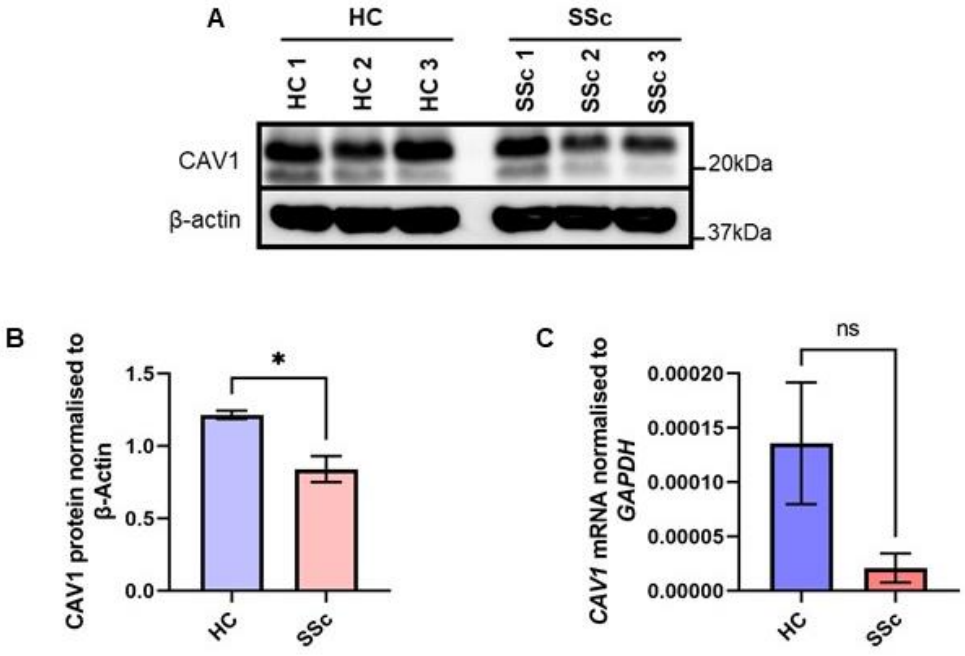

Figure 6.1: Reduced CAV1 expression at protein and mRNA level in SSc dermal fibroblasts compared to HC

Confluent HC and SSc fibroblasts were cultured in 0.5 % serum media for 48 h before protein and RNA were harvested. A) Western Blots showing CAV1 protein levels in three HC and SSc fibroblast lines. β-Actin included as a loading control. B) CAV1 densitometry of (A). C) *CAV1* mRNA levels normalised to housekeeping gene *GAPDH*, quantified by qPCR. HC and SSc n=3. Bars show the mean of three donor

lines, and error bars show standard error of the mean. P values were calculated with unpaired two-tailed t-tests (ns = non-significant, *P<0.05).

To study any pathological effect of CAV1 downregulation in SSc dermal fibroblasts, a model was created by silencing of CAV1 in healthy fibroblasts. Briefly, healthy dermal fibroblasts were transduced with short hairpin RNA (shRNA) specific to the gene sequence of CAV1 in order to generate a long-term stable CAV1 knockdown fibroblast line (Liakouli et al., 2018). Compared to fibroblasts transduced with scramble control sequence shRNA (shSCR), those transduced with CAV1-targeting shRNA (shCAV1) had significantly reduced CAV1 protein levels (Fig. 6.2A, B). This knockdown was monitored over the course of experimental use and remained stable – data shown in Fig 6.2B comprises of results from independent experiments conducted over several months, with continued Puromycin selection for successful shRNA transduction and a maximum of 10 passages during culture of each batch of cells.

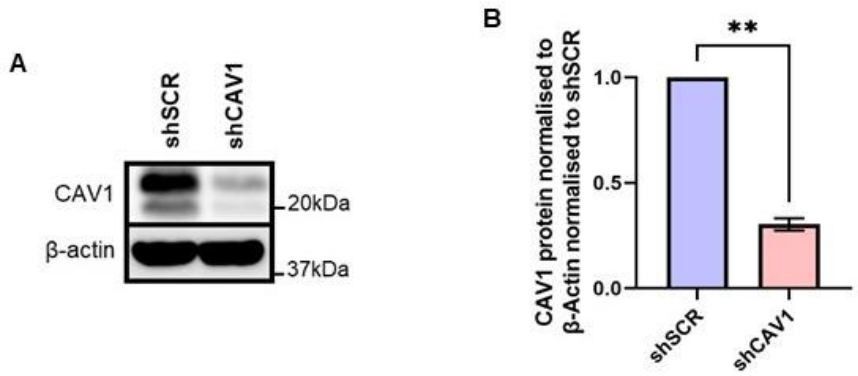

Figure 6.2: Generation of a stable CAV1 knockdown healthy fibroblast line using short hairpin RNA to reduce protein expression

Confluent shSCR and shCAV1 fibroblasts were cultured in 0.5 % serum media for 48 h before protein was harvested. A) Representative Western Blots showing CAV1 protein levels in shSCR vs shCAV1. β-Actin included as a loading control. B) CAV1 protein densitometry of shSCR vs shCAV1 (n=3 biological replicates). Bars show the

mean and error bars show standard error of the mean. P value calculated by unpaired two-tailed t-test (**P<0.01).

To characterise the effect of CAV1 downregulation, the expression of selected transcripts and proteins recognised as characteristically upregulated in SSc compared to HC (Mouawad & Feghali-Bostwick, 2023), considered to be ‘markers’ of fibrotic activity, were studied by qPCR and Western Blot. Although mRNA levels of *ACTA2* (Fig. 6.3A) and *COL1A2* (Fig. 6.3E) were similar between shSCR and shCAV1, shCAV1 fibroblasts showed increased expression of *CCN2* (Fig. 6.3B), *FN1* (Fig. 6.3C), and *COL1A1* (Fig. 6.3E) mRNA. At the protein level, shCAV1 fibroblasts were found to have a significantly increased abundance of CTGF, encoded by the *CCN2* gene (Fig. 6.3F, G), αSMA, encoded by the *ACTA2* gene (Fig. 6.3F, H), and phosphorylated SMAD3 (Fig. 6.3F, I) compared to shSCR, suggesting activation of the TGFβ pathway. This data shows that knockdown of CAV1 in healthy dermal fibroblasts induces a gene and protein expression profile which largely mimics that of SSc, including genes and proteins of known pathological contribution to the disease phenotype.

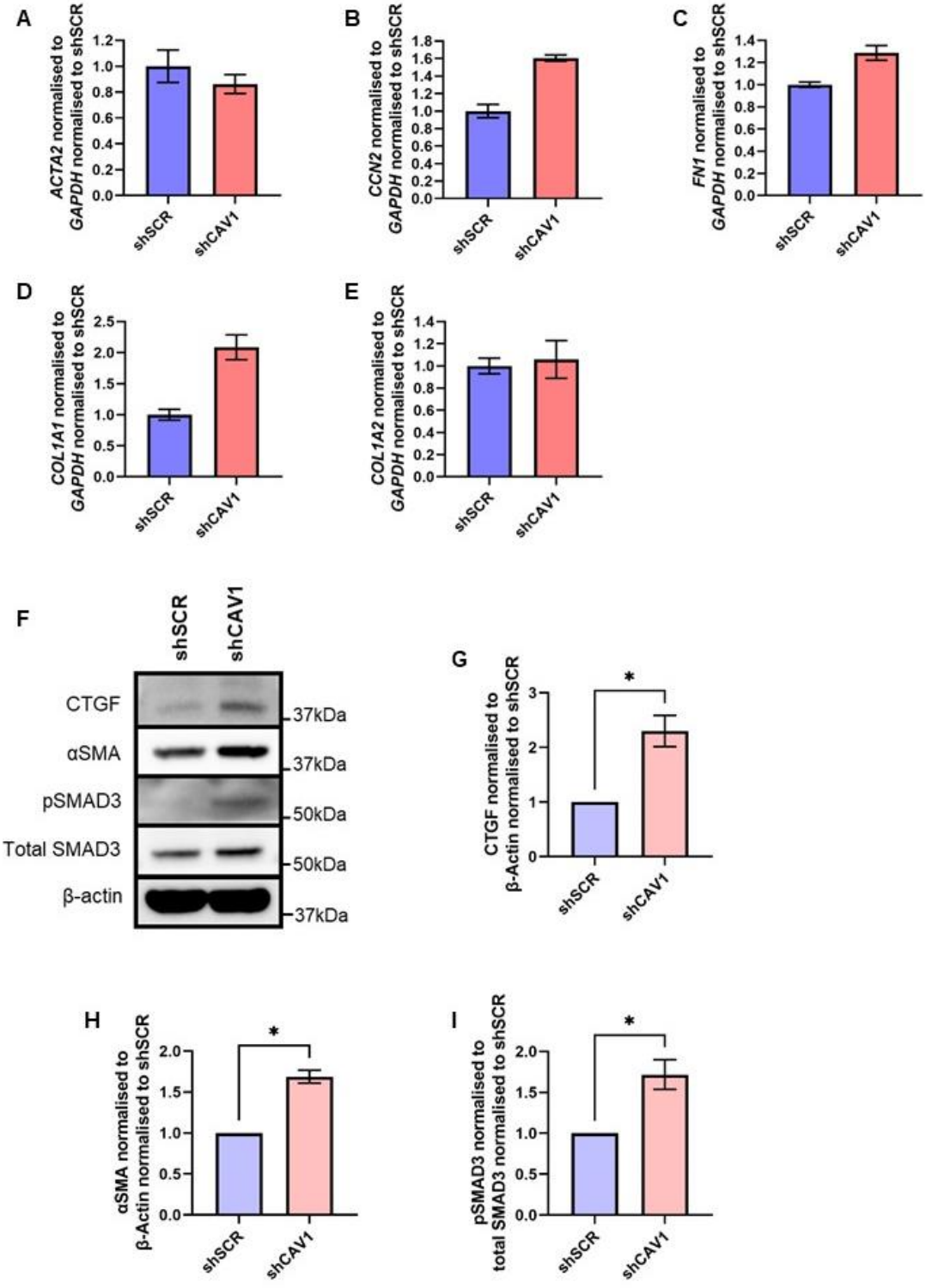

Figure 6.3: shCAV1 fibroblast lines show increased expression of classic fibrotic markers at the mRNA and protein level

Confluent shSCR and shCAV1 fibroblasts were cultured in 0.5 % serum media for 48 h before RNA and protein were harvested. Transcript levels were quantified by qPCR with normalisation to housekeeping gene *GAPDH*. A) Transcript levels of *ACTA2*. B) Transcript levels of *CCN2*. C) Transcript levels of *FN1*. D) Transcript levels of

COL1A1. E) Transcript levels of *COL1A2*. For mRNA data, n=1. Bars show the mean of triplicate well results for each transcript analysed. Error bars show standard error of the mean. F) Representative Western Blots showing protein levels of CTGF, αSMA, pSMAD3 and total SMAD3 in shSCR vs shCAV1. β-Actin included as a loading control. G) CTGF densitometry in shSCR vs shCAV1. H) αSMA densitometry in shSCR vs shCAV1. I) pSMAD3/total SMAD3 densitometry in shSCR vs shCAV1. For protein data, n=3 biological replicates. Bars show the mean and error bars show standard error of the mean. P values were calculated with unpaired two-tailed t-tests (*P<0.05).

6.2.2 Primary cilia are shorter in shCAV1 fibroblasts

Next, primary cilia of healthy shCAV1 dermal fibroblasts were examined by immunofluorescence for Ac-α-Tub (Fig. 6.4A) and compared to that of healthy shSCR fibroblasts, along with HC and SSc fibroblasts. There was no significant difference in cilia incidence between any cell line (Fig. 6.4B), consistent with findings presented previously that showed cilia incidence does not differ between HC and SSc (Fig. 3.1). Primary cilia were shorter in shCAV1 fibroblasts compared to shSCR (3.1±0.3 μm (Mean±SEM) vs 4.4±0.2 μm, p<0.01). There was no significant difference between shSCR primary cilium length and HC cilium length at 4.4±0.1 μm. Interestingly, there was also no significant difference between shCAV1 primary cilium length and SSc primary cilium length at 2.8±0.1 μm (Fig. 6.4A, C). Visual representation of the distribution of cilia lengths within each population shows close alignment between the distribution profiles of HC and shSCR fibroblast cilia at longer lengths, and of SSc and shCAV1 fibroblast cilia at shorter lengths (Fig. 6.4D). These data suggest that CAV1 knockdown in healthy fibroblasts is sufficient to induce a ciliary phenotype which mimics that of SSc.

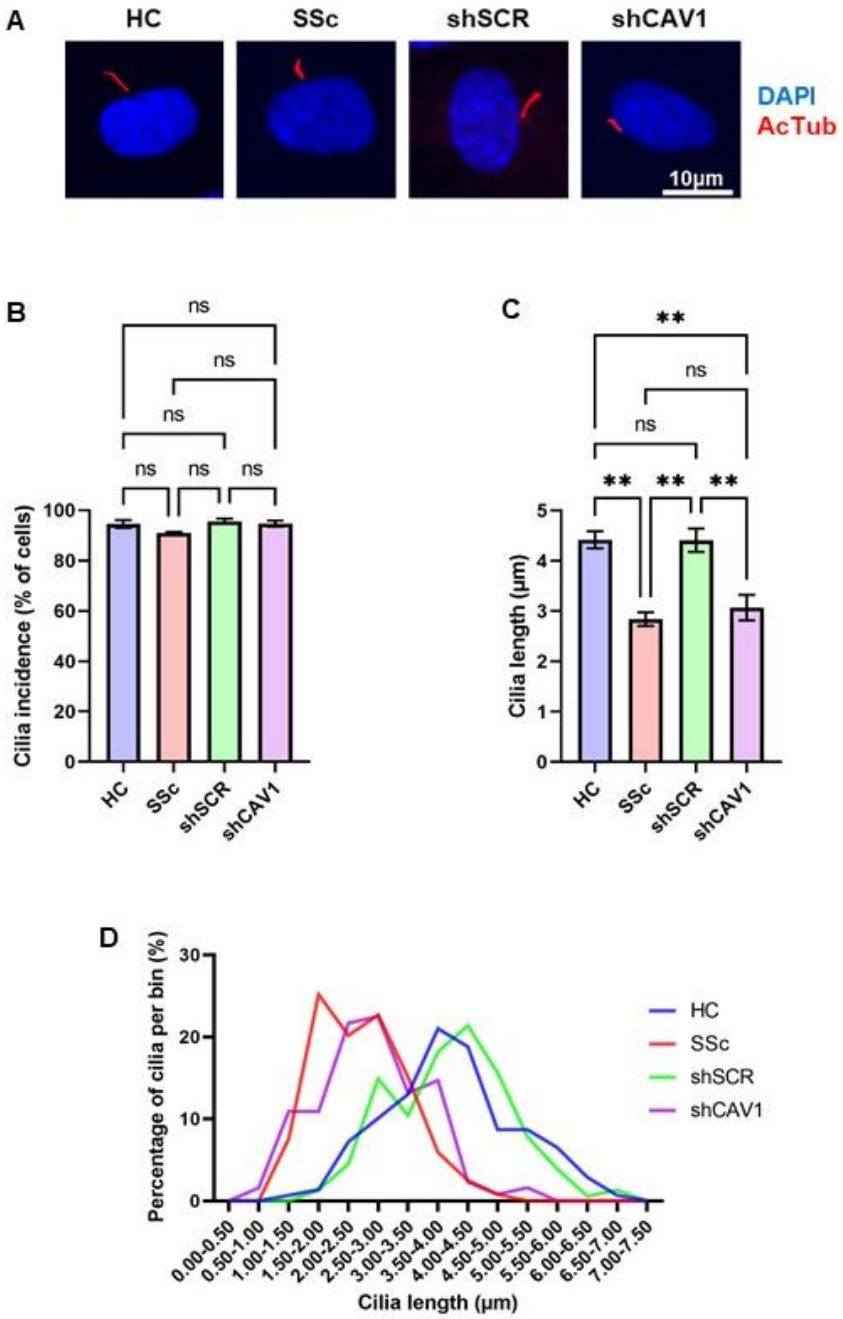

Figure 6.4: Primary cilia are shorter in healthy shCAV1 fibroblasts compared to shSCR controls, and are similar in length to SSc fibroblast cilia

Confluent fibroblasts were cultured in 0.5 % serum media for 48 h, and cilia measured using immunofluorescence for Ac-α-Tub. A) Representative immunofluorescence images taken at 400 x magnification showing cilia (stained for Ac-α-Tub in red) of individual fibroblasts (DAPI nuclear staining in blue). Scale bar shown at 10 µm. B) Cilia incidence observed in each group. C) Length of cilia observed in (B). HC and SSc n=3 donor lines, shSCR and shCAV1 n=3 biological replicates. Bars show the mean and error bars show standard error of the mean. P values were calculated by one-way ANOVA with Tukey's multiple comparisons test

(ns = non-significant, **P<0.01). D) Distribution of cilia length in a representative replicate of each fibroblast line, showing the percentage of total cilia in each 0.5 μm length category.

The effect of stimulation with exogenous TGFβ in these fibroblast lines was also studied. As observed in HC and SSc in earlier experiments (Fig 3.3), TGFβ was again able to induce a reduction in ciliary incidence in all cell lines (Fig. 6.5A). Similarly, TGFβ treatment was also able to reduce ciliary length in all cell lines, shortening HC to 1.6±0.02 μm, SSc to 1.6±0.1 μm, shSCR to 1.5±0.05 μm, and shCAV1 to 1.5±0.02 μm, all significantly shorter than their respective untreated controls (Fig 6.5B).

The effect of TGFβ treatment on primary cilia over a time course was also studied in shSCR and shCAV1 fibroblasts. The previously described results of this experiment carried out on HC and SSc fibroblasts (Fig. 3.5) showed a reduction in cilia incidence identifiable by 18 h in both HC and SSc fibroblasts, but a faster reduction in length in SSc fibroblasts (by 4 h) than HC (by 18 h). The same result was observed on cilia incidence in shSCR and shCAV1 fibroblasts, with TGFβ-induced shortening evident in both by 18 h (Fig. 6.5C). Ciliary length, as in SSc fibroblasts, was reduced by 4 h in shCAV1 fibroblasts. However, unlike the HC fibroblasts, shSCR cells also showed a faster reduction in cilia length, evident at 4 h post-TGFβ addition (Fig. 6.5D). Therefore, despite shCAV1 fibroblast cilia shortening as quickly as SSc cilia in response to TGFβ treatment, and more quickly than HC, this cannot be described as an effect of CAV1 downregulation due to control shSCR fibroblast cilia shortening as quickly.

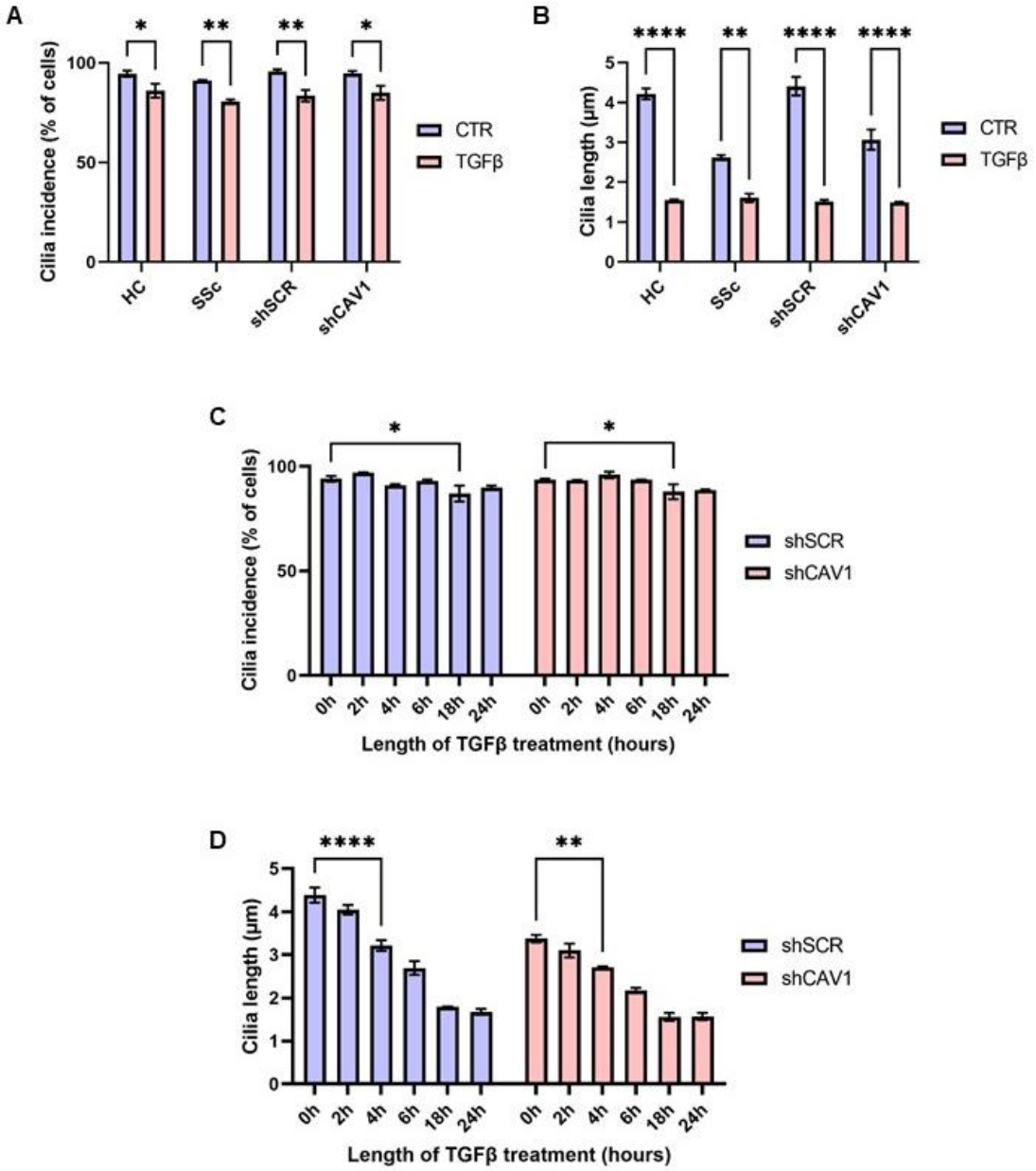

Figure 6.5: TGFβ decreases primary cilia incidence and length in shSCR and shCAV1 fibroblasts, with similar timing

For (A) and (B), confluent fibroblasts were cultured in 0.5 % serum media for 24 h, followed by 24 h in the presence or absence of 10 ng/mL TGFβ. Cilia were measured using immunofluorescence for Ac-α-Tub. A) Cilia incidence observed in each group. B) Length of cilia observed in (A). HC and SSc n=3 donor lines, shSCR and shCAV1 n=3 biological replicates. Bars show the mean and error bars show standard error of the mean. P values were calculated by two-way ANOVA with Tukey's multiple comparisons test (*P<0.05, **P<0.01, ****P<0.0001). For (C) and (D), confluent fibroblasts were cultured in 0.5 % serum media for a total of 48 h, with 10 ng/mL TGFβ added for the indicated periods of time before cilia measurement. C) Time course reduction of cilia incidence in response to TGFβ. D) Length of cilia observed

in (C). shSCR and shCAV1 n=2 biological replicates. Bars show the mean and error bars show standard error of the mean. P values were calculated by two-way ANOVA with Dunnet's multiple comparisons test (*P<0.05, **P<0.01, ****P<0.0001).

These data support the hypothesis that CAV1 downregulation characteristic of SSc may contribute to the shortened cilia phenotype of SSc dermal fibroblasts, as knockdown of CAV1 in healthy dermal fibroblasts causes cilia length to shorten to that of SSc.

6.2.3 Inhibition of Aurora A Kinase and HDAC6 rescues cilia length in shCAV1 fibroblasts

Previously described data showed an SSc-specific rescue of cilia length upon inhibition of AURKA and HDAC6 (Fig. 4.10, Fig. 5.3). Since shCAV1 fibroblasts possess primary cilia as short as SSc, the effect of inhibition of AURKA with MLN8054 and of HDAC6 with Tubacin on primary cilia was also investigated in a preliminary experiment in this model by immunofluorescence for Ac-α-Tub (Fig 6.6A).

Mirroring the results shown for HC and SSc (Chapter 5), inhibition of either AURKA or HDAC6 had no effect on ciliary incidence in shSCR and shCAV1 (Fig. 6.6B, E). Inhibition of AURKA or HDAC6 in combination with TGFβ treatment also had no effect on the ability of TGFβ to induce ciliary shortening in shSCR and shCAV1 (Fig. 6.6C, F), as seen in HC and SSc (Chapter 5). This supports the notion that the mechanism by which TGFβ shortens cilia is independent of the AURKA-HDAC6 axis.

Inhibition of AURKA increased cilia length in shCAV1 cells to the level of shSCR control cells while leaving cilia length in shSCR cells unaffected – mean shSCR cilia length after AURKA inhibition with MLN8054 was 4.3±0.2 μm (Mean±STDEV), similar to the CTR length of 4.4±0.3 μm, while shCAV1 cilia length after MLN8054 treatment was 4.3±0.3 μm, increased from 3.4±0.1 μm in CTR conditions (Fig. 6.6A, C, D). Similarly, HDAC6 inhibition with Tubacin increased cilia length in shCAV1 cells but not in shSCR cells (Fig. 6.6A, F, G).

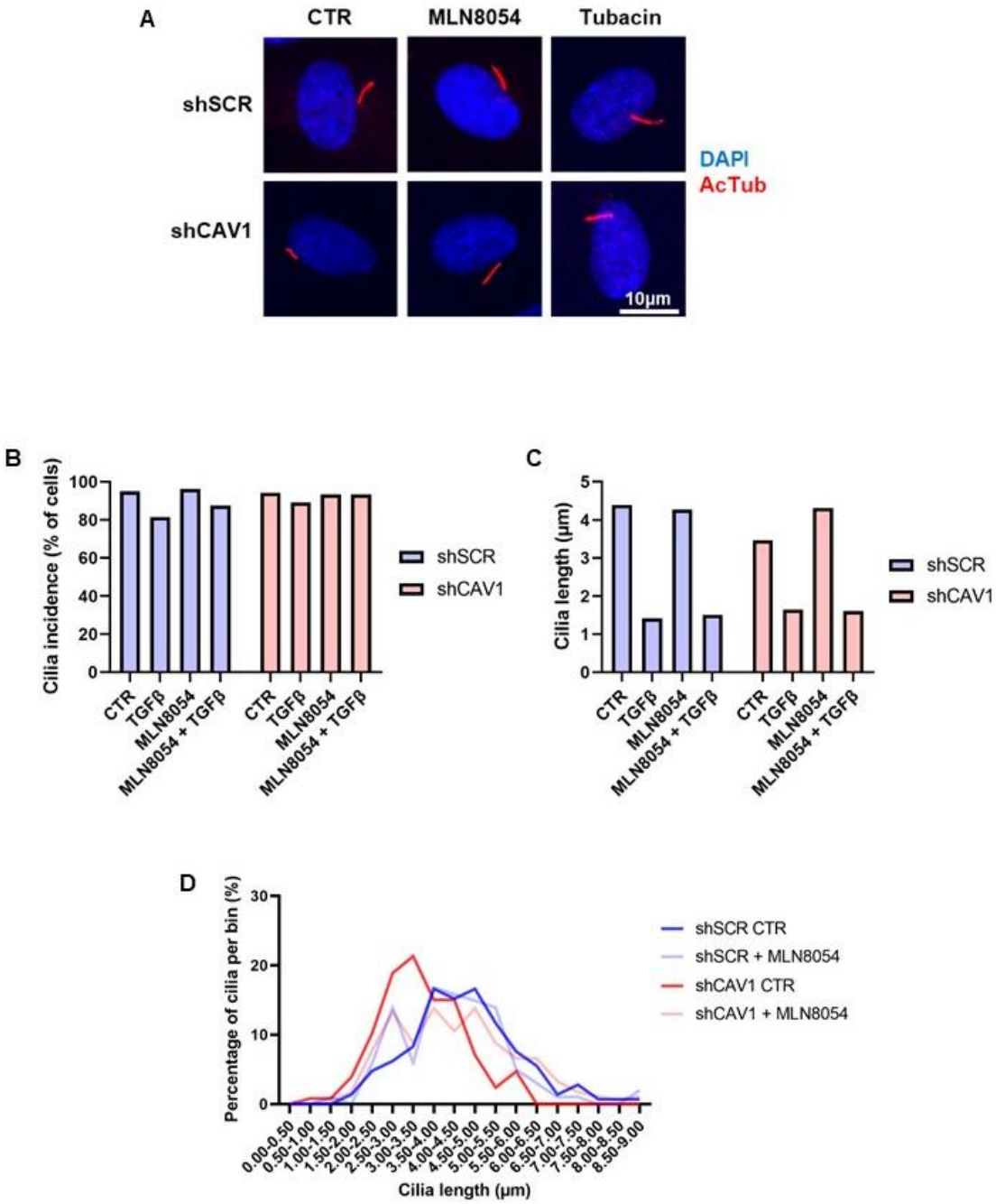

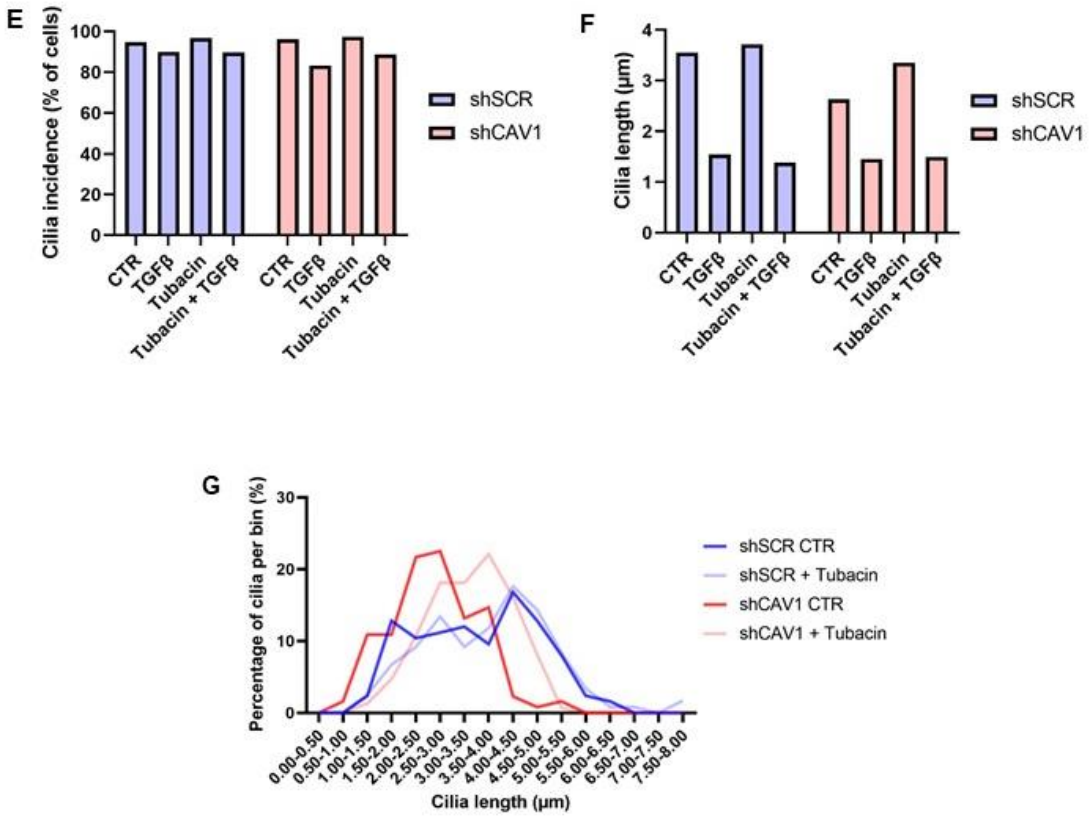

Figure 6.6: AURKA inhibition with MLN8054 and HDAC6 inhibition with Tubacin rescues cilia length in shCAV1 fibroblasts

Confluent fibroblasts were cultured in 0.5 % serum media for 24 h followed by 24 h treatment with either 10 µM MLN8054, 10 µM Tubacin or DMSO control, with or without 10 ng/mL TGFβ in 0.5 % serum media. Cilia were measured by immunofluorescence for Ac-α-Tub. A) Representative immunofluorescence images taken at 400 x magnification showing cilia (stained for Ac-α-Tub in red) of individual fibroblasts (DAPI nuclear staining in blue). Scale bar shown at 10 µm. B) Cilia incidence changes in response to MLN8054/TGFβ treatment. C) Length of cilia observed in (B). D) Distribution of lengths of cilia observed in (C), showing the percentage of total cilia in each 0.5 µm length category. E) Cilia incidence changes in response to Tubacin/TGFβ treatment. F) Length of cilia observed in (E). G) Distribution of lengths of cilia observed in (F), showing the percentage of total cilia in each 0.5 µm length category. shSCR and shCAV1 n=1. Bars show the mean.

These preliminary data show that shCAV1-induced reduction of primary cilia length is dependent upon AURKA-HDAC6, mirroring the findings in SSc dermal fibroblasts. This suggests that the AURKA-HDAC6 induced shortened cilia

phenotype of SSc could be a direct consequence of downregulation of CAV1 characteristic of SSc fibroblasts.

6.2.4 Investigation of interaction between Caveolin-1 and AURKA

The results discussed so far suggest that AURKA hyperactivity and its effect on primary cilium length in SSc may be a downstream consequence of CAV1 downregulation, as the shorter primary cilia of shCAV1 fibroblasts are rescued by AURKA inhibition. As the exact mechanism of CAV1 downregulation in SSc remains elusive, we decided to investigate the hypothesis that this may be a two-way interaction, and that AURKA hyperactivity could contribute to CAV1 downregulation. In order to do this, AURKA was inhibited with MLN8054 in HC, SSc, shSCR and shCAV1 fibroblasts followed by assessment of CAV1 protein levels.

Additionally, since TGFβ has been shown to reduce the expression of CAV1 in fibroblasts (Del Galdo et al., 2008, Hou et al., 2017, Liakouli et al., 2018), stimulation with exogenous TGFβ alone and in combination with MLN8054 was also performed to determine the ability of TGFβ to influence CAV1 expression in the dermal fibroblast lines used in this study, and any involvement of AURKA in this process.

Inhibition of AURKA did not affect CAV1 protein levels in any cell line (Fig. 6.7A-C). TGFβ had no effect on CAV1 protein expression in HC nor in shSCR fibroblasts (Fig. 6.7A-C). However, in SSc and shCAV1 fibroblasts, TGFβ reduced CAV1 protein levels. This reduction was independent of AURKA activity, as seen in samples treated with MLN8054 (Fig. 6.7A-C).

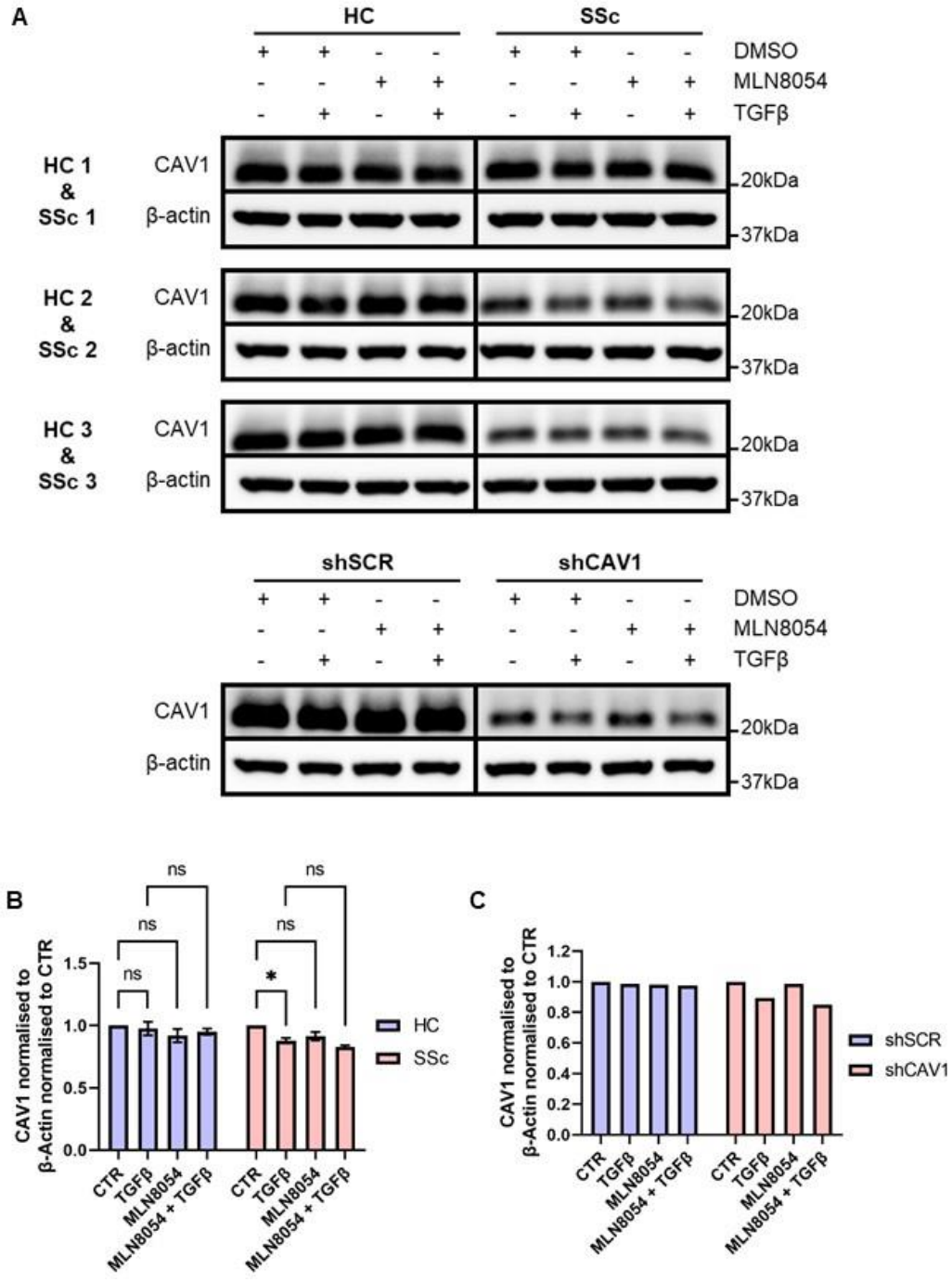

Figure 6.7: Inhibition of AURKA has no effect on levels of CAV1, nor SSc and shCAV1-specific TGFβ-induced downregulation of CAV1

Confluent HC, SSc, shSCR and shCAV1 fibroblasts were cultured in 0.5 % serum media for 24 h followed by 24 h treatment with 10 μM MLN8054 or DMSO control in 0.5 % serum media, with or without the addition of 10 ng/mL TGFβ. Protein was harvested for quantification by Western Blot. A) Western Blots showing CAV1 protein levels in response to treatments comprising of MLN8054 or DMSO control with or without TGFβ. β-Actin included as a loading control. B) Protein densitometry of CAV1 in HC vs SSc, quantified from (A), relative to each group's CTR. HC and SSc n=3

donor lines. Bars show the mean and error bars show standard error of the mean. P values were calculated with paired two-tailed t-tests (ns = non-significant). C) Protein densitometry of CAV1 in shSCR vs shCAV1, quantified from (A), relative to each line's CTR. shSCR and shCAV1 n=1.

Inhibition of AURKA in HC, SSc, shSCR and shCAV1 did not change the abundance of CAV1, nor rescue SSc and shCAV1-specific TGFβ-induced CAV1 downregulation. This refutes the hypotheses that AURKA hyperactivation in SSc could be the cause of CAV1 downregulation, and that AURKA may mediate TGFβ-induced CAV1 downregulation.

6.2.5 The effect of Aurora A Kinase inhibition on the fibrotic phenotype of shCAV1 fibroblasts at the transcript level

shCAV1 fibroblasts show elevated levels of *CCN2*, *FN1*, and *COL1A1* transcripts compared to shSCR (Fig. 6.3). These transcripts are also elevated in SSc fibroblasts, along with *ACTA2* and *COL1A2* (Fig 5.4). AURKA inhibition led to a partial reduction in levels of some of these fibrosis-associated and TGFβ-inducible transcripts in some SSc fibroblast lines (Fig. 5.5). As inhibition of AURKA in shCAV1 fibroblasts rescues cilia length (Fig. 6.6) as it does in SSc fibroblasts (Fig. 5.3), the effect of AURKA inhibition on expression of these transcripts in shCAV1 fibroblasts was next investigated by a preliminary qPCR experiment.

Treatment of shSCR or shCAV1 fibroblasts with MLN8054 did not alter basal *ACTA2, FN1,* or *COL1A1* expression (Fig. 6.8A, C, D), while *COL1A2* expression was slightly increased in shCAV1 (Fig. 6.8E). Basal *CCN2*

expression, however, was reduced by MLN8054 in both cell lines, to a greater degree in shCAV1 than in shSCR fibroblasts (Fig. 6.8B).

All genes were, as expected, upregulated upon TGFβ stimulation in both cell lines. Comparing TGFβ-treated fibroblasts to those treated with TGFβ in the presence of MLN8054, there was some shCAV1-specific rescue of TGFβ-induced *ACTA2*, *FN1*, and *COL1A1* expression (Fig. 6.8A, C, D). TGFβ-induced *CCN2* expression was reduced slightly in both cell lines upon co-treatment with MLN8054 (Fig. 6.8B), while TGFβ-induced *COL1A2* expression increased in shSCR and remained similar in shCAV1 (Fig. 6.8E).

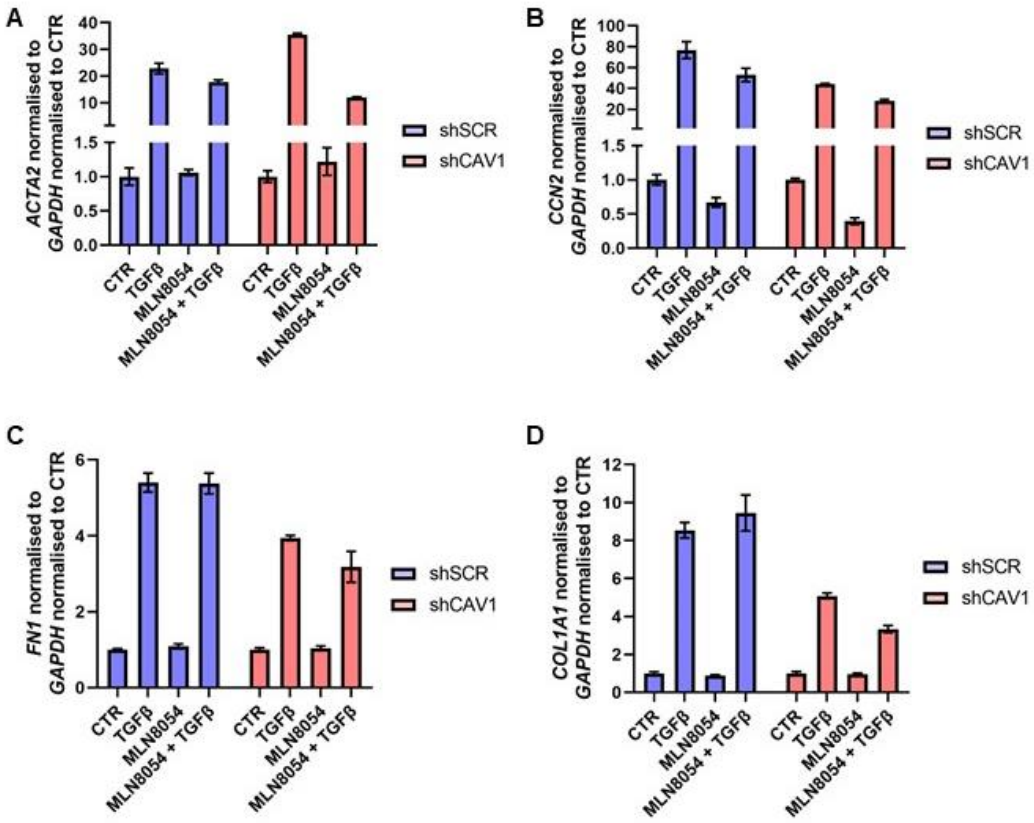

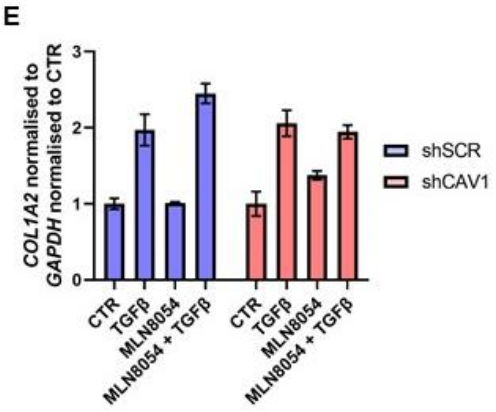

Figure 6.8: Inhibition of Aurora A Kinase partially rescues the fibrotic phenotype of shCAV1 fibroblasts and response to TGFβ at transcript level
Confluent shSCR and shCAV1 fibroblasts were cultured in 0.5 % serum media for 24 h followed by 24 h treatment with 10 μM MLN8054 or DMSO control in 0.5 % serum media, with or without the addition of 10 ng/mL TGFβ. RNA was harvested for quantification by qPCR, with normalisation to housekeeping gene *GAPDH*, and results presented relative to each line's CTR. A) Transcript levels of *ACTA2*. B) Transcript levels of *CCN2*. C) Transcript levels of *FN1*. D) Transcript levels of *COL1A1*. E) Transcript levels of *COL1A2*. shSCR and shCAV1 n=1. Bars show the mean of triplicate well results for each transcript analysed. Error bars show standard error of the mean.

Overall, the response at the transcript level to AURKA inhibition with MLN8054 both alone and in combination with TGFβ was similar in shSCR and shCAV1 fibroblasts to the observations in HC and SSc fibroblasts (Fig 5.5), with a limited effect on basal expression of fibrosis-associated transcripts, and some reduction of TGFβ-induced expression.

6.2.6 The effect of Aurora A Kinase inhibition on the fibrotic phenotype of shCAV1 fibroblasts at the protein level

Next, to compare with data of HC and SSc fibroblasts (Fig. 5.7, 5.8), we started to explore the effect of AURKA inhibition with MLN8054 in shSCR and shCAV1

fibroblasts, both alone and in combination with TGFβ, was investigated after 24 h and 48 h on the same panel of typically fibrosis-associated and TGFβ-inducible proteins by Western Blot in preliminary experiments.

After treatment with MLN8054 for 24 h, the basal CTGF protein level was reduced in shCAV1 but remained unchanged in shSCR fibroblasts (Fig. 6.9A, B), while αSMA protein levels remained largely the same in both cell lines (Fig. 6.9A, C). Phosphorylated SMAD3 was slightly increased in shSCR after MLN8054 treatment, and slightly decreased in shCAV1 fibroblasts (Fig. 6.9A, D).

Levels of all proteins were increased by TGFβ stimulation in both cell lines, as expected. However, the upregulation of CTGF and αSMA was lowered by co-treatment with MLN8054. Abundance of phosphorylated SMAD3 remained largely unchanged in both cell lines (Fig. 6.9A-D).

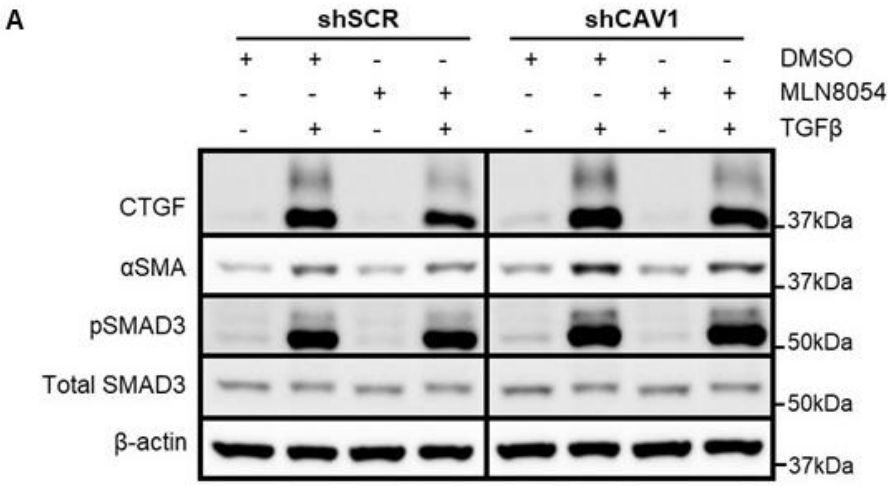

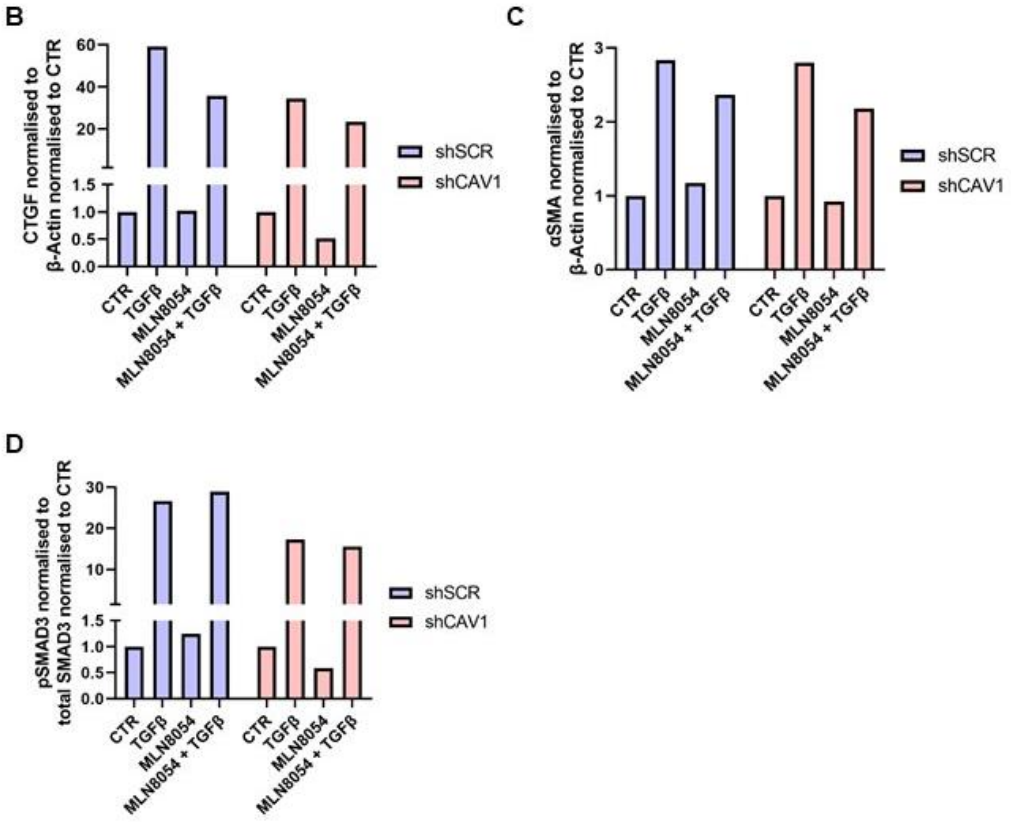

Figure 6.9: Inhibition of Aurora A Kinase for 24 h partially rescues the fibrotic phenotype of shCAV1 fibroblasts and their response to TGFβ

Confluent shSCR and shCAV1 fibroblasts were cultured in 0.5 % serum media for 24 h followed by 24 h treatment with 10 μM MLN8054 or DMSO control in 0.5 % serum media, with or without the addition of 10 ng/mL TGFβ. Protein was harvested for quantification by Western Blot. A) Western Blots showing CTGF, αSMA, pSMAD3 and total SMAD3 protein expression in response to treatments comprising of MLN8054 or DMSO control with or without TGFβ. β-Actin included as a loading control. B) αSMA densitometry of (A). C) CTGF densitometry of (A). D) pSMAD3/total SMAD3 densitometry of (A). Densitometry presented relative to each line's CTR. shSCR and shCAV1 n=1.

After treatment with MLN8054 for 48 h, basal CTGF protein remained unchanged in both cell lines (Fig. 6.10A, B), while αSMA protein decreased slightly in both cell lines (Fig. 6.10A, C), and phosphorylated SMAD3 abundance also decreased in both cell lines (Fig. 6.10A, D).

TGFβ-induced upregulation of CTGF expression was slightly reduced in shCAV1 but not shSCR fibroblasts (Fig. 6.10A, B), as was TGFβ-induced αSMA expression in both cell lines (Fig. 6.10A, C), while abundance of phosphorylated SMAD3 slightly increased in both cell lines (Fig. 6.10A, D).

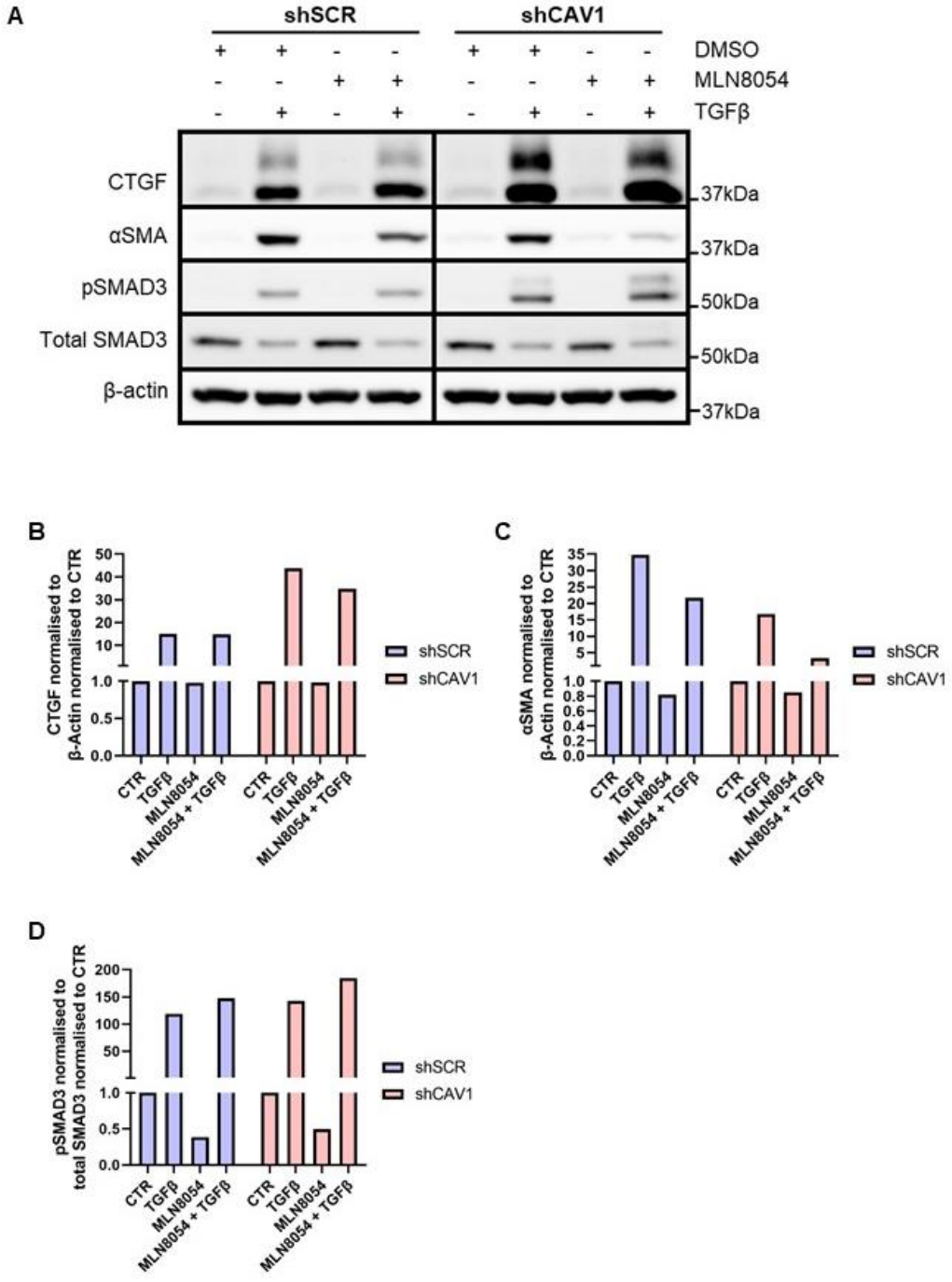

Figure 6.10: Inhibition of Aurora A Kinase for 48 h partially rescues the fibrotic phenotype of shCAV1 fibroblasts and response to TGFβ at protein level

Confluent shSCR and shCAV1 fibroblasts were cultured in 0.5 % serum media for 24 h followed by 48 h treatment with 10 μM MLN8054 or DMSO control in 0.5 % serum media, with or without the addition of 10 ng/mL TGFβ. Protein was harvested for quantification by Western Blot. A) Western Blots showing CTGF, αSMA, pSMAD3 and total SMAD3 protein expression in response to treatments comprising of MLN8054 or DMSO control with or without TGFβ. β-Actin included as a loading control. B) αSMA densitometry of (A). C) CTGF densitometry of (A). D) pSMAD3/total SMAD3 densitometry of (A).). Densitometry presented relative to each line's CTR. shSCR and shCAV1 n=1.

These preliminary results mirror those observed in HC vs SSc fibroblasts, with AURKA inhibition with MLN8054 conferring a partial reduction of fibrosis-associated protein expression both at the basal level and in response to TGFβ, though this was not specific to shCAV1 fibroblasts.

6.2.7 The effect of Aurora A Kinase inhibition on TGFβ-induced shCAV1 fibroblast contractility

Previously described data showed that inhibition of AURKA with MLN8054 was able to rescue the contractile phenotype of SSc fibroblasts in response to TGFβ, in functional collagen-cell contraction assays (Fig. 5.9). Therefore, the same experimental approach was used to study the effect of MLN8054 in shSCR and shCAV1 fibroblasts in a preliminary experiment (Fig. 6.11A), to determine whether CAV1 downregulation was sufficient to yield similar experimental results at the functional level.

While unstimulated shSCR and shCAV1 fibroblasts exhibited similar contractility over the time course (Fig. 6.11B) and by 48 h there was little difference in gel contraction in CTR conditions or in fibroblasts treated with MLN8054 (Fig.

6.11C), upon stimulation with exogenous TGFβ, shCAV1 fibroblasts contracted the gel more than shSCR fibroblasts (to 79.2±2.9 % vs 89.4±0.2 % respectively by 48 h) (Fig. 6.11B, C). The increased contraction of shCAV1 fibroblasts compared to shSCR fibroblasts in response to TGFβ was effectively rescued by co-treatment with MLN8054 (87.6±0.6 % for shSCR vs 87.8±2.1 % for shCAV1) (Fig. 6.11B, C).

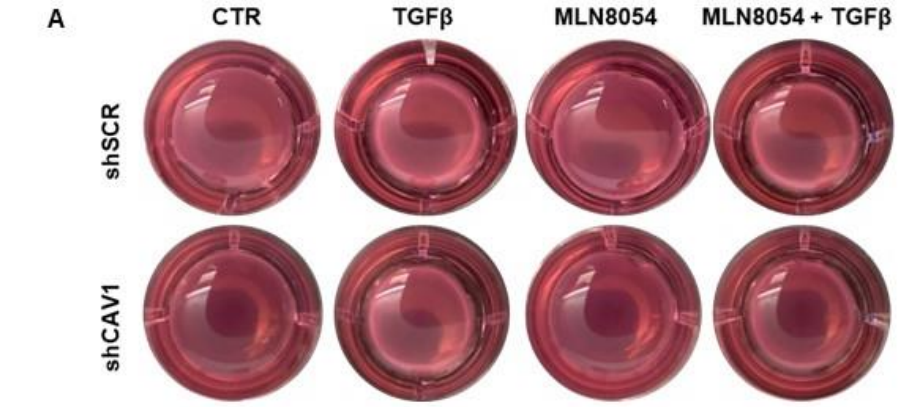

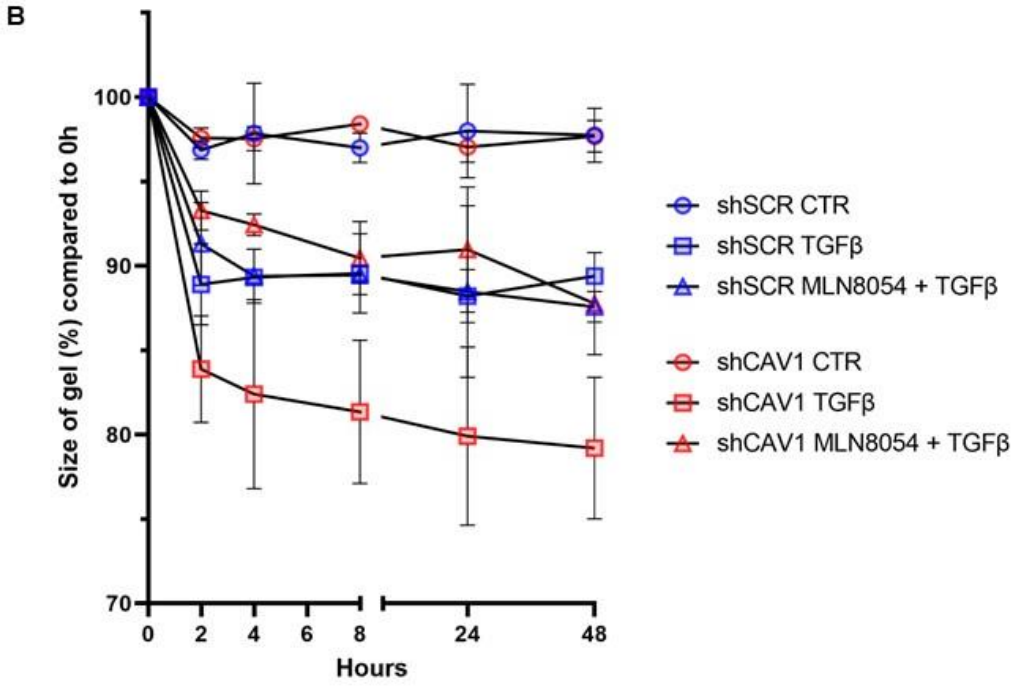

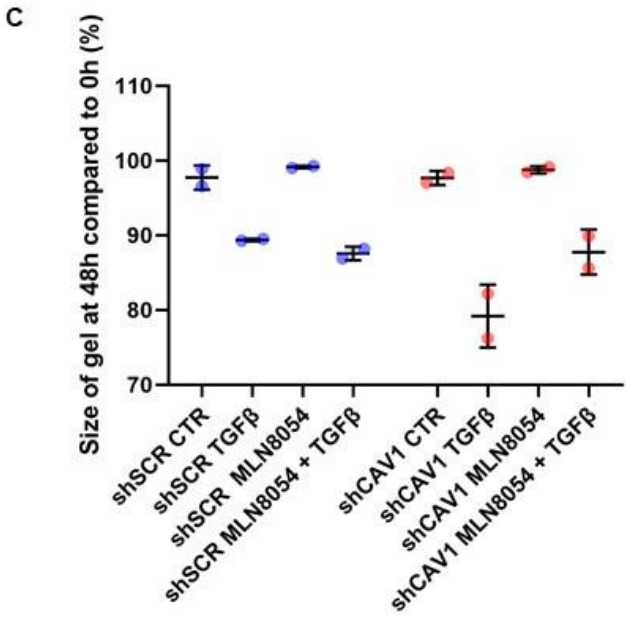

Figure 6.11: Inhibition of AURKA rescues the contractile phenotype of shCAV1 fibroblasts in response to stimulation with TGFβ

Confluent shSCR and shCAV1 fibroblasts were cultured in 0.5 % serum media for 24 h followed by 2 h pre-treatment with 10 μM MLN8054 or DMSO control in 0.5 % serum media. Fibroblasts were seeded into cell-collagen gels which were allowed to set, then incubated for 16 h in 10 μM MLN8054 or DMSO control in 0.5 % serum media, with or without the addition of 10 ng/mL TGFβ. Gels were released from the wells, and gel area measured at the indicated time points over a time course of 48 h. A) Representative images of cell-collagen gels taken at 48 h. B) Cell-collagen gel contraction in each of the experimental conditions, shown as the area of the gel at each time point, as a percentage of the gel area at 0 h. Each point plotted shows the mean and bars show standard deviation of the mean (shSCR and shCAV1 n=2). C) Gel areas of the 48 h time point of (B), with each replicate shown as an individual point. Box and whisker plots show the mean and standard deviation of the mean.

As the observations in this preliminary experiment closely match those of experimental comparison of HC and SSc, and can be modulated by AURKA inhibition, these data suggest that the increased fibroblast contractility in response to TGFβ in SSc and shCAV1 dermal fibroblasts may share the same AURKA-dependent mechanism.

6.3 Discussion

The results presented in this chapter are the first to demonstrate that primary ciliary shortening can be induced by CAV1 downregulation in dermal fibroblasts. Thus, it is proposed that the shortened primary cilia characteristic of SSc dermal fibroblasts may be a consequence of CAV1 downregulation.

This finding is novel, and is interestingly paradoxical to the results obtained in limited previous work which has demonstrated a link between CAV1 and primary cilia length in which experimental depletion of CAV1 in epithelial cell lines was shown to lead to elongation of primary cilia (Schou et al., 2017, Rangel et al., 2019). It was shown that two components of the ciliary transition zone, NPHP4 and KIF13B, are required to establish a CAV1-enriched microdomain at the transition zone of retinal pigment epithelial (RPE-1) cells, required for functional SHH signalling at the primary cilium (Schou et al., 2017). In this study, siRNA-mediated knockdown of CAV1 (siCAV1) in serum starved RPE-1 cells was shown to reduce ciliary incidence, but increase cilia length. However, this was supported by a single representative immunofluorescence image of a cilium in siCAV1 conditions, and was not quantified. Nevertheless, in a subsequent study, Rangel et al. showed that siRNA-mediated knockdown of CAV1 in serum starved RPE-1 cells led to cytoskeletal impairments caused by reduced RhoA GTPase activity at the apical membrane, along with slightly decreased ciliary incidence, and increased ciliary length (Rangel et al., 2019). The latter finding was replicated in both Madin-Darby canine kidney (MDCK) and inner medullary collecting duct (IMCD3) epithelial cell lines, although the scale of ciliary length increase was variable between the three cell lines. Although these two studies in epithelial cells oppose the observations of the current study conducted in dermal fibroblasts, they demonstrate that CAV1 can

regulate ciliary morphology and, given that primary cilia are known to exhibit cell-type specific diversity in their structure, composition, and functions (Mill et al., 2023), it is plausible that downregulation of CAV1 may confer differential effects on ciliary morphology depending on the cellular context. Taken together, this highlights the need for more extensive research to elucidate the mechanism by which CAV1 influences ciliary length.

Our preliminary data indicated that the shortened ciliary length observed in shCAV1 dermal fibroblasts can be rescued by inhibition of AURKA and HDAC6, as was previously also shown in SSc dermal fibroblasts. Therefore, with the caveat that experimental repeats are required, it is proposed that ciliary shortening in both SSc and shCAV1 dermal fibroblasts may share the same AURKA-HDAC6 dependent mechanism of ciliary disassembly, and that downregulation of CAV1 in SSc may lead to aberrant increased activity of AURKA and drive subsequent ciliary shortening.

Only one previously published study has linked both CAV1 and AURKA, and the primary cilium. In contrast to the relationship suggested here, Jeffries et al. showed that siRNA and shRNA-mediated depletion of CAV1 in two foetal lung fibroblast cell lines led to decrease of total AURKA protein levels, accompanied by an increase in primary cilia incidence, although cilia length was not measured (Jeffries et al., 2019). Based on these observations, the authors suggested that CAV1 depletion in these cells may reduce the activity of AURKA at the primary cilium. To give greater insight into the effect of CAV1 depletion on AURKA stability and activity in dermal fibroblasts and other cell types, it would be interesting to assess the abundance of active and phosphorylated AURKA (pAURKA) in CAV1-depleted cells. Western Blots used to demonstrate AURKA protein degradation after CAV1 depletion in the Jeffries et al. study only

evaluated total AURKA protein levels, not of active pAURKA. During the course of this study, we attempted to quantify pAURKA levels by Western Blot, but this was impeded by the poor suitability of multiple pAURKA antibodies tested for this assay. In order to circumvent this issue, we also begun to optimise the conditions for immunoprecipitation of AURKA in order to enable analysis of pAURKA by mass spectrometry. This method, once fully optimised, will allow determination of the effect of CAV1 depletion on AURKA activity.

It is also possible that the mechanism of interaction between CAV1 and AURKA and the subsequent effects on cilia morphology may differ depending on cellular type and context. In support of this, the depletion of CAV1 in the Jeffries et al. study led to a significant increase in cilia incidence in the foetal lung fibroblast cell lines studied, whereas cilia incidence was unchanged in the shCAV1 dermal fibroblasts in our experiments, and in the two studies discussed previously in epithelial cell lines, CAV1 depletion led to a slight decrease in ciliary incidence (Schou et al., 2017, Rangel et al., 2019).

Jeffries et al. showed that pharmacological inhibition of AURKA increased cilia incidence, but did not show the effect of this inhibitor in the context of CAV1 depletion, as we did. It is important to note, however, that the data presented in the current study in which AURKA and HDAC6 were inhibited in shCAV1 fibroblasts are preliminary, and reproduction of results would be necessary to verify the findings. To formally prove that CAV1 modulates cilia length through AURKA-HDAC6 in SSc, an alternative method of experimental downregulation of CAV1 could be utilised, along with an additional method of AURKA inhibition in CAV1-depleted fibroblasts. Additionally, it would be interesting to overexpress CAV1, in SSc dermal fibroblasts, to see if cilium length could be increased to healthy control levels, and if AURKA and HDAC6 activity are reduced.

Since the simplest explanation of the regulation of AURKA by CAV1 is through a direct physical interaction, co-immunoprecipitation (CoIP) of AURKA with CAV1 and other binding partners was attempted. While CAV1 did appear in some CoIP samples along with AURKA, it was also sporadically present in some control conditions and therefore no conclusions regarding a specific interaction between the two proteins could be drawn from this data, and further optimisation would be required. In addition to this methodology, super-resolution immunofluorescence microscopy at the primary cilium may identify whether there is any overlap between the specific localisation of CAV1 and AURKA at the ciliary base, with both proteins having been shown independently to localise there (Schou et al., 2017, Pugacheva et al., 2007). Proximity ligation assays or FRET analysis could also be employed to investigate whether there is a direct protein-protein interaction between AURKA and CAV1 (Hochreiter et al., 2019, Qin et al., 2021).

Once optimised, AURKA CoIP will allow not only for the investigation of the possibility that AURKA and CAV1 may interact, but also allow for investigation by proteomic analysis of any alterations to the binding partners of AURKA in control and CAV1-depleted conditions, and in healthy control and SSc dermal fibroblasts, that may influence its activity in these different contexts.

While it is important to note that our investigation of AURKA inhibition in CAV1-depleted fibroblasts was exploratory and requires recapitulation, we hypothesise that CAV1 downregulation and subsequent aberrant AURKA activity may contribute to the fibrotic phenotype of SSc dermal fibroblasts, potentially via shortening of the primary cilium and dysregulation of signalling pathways transduced at the cilium. This hypothesis was supported by preliminary data showing a similar response after inhibition of AURKA in

shCAV1 fibroblasts as was observed in SSc fibroblasts. Correlating with increased ciliary length, there was a partial reduction in the levels of some fibrosis-associated transcripts and proteins assessed by qPCR and Western Blotting after AURKA inhibition, particularly that which was induced by treatment with exogenous TGFβ, although this was sometimes also observed in control shSCR fibroblasts. Importantly, inhibition of AURKA reduced the increased TGFβ-induced fibroblast contraction in shCAV1 fibroblasts to the level of shSCR fibroblasts, as it did in SSc fibroblasts compared to HC.

CAV1 is known to act as a negative regulator of TGFβ signalling (Razani et al., 2001, Di Guglielmo et al., 2003), and TGFβ signalling is known to reduce CAV1 expression (Del Galdo et al., 2008, Liakouli et al., 2018). Our data showing increased TGFβ-induced contraction of SSc and shCAV fibroblasts compared to controls, in addition to SSc- and shCAV1-specific TGFβ-induced downregulation of CAV1 protein levels, supports the existence of a feedback loop between CAV1 downregulation and TGFβ amplification in dermal fibroblasts. We speculate that a differential coordination of TGFβ signalling by the shortened primary cilium of SSc dermal fibroblasts could also be implicated in this feedback mechanism.

Along with TGFβ signalling, hyperactivation of both the SHH and Wnt signalling pathways is known to be implicated in SSc fibrosis (Horn et al., 2012, Dees & Distler, 2013). The primary cilium has long been implicated in the coordination and balance of these signalling pathways, being essential for full activation as well as full repression of the SHH pathway, and inhibitory in the case of canonical Wnt signalling (Zingg et al., 2018). Interestingly, ciliary sphingolipids have been shown to facilitate the interaction between TGFβ receptors (TGFβRs) and the inhibitory SMAD7, which prevents TGFβR recycling to the

primary cilium and instead targets them for degradation (Gencer et al., 2017). Additionally, siRNA-mediated knockdown of ciliary protein Alstrom Syndrome-1 (ALSM1) in RPE-1 cells was recently shown to induce cilium elongation, and reduced TGFβ-mediated SMAD2 phosphorylation (Álvarez-Satta et al., 2021). It is therefore interesting to consider that such a signalling fine-tuning role may also exist for the cilium in its coordination of TGFβ signalling, and that aberrations to the primary cilium such as those observed in SSc may contribute to constitutive pathway activation. Further investigation into this possibility will be important to fully understand the pathological relevance that the primary cilium may have in the molecular pathogenesis of SSc, and other fibrotic diseases.

Overall, the results presented in this chapter, if recapitulated, could support the existence of a hierarchical relationship among CAV1, AURKA, and the primary cilium in the pathogenesis of SSc. Future studies to understand their mechanistic relationship will confer greater insight into a disease for which the cellular and molecular mechanisms of pathogenesis are still poorly understood, and allow for determination of the potential for CAV1 or defective primary cilia as targets for future therapeutic intervention strategies in SSc.

6.4 Summary

The data discussed in this chapter show that CAV1 downregulation is sufficient to produce a ciliary phenotype in HC fibroblasts which mimics the SSc shortened cilia phenotype, coupled with an increase in fibrotic marker expression. This model of the SSc cilia phenotype was rescued in preliminary experiments by the inhibition of AURKA and HDAC6, coupled with a reduction in fibrotic characteristics including fibroblast contractility in response to TGFβ,

suggesting that CAV1 may be upstream of AURKA. If recapitulated, these findings could suggest that hyperactivity of AURKA-HDAC6 and consequent increased ciliary disassembly in SSc fibroblasts may be a result of CAV1 downregulation, and data supports the possibility that this could contribute to the pathogenesis of SSc myofibroblasts. This warrants further investigation in order to elucidate the mechanism by which CAV1 may influence AURKA activity to modulate primary cilium length, the influence that this has on SSc fibroblast phenotype in disease, and the potential scope for therapeutic intervention which could target ciliary length rescue in SSc in order to ameliorate fibrosis.

Chapter 7. Characterisation of SPAG17 expression and localisation at the Systemic Sclerosis primary cilium

7.1 Introduction

The experimental results discussed so far have shown that a shortened primary cilium is characteristic of SSc dermal fibroblasts, with previously described work focussing on analysis of ciliary length. However, changes to the composition of the primary cilia proteome were not investigated. Sperm Associated Antigen 17 (SPAG17) is an essential component of the central pair complex of motile cilia (Zhang et al., 2005, Zhang et al., 2007), and has also been implicated in the formation and function of primary cilia, in a study which demonstrated that SPAG17 knockdown in a murine model led to shortened primary cilia in chondrocytes, osteoblasts, and mouse embryonic fibroblasts (Teves et al., 2015). It was recently reported that SPAG17 is downregulated in SSc skin, and that its deficiency is sufficient to induce myofibroblast transition (Sapao et al., 2023). Based on the implications of these studies, we investigated SPAG17 in HC and SSc dermal fibroblasts to gain insight into the primary cilium outside of length alone, focussing on a ciliary component with evidence to suggest a link to SSc pathogenesis.

7.2 Results

7.2.1 SPAG17 expression and localisation

To investigate SPAG17 expression levels in skin, fixed and mounted skin sections from an SSc patient and HC donor were stained using

immunohistochemistry. Within the epidermis, expression levels appeared similar between HC and SSc, with staining most intense in the upper regions of the epidermis. In the SSc dermis, however, expression appeared to be reduced compared to HC dermis (Fig. 7.1).

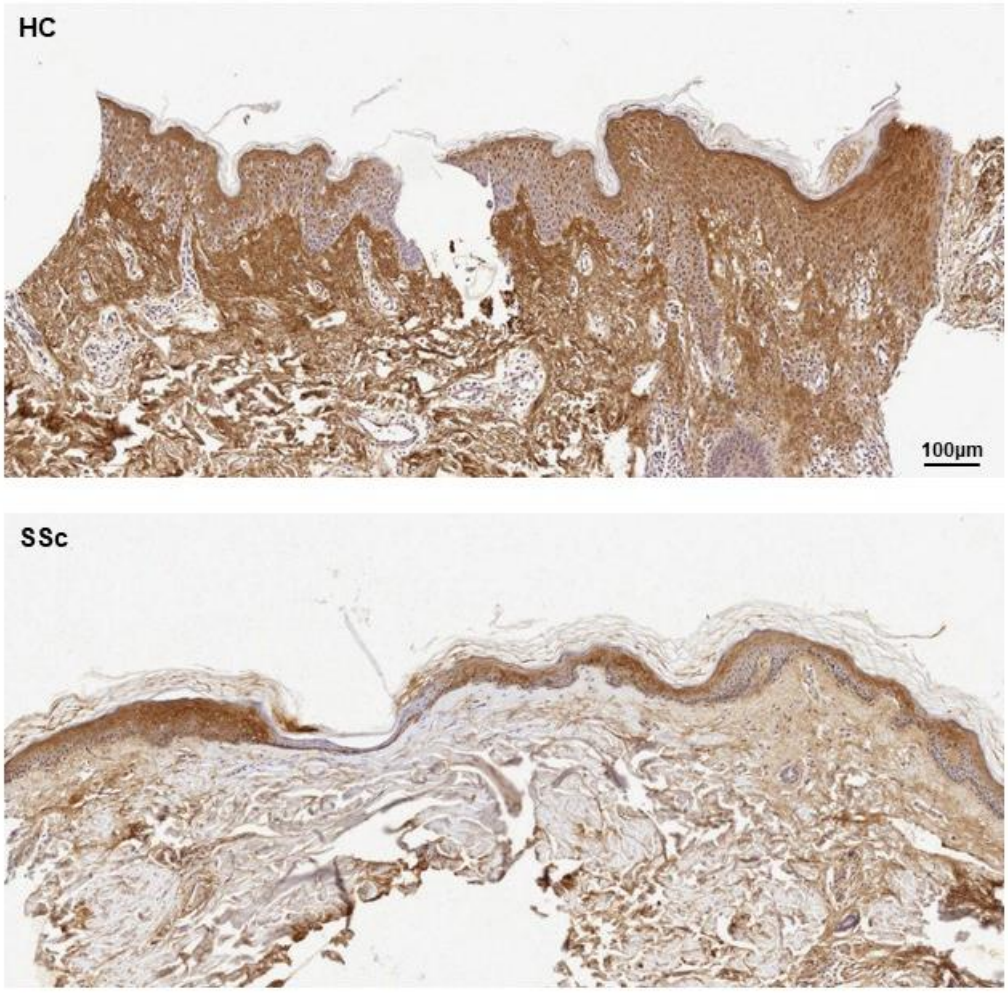

Figure 7.1: SPAG17 expression is reduced in the SSc dermis compared to HC
Immunohistochemistry staining of SPAG17 in skin sections from one HC donor and one SSc patient. Images taken at 20 x magnification. Scale bar shown at 100 µm.

In order to investigate SPAG17 expression in dermal fibroblasts specifically, transcript and protein levels were quantified in immortalised dermal fibroblast cell lines from three HC and three SSc donors. At the transcript level, *SPAG17* was variable between fibroblasts from different donors (Fig. 7.1A). Expression

was lower in HC 1 and HC 3 than in all three SSc lines, while HC 2 and SSc 1 – the lowest of the three SSc lines – showed comparable expression levels. When results from these triplicate lines were combined, *SPAG17* expression was overall lower in HC than SSc, but this was not statistically significant. At the protein level, SPAG17 was again variable between cell lines from different donors (Fig. 7.2B, C), though differences in protein levels between cell lines did not seem to match the variability observed at the transcript level (Fig. 7.2A). SSc 1 had the highest level of SPAG17 of all the cell lines, while HC 1 and HC 3 had greater levels of SPAG17 than SSc 2 and SSc 3, and HC 2 was comparable to SSc 3. When triplicate results were combined, there was no significant difference in SPAG17 protein abundance between HC and SSc.

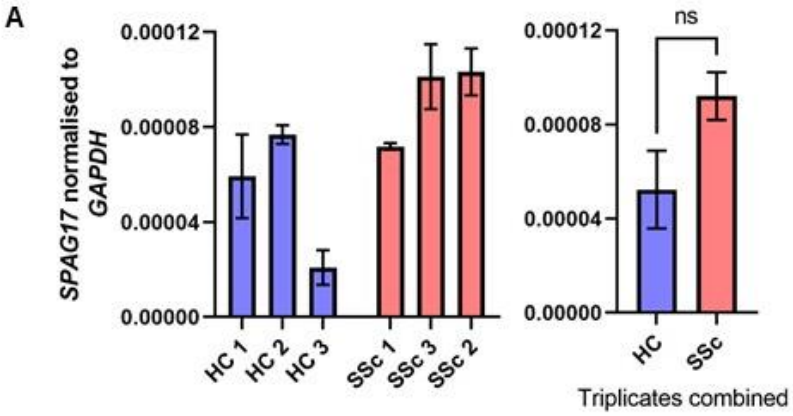

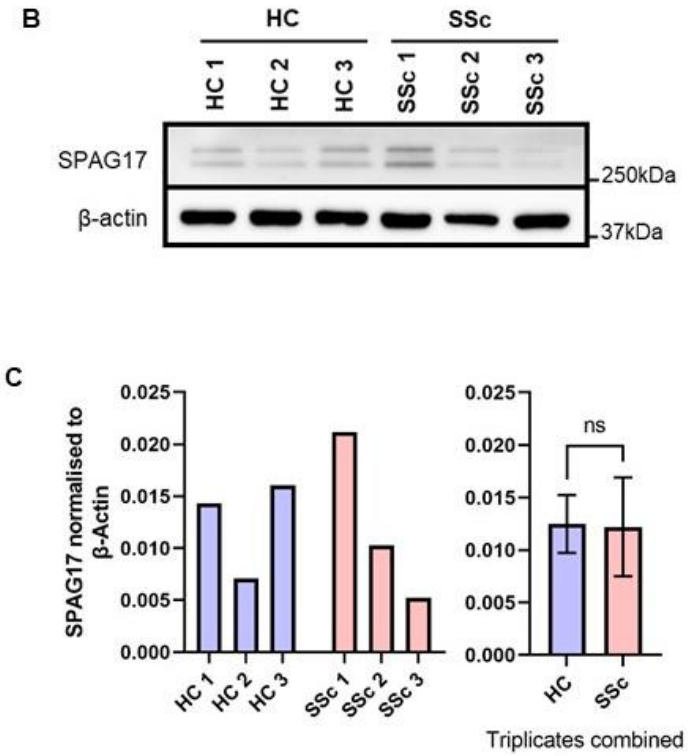

Figure 7.2: SPAG17 expression at the transcript and protein level vary between fibroblasts from different HC and SSc donors

Confluent HC and SSc fibroblasts were cultured in 0.5 % serum media for 48 h. RNA was harvested for quantification by qPCR, and protein harvested for quantification by Western Blot. A) Transcript levels of *SPAG17* normalised to housekeeping gene *GAPDH.* Bars show the mean of triplicate well results for each transcript analysed in each donor line, or the mean of the three donor lines in the combined triplicate graph. Error bars show standard error of the mean. B) Western Blots showing SPAG17 protein levels with β-Actin included as a loading control. C) SPAG17 densitometry of (B). Bars show the quantified protein levels from each individual donor line, or the mean of the three donor lines in the combined triplicate graph. Error bars show standard error of the mean. HC and SSc n=3. P values were calculated with unpaired two-tailed t-tests (ns = non-significant).

Next, the subcellular localisation of SPAG17 in dermal fibroblasts was investigated using immunofluorescence, with co-staining for nuclei and primary cilia using Ac-α-Tub. With standard confocal microscopy, SPAG17 was observed with some nuclear localisation in addition to distinct localisation of SPAG17 at the base of primary cilia (Fig. 7.3A, first panel). Airyscan detection

allowed for this ciliary base localisation to be observed with increased image resolution, revealing the presence of clearly visible SPAG17 localisation in puncta around the ciliary base (Fig. 7.3A, second panel).

SPAG17 localisation in HC fibroblasts was quantified and compared to SSc fibroblasts (Fig. 7.3B). The total number of cells were counted as well as the proportion of those cells that were identified as having a SPAG17-positive region at the ciliary base. SSc fibroblasts had a lower percentage of total cells with a SPAG17-positive ciliary base region than HC ($P<0.05$) (Fig. 7.3C). Furthermore, after fluorescence intensity of SPAG17 at the ciliary base was quantified, the intensity of SPAG17 at those regions was found to be lower in SSc than in HC ($P<0.05$) (Fig. 7.3D).

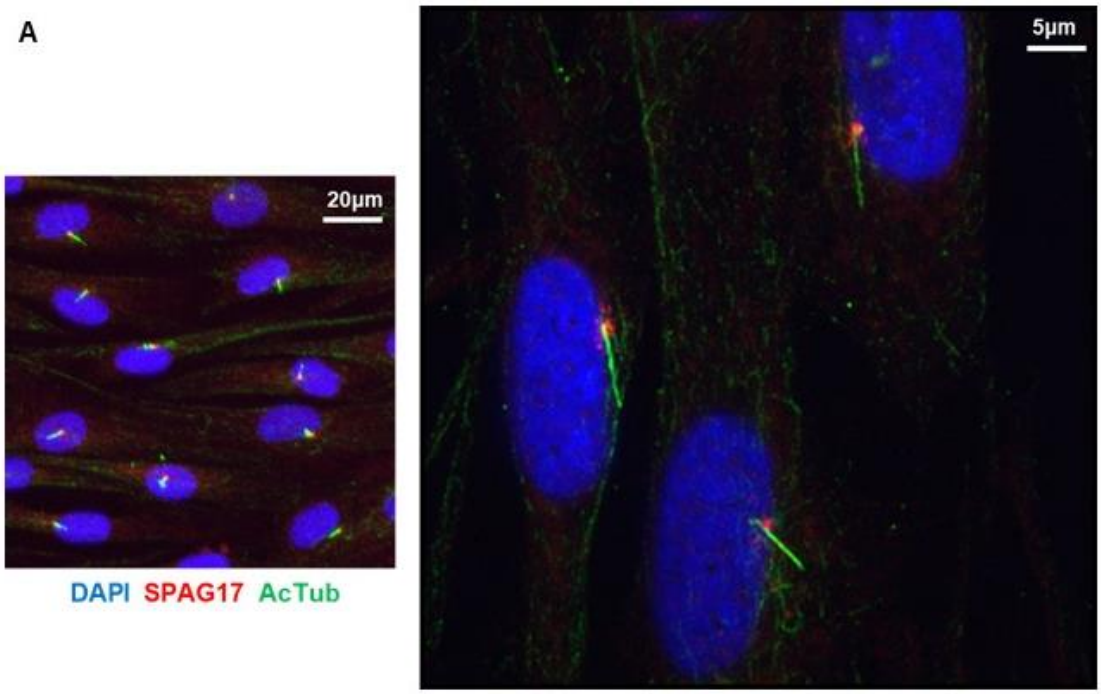

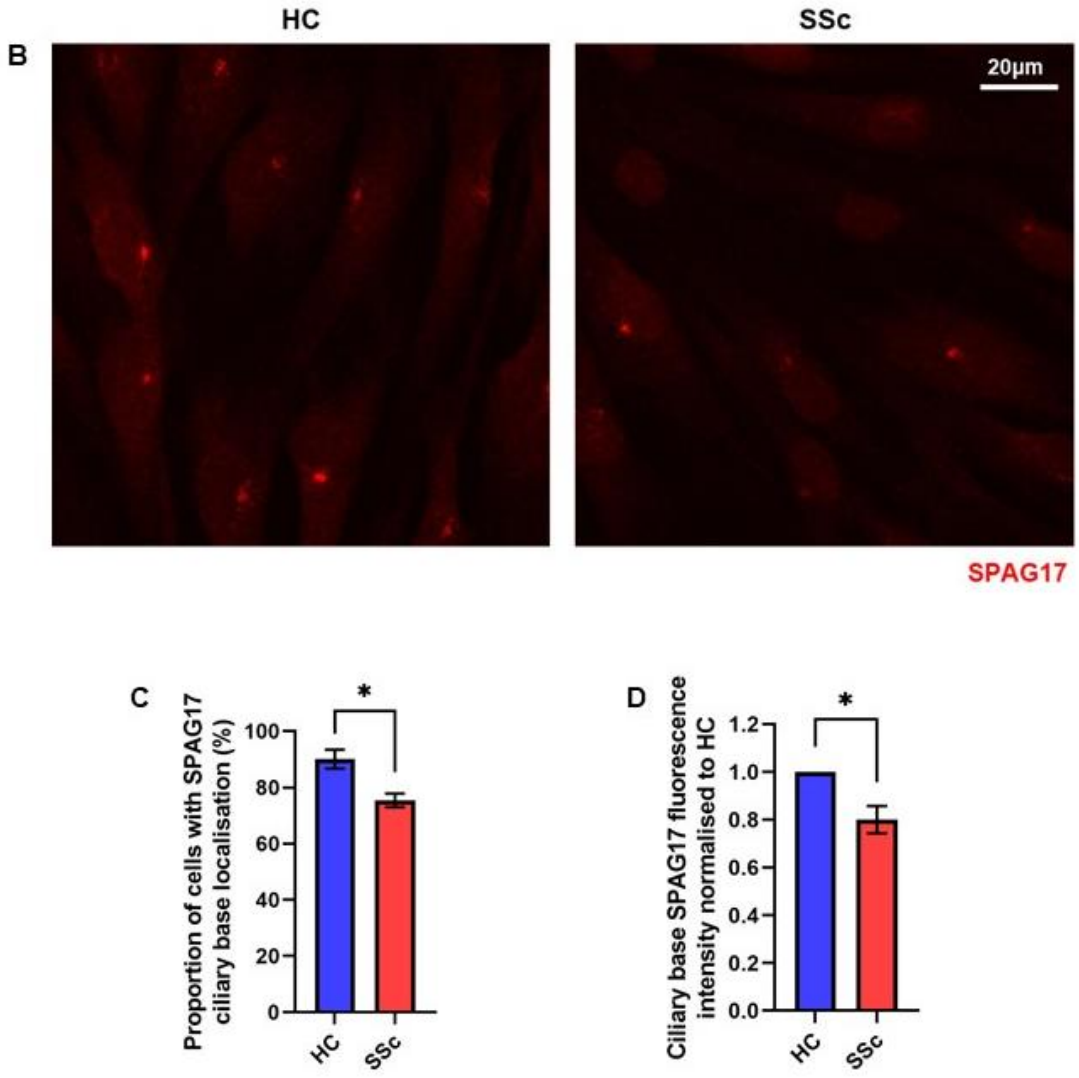

Figure 7.3: Ciliary base specific localisation of SPAG17 is reduced in SSc fibroblasts compared to HC

Confluent HC and SSc fibroblasts were cultured in 0.5 % serum media for 48 h to induce ciliogenesis, then fixed for SPAG17 staining by immunofluorescence. A) Representative immunofluorescence images taken at 400 x magnification showing cilia (stained for Ac-α-Tub in green) of individual healthy fibroblasts (DAPI nuclear staining in blue), and the subcellular localisation of SPAG17 (stained red). Scale bar shown at 20 µm for one image taken using standard confocal microscopy, and at 5 µm for one image taken using Airyscan detection to increase image resolution. B) Representative immunofluorescence images taken at 400 x magnification showing SPAG17 (stained in red) localisation foci in HC and SSc fibroblasts. Scale bar shown at 20 µm. C) Proportion of total cells imaged that had a SPAG17-positive region at their ciliary base in HC and SSc, from a minimum of 100 cells imaged across three fields of view per donor line. D) Fluorescence intensity of the SPAG17-positive ciliary base regions identified in (C) relative to HC. Bars show the mean and error bars

show standard error of the mean. HC and SSc n=3 donor lines. P values were calculated with unpaired two-tailed t-tests (*P<0.05).

Taken together, these data show a reduction of SPAG17 in the SSc dermis compared to HC at the whole skin level, while in fibroblasts specifically, both mRNA and protein expression were found to be variable between cell lines from different donors at the whole cell level, with no significant difference between HC and SSc when triplicate lines were combined. However, the subcellular localisation of SPAG17 at the ciliary base region was consistently and significantly reduced in all SSc fibroblast lines compared to all HC fibroblast lines. This suggests that loss of SPAG17 from the ciliary base could be another characteristic of the SSc-specific primary cilia phenotype.

7.2.2 The effect of TGFβ on SPAG17 expression and localisation

The effect of TGFβ on SPAG17 expression and subcellular localisation in dermal fibroblasts was also of interest, due to the ability of TGFβ to influence cilia incidence and length. TGFβ treatment significantly downregulated *SPAG17* mRNA expression in both HC and SSc (P<0.01) (Fig. 7.4A), consistent in all three HC and all three SSc donor fibroblast lines. However, at the protein level, the response to TGFβ was varied between cell lines from different donors, with SPAG17 increasing in some cell lines and decreasing in others after TGFβ treatment. When triplicate HC and SSc data were combined, there was an increase in SPAG17 protein abundance in response to TGFβ in both HC and SSc, although this was not statistically significant (Fig. 7.4B, C).

TGFβ reduced the proportion of cells with a SPAG17-positive region at the ciliary base in both HC (P<0.01) and SSc (P<0.05) (Fig. 7.4D). It also reduced the fluorescence intensity of SPAG17 at the base region in both HC (<P<0.01) and SSc (P<0.05) (Fig. 7.4E).

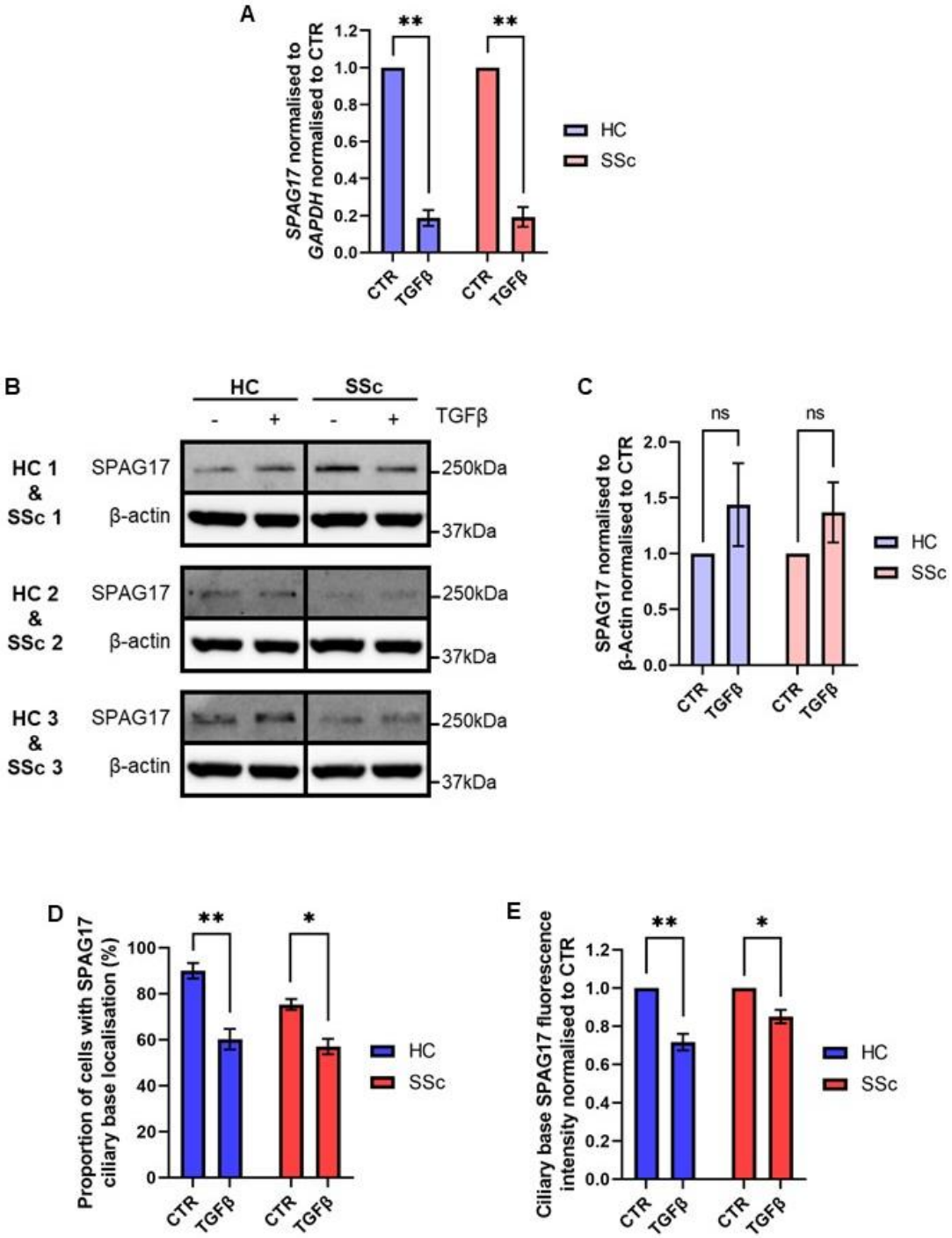

Figure 7.4: Despite variable response at the protein level, TGFβ reduces *SPAG17* mRNA and ciliary base-specific localisation of SPAG17 in HC and SSc fibroblasts

Confluent HC and SSc fibroblasts were cultured in 0.5 % serum media for 24 h, followed by 24 h in the presence/absence of 10 ng/mL TGFβ. RNA was harvested for quantification by qPCR, protein harvested for quantification by Western Blot, and cells fixed for SPAG17 staining and quantification by immunofluorescence. A) Transcript levels of *SPAG17* normalised to housekeeping gene *GAPDH*, relative to each group's CTR. B) Western Blots showing SPAG17 protein levels with β-Actin included as a loading control. C) SPAG17 densitometry of (B), relative to each group's CTR. D) Proportion of total cells imaged that had a SPAG17-positive region at their ciliary base in HC and SSc, from a minimum of 100 cells imaged across three fields of view per donor line. E) Fluorescence intensity of the SPAG17-positive ciliary base regions identified in (D) relative to each group's CTR. HC and SSc n=3 donor lines. Bars show the mean and error bars show standard error of the mean. P values were calculated with unpaired two-tailed t-tests (ns = non-significant, *P<0.05, **P<0.01).

The data presented in previous chapters strongly suggest that the mechanism by which TGFβ shortens primary cilia is independent of the mechanism by which SSc fibroblasts possess a stably shortened primary cilia phenotype. Due to the fact that SPAG17 localisation at the ciliary base region is lessened in the shorter cilia of SSc compared to HC, and that TGFβ reduces SPAG17 ciliary localisation alongside shortening cilia, this could be indicative that SPAG17 loss at the cilium is central to both SSc and TGFβ-induced ciliary shortening.

7.2.3 Characterisation of SPAG17 expression and localisation in Caveolin-1 knockdown fibroblasts

Next, we begun to investigate SPAG17 in preliminary experiments in the shCAV1 model of SSc, which possess shorter primary cilia. At the transcript level, knockdown of Caveolin-1 led to a reduction of *SPAG17* (Fig. 7.5A). Western Blot results did not show any SPAG17 protein in shCAV1 (Fig. 7.5C), but its detection by immunofluorescence in this condition, though lower than

control (Fig 7.5G), suggests that complete absence is unlikely and that this result is likely a consequence of insufficient detection sensitivity in the Western Blot assay. In both shSCR and shCAV1, treatment with TGFβ led to a reduction in *SPAG17* mRNA expression (Fig. 7.5B), as well as a reduction of SPAG17 protein levels in shSCR fibroblasts, though lack of detection of SPAG17 protein in shCAV1 fibroblasts by Western Blot made assessment of the effect of TGFβ impossible (Fig. 7.5C).

Subcellular ciliary localisation of SPAG17 in shCAV1 was found to mimic the phenotype observed in SSc fibroblasts, with fewer cells possessing a SPAG17 positive region at the ciliary base (Fig. 7.5D, G), and the fluorescence intensity of SPAG17 at these regions being reduced in shCAV1 compared to shSCR (Fig. 7.5E, G). In both cell types, as observed in HC and SSc, TGFβ again exacerbated both of these observations (Fig. 7.5D, F).

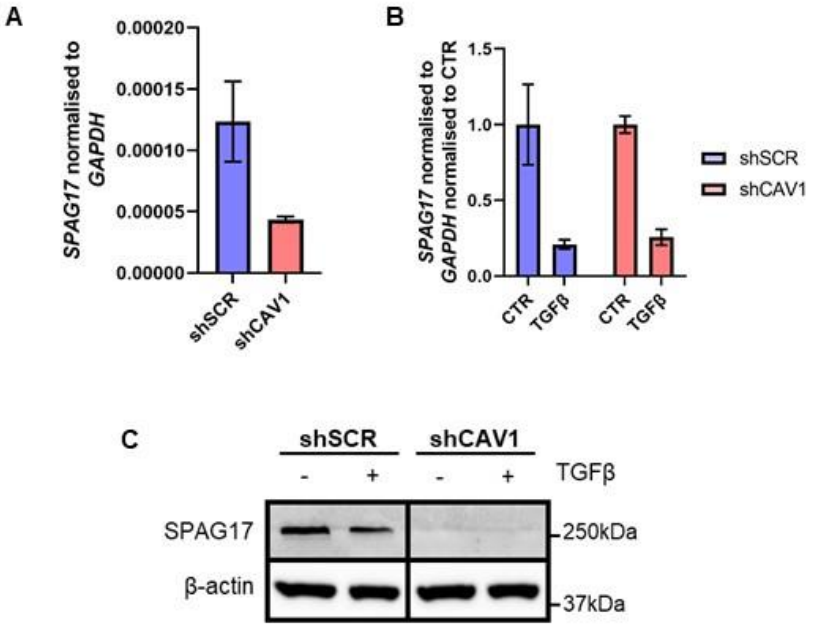

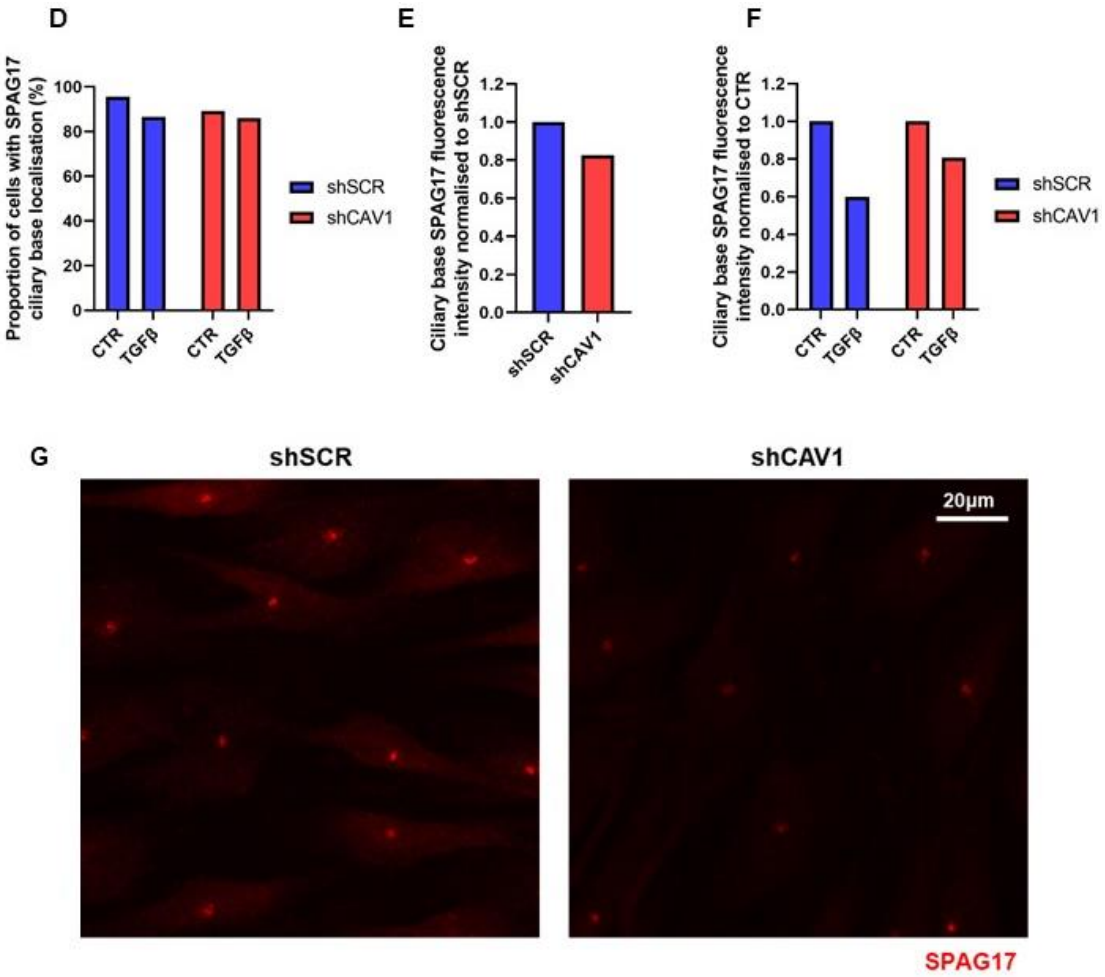

Figure 7.5: *SPAG17* mRNA levels, SPAG17 protein levels, and ciliary base localisation of SPAG17 are reduced in shCAV1 fibroblasts compared to shSCR

Confluent shSCR and shCAV1 fibroblasts were cultured in 0.5 % serum media for 24 h, followed by 24 h in the presence/absence of 10 ng/mL TGFβ. RNA was harvested for quantification by qPCR, protein harvested for quantification by Western Blot, and cells fixed for SPAG17 staining and quantification by immunofluorescence. A) Transcript levels of *SPAG17* normalised to housekeeping gene *GAPDH* in shSCR and shCAV1. Bars show the mean of triplicate well results for each transcript analysed in each cell line, error bars show standard error of the mean. B) As for (A), but showing transcript level changes in response to TGFβ, relative to each line's CTR. C) Western Blots showing SPAG17 protein levels with β-Actin included as a loading control. D) Proportion of total cells imaged that had a SPAG17-positive region at their ciliary base, from a minimum of 100 cells imaged across three fields of view per cell line. E) Fluorescence intensity of the SPAG17-positive ciliary base regions in shSCR and shCAV1 identified in (D) relative to shSCR. F) As for (E), but showing fluorescence intensity changes in response to TGFβ, relative to each line's CTR. G) Representative immunofluorescence images taken at 400 x magnification

showing SPAG17 (stained in red) localisation foci in shSCR and shCAV1 fibroblasts. Scale bar shown at 20 μm. shSCR and shCAV1 n=1.

As inhibition of AURKA with MLN8054 was sufficient to rescue shortened ciliary length in SSc and shCAV1 fibroblasts, the effect of MLN8054 on SPAG17 subcellular localisation in shSCR and shCAV1 fibroblasts was also studied in a preliminary experiment. There was little effect on the proportion of cells which possess a SPAG17-positive region at the ciliary base in any cell line (Fig. 7.6A). However, AURKA inhibition did increase the fluorescence intensity of SPAG17 at these regions in shCAV1 fibroblasts, while in shSCR fibroblasts, intensity was decreased (Fig. 7.6B). This could suggest that the ciliary SPAG17 localisation induced by CAV1 knockdown may be at least partially dependent on AURKA activity, as is its shorter cilia phenotype.

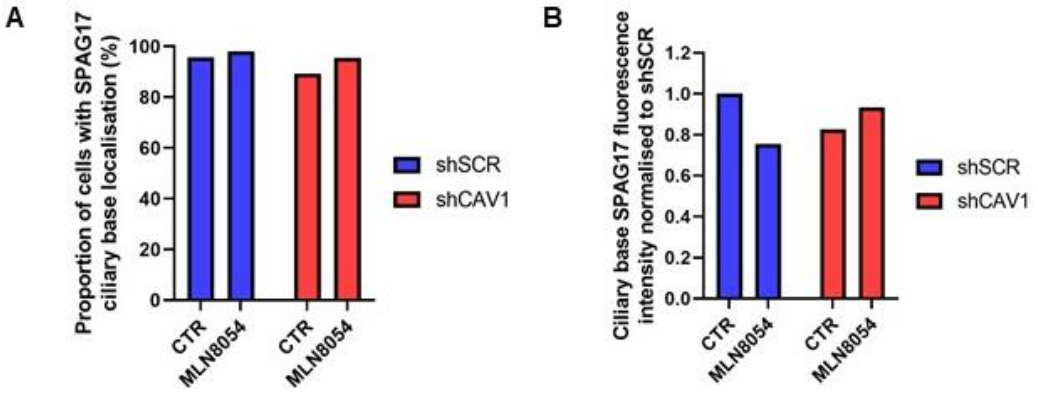

Figure 7.6: Inhibition of AURKA partially ameliorates the reduced SPAG17 localisation at the ciliary base in shCAV1 fibroblasts

Confluent shSCR and shCAV1 fibroblasts were cultured in 0.5 % serum media for 24 h followed by 24 h treatment with 10 μM MLN8054 or DMSO control in 0.5 % serum media. Cells were fixed for SPAG17 staining and quantification by immunofluorescence. A) Proportion of total shSCR and shCAV1 cells imaged that had a SPAG17-positive region at their ciliary base, from a minimum of 100 cells imaged across three fields of view per cell line. B) Fluorescence intensity of the SPAG17-positive ciliary base regions in shSCR and shCAV1 identified in (A), in CTR and MLN8054-treated conditions, relative to shSCR. shSCR and shCAV1 n=1.

7.3 Discussion

In this chapter, we show novel evidence of reduced localisation of SPAG17 at the base of primary cilia in SSc dermal fibroblasts. Research into the ciliary role of SPAG17 has primarily been conducted in the context of motile cilia, where it has been shown to be a component of the central pair complex (Zhang et al., 2005, Zhang et al., 2007), and to be essential for motile cilia ultrastructural integrity (Teves et al., 2013). In a subsequent study, Teves et al. demonstrated that experimental depletion of SPAG17 led to significantly shortened primary cilia in chondrocytes, osteoblasts, and mouse embryonic fibroblasts (MEFs) (Teves et al., 2015), leading the authors to propose a role for SPAG17 in the structural integrity of immotile primary cilia as well as in motile cilia. The current study adds to the still limited understanding of the role of SPAG17 at the primary cilium, by being the first to show specific localisation foci of SPAG17 at the base of the primary cilium in dermal fibroblasts by immunofluorescence.

Our data also adds evidence to the association of SPAG17 with primary cilia morphology proposed by Teves et al., by demonstrating that ciliary shortening consistently correlated with loss of SPAG17 localisation to the ciliary base in both SSc fibroblasts and CAV1-depleted fibroblasts with shorter cilia, as well as during TGFβ-induced cilia shortening. The latter is an interesting observation since our data indicates an alternative mechanism of cilia shortening by TGFβ compared to that regulating cilia length in SSc and shCAV1 dermal fibroblasts. It would be interesting to examine SPAG17 expression and localisation in other contexts of ciliary shortening.

A recent study linked SPAG17 to SSc, where RNA-sequencing analysis of skin biopsies from SSc patients found a marked decreased in *SPAG17* expression compared to healthy controls (E. D. O. Roberson et al., 2023). Our observation

of reduced SPAG17 staining by immunohistochemistry in SSc skin biopsies compared to healthy control skin sections is in accordance with this finding. In a subsequent study, single-cell RNA-sequencing of skin biopsies showed that *SPAG17*-expressing microvascular endothelial cells and fibroblasts were less frequent in SSc compared to HC, and reduced SPAG17 protein in skin biopsy sections and in cultured SSc dermal fibroblasts was identified by immunofluorescence (Sapao et al., 2023). While our analysis of SPAG17 expression at the transcript and protein level did not find significantly reduced SPAG17 expression in SSc donor dermal fibroblast lines compared to HC, the loss of SPAG17 fluorescence at the ciliary base was consistently observed in each SSc line, and we propose that SPAG17 loss specifically at its ciliary localisation foci may be of importance in any contribution to SSc pathogenesis.

Sapao et al. went on to demonstrate that CRISPR-mediated knockout of SPAG17 in human dermal fibroblasts led to increased expression of αSMA and procollagen I. Additionally, in a conditional SPAG17 knockout mouse model, animals developed spontaneous skin fibrosis which phenocopied characteristic observations of SSc patient skin. By unbiased transcriptome profiling, explanted dermal fibroblasts from these mice were shown to have an enrichment of fibrotic hallmarks which consistently overlapped with those expressed in explanted SSc patient dermal fibroblasts. Interestingly, explanted SPAG17 deficient mouse fibroblasts displayed constitutive activation of the TGFβ signalling pathway, with heightened nuclear accumulation of SMAD2/3. Both nuclear SMAD2/3 accumulation, along with upregulation of αSMA and procollagen I, was ameliorated by treatment with TGFβ pathway inhibitors, leading the authors to propose that the observed profibrotic phenotype resulting from SPAG17 depletion was mediated by TGFβ pathway activation. While ciliary length and

morphology was not assessed by Sapao et al., previously published work showed that SPAG17 knockout can induce ciliary shortening (Teves et al., 2015). Additionally, our current study shows ciliary shortening in SSc associated with SPAG17 loss at the ciliary base and as demonstrated in previous chapters, we showed that rescue of SSc cilia length correlated with some reduction of TGFβ-induced fibrotic marker expression and fibroblast contractility. Considering these results together, we propose that shortened primary cilia may be implicated in the TGFβ-mediated profibrotic phenotype that Sapao et al. reported in their SPAG17 deficient animal model. Collectively, this data warrants consideration of the hypothesis discussed in the previous chapter: that primary cilia may exert negative regulation of TGFβ signalling, and their shortening may contribute to the pathogenesis of fibrotic diseases such as SSc. It would be extremely interesting to overexpress SPAG17 in SSc dermal fibroblasts and assess any effect on both ciliary length and the fibrotic phenotype.

ATAC-sequencing conducted by Sapao et al. in microvascular endothelial cells explanted from skin biopsies showed significantly reduced chromatin accessibility at the *SPAG17* locus in SSc compared to HC, which they suggest may be responsible for loss of SPAG17, but the same experiment in explanted SSc and HC dermal fibroblasts yielded mostly insignificant results. Preliminary data obtained in the current study, if recapitulated in experimental repeats, could suggest an alternative mechanism for aberrant SPAG17 in dermal fibroblasts driven by CAV1 downregulation and aberrant AURKA activity. While it is important to note that this data requires replication, shCAV1 fibroblasts had reduced SPAG17 expression at both the transcript and protein level, and a reduced SPAG17 localisation to the ciliary base, mimicking the observation in

SSc. While the effect of AURKA inhibition on SPAG17 localisation was not examined in HC and SSc dermal fibroblasts and would be important to establish, AURKA inhibition increased SPAG17 ciliary base localisation in shCAV1 fibroblasts in a preliminary experiment, to similar levels observed in shSCR control fibroblasts.

Replication of this experiment in both shCAV1 fibroblasts and shSCR fibroblasts, in addition to SSc and HC fibroblasts, will be crucial to elucidate whether SPAG17 loss at the primary cilium is a consequence of ciliary shortening in SSc and CAV1-depleted fibroblasts, which in this study are suggested to be a consequence of aberrant AURKA activity, or whether it plays a driving role in ciliary disassembly, with previous research showing that SPAG17 depletion is sufficient to induce ciliary shortening by itself (Teves et al., 2015). To further understand this, it would be interesting to overexpress SPAG17 in SSc and shCAV1 dermal fibroblasts as previously mentioned, and to inhibit AURKA in SPAG17-depleted cells, followed by assessment of primary cilia morphology. While the data shown here is exploratory, further investigation into the roles of SPAG17, AURKA, CAV1, and primary cilia in dermal fibroblasts, and the mechanisms of their interactions, could shed significant insight into the molecular pathogenesis of SSc.

7.4 Summary

These data show for the first time that SPAG17 localises at the base of primary cilia in healthy dermal fibroblasts, and provides evidence of reduced ciliary localisation of SPAG17 in SSc. This phenotype was also observed in the shCAV1 fibroblast model of SSc, which suggests that downregulation of Caveolin-1 is able to induce SPAG17 downregulation, as well as in cilia

shortened by TGFβ treatment. Thus, SPAG17 loss at the primary cilium is consistently correlated with ciliary shortening, but whether SPAG17 loss is an initiator of ciliary shortening in these cells or a consequence of it remains to be elucidated. Deeper understanding of this mechanism and of the relevance of SPAG17 loss to proper ciliary function will provide interesting insight to better understand the role of an aberrant primary cilium in SSc, and potentially other fibrotic conditions, as well as help to guide efforts to assess the potential therapeutic benefits of making the primary cilium a target for medical intervention.

Chapter 8. Concluding remarks

In this study, we identified that primary cilia of systemic sclerosis (SSc) dermal fibroblasts are significantly and stably shorter than those of healthy controls. Cilia length was remarkably consistent between fibroblasts in explanted cultures consisting of heterogeneous fibroblast populations, suggesting that this phenotype is a tightly regulated, stable hallmark of these cells. Shortened primary cilia were found even in very early diagnosis of systemic sclerosis (VEDOSS) patient fibroblasts, a diagnosis made before the appearance of clinically detectable fibrosis. This suggests that shortened primary cilia may be implicated in the development of the disease, rather than a consequence of it. As well as increasing sample sizes, future work to elaborate on these findings should include high resolution imaging such as electron microscopy to investigate the structural integrity of these shortened cilia. It would also be interesting to investigate cilium length in cells of other organs implicated in SSc pathogenesis, such as the lungs.

Consistent with studies in other cell types, we also showed that TGFβ treatment significantly shortens cilia in healthy and SSc-derived dermal fibroblasts. We suggest that in dermal fibroblasts – different to the various previously reported mechanisms in other cell types – TGFβ-induced ciliary shortening is at least partially dependent on activation of ROCK2, and is not mediated by activation of HDAC6. It would be interesting to explore the effect of TGFβ treatment on the expression and activity of IFT88 in dermal fibroblasts, another proposed mechanism of TGFβ-induced ciliary shortening in other cell types.

Importantly, we show that despite the demonstrated activation of TGFβ signalling as a fibrotic hallmark in SSc and the ability of TGFβ to shorten cilia

length, this shortening effect is not stably maintained, and inhibition of the TGFβ signalling pathway does not restore the shortened cilia phenotype of SSc dermal fibroblasts to normal length. Therefore, we demonstrate that the stable reduced primary cilium length phenotype of SSc is maintained by a TGFβ-independent mechanism.

Furthermore, we showed that inhibition of the AURKA-HDAC6 axis, a known negative regulator of ciliary length, restored the cilia of SSc dermal fibroblasts to normal length, while leaving healthy control cilia unaffected. Therefore, we propose that the stable reduction of ciliary length in SSc may be mediated by aberrant activity of the AURKA-HDAC6 axis. Future work should employ additional methods of inhibition of the AURKA-HDAC6 axis to validate these findings, and it would also be interesting to explore the effect of experimental AURKA or HDAC6 overexpression in healthy dermal fibroblasts.

Interestingly, along with increased expression of profibrotic markers typical of SSc, dermal fibroblasts with experimentally induced silencing of CAV1 – reported to be downregulated in SSc and reported to play poorly defined roles in ciliary structure and function – was sufficient to induce a stably shortened cilium phenotype which mimics that of SSc. Preliminary data showed that inhibition of the AURKA-HDAC6 axis restored cilium length in CAV1-depleted fibroblasts to the same length as control, suggesting that ciliary shortening in SSc and in CAV1-deficiency may share the same AURKA-HDAC6 dependent mechanism. It is therefore pertinent to consider that CAV1 downregulation may drive ciliary shortening in SSc by inducing aberrant activity of AURKA. The molecular mechanism of this proposed interaction remains to be elucidated, and should be a focus of future work.

In our experiments, restoration of cilium length in SSc and CAV1-depleted dermal fibroblasts by AURKA inhibition correlated with some reduction of the expression of profibrotic gene and protein expression, particularly that which was induced by treatment with exogenous TGFβ. Crucially, in an experimental model of fibroblast contractility, a key TGFβ-inducible feature of fibrotic myofibroblasts, inhibition of AURKA reduced the increased contractility of both SSc dermal fibroblasts and CAV1-depleted fibroblasts in response to TGFβ.

Finally, we demonstrated for the first time that SPAG17 localises at the base of the primary cilium in healthy fibroblasts and that the shortened cilia of SSc dermal fibroblasts, CAV1-depleted fibroblasts, and TGFβ-treated fibroblasts share markedly reduced ciliary localisation of SPAG17. It will be interesting to further explore the poorly defined role of SPAG17 at the primary cilium, the consequences of its loss, and how this protein may be implicated in the proposed model of cilium length modulation by CAV1 and AURKA.

Based on these findings, we propose that it is pertinent to consider that an aberrant primary cilium may be implicated in the pathogenesis of fibrosis in SSc, particularly that which is mediated by the activation of TGFβ signalling, and propose that a functional primary cilium may be essential for balancing TGFβ signalling output. In order to elaborate on these findings, further research should explore the effects of experimental modulation of cilium length on cellular signalling output and the fibrotic phenotype. Organotypic skin culture models and *in vivo* mouse models such as the bleomycin model of fibrosis, should be employed in combination with experimental modulation of AURKA and CAV1, to explore their contribution to fibrosis in contexts that will be more representative of complex physiological tissue homeostasis. Models such as

these will be more informative than the fibroblast culture models employed in this study.

The Wnt and HH signalling pathways are both coordinated by the primary cilium and dysregulated in SSc, but were not explored in this study. Future work should investigate the effects of experimental modulation of dermal fibroblast cilium length on the signalling output of these pathways. It would be interesting, for these pathways and for TGFβ signalling, to employ super-resolution microscopy and live imaging to observe specific spatio-temporal regulation of signalling pathway components at the shortened primary cilia of both SSc and CAV1-depleted fibroblasts, as well as in cells with restored cilium length after inhibition of AURKA.

It is well known from the study of human diseases driven by genetic ciliary defects – the ciliopathies – that defective primary cilia can contribute to human diseases. However, their implication in diseases outside of the ciliopathies, including fibrotic diseases, is only beginning to be explored. We propose that SSc may be one such disease, characterised from early onset by shortened cilia of dermal fibroblasts, which may contribute to the pathogenesis of SSc fibrosis. In SSc, a disease of unknown aetiology for which there remains no cure and limited treatment options, the identification of potential pathogenic contributors is crucial to direct the search for effective therapeutic targets. We propose that the primary cilium should be explored as one such potential target. The cilium is known to be important in the transduction of a multitude of interacting signalling pathways, including those known to be dysregulated in SSc. Therefore, therapeutic targeting of this organelle could prove uniquely beneficial to restore normal regulation to a number of signalling pathways, compared to therapeutic targeting of individual signalling components.

Additionally, the dysregulated cellular behaviour of fibrosis is shared between its presentations in numerous clinical contexts. With fibrosis known to be a clinical characteristic of several ciliopathies, and recent studies such as ours proposing pathogenic roles for aberrant primary cilia in fibrotic diseases, the hypothesis that primary cilia may be implicated in the pathogenesis of a broad range of fibrotic conditions which contribute to significant human morbidity and mortality warrants further investigation.

Bibliography

Abdelhamed, Z. A., Wheway, G., Szymanska, K., Natarajan, S., Toomes, C., Inglehearn, C., & Johnson, C. A. (2013). Variable expressivity of ciliopathy neurological phenotypes that encompass Meckel–Gruber syndrome and Joubert syndrome is caused by complex de-regulated ciliogenesis, Shh and Wnt signalling defects. *Human Molecular Genetics*, *22*(7), 1358–1372. https://doi.org/10.1093/hmg/dds546

Adams, M., Smith, U. M., Logan, C. V., & Johnson, C. A. (2008). Recent advances in the molecular pathology, cell biology and genetics of ciliopathies. *Journal of Medical Genetics*, *45*(5), 257–267. https://doi.org/10.1136/jmg.2007.054999

Akhmetshina, A., Palumbo, K., Dees, C., Bergmann, C., Venalis, P., Zerr, P., Horn, A., Kireva, T., Beyer, C., Zwerina, J., Schneider, H., Sadowski, A., Riener, M.-O., MacDougald, O. A., Distler, O., Schett, G., & Distler, J. H. W. (2012). Activation of canonical Wnt signalling is required for TGF-β-mediated fibrosis. *Nature Communications*, *3*(1), 735. https://doi.org/10.1038/ncomms1734

Alessi, D. R., Andjelkovic, M., Caudwell, B., Cron, P., Morrice, N., Cohen, P., & Hemmings, B. A. (1996). Mechanism of activation of protein kinase B by insulin and IGF-1. *The EMBO Journal*, *15*(23), 6541–6551. https://doi.org/10.1002/j.1460-2075.1996.tb01045.x

Allanore, Y., Simms, R., Distler, O., Trojanowska, M., Pope, J., Denton, C. P., & Varga, J. (2015). Systemic sclerosis. *Nature Reviews Disease Primers*, *1*(1), 15002. https://doi.org/10.1038/nrdp.2015.2

Álvarez-Satta, M., Lago-Docampo, M., Bea-Mascato, B., Solarat, C., Castro-Sánchez, S., Christensen, S. T., & Valverde, D. (2021). ALMS1 Regulates TGF-β Signaling and Morphology of Primary Cilia. *Frontiers in Cell and Developmental Biology*, *9*, 623829. https://doi.org/10.3389/fcell.2021.623829

Antar, S. A., Ashour, N. A., Marawan, M. E., & Al-Karmalawy, A. A. (2023). Fibrosis: Types, Effects, Markers, Mechanisms for Disease Progression, and Its Relation with Oxidative Stress, Immunity, and Inflammation. *International Journal of Molecular Sciences*, *24*(4), 4004. https://doi.org/10.3390/ijms24044004

Anvarian, Z., Mykytyn, K., Mukhopadhyay, S., Pedersen, L. B., & Christensen, S. T. (2019). Cellular signalling by primary cilia in development, organ function and

disease. *Nature Reviews Nephrology*, *15*(4), 199–219. https://doi.org/10.1038/s41581-019-0116-9

Arrighi, N., Lypovetska, K., Moratal, C., Giorgetti-Peraldi, S., Dechesne, C. A., Dani, C., & Peraldi, P. (2017). The primary cilium is necessary for the differentiation and the maintenance of human adipose progenitors into myofibroblasts. *Scientific Reports*, *7*(1), 15248. https://doi.org/10.1038/s41598-017-15649-2

Asano, Y., Ihn, H., Jinnin, M., Tamaki, K., & Sato, S. (2011). Altered dynamics of transforming growth factor (TGF-) receptors in scleroderma fibroblasts. *Annals of the Rheumatic Diseases*, *70*(2), 384–387. https://doi.org/10.1136/ard.2009.127811

Asano, Y., Ihn, H., Yamane, K., Jinnin, M., Mimura, Y., & Tamaki, K. (2005). Increased Expression of Integrin αvβ3 Contributes to the Establishment of Autocrine TGF-β Signaling in Scleroderma Fibroblasts. *The Journal of Immunology*, *175*(11), 7708–7718. https://doi.org/10.4049/jimmunol.175.11.7708

Asano, Y., Ihn, H., Yamane, K., Kubo, M., & Tamaki, K. (2004). Impaired Smad7-Smurf–mediated negative regulation of TGF-β signaling in scleroderma fibroblasts. *Journal of Clinical Investigation*, *113*(2), 253–264. https://doi.org/10.1172/JCI16269

Avasthi, P., & Marshall, W. F. (2012). Stages of ciliogenesis and regulation of ciliary length. *Differentiation*, *83*(2), 30–42. https://doi.org/10.1016/j.diff.2011.11.015

Avouac, J., Fransen, J., Walker, U., Riccieri, V., Smith, V., Muller, C., Miniati, I., Tarner, I., Randone, S. B., Cutolo, M., Allanore, Y., Distler, O., Valentini, G., Czirjak, L., Müller-Ladner, U., Furst, D., Tyndall, A., Matucci-Cerinic, M., & EUSTAR Group. (2011). Preliminary criteria for the very early diagnosis of systemic sclerosis: Results of a Delphi Consensus Study from EULAR Scleroderma Trials and Research Group. *Annals of the Rheumatic Diseases*, *70*(3), 476–481. https://doi.org/10.1136/ard.2010.136929

Ayers, N. B., Chenming, S., & Shi-You, C. (2018). Transforming growth factor-β signaling in systemic sclerosis. *The Journal of Biomedical Research*, *32*(1), 3. https://doi.org/10.7555/JBR.31.20170034

Bachmann-Gagescu, R., Dempsey, J. C., Phelps, I. G., O'Roak, B. J., Knutzen, D. M., Rue, T. C., Ishak, G. E., Isabella, C. R., Gorden, N., Adkins, J., Boyle, E. A., De Lacy, N., O'Day, D., Alswaid, A., Ramadevi A, R., Lingappa, L., Lourenço, C.,

Martorell, L., Garcia-Cazorla, À., … Doherty, D. (2015). Joubert syndrome: A model for untangling recessive disorders with extreme genetic heterogeneity. *Journal of Medical Genetics*, *52*(8), 514–522. https://doi.org/10.1136/jmedgenet-2015-103087

Bairkdar, M., Rossides, M., Westerlind, H., Hesselstrand, R., Arkema, E. V., & Holmqvist, M. (2021). Incidence and prevalence of systemic sclerosis globally: A comprehensive systematic review and meta-analysis. *Rheumatology*, *60*(7), 3121–3133. https://doi.org/10.1093/rheumatology/keab190

Bangs, F., & Anderson, K. V. (2017). Primary Cilia and Mammalian Hedgehog Signaling. *Cold Spring Harbor Perspectives in Biology*, *9*(5), a028175. https://doi.org/10.1101/cshperspect.a028175

Barnes, C. L., Malhotra, H., & Calvert, P. D. (2021). Compartmentalization of Photoreceptor Sensory Cilia. *Frontiers in Cell and Developmental Biology*, *9*, 636737. https://doi.org/10.3389/fcell.2021.636737

Basten, S. G., Willekers, S., Vermaat, J. S., Slaats, G. G., Voest, E. E., Van Diest, P. J., & Giles, R. H. (2013). Reduced cilia frequencies in human renal cell carcinomas versus neighboring parenchymal tissue. *Cilia*, *2*(1), 2. https://doi.org/10.1186/2046-2530-2-2

Bellando-Randone, S., Del Galdo, F., Lepri, G., Minier, T., Huscher, D., Furst, D. E., Allanore, Y., Distler, O., Czirják, L., Bruni, C., Guiducci, S., Avouac, J., Cutolo, M., Smith, V., & Matucci-Cerinic, M. (2021). Progression of patients with Raynaud's phenomenon to systemic sclerosis: A five-year analysis of the European Scleroderma Trial and Research group multicentre, longitudinal registry study for Very Early Diagnosis of Systemic Sclerosis (VEDOSS). *The Lancet Rheumatology*, *3*(12), e834–e843. https://doi.org/10.1016/S2665-9913(21)00244-7

Bergmann, C. (2019). Early and Severe Polycystic Kidney Disease and Related Ciliopathies: An Emerging Field of Interest. *Nephron*, *141*(1), 50–60. https://doi.org/10.1159/000493532

Bergmann, C., Chenguiti Fakhouri, S., Thuong, T., Filla, T., Rigau, A. R., Ekici, A. B., Merlevede, B., Hallenberger, L., Zhu, H., Dees, C., Matei, A., Auth, J., Györfi, A., Zhou, X., Rauber, S., Bozec, A., Dickel, N., Liang, C., Kunz, M., … Distler, J. H. W. (2024). Mutual amplification of GLI2 /Hedgehog and cJUN / AP1

signaling in fibroblasts in Systemic Sclerosis (SSc) – potential implications for combined therapies. *Arthritis & Rheumatology*, art.42979. https://doi.org/10.1002/art.42979

Bertolin, G., & Tramier, M. (2020). Insights into the non-mitotic functions of Aurora kinase A: More than just cell division. *Cellular and Molecular Life Sciences*, *77*(6), 1031–1047. https://doi.org/10.1007/s00018-019-03310-2

Beyer, C., Huscher, D., Ramming, A., Bergmann, C., Avouac, J., Guiducci, S., Meier, F., Vettori, S., Siegert, E., Jaeger, V. K., Maurer, B., Riemekasten, G., Walker, U., Müller-Ladner, U., Valentini, G., Matucci-Cerinic, M., Allanore, Y., Distler, O., Schett, G., & Distler, J. H. W. (2018). Elevated serum levels of sonic hedgehog are associated with fibrotic and vascular manifestations in systemic sclerosis. *Annals of the Rheumatic Diseases*, *77*(4), 626–628. https://doi.org/10.1136/annrheumdis-2016-210834

Beyer, C., Schramm, A., Akhmetshina, A., Dees, C., Kireva, T., Gelse, K., Sonnylal, S., De Crombrugghe, B., Taketo, M. M., Distler, O., Schett, G., & Distler, J. H. W. (2012). β-catenin is a central mediator of pro-fibrotic Wnt signaling in systemic sclerosis. *Annals of the Rheumatic Diseases*, *71*(5), 761–767. https://doi.org/10.1136/annrheumdis-2011-200568

Biernacka, A., Dobaczewski, M., & Frangogiannis, N. G. (2011). TGF-β signaling in fibrosis. *Growth Factors*, *29*(5), 196–202. https://doi.org/10.3109/08977194.2011.595714

Boerma, M., Fu, Q., Wang, J., Loose, D. S., Bartolozzi, A., Ellis, J. L., McGonigle, S., Paradise, E., Sweetnam, P., Fink, L. M., Vozenin-Brotons, M.-C., & Hauer-Jensen, M. (2008). Comparative gene expression profiling in three primary human cell lines after treatment with a novel inhibitor of Rho kinase or atorvastatin. *Blood Coagulation & Fibrinolysis*, *19*(7), 709–718. https://doi.org/10.1097/MBC.0b013e32830b2891

Bolaños, A. L., Milla, C. M., Lira, J. C., Ramírez, R., Checa, M., Barrera, L., García-Alvarez, J., Carbajal, V., Becerril, C., Gaxiola, M., Pardo, A., & Selman, M. (2012). Role of Sonic Hedgehog in idiopathic pulmonary fibrosis. *American Journal of Physiology-Lung Cellular and Molecular Physiology*, *303*(11), L978–L990. https://doi.org/10.1152/ajplung.00184.2012

Borgal, L., Habbig, S., Hatzold, J., Liebau, M. C., Dafinger, C., Sacarea, I., Hammerschmidt, M., Benzing, T., & Schermer, B. (2012). The Ciliary Protein Nephrocystin-4 Translocates the Canonical Wnt Regulator Jade-1 to the Nucleus to Negatively Regulate β-Catenin Signaling. *Journal of Biological Chemistry*, *287*(30), 25370–25380. https://doi.org/10.1074/jbc.M112.385658

Brachmann, S. M., Kleylein-Sohn, J., Gaulis, S., Kauffmann, A., Blommers, M. J. J., Kazic-Legueux, M., Laborde, L., Hattenberger, M., Stauffer, F., Vaxelaire, J., Romanet, V., Henry, C., Murakami, M., Guthy, D. A., Sterker, D., Bergling, S., Wilson, C., Brümmendorf, T., Fritsch, C., … Maira, S.-M. (2012). Characterization of the Mechanism of Action of the Pan Class I PI3K Inhibitor NVP-BKM120 across a Broad Range of Concentrations. *Molecular Cancer Therapeutics*, *11*(8), 1747–1757. https://doi.org/10.1158/1535-7163.MCT-11-1021

Breslow, D. K., Koslover, E. F., Seydel, F., Spakowitz, A. J., & Nachury, M. V. (2013). An in vitro assay for entry into cilia reveals unique properties of the soluble diffusion barrier. *Journal of Cell Biology*, *203*(1), 129–147. https://doi.org/10.1083/jcb.201212024

Budi, E. H., Schaub, J. R., Decaris, M., Turner, S., & Derynck, R. (2021). TGF -β as a driver of fibrosis: Physiological roles and therapeutic opportunities. *The Journal of Pathology*, *254*(4), 358–373. https://doi.org/10.1002/path.5680

Burgy, O., & Königshoff, M. (2018). The WNT signaling pathways in wound healing and fibrosis. *Matrix Biology*, *68–69*, 67–80. https://doi.org/10.1016/j.matbio.2018.03.017

Cao, H.-L., Zhou, J., Chen, X.-B., Landeck, L., Jian-Qiang, Y., Chen, J.-Q., Li, W., Cai, S.-Q., Zheng, M., & Man, X.-Y. (2016). Inhibition of the hedgehog pathway leads to antifibrotic effects in dermal fibrosis. *Discovery Medicine*, *22*(122), 311–318.

Carotenuto, P., Gradilone, S. A., & Franco, B. (2023). Cilia and Cancer: From Molecular Genetics to Therapeutic Strategies. *Genes*, *14*(7), 1428. https://doi.org/10.3390/genes14071428

Carvalho-Santos, Z., Azimzadeh, J., Pereira-Leal, José. B., & Bettencourt-Dias, M. (2011). Tracing the origins of centrioles, cilia, and flagella. *Journal of Cell Biology*, *194*(2), 165–175. https://doi.org/10.1083/jcb.201011152

Carver, L. A., & Schnitzer, J. E. (2003). Caveolae: Mining little caves for new cancer targets. *Nature Reviews Cancer*, *3*(8), 571–581. https://doi.org/10.1038/nrc1146

Chakravarthy, B., Gaudet, C., Ménard, M., Brown, L., Atkinson, T., LaFerla, F. M., Ito, S., Armato, U., Dal Prà, I., & Whitfield, J. (2012). Reduction of the immunostainable length of the hippocampal dentate granule cells' primary cilia in 3xAD-transgenic mice producing human Aβ1-42 and tau. *Biochemical and Biophysical Research Communications*, *427*(1), 218–222. https://doi.org/10.1016/j.bbrc.2012.09.056

Choi, S. Y., Chacon-Heszele, M. F., Huang, L., McKenna, S., Wilson, F. P., Zuo, X., & Lipschutz, J. H. (2013). Cdc42 Deficiency Causes Ciliary Abnormalities and Cystic Kidneys. *Journal of the American Society of Nephrology*, *24*(9), 1435–1450. https://doi.org/10.1681/ASN.2012121236

Chowdhury, P., Perera, D., Powell, R. T., Talley, T., Tripathi, D. N., Park, Y. S., Mancini, M. A., Davies, P., Stephan, C., Coarfa, C., & Dere, R. (2021). Therapeutically actionable signaling node to rescue AURKA driven loss of primary cilia in VHL-deficient cells. *Scientific Reports*, *11*(1), 10461. https://doi.org/10.1038/s41598-021-89933-7

Chowdhury, P., Powell, R. T., Stephan, C., Uray, I. P., Talley, T., Karki, M., Tripathi, D. N., Park, Y. S., Mancini, M. A., Davies, P., & Dere, R. (2018). Bexarotene – a novel modulator of AURKA and the primary cilium in *VHL* -deficient cells. *Journal of Cell Science*, *131*(24), jcs219923. https://doi.org/10.1242/jcs.219923

Christensen, S. T., Morthorst, S. K., Mogensen, J. B., & Pedersen, L. B. (2017). Primary Cilia and Coordination of Receptor Tyrosine Kinase (RTK) and Transforming Growth Factor β (TGF-β) Signaling. *Cold Spring Harbor Perspectives in Biology*, *9*(6), a028167. https://doi.org/10.1101/cshperspect.a028167

Cipriani, P., Di Benedetto, P., Capece, D., Zazzeroni, F., Liakouli, V., Ruscitti, P., Pantano, I., Berardicurti, O., Carubbi, F., Alesse, E., & Giacomelli, R. (2014). Impaired Cav-1 expression in SSc mesenchymal cells upregulates VEGF signaling: A link between vascular involvement and fibrosis. *Fibrogenesis & Tissue Repair*, *7*(1), 13. https://doi.org/10.1186/1755-1536-7-13

Clark, K., Xu, S., Ong, V., Buckley, C., & Denton, C. (2023). Understanding Distinct Resident and Migratory Fibroblast Populations in Systemic Sclerosis Skin

Through Single-cell RNAseq and Immunohistochemistry [abstract]. *Arthritis & Rheumatology*, *75*(suppl 9).

Clement, C. A., Ajbro, K. D., Koefoed, K., Vestergaard, M. L., Veland, I. R., Henriques de Jesus, M. P. R., Pedersen, L. B., Benmerah, A., Andersen, C. Y., Larsen, L. A., & Christensen, S. T. (2013). TGF-β Signaling Is Associated with Endocytosis at the Pocket Region of the Primary Cilium. *Cell Reports*, *3*(6), 1806–1814. https://doi.org/10.1016/j.celrep.2013.05.020

Conkar, D., & Firat-Karalar, E. N. (2021). Microtubule-associated proteins and emerging links to primary cilium structure, assembly, maintenance, and disassembly. *The FEBS Journal*, *288*(3), 786–798. https://doi.org/10.1111/febs.15473

Corbit, K. C., Shyer, A. E., Dowdle, W. E., Gaulden, J., Singla, V., & Reiter, J. F. (2008). Kif3a constrains β-catenin-dependent Wnt signalling through dual ciliary and non-ciliary mechanisms. *Nature Cell Biology*, *10*(1), 70–76. https://doi.org/10.1038/ncb1670

Dallon, J. C., & Ehrlich, H. P. (2008). A review of fibroblast-populated collagen lattices. *Wound Repair and Regeneration*, *16*(4), 472–479. https://doi.org/10.1111/j.1524-475X.2008.00392.x

Dantas, A. T., Gonçalves, S. M. C., Almeida, A. R. D., Gonçalves, R. S. G., Sampaio, M. C. P. D., Vilar, K. D. M., Pereira, M. C., Rêgo, M. J. B. D. M., Pitta, I. D. R., Marques, C. D. L., Duarte, A. L. B. P., & Pitta, M. G. D. R. (2016). Reassessing the Role of the Active TGF- *β* 1 as a Biomarker in Systemic Sclerosis: Association of Serum Levels with Clinical Manifestations. *Disease Markers*, *2016*, 1–6. https://doi.org/10.1155/2016/6064830

Darby, I. A., Zakuan, N., Billet, F., & Desmoulière, A. (2016). The myofibroblast, a key cell in normal and pathological tissue repair. *Cellular and Molecular Life Sciences*, *73*(6), 1145–1157. https://doi.org/10.1007/s00018-015-2110-0

De Mori, R., Tardivo, S., Pollara, L., Giliani, S. C., Ali, E., Giordano, L., Leuzzi, V., Fischetto, R., Gener, B., Diprima, S., Morelli, M. J., Monti, M. C., Sottile, V., & Valente, E. M. (2024). Joubert syndrome-derived induced pluripotent stem cells show altered neuronal differentiation in vitro. *Cell and Tissue Research*, *396*(2), 255–267. https://doi.org/10.1007/s00441-024-03876-9

Deane, J. A., Verghese, E., Martelotto, L. G., Cain, J. E., Galtseva, A., Rosenblum, N. D., Watkins, D. N., & Ricardo, S. D. (2013). Visualizing renal primary cilia. *Nephrology*, *18*(3), 161–168. https://doi.org/10.1111/nep.12022

Dees, C., & Distler, J. H. W. (2013). Canonical Wnt signalling as a key regulator of fibrogenesis – implications for targeted therapies? *Experimental Dermatology*, *22*(11), 710–713. https://doi.org/10.1111/exd.12255

Del Galdo, F., Hartley, C., & Allanore, Y. (2020). Randomised controlled trials in systemic sclerosis: Patient selection and endpoints for next generation trials. *The Lancet Rheumatology*, *2*(3), e173–e184. https://doi.org/10.1016/S2665-9913(20)30007-2

Del Galdo, F., Lescoat, A., Conaghan, P. G., Bertoldo, E., Čolić, J., Santiago, T., Suliman, Y. A., Matucci-Cerinic, M., Gabrielli, A., Distler, O., Hoffmann-Vold, A.-M., Castellví, I., Balbir-Gurman, A., Vonk, M., Ananyeva, L., Rednic, S., Tarasova, A., Ostojic, P., Boyadzhieva, V., … Allanore, Y. (2024). EULAR recommendations for the treatment of systemic sclerosis: 2023 update. *Annals of the Rheumatic Diseases*, ard-2024-226430. https://doi.org/10.1136/ard-2024-226430

Del Galdo, F., Sotgia, F., De Almeida, C. J., Jasmin, J., Musick, M., Lisanti, M. P., & Jiménez, S. A. (2008). Decreased expression of caveolin 1 in patients with systemic sclerosis: Crucial role in the pathogenesis of tissue fibrosis. *Arthritis & Rheumatism*, *58*(9), 2854–2865. https://doi.org/10.1002/art.23791

Dere, R., Perkins, A. L., Bawa-Khalfe, T., Jonasch, D., & Walker, C. L. (2015). β-Catenin Links von Hippel-Lindau to Aurora Kinase A and Loss of Primary Cilia in Renal Cell Carcinoma. *Journal of the American Society of Nephrology*, *26*(3), 553–564. https://doi.org/10.1681/ASN.2013090984

Di Guglielmo, G. M., Le Roy, C., Goodfellow, A. F., & Wrana, J. L. (2003). Distinct endocytic pathways regulate TGF-β receptor signalling and turnover. *Nature Cell Biology*, *5*(5), 410–421. https://doi.org/10.1038/ncb975

Ding, H., Zhou, D., Hao, S., Zhou, L., He, W., Nie, J., Hou, F. F., & Liu, Y. (2012). Sonic Hedgehog Signaling Mediates Epithelial–Mesenchymal Communication and Promotes Renal Fibrosis. *Journal of the American Society of Nephrology*, *23*(5), 801–813. https://doi.org/10.1681/ASN.2011060614

Do, N. N., & Eming, S. A. (2016). Skin fibrosis: Models and mechanisms. *Current Research in Translational Medicine*, *64*(4), 185–193. https://doi.org/10.1016/j.retram.2016.06.003

Doherty, D., Parisi, M. A., Finn, L. S., Gunay-Aygun, M., Al-Mateen, M., Bates, D., Clericuzio, C., Demir, H., Dorschner, M., Van Essen, A. J., Gahl, W. A., Gentile, M., Gorden, N. T., Hikida, A., Knutzen, D., Ozyurek, H., Phelps, I., Rosenthal, P., Verloes, A., … Glass, I. A. (2010). Mutations in 3 genes (MKS3, CC2D2A and RPGRIP1L) cause COACH syndrome (Joubert syndrome with congenital hepatic fibrosis). *Journal of Medical Genetics*, *47*(1), 8–21. https://doi.org/10.1136/jmg.2009.067249

Dziadzio, M., Smith, R. E., Abraham, D. J., Black, C. M., & Denton, C. P. (2005). Circulating levels of active transforming growth factor β1 are reduced in diffuse cutaneous systemic sclerosis and correlate inversely with the modified Rodnan skin score. *Rheumatology*, *44*(12), 1518–1524. https://doi.org/10.1093/rheumatology/kei088

Egger, A. N., Rajabi-Estarabadi, A., Williams, N. M., Resnik, S. R., Fox, J. D., Wong, L. L., & Jozic, I. (2020). The importance of caveolins and caveolae to dermatology: Lessons from the caves and beyond. *Experimental Dermatology*, *29*(2), 136–148. https://doi.org/10.1111/exd.14068

Egorova, A. D., Khedoe, P. P. S. J., Goumans, M.-J. T. H., Yoder, B. K., Nauli, S. M., Ten Dijke, P., Poelmann, R. E., & Hierck, B. P. (2011). Lack of Primary Cilia Primes Shear-Induced Endothelial-to-Mesenchymal Transition. *Circulation Research*, *108*(9), 1093–1101. https://doi.org/10.1161/CIRCRESAHA.110.231860

Ehnert, S., Sreekumar, V., Aspera-Werz, R. H., Sajadian, S. O., Wintermeyer, E., Sandmann, G. H., Bahrs, C., Hengstler, J. G., Godoy, P., & Nussler, A. K. (2017). TGF-β1 impairs mechanosensation of human osteoblasts via HDAC6-mediated shortening and distortion of primary cilia. *Journal of Molecular Medicine*, *95*(6), 653–663. https://doi.org/10.1007/s00109-017-1526-4

Fabbri, L., Bost, F., & Mazure, N. M. (2019). Primary Cilium in Cancer Hallmarks. *International Journal of Molecular Sciences*, *20*(6), 1336. https://doi.org/10.3390/ijms20061336

Ferchichi, I., Kourda, N., Sassi, S., Romdhane, K. B., Balatgi, S., Cremet, J. Y., Prigent, C., & Elgaaied, A. B. (2012). Aurora a Overexpression and pVHL Reduced Expression Are Correlated with a Bad Kidney Cancer Prognosis. *Disease Markers*, *33*(6), 333–340. https://doi.org/10.1155/2012/804708

Fisch, C., & Dupuis-Williams, P. (2011). Ultrastructure of cilia and flagella—Back to the future! *Biology of the Cell*, *103*(6), 249–270. https://doi.org/10.1042/BC20100139

Focșa, I., Budișteanu, M., & Bălgrădean, M. (2021). Clinical and genetic heterogeneity of primary ciliopathies (Review). *International Journal of Molecular Medicine*, *48*(3), 176. https://doi.org/10.3892/ijmm.2021.5009

Gadadhar, S., Dadi, H., Bodakuntla, S., Schnitzler, A., Bièche, I., Rusconi, F., & Janke, C. (2017). Tubulin glycylation controls primary cilia length. *Journal of Cell Biology*, *216*(9), 2701–2713. https://doi.org/10.1083/jcb.201612050

Garcia, G., Raleigh, D. R., & Reiter, J. F. (2018). How the Ciliary Membrane Is Organized Inside-Out to Communicate Outside-In. *Current Biology*, *28*(8), 421–434. https://doi.org/10.1016/j.cub.2018.03.010

Garcia-Gonzalo, F. R., & Reiter, J. F. (2017). Open Sesame: How Transition Fibers and the Transition Zone Control Ciliary Composition. *Cold Spring Harbor Perspectives in Biology*, *9*(2), a028134. https://doi.org/10.1101/cshperspect.a028134

Gascue, C., Katsanis, N., & Badano, J. L. (2011). Cystic diseases of the kidney: Ciliary dysfunction and cystogenic mechanisms. *Pediatric Nephrology*, *26*(8), 1181–1195. https://doi.org/10.1007/s00467-010-1697-5

Gencer, S., Oleinik, N., Kim, J., Selvam, S. P., Palma, R. D., Dany, M., Nganga, R., Thomas, R. J., Senkal, C. E., Howe, P. H., & Ogretmen, B. (2017). TGF-b receptor I/II trafficking and signaling at primary cilia are inhibited by ceramide to attenuate cell migration and tumor metastasis. *SCIENCE SIGNALING*.

Gerdes, J. M., Liu, Y., Zaghloul, N. A., Leitch, C. C., Lawson, S. S., Kato, M., Beachy, P. A., Beales, P. L., DeMartino, G. N., Fisher, S., Badano, J. L., & Katsanis, N. (2007). Disruption of the basal body compromises proteasomal function and perturbs intracellular Wnt response. *Nature Genetics*, *39*(11), 1350–1360. https://doi.org/10.1038/ng.2007.12

Gilbane, A. J., Denton, C. P., & Holmes, A. M. (2013). Scleroderma pathogenesis: A pivotal role for fibroblasts as effector cells. *Arthritis Research & Therapy*, *15*(3), 215. https://doi.org/10.1186/ar4230

Gillespie, J., Ross, R. L., Corinaldesi, C., Esteves, F., Derrett-Smith, E., McDermott, M. F., Doody, G. M., Denton, C. P., Emery, P., & Del Galdo, F. (2018). Transforming Growth Factor β Activation Primes Canonical Wnt Signaling Through Down-Regulation of Axin-2. *Arthritis & Rheumatology*, *70*(6), 932–942. https://doi.org/10.1002/art.40437

Görgün, G., Calabrese, E., Hideshima, T., Ecsedy, J., Perrone, G., Mani, M., Ikeda, H., Bianchi, G., Hu, Y., Cirstea, D., Santo, L., Tai, Y.-T., Nahar, S., Zheng, M., Bandi, M., Carrasco, R. D., Raje, N., Munshi, N., Richardson, P., & Anderson, K. C. (2010). A novel Aurora-A kinase inhibitor MLN8237 induces cytotoxicity and cell-cycle arrest in multiple myeloma. *Blood*, *115*(25), 5202–5213. https://doi.org/10.1182/blood-2009-12-259523

Griffin, M. F., Huber, J., Evan, F. J., Quarto, N., & Longaker, M. T. (2022). The role of Wnt signaling in skin fibrosis. *Medicinal Research Reviews*, *42*(1), 615–628. https://doi.org/10.1002/med.21853

Gunay-Aygun, M. (2009). Liver and kidney disease in ciliopathies. *American Journal of Medical Genetics Part C: Seminars in Medical Genetics*, *151C*(4), 296–306. https://doi.org/10.1002/ajmg.c.30225

Györfi, A. H., Matei, A.-E., & Distler, J. H. W. (2018). Targeting TGF-β signaling for the treatment of fibrosis. *Matrix Biology*, *68–69*, 8–27. https://doi.org/10.1016/j.matbio.2017.12.016

Haddad, T. C., Suman, V. J., D'Assoro, A. B., Carter, J. M., Giridhar, K. V., McMenomy, B. P., Santo, K., Mayer, E. L., Karuturi, M. S., Morikawa, A., Marcom, P. K., Isaacs, C. J., Oh, S. Y., Clark, A. S., Mayer, I. A., Keyomarsi, K., Hobday, T. J., Peethambaram, P. P., O'Sullivan, C. C., … Goetz, M. P. (2023). Evaluation of Alisertib Alone or Combined With Fulvestrant in Patients With Endocrine-Resistant Advanced Breast Cancer: The Phase 2 TBCRC041 Randomized Clinical Trial. *JAMA Oncology*, *9*(6), 815. https://doi.org/10.1001/jamaoncol.2022.7949

Haggarty, S. J., Koeller, K. M., Wong, J. C., Grozinger, C. M., & Schreiber, S. L. (2003). Domain-selective small-molecule inhibitor of histone deacetylase 6

(HDAC6)-mediated tubulin deacetylation. *Proceedings of the National Academy of Sciences*, *100*(8), 4389–4394. https://doi.org/10.1073/pnas.0430973100

Hamburg-Shields, E., DiNuoscio, G. J., Mullin, N. K., Lafyatis, R., & Atit, R. P. (2015). Sustained β-catenin activity in dermal fibroblasts promotes fibrosis by up-regulating expression of extracellular matrix protein-coding genes. *The Journal of Pathology*, *235*(5), 686–697. https://doi.org/10.1002/path.4481

Han, S. J., Jung, J. K., Im, S.-S., Lee, S.-R., Jang, B.-C., Park, K. M., & Kim, J. I. (2018). Deficiency of primary cilia in kidney epithelial cells induces epithelial to mesenchymal transition. *Biochemical and Biophysical Research Communications*, *496*(2), 450–454. https://doi.org/10.1016/j.bbrc.2018.01.079

Harris, P. C., & Torres, V. E. (2009). Polycystic Kidney Disease. *Annual Review of Medicine*, *60*(1), 321–337. https://doi.org/10.1146/annurev.med.60.101707.125712

Hartill, V., Szymanska, K., Sharif, S. M., Wheway, G., & Johnson, C. A. (2017). Meckel–Gruber Syndrome: An Update on Diagnosis, Clinical Management, and Research Advances. *Frontiers in Pediatrics*, *5*, 244. https://doi.org/10.3389/fped.2017.00244

Hasanov, E., Chen, G., Chowdhury, P., Weldon, J., Ding, Z., Jonasch, E., Sen, S., Walker, C. L., & Dere, R. (2017). Ubiquitination and regulation of AURKA identifies a hypoxia-independent E3 ligase activity of VHL. *Oncogene*, *36*(24), 3450–3463. https://doi.org/10.1038/onc.2016.495

He, K., Yan, X., Li, N., Dang, S., Xu, L., Zhao, B., Li, Z., Lv, Z., Fang, X., Zhang, Y., & Chen, Y.-G. (2015). Internalization of the TGF-β type I receptor into caveolin-1 and EEA1 double-positive early endosomes. *Cell Research*, *25*(6), 738–752. https://doi.org/10.1038/cr.2015.60

Henderson, J., Pryzborski, S., Stratton, R., & O'Reilly, S. (2021). Wnt antagonist DKK-1 levels in systemic sclerosis are lower in skin but not in blood and are regulated by microRNA33a-3p. *Experimental Dermatology*, *30*(1), 162–168. https://doi.org/10.1111/exd.14136

Henderson, N. C., Rieder, F., & Wynn, T. A. (2020). Fibrosis: From mechanisms to medicines. *Nature*, *587*(7835), 555–566. https://doi.org/10.1038/s41586-020-2938-9

Herrera, J., Henke, C. A., & Bitterman, P. B. (2018). Extracellular matrix as a driver of progressive fibrosis. *Journal of Clinical Investigation*, *128*(1), 45–53. https://doi.org/10.1172/JCI93557

Herrick, A. L., Assassi, S., & Denton, C. P. (2022). Skin involvement in early diffuse cutaneous systemic sclerosis: An unmet clinical need. *Nature Reviews Rheumatology*, *18*(5), 276–285. https://doi.org/10.1038/s41584-022-00765-9

Hilgendorf, K. I., Myers, B. R., & Reiter, J. F. (2024). Emerging mechanistic understanding of cilia function in cellular signalling. *Nature Reviews Molecular Cell Biology*, *25*(7), 555–573. https://doi.org/10.1038/s41580-023-00698-5

Hochreiter, B., Kunze, M., Moser, B., & Schmid, J. A. (2019). Advanced FRET normalization allows quantitative analysis of protein interactions including stoichiometries and relative affinities in living cells. *Scientific Reports*, *9*(1), 8233. https://doi.org/10.1038/s41598-019-44650-0

Horn, A., Kireva, T., Palumbo-Zerr, K., Dees, C., Tomcik, M., Cordazzo, C., Zerr, P., Akhmetshina, A., Ruat, M., Distler, O., Beyer, C., Schett, G., & Distler, J. H. W. (2012). Inhibition of hedgehog signalling prevents experimental fibrosis and induces regression of established fibrosis. *Annals of the Rheumatic Diseases*, *71*(5), 785–789. https://doi.org/10.1136/annrheumdis-2011-200883

Horn, A., Palumbo, K., Cordazzo, C., Dees, C., Akhmetshina, A., Tomcik, M., Zerr, P., Avouac, J., Gusinde, J., Zwerina, J., Roudaut, H., Traiffort, E., Ruat, M., Distler, O., Schett, G., & Distler, J. H. W. (2012). Hedgehog signaling controls fibroblast activation and tissue fibrosis in systemic sclerosis. *Arthritis & Rheumatism*, *64*(8), 2724–2733. https://doi.org/10.1002/art.34444

Hou, X., Zhang, J., Wang, Y., Xiong, W., & Mi, J. (2017). TGFBR-IDH1-Cav1 axis promotes TGF-β signalling in cancer-associated fibroblast. *Oncotarget*, *8*(48), 83962–83974. https://doi.org/10.18632/oncotarget.20861

Hu, H. H., Chen, D. Q., Wang, Y. N., Feng, Y. L., Cao, G., Vaziri, N. D., & Zhao, Y. Y. (2018). New insights into TGF-β/Smad signaling in tissue fibrosis. *Chemico-Biological Interactions*, *292*, 76–83. https://doi.org/10.1016/j.cbi.2018.07.008

Hu, L., Lin, X., Lu, H., Chen, B., & Bai, Y. (2015). An Overview of Hedgehog Signaling in Fibrosis. *Molecular Pharmacology*, *87*(2), 174–182. https://doi.org/10.1124/mol.114.095141

Hughes, M., Allanore, Y., Denton, C. P., & Matucci-Cerinic, M. (2020). Systemic Sclerosis. *EMJ Rheumatol.*, *7*(1), 100–109.

Ingegnoli, F., Ughi, N., & Mihai, C. (2018). Update on the epidemiology, risk factors, and disease outcomes of systemic sclerosis. *Best Practice & Research Clinical Rheumatology*, *32*(2), 223–240. https://doi.org/10.1016/j.berh.2018.08.005

Ishizaki, T., Uehata, M., Tamechika, I., Keel, J., Nonomura, K., Maekawa, M., & Narumiya, S. (2000). Pharmacological Properties of Y-27632, a Specific Inhibitor of Rho-Associated Kinases. *Molecular Pharmacology*, *57*, 976–983.

Jeffries, E. P., Di Filippo, M., & Galbiati, F. (2019). Failure to reabsorb the primary cilium induces cellular senescence. *The FASEB Journal*, *33*(4), 4866–4882. https://doi.org/10.1096/fj.201801382R

Jinnin, M., Ihn, H., & Tamaki, K. (2006). Characterization of SIS3, a Novel Specific Inhibitor of Smad3, and Its Effect on Transforming Growth Factor-β1-Induced Extracellular Matrix Expression. *Molecular Pharmacology*, *69*(2), 597–607. https://doi.org/10.1124/mol.105.017483

Kasahara, K., & Inagaki, M. (2021). Primary ciliary signaling: Links with the cell cycle. *Trends in Cell Biology*, *31*(12), 954–964. https://doi.org/10.1016/j.tcb.2021.07.009

Katayama, H., Sasai, K., Kawai, H., Yuan, Z.-M., Bondaruk, J., Suzuki, F., Fujii, S., Arlinghaus, R. B., Czerniak, B. A., & Sen, S. (2004). Phosphorylation by aurora kinase A induces Mdm2-mediated destabilization and inhibition of p53. *Nature Genetics*, *36*(1), 55–62. https://doi.org/10.1038/ng1279

Kawasaki, M., Al-Shama, R. F. M., Nariswari, F. A., Fabrizi, B., Van Den Berg, N. W. E., Wesselink, R., Neefs, J., Meulendijks, E. R., Baalman, S. W. E., Driessen, A. H. G., & De Groot, J. R. (2024). Primary cilia suppress the fibrotic activity of atrial fibroblasts from patients with atrial fibrillation in vitro. *Scientific Reports*, *14*(1), 12470. https://doi.org/10.1038/s41598-024-60298-x

Kawasaki, M., Ezura, Y., Hayata, T., Notomi, T., Izu, Y., & Noda, M. (2015). TGF-β Suppresses Ift88 Expression in Chondrocytic ATDC5 Cells: TGF-β REGULATES IFT88. *Journal of Cellular Physiology*, *230*(11), 2788–2795. https://doi.org/10.1002/jcp.25005

Keeling, J., Tsiokas, L., & Maskey, D. (2016). Cellular Mechanisms of Ciliary Length Control. *Cells*, *5*(1). https://doi.org/10.3390/cells5010006

Kiesel, P., Alvarez Viar, G., Tsoy, N., Maraspini, R., Gorilak, P., Varga, V., Honigmann, A., & Pigino, G. (2020). The molecular structure of mammalian primary cilia revealed by cryo-electron tomography. *Nature Structural & Molecular Biology*, *27*(12), 1115–1124. https://doi.org/10.1038/s41594-020-0507-4

Kim, J., Jo, H., Hong, H., Kim, M. H., Kim, J. M., Lee, J.-K., Heo, W. D., & Kim, J. (2015). Actin remodelling factors control ciliogenesis by regulating YAP/TAZ activity and vesicle trafficking. *Nature Communications*, *6*(1), 6781. https://doi.org/10.1038/ncomms7781

Kimura, K., Ito, M., Amano, M., Chihara, K., Fukata, Y., Nakafuku, M., Yamamori, B., Feng, J., Nakano, T., Okawa, K., Iwamatsu, A., & Kaibuchi, K. (1996). Regulation of Myosin Phosphatase by Rho and Rho-Associated Kinase (Rho-Kinase). *Science*, *273*(5272), 245–248. https://doi.org/10.1126/science.273.5272.245

Kis, K., Liu, X., & Hagood, J. S. (2011). Myofibroblast differentiation and survival in fibrotic disease. *Expert Reviews in Molecular Medicine*, *13*, e27. https://doi.org/10.1017/S1462399411001967

Klingberg, F., Hinz, B., & White, E. S. (2013). The myofibroblast matrix: Implications for tissue repair and fibrosis. *The Journal of Pathology*, *229*(2), 298–309. https://doi.org/10.1002/path.4104

Kobayashi, Y., Hamamoto, A., & Saito, Y. (2024). Ciliary length variations impact cilia-mediated signaling and biological responses. *The Journal of Biochemistry*, 1–15. https://doi.org/10.1093/jb/mvae057

Kobayashi, Y., Kohbuchi, S., Koganezawa, N., Sekino, Y., Shirao, T., Saido, T. C., Saito, T., & Saito, Y. (2022). Impairment of ciliary dynamics in an APP knock-in mouse model of Alzheimer's disease. *Biochemical and Biophysical Research Communications*, *610*, 85–91. https://doi.org/10.1016/j.bbrc.2022.04.050

Koçak, A., Harmancı, D., Güner Akdoğan, G., & Birlik, M. (2020). Relationship of Wnt pathway activity and organ involvement in scleroderma types. *International Journal of Rheumatic Diseases*, *23*(11), 1558–1567. https://doi.org/10.1111/1756-185X.13973

Koefoed, K., Skat-Rørdam, J., Andersen, P., Warzecha, C. B., Pye, M., Andersen, T. A., Ajbro, K. D., Bendsen, E., Narimatsu, M., Vilhardt, F., Pedersen, L. B., Wrana, J. L., Anderson, R. H., Møllgård, K., Christensen, S. T., & Larsen, L. A. (2018). The E3 ubiquitin ligase SMURF1 regulates cell-fate specification and outflow tract septation during mammalian heart development. *Scientific Reports*, *8*(1), 9542. https://doi.org/10.1038/s41598-018-27854-8

Komura, K., Yanaba, K., Bouaziz, J.-D., Yoshizaki, A., Hasegawa, M., Varga, J., Takehara, K., & Matsushita, T. (2024). Perspective to precision medicine in scleroderma. *Frontiers in Immunology*, *14*, 1298665. https://doi.org/10.3389/fimmu.2023.1298665

Korobeynikov, V., Deneka, A. Y., & Golemis, E. A. (2017). Mechanisms for nonmitotic activation of Aurora-A at cilia. *Biochemical Society Transactions*, *45*(1), 37–49. https://doi.org/10.1042/BST20160142

Korol, A., Taiyab, A., & West-Mays, J. A. (2016). RhoA/ROCK Signaling Regulates TGFβ-Induced Epithelial-Mesenchymal Transition of Lens Epithelial Cells through MRTF-A. *Molecular Medicine*, *22*(1), 713–723. https://doi.org/10.2119/molmed.2016.00041

Ku, J. C., Raiten, J., & Li, Y. (2024). Understanding fibrosis: Mechanisms, clinical implications, current therapies, and prospects for future interventions. *Biomedical Engineering Advances*, *7*, 100118. https://doi.org/10.1016/j.bea.2024.100118

Kulshrestha, R., Singh, H., Pandey, A., Mehta, A., Bhardwaj, S., & Jaggi, A. S. (2019). Caveolin-1 as a critical component in the pathogenesis of lung fibrosis of different etiology: Evidences and mechanisms. *Experimental and Molecular Pathology*, *111*, 104315. https://doi.org/10.1016/j.yexmp.2019.104315

Labour, M.-N., Riffault, M., Christensen, S. T., & Hoey, D. A. (2016). TGFβ1 – induced recruitment of human bone mesenchymal stem cells is mediated by the primary cilium in a SMAD3-dependent manner. *Scientific Reports*, *6*(1), 35542. https://doi.org/10.1038/srep35542

Lafyatis, R. (2014). Transforming growth factor β—At the centre of systemic sclerosis. *Nature Reviews Rheumatology*, *10*(12), 706–719. https://doi.org/10.1038/nrrheum.2014.137

Lake, A. V. R., Smith, C. E. L., Natarajan, S., Basu, B., Best, S. K., Stevenson, T., Trowbridge, R., Grellscheid, S. N., Bond, J., Foster, R., & Johnson, C. A. (2020). *Drug and siRNA screens identify ROCK2 as a therapeutic target for ciliopathies*. bioRxiv. https://doi.org/10.1101/2020.11.26.393801

Lancaster, M. A., Schroth, J., & Gleeson, J. G. (2011). Subcellular spatial regulation of canonical Wnt signalling at the primary cilium. *Nature Cell Biology*, *13*(6), 700–707. https://doi.org/10.1038/ncb2259

Lee, E. K., Lee, Y. S., Han, I.-O., & Park, S. H. (2007). Expression of Caveolin-1 reduces cellular responses to TGF-β1 through down-regulating the expression of TGF-β type II receptor gene in NIH3T3 fibroblast cells. *Biochemical and Biophysical Research Communications*, *359*(2), 385–390. https://doi.org/10.1016/j.bbrc.2007.05.121

LeRoy, E. C., & Medsger, T. A. (2001). Criteria for the Classification of Early Systemic Sclerosis. *The Journal of Rheumatology*, *28*, 1573–1576.

Li, J., Qi, Y., Li, B., Liu, Y., Yang, K., Zhang, Z., Zhu, J., & Du, E. (2023). STIL/AURKA axis promotes cell proliferation by influencing primary cilia formation in bladder cancer. *Journal of Translational Medicine*, *21*(1), 281. https://doi.org/10.1186/s12967-023-04118-2

Li, Z., Wermuth, P. J., Benn, B. S., Lisanti, M. P., & Jimenez, S. A. (2013). Caveolin-1 Deficiency Induces Spontaneous Endothelial-to-Mesenchymal Transition in Murine Pulmonary Endothelial Cells in Vitro. *The American Journal of Pathology*, *182*(2), 325–331. https://doi.org/10.1016/j.ajpath.2012.10.022

Liakouli, V., Elies, J., El-Sherbiny, Y. M., Scarcia, M., Grant, G., Abignano, G., Derrett-Smith, E. C., Esteves, F., Cipriani, P., Emery, P., Denton, C. P., Giacomelli, R., Mavria, G., & Del Galdo, F. (2018). Scleroderma fibroblasts suppress angiogenesis via TGF-β/caveolin-1 dependent secretion of pigment epithelium-derived factor. *Annals of the Rheumatic Diseases*, *77*(3), 431–440. https://doi.org/10.1136/annrheumdis-2017-212120

Liang, R., Kagwiria, R., Zehender, A., Dees, C., Bergmann, C., Ramming, A., Krasowska, D., Michalska-Jakubus, M., Kreuter, A., Kraner, M. E., Schett, G., & Distler, J. H. W. (2019). Acyltransferase skinny hedgehog regulates TGFβ-dependent fibroblast activation in SSc. *Annals of the Rheumatic Diseases*, *78*(9), 1269–1273. https://doi.org/10.1136/annrheumdis-2019-215066

Liang, R., Šumová, B., Cordazzo, C., Mallano, T., Zhang, Y., Wohlfahrt, T., Dees, C., Ramming, A., Krasowska, D., Michalska-Jakubus, M., Distler, O., Schett, G., Šenolt, L., & Distler, J. H. W. (2017). The transcription factor GLI2 as a downstream mediator of transforming growth factor-β-induced fibroblast activation in SSc. *Annals of the Rheumatic Diseases*, *76*(4), 756–764. https://doi.org/10.1136/annrheumdis-2016-209698

Liewer, S., & Huddleston, A. (2018). Alisertib: A review of pharmacokinetics, efficacy and toxicity in patients with hematologic malignancies and solid tumors. *Expert Opinion on Investigational Drugs*, *27*(1), 105–112.

Liu, A., Wang, B., & Niswander, L. A. (2005). Mouse intraflagellar transport proteins regulate both the activator and repressor functions of Gli transcription factors. *Development*, *132*(13), 3103–3111. https://doi.org/10.1242/dev.01894

Liu, H., & Chen, Y.-G. (2022). The Interplay Between TGF-β Signaling and Cell Metabolism. *Frontiers in Cell and Developmental Biology*, *10*, 846723. https://doi.org/10.3389/fcell.2022.846723

Liu, S., Kapoor, M., Denton, C. P., Abraham, D. J., & Leask, A. (2009). Loss of β1 integrin in mouse fibroblasts results in resistance to skin scleroderma in a mouse model. *Arthritis & Rheumatism*, *60*(9), 2817–2821. https://doi.org/10.1002/art.24801

Lomelí-Nieto, J. A., Muñoz-Valle, J. F., Baños-Hernández, C. J., Navarro-Zarza, J. E., Godínez-Rubí, J. M., García-Arellano, S., Ramírez-Dueñas, M. G., Parra-Rojas, I., Villanueva-Pérez, A., & Hernández-Bello, J. (2022). Transforming growth factor beta isoforms and TGF-βR1 and TGF-βR2 expression in systemic sclerosis patients. *Clinical and Experimental Medicine*, *23*(2), 471–481. https://doi.org/10.1007/s10238-022-00841-0

Lovera, M., & Lüders, J. (2021). The ciliary impact of nonciliary gene mutations. *Trends in Cell Biology*, *31*(11), 876–887. https://doi.org/10.1016/j.tcb.2021.06.001

Lu, J., Liu, Q., Wang, L., Tu, W., Chu, H., Ding, W., Jiang, S., Ma, Y., Shi, X., Pu, W., Zhou, X., Jin, L., Wang, J., & Wu, W. (2017). Increased expression of latent TGF-β-binding protein 4 affects the fibrotic process in scleroderma by TGF-β/SMAD signaling. *Laboratory Investigation*, *97*(5), 591–601. https://doi.org/10.1038/labinvest.2017.20

Macarelli, V., Leventea, E., & Merkle, F. T. (2023). Regulation of the length of neuronal primary cilia and its potential effects on signalling. *Trends in Cell Biology*, *33*(11), 979–990. https://doi.org/10.1016/j.tcb.2023.05.005

Mahoney, J. M., Taroni, J., Martyanov, V., Wood, T. A., Greene, C. S., Pioli, P. A., Hinchcliff, M. E., & Whitfield, M. L. (2015). Systems Level Analysis of Systemic Sclerosis Shows a Network of Immune and Profibrotic Pathways Connected with Genetic Polymorphisms. *PLoS Computational Biology*, *11*(1), e1004005. https://doi.org/10.1371/journal.pcbi.1004005

Malicki, J. J., & Johnson, C. A. (2017). The Cilium: Cellular Antenna and Central Processing Unit. *Trends in Cell Biology*, *27*(2), 126–140. https://doi.org/10.1016/j.tcb.2016.08.002

Manetti, M., Allanore, Y., Saad, M., Fatini, C., Cohignac, V., Guiducci, S., Romano, E., Airó, P., Caramaschi, P., Tinazzi, I., Riccieri, V., Rossa, A. D., Abbate, R., Caporali, R., Cuomo, G., Valesini, G., Dieudé, P., Hachulla, E., Cracowski, J.-L., … Matucci-Cerinic, M. (2012). Evidence for caveolin-1 as a new susceptibility gene regulating tissue fibrosis in systemic sclerosis. *Annals of the Rheumatic Diseases*, *71*(6), 1034–1041. https://doi.org/10.1136/annrheumdis-2011-200986

Manfredi, M. G., Ecsedy, J. A., Meetze, K. A., Balani, S. K., Burenkova, O., Chen, W., Galvin, K. M., Hoar, K. M., Huck, J. J., LeRoy, P. J., Ray, E. T., Sells, T. B., Stringer, B., Stroud, S. G., Vos, T. J., Weatherhead, G. S., Wysong, D. R., Zhang, M., Bolen, J. B., & Claiborne, C. F. (2007). Antitumor activity of MLN8054, an orally active small-molecule inhibitor of Aurora A kinase. *Proceedings of the National Academy of Sciences*, *104*(10), 4106–4111. https://doi.org/10.1073/pnas.0608798104

Marumoto, T., Zhang, D., & Saya, H. (2005). Aurora-A — A guardian of poles. *Nature Reviews Cancer*, *5*(1), 42–50. https://doi.org/10.1038/nrc1526

May-Simera, H. L., & Kelley, M. W. (2012). Cilia, Wnt signaling, and the cytoskeleton. *Cilia*, *7*(1). https://doi.org/10.1186/2046-2530-1-7

Mendoza, F. A., & Jimenez, S. A. (2022). Serine/threonine kinase inhibition as antifibrotic therapy: Transforming growth factor-β and Rho kinase inhibitors. *Rheumatology*, *61*(4), 1354–1365. https://doi.org/10.1093/rheumatology/keab762

Meng, X., Nikolic-Paterson, D. J., & Lan, H. Y. (2016). TGF-β: The master regulator of fibrosis. *Nature Reviews Nephrology*, *12*(6), 325–338. https://doi.org/10.1038/nrneph.2016.48

Mick, D. U., Rodrigues, R. B., Leib, R. D., Adams, C. M., Chien, A. S., Gygi, S. P., & Nachury, M. V. (2015). Proteomics of Primary Cilia by Proximity Labeling. *Developmental Cell*, *35*(4), 497–512. https://doi.org/10.1016/j.devcel.2015.10.015

Mill, P., Christensen, S. T., & Pedersen, L. B. (2023). Primary cilia as dynamic and diverse signalling hubs in development and disease. *Nature Reviews Genetics*, *24*(7), 421–441. https://doi.org/10.1038/s41576-023-00587-9

Mirvis, M., Siemers, K. A., Nelson, W. J., & Stearns, T. P. (2019). Primary cilium loss in mammalian cells occurs predominantly by whole-cilium shedding. *PLOS Biology*, *17*(7), e3000381. https://doi.org/10.1371/journal.pbio.3000381

Mirvis, M., Stearns, T., & James Nelson, W. (2018). Cilium structure, assembly, and disassembly regulated by the cytoskeleton. *Biochemical Journal*, *475*(14), 2329–2353. https://doi.org/10.1042/BCJ20170453

Miyasato, S. K., Loeffler, J., Shohet, R., Zhang, J., Lindsey, M., & Le Saux, C. J. (2011). Caveolin-1 modulates TGF-β1 signaling in cardiac remodeling. *Matrix Biology*, *30*(5–6), 318–329. https://doi.org/10.1016/j.matbio.2011.05.003

Molla-Herman, A., Ghossoub, R., Blisnick, T., Meunier, A., Serres, C., Silbermann, F., Emmerson, C., Romeo, K., Bourdoncle, P., Schmitt, A., Saunier, S., Spassky, N., Bastin, P., & Benmerah, A. (2010). The ciliary pocket: An endocytic membrane domain at the base of primary and motile cilia. *Journal of Cell Science*, *123*(10), 1785–1795. https://doi.org/10.1242/jcs.059519

Mönnich, M., Borgeskov, L., Breslin, L., Jakobsen, L., Rogowski, M., Doganli, C., Schrøder, J. M., Mogensen, J. B., Blinkenkjær, L., Harder, L. M., Lundberg, E., Geimer, S., Christensen, S. T., Andersen, J. S., Larsen, L. A., & Pedersen, L. B. (2018). CEP128 Localizes to the Subdistal Appendages of the Mother Centriole and Regulates TGF-β/BMP Signaling at the Primary Cilium. *Cell Reports*, *22*(10), 2584–2592. https://doi.org/10.1016/j.celrep.2018.02.043

Moore, E. R. (2022). Primary Cilia: The New Face of Craniofacial Research. *Biomolecules*, *12*(12), 1724. https://doi.org/10.3390/biom12121724

Mouawad, J. E., & Feghali-Bostwick, C. (2023). The Molecular Mechanisms of Systemic Sclerosis-Associated Lung Fibrosis. *International Journal of Molecular Sciences*, *24*(3), 2963. https://doi.org/10.3390/ijms24032963

Murphy, S. L., Chen, Y. T., Lee, Y. C., Carns, M., Aren, K., Korman, B., Hinchcliff, M., & Varga, J. (2023). Differences in symptom experience among patients with systemic sclerosis: A cluster analytic approach to identifying subgroups. *Rheumatology*, *62*(SI), SI64–SI73. https://doi.org/10.1093/rheumatology/keac444

Neary, R., Watson, C. J., & Baugh, J. A. (2015). Epigenetics and the overhealing wound: The role of DNA methylation in fibrosis. *Fibrogenesis & Tissue Repair*, *8*(18). https://doi.org/10.1186/s13069-015-0035-8

Newell-Litwa, K. A., Badoual, M., Asmussen, H., Patel, H., Whitmore, L., & Horwitz, A. R. (2015). ROCK1 and 2 differentially regulate actomyosin organization to drive cell and synaptic polarity. *Journal of Cell Biology*, *210*(2), 225–242. https://doi.org/10.1083/jcb.201504046

Nikonova, A. S., Astsaturov, I., Serebriiskii, I. G., Dunbrack, R. L., & Golemis, E. A. (2013). Aurora A kinase (AURKA) in normal and pathological cell division. *Cellular and Molecular Life Sciences*, *70*(4), 661–687. https://doi.org/10.1007/s00018-012-1073-7

Ning, K., Bhuckory, M. B., Lo, C.-H., Sendayen, B. E., Kowal, T. J., Chen, M., Bansal, R., Chang, K.-C., Vollrath, D., Berbari, N. F., Mahajan, V. B., Hu, Y., & Sun, Y. (2023). Cilia-associated wound repair mediated by IFT88 in retinal pigment epithelium. *Scientific Reports*, *13*(1), 8205. https://doi.org/10.1038/s41598-023-35099-3

Nishimura, Y., Yamakawa, D., Shiromizu, T., & Inagaki, M. (2021). Aurora A and AKT Kinase Signaling Associated with Primary Cilia. *Cells*, *10*(12), 3602. https://doi.org/10.3390/cells10123602

Oud, M. M., Latour, B. L., Bakey, Z., Letteboer, S. J., Lugtenberg, D., Wu, K. M., Cornelissen, E. A. M., Yntema, H. G., Schmidts, M., Roepman, R., & Bongers, E. M. H. F. (2018). Cellular ciliary phenotyping indicates pathogenicity of novel variants in IFT140 and confirms a Mainzer–Saldino syndrome diagnosis. *Cilia*, *7*(1), 1. https://doi.org/10.1186/s13630-018-0055-2

Pala, R., Alomari, N., & Nauli, S. (2017). Primary Cilium-Dependent Signaling Mechanisms. *International Journal of Molecular Sciences*, *18*(11), 2272. https://doi.org/10.3390/ijms18112272

Park, D. S., Cohen, A. W., Frank, P. G., Razani, B., Lee, H., Williams, T. M., Chandra, M., Shirani, J., De Souza, A. P., Tang, B., Jelicks, L. A., Factor, S. M., Weiss, L. M., Tanowitz, H. B., & Lisanti, M. P. (2003). Caveolin-1 Null (−/−) Mice Show Dramatic Reductions in Life Span. *Biochemistry*, *42*(51), 15124–15131. https://doi.org/10.1021/bi0356348

Peixoto, E., Jin, S., Thelen, K., Biswas, A., Richard, S., Morleo, M., Mansini, A., Holtorf, S., Carbone, F., Pastore, N., Ballabio, A., Franco, B., & Gradilone, S. A. (2020). HDAC6-dependent ciliophagy is involved in ciliary loss and cholangiocarcinoma growth in human cells and murine models. *American Journal of Physiology-Gastrointestinal and Liver Physiology*, *318*(6), G1022–G1033. https://doi.org/10.1152/ajpgi.00033.2020

Pellar, R. E., & Pope, J. E. (2017). Evidence-based management of systemic sclerosis: Navigating recommendations and guidelines. *Seminars in Arthritis and Rheumatism*, *46*(6), 767–774. https://doi.org/10.1016/j.semarthrit.2016.12.003

Perrault, I., Saunier, S., Hanein, S., Filhol, E., Bizet, A. A., Collins, F., Salih, M. A. M., Gerber, S., Delphin, N., Bigot, K., Orssaud, C., Silva, E., Baudouin, V., Oud, M. M., Shannon, N., Le Merrer, M., Roche, O., Pietrement, C., Goumid, J., … Rozet, J.-M. (2012). Mainzer-Saldino Syndrome Is a Ciliopathy Caused by IFT140 Mutations. *The American Journal of Human Genetics*, *90*(5), 864–870. https://doi.org/10.1016/j.ajhg.2012.03.006

Philippeos, C., Telerman, S. B., Oulès, B., Pisco, A. O., Shaw, T. J., Elgueta, R., Lombardi, G., Driskell, R. R., Soldin, M., Lynch, M. D., & Watt, F. M. (2018). Spatial and Single-Cell Transcriptional Profiling Identifies Functionally Distinct Human Dermal Fibroblast Subpopulations. *Journal of Investigative Dermatology*, *138*(4), 811–825. https://doi.org/10.1016/j.jid.2018.01.016

Plotnikova, O. V., Pugacheva, E. N., & Golemis, E. A. (2009). Primary Cilia and the Cell Cycle. *Methods in Cell Biology*, *94*, 137–160. https://doi.org/10.1016/S0091-679X(08)94007-3

Pugacheva, E. N., Jablonski, S. A., Hartman, T. R., Henske, E. P., & Golemis, E. A. (2007). HEF1-Dependent Aurora A Activation Induces Disassembly of the

Primary Cilium. *Cell*, *129*(7), 1351–1363. https://doi.org/10.1016/j.cell.2007.04.035

Qin, W., Cho, K. F., Cavanagh, P. E., & Ting, A. Y. (2021). Deciphering molecular interactions by proximity labeling. *Nature Methods*, *18*(2), 133–143. https://doi.org/10.1038/s41592-020-01010-5

Rangel, L., Bernabé-Rubio, M., Fernández-Barrera, J., Casares-Arias, J., Millán, J., Alonso, M. A., & Correas, I. (2019). Caveolin-1α regulates primary cilium length by controlling RhoA GTPase activity. *Scientific Reports*, *9*(1), 1116. https://doi.org/10.1038/s41598-018-38020-5

Razani, B., Zhang, X. L., Bitzer, M., Von Gersdorff, G., Böttinger, E. P., & Lisanti, M. P. (2001). Caveolin-1 Regulates Transforming Growth Factor (TGF)-β/SMAD Signaling through an Interaction with the TGF-β Type I Receptor. *Journal of Biological Chemistry*, *276*(9), 6727–6738. https://doi.org/10.1074/jbc.M008340200

Reese, C. F., Chinnakkannu, P., Tourkina, E., Hoffman, S., & Kuppuswamy, D. (2022). Multiple subregions within the caveolin-1 scaffolding domain inhibit fibrosis, microvascular leakage, and monocyte migration. *PLOS ONE*, *17*(2), e0264413. https://doi.org/10.1371/journal.pone.0264413

Reese, C. F., Perry, B., Heywood, J., Bonner, M., Visconti, R. P., Lee, R., Hatfield, C. M., Silver, R. M., Hoffman, S., & Tourkina, E. (2014). Caveolin-1 Deficiency May Predispose African Americans to Systemic Sclerosis–Related Interstitial Lung Disease. *Arthritis & Rheumatology*, *66*(7), 1909–1919. https://doi.org/10.1002/art.38572

Reiter, J. F., & Leroux, M. R. (2017). Genes and molecular pathways underpinning ciliopathies. *Nature Reviews Molecular Cell Biology*, *18*(9), 533–547. https://doi.org/10.1038/nrm.2017.60

Revell, D. Z., & Yoder, B. K. (2019). Intravital visualization of the primary cilium, tubule flow, and innate immune cells in the kidney utilizing an abdominal window imaging approach. *Methods in Cell Biology*, *154*, 67–83.

Riemekasten, G., & Distler, J. H. W. (2022). A broad look into the future of systemic sclerosis. *Therapeutic Advances in Musculoskeletal Disease*, *14*, 1759720X221109404. https://doi.org/10.1177/1759720X221109404

Roberson, E. C., Dowdle, W. E., Ozanturk, A., Garcia-Gonzalo, F. R., Li, C., Halbritter, J., Elkhartoufi, N., Porath, J. D., Cope, H., Ashley-Koch, A., Gregory, S., Thomas, S., Sayer, J. A., Saunier, S., Otto, E. A., Katsanis, N., Davis, E. E., Attié-Bitach, T., Hildebrandt, F., … Reiter, J. F. (2015). TMEM231, mutated in orofaciodigital and Meckel syndromes, organizes the ciliary transition zone. *Journal of Cell Biology*, *209*(1), 129–142. https://doi.org/10.1083/jcb.201411087

Roberson, E. D. O., Carns, M., Cao, L., Aren, K., Goldberg, I. A., Morales-Heil, D. J., Korman, B. D., Atkinson, J. P., & Varga, J. (2023). Alterations of the Primary Cilia Gene *SPAG17* and *SOX9* Locus Noncoding RNAs Identified by RNA-Sequencing Analysis in Patients With Systemic Sclerosis. *Arthritis & Rheumatology*, *75*(1), 108–119. https://doi.org/10.1002/art.42281

Rodnan, G. P., Lipinski, E., & Luksick, J. (1979). Skin thickness and collagen content in progressive systemic sclerosis and localized scleroderma. *Arthritis & Rheumatism*, *22*(2), 130–140. https://doi.org/10.1002/art.1780220205

Rowson, D. T., Shelton, J. C., Screen, H. R. C., & Knight, M. M. (2018). Mechanical loading induces primary cilia disassembly in tendon cells via TGFβ and HDAC6. *Scientific Reports*, *8*(1), 11107. https://doi.org/10.1038/s41598-018-29502-7

Rozycki, M., Lodyga, M., Lam, J., Miranda, M. Z., Fátyol, K., Speight, P., & Kapus, A. (2014). The fate of the primary cilium during myofibroblast transition. *Molecular Biology of the Cell*, *25*(5), 643–657. https://doi.org/10.1091/mbc.e13-07-0429

Saito, M., Otsu, W., Miyadera, K., & Nishimura, Y. (2023). Recent advances in the understanding of cilia mechanisms and their applications as therapeutic targets. *Frontiers in Molecular Biosciences*, *10*, 1232188. https://doi.org/10.3389/fmolb.2023.1232188

Sapao, P., Roberson, E. D. O., Shi, B., Assassi, S., Skaug, B., Lee, F., Naba, A., Perez White, B. E., Córdova-Fletes, C., Tsou, P.-S., Sawalha, A. H., Gudjonsson, J. E., Ma, F., Verma, P., Bhattacharyya, D., Carns, M., Strauss, J. F., Sicard, D., Tschumperlin, D. J., … Varga, J. (2023). Reduced SPAG17 Expression in Systemic Sclerosis Triggers Myofibroblast Transition and Drives Fibrosis. *Journal of Investigative Dermatology*, *143*(2), 284–293. https://doi.org/10.1016/j.jid.2022.08.052

Sargent, J. L., Milano, A., Bhattacharyya, S., Varga, J., Connolly, M. K., Chang, H. Y., & Whitfield, M. L. (2010). A TGFβ-Responsive Gene Signature Is Associated

with a Subset of Diffuse Scleroderma with Increased Disease Severity. *Journal of Investigative Dermatology*, *130*(3), 694–705. https://doi.org/10.1038/jid.2009.318

Sargent, J. L., & Whitfield, M. L. (2011). Capturing the heterogeneity in systemic sclerosis with genome-wide expression profiling. *Expert Review of Clinical Immunology*, *7*(4), 463–473. https://doi.org/10.1586/eci.11.41

Satir, P., & Christensen, S. T. (2007). Overview of Structure and Function of Mammalian Cilia. *Annual Review of Physiology*, *69*(1), 377–400. https://doi.org/10.1146/annurev.physiol.69.040705.141236

Satir, P., Pedersen, L. B., & Christensen, S. T. (2010). The primary cilium at a glance. *Journal of Cell Science*, *123*(4), 499–503. https://doi.org/10.1242/jcs.050377

Scheidel, N., Kennedy, J., & Blacque, O. E. (2018). Endosome maturation factors Rabenosyn-5/VPS45 and caveolin-1 regulate ciliary membrane and polycystin-2 homeostasis. *The EMBO Journal*, *37*(9), e98248. https://doi.org/10.15252/embj.201798248

Schneider, L., Cammer, M., Lehman, J., Nielsen, S., Guerra, C., Veland, I., Stock, C., Hoffmann, E., Yoder, B., Schwab, A., Satir, P., & Christensen, S. (2010). Directional Cell Migration and Chemotaxis in Wound Healing Response to PDGF-AA are Coordinated by the Primary Cilium in Fibroblasts. *Cellular Physiology and Biochemistry*, *25*(2–3), 279–292. https://doi.org/10.1159/000276562

Schou, K. B., Mogensen, J. B., Morthorst, S. K., Nielsen, B. S., Aleliunaite, A., Serra-Marques, A., Fürstenberg, N., Saunier, S., Bizet, A. A., Veland, I. R., Akhmanova, A., Christensen, S. T., & Pedersen, L. B. (2017). KIF13B establishes a CAV1-enriched microdomain at the ciliary transition zone to promote Sonic hedgehog signalling. *Nature Communications*, *8*(1), 14177. https://doi.org/10.1038/ncomms14177

Schubert, W., Sotgia, F., Cohen, A. W., Capozza, F., Bonuccelli, G., Bruno, C., Minetti, C., Bonilla, E., DiMauro, S., & Lisanti, M. P. (2007). Caveolin-1(−/−)- and Caveolin-2(−/−)-Deficient Mice Both Display Numerous Skeletal Muscle Abnormalities, with Tubular Aggregate Formation. *The American Journal of Pathology*, *170*(1), 316–333. https://doi.org/10.2353/ajpath.2007.060687

Shagisultanova, E., Gaponova, A. V., Gabbasov, R., Nicolas, E., & Golemis, E. A. (2015). Preclinical and clinical studies of the NEDD9 scaffold protein in cancer and other diseases. *Gene*, *567*(1), 1–11. https://doi.org/10.1016/j.gene.2015.04.086

Shao, L., El-Jouni, W., Kong, F., Ramesh, J., Kumar, R. S., Shen, X., Ren, J., Devendra, S., Dorschel, A., Wu, M., Barrera, I., Tabari, A., Hu, K., Haque, N., Yambayev, I., Li, S., Kumar, A., Behera, T. R., McDonough, G., … Zhou, J. (2020). Genetic reduction of cilium length by targeting intraflagellar transport 88 protein impedes kidney and liver cyst formation in mouse models of autosomal polycystic kidney disease. *Kidney International*, *98*(5), 1225–1241. https://doi.org/10.1016/j.kint.2020.05.049

Shida, T., Cueva, J. G., Xu, Z., Goodman, M. B., & Nachury, M. V. (2010). The major α-tubulin K40 acetyltransferase αTAT1 promotes rapid ciliogenesis and efficient mechanosensation. *Proceedings of the National Academy of Sciences*, *107*(50), 21517–21522. https://doi.org/10.1073/pnas.1013728107

Smith, C. E. L., Lake, A. V. R., & Johnson, C. A. (2020). Primary Cilia, Ciliogenesis and the Actin Cytoskeleton: A Little Less Resorption, A Little More Actin Please. *Frontiers in Cell and Developmental Biology*, *8*, 622822. https://doi.org/10.3389/fcell.2020.622822

Sobolewski, P., Maślińska, M., Wieczorek, M., Łagun, Z., Malewska, A., Roszkiewicz, M., Nitskovich, R., Szymańska, E., & Walecka, I. (2019). Systemic sclerosis – multidisciplinary disease: Clinical features and treatment. *Rheumatology*, *57*(4), 221–233. https://doi.org/10.5114/reum.2019.87619

Sorokin, S. (1962). CENTRIOLES AND THE FORMATION OF RUDIMENTARY CILIA BY FIBROBLASTS AND SMOOTH MUSCLE CELLS. *The Journal of Cell Biology*, *15*(2), 363–377. https://doi.org/10.1083/jcb.15.2.363

Sorokin, S. P. (1968). Reconstructions of centriole formation and ciliogenesis in mammalian lungs. *Journal of Cell Science*, *3*(2), 207–230. https://doi.org/10.1242/jcs.3.2.207

Spahiu, L., Behluli, E., Graiqevci Uka, V., Liehr, T., & Temaj, G. (2022). Joubert syndrome: Molecular basis and treatment. *Journal of Mother and Child. Medycyna Wieku Rozwojowego*, *26*(1), 118–123. https://doi.org/10.34763/JMOTHERANDCHILD.20222601.D-22-00034

Stam, L. B., & Clark, A. L. (2023). Chondrocyte primary cilia lengthening and shortening in response to mediators of osteoarthritis; a role for integrin α1β1 and focal adhesions. *Osteoarthritis and Cartilage Open*, *5*(2), 100357. https://doi.org/10.1016/j.ocarto.2023.100357

Steen, V. D., & Medsger, T. A. (2000). Severe organ involvement in systemic sclerosis with diffuse scleroderma. *Arthritis & Rheumatism*, *43*(11), 2437–2444. https://doi.org/10.1002/1529-0131(200011)43:11<2437::AID-ANR10>3.0.CO;2-U

Strippoli, R., Loureiro, J., Moreno, V., Benedicto, I., Pérez Lozano, M. L., Barreiro, O., Pellinen, T., Minguet, S., Foronda, M., Osteso, M. T., Calvo, E., Vázquez, J., López Cabrera, M., & Del Pozo, M. A. (2015). Caveolin-1 deficiency induces a MEK - ERK 1/2-Snail-1-dependent epithelial–mesenchymal transition and fibrosis during peritoneal dialysis. *EMBO Molecular Medicine*, *7*(1), 102–123. https://doi.org/10.15252/emmm.201404127

Sun, S., Fisher, R. L., Bowser, S. S., Pentecost, B. T., & Sui, H. (2019). Three-dimensional architecture of epithelial primary cilia. *Proceedings of the National Academy of Sciences*, *116*(19), 9370–9379. https://doi.org/10.1073/pnas.1821064116

Sun, T., Vander Heiden, J. A., Gao, X., Yin, J., Uttarwar, S., Liang, W.-C., Jia, G., Yadav, R., Huang, Z., Mitra, M., Halpern, W., Bender, H. S., Brightbill, H. D., Wu, Y., Lupardus, P., Ramalingam, T., & Arron, J. R. (2024). Isoform-selective TGF-β3 inhibition for systemic sclerosis. *Med*, *5*(2), 132-147.e7. https://doi.org/10.1016/j.medj.2023.12.011

Svegliati, S., Marrone, G., Pezone, A., Spadoni, T., Grieco, A., Moroncini, G., Grieco, D., Vinciguerra, M., Agnese, S., Jüngel, A., Distler, O., Musti, A. M., Gabrielli, A., & Avvedimento, E. V. (2014). Oxidative DNA damage induces the ATM-mediated transcriptional suppression of the Wnt inhibitor WIF-1 in systemic sclerosis and fibrosis. *Science Signaling*, *7*(341). https://doi.org/10.1126/scisignal.2004592

Tabib, T., Morse, C., Wang, T., Chen, W., & Lafyatis, R. (2018). SFRP2/DPP4 and FMO1/LSP1 Define Major Fibroblast Populations in Human Skin. *Journal of Investigative Dermatology*, *138*(4), 802–810. https://doi.org/10.1016/j.jid.2017.09.045

Tai, Y., Woods, E. L., Dally, J., Kong, D., Steadman, R., Moseley, R., & Midgley, A. C. (2021). Myofibroblasts: Function, Formation, and Scope of Molecular Therapies for Skin Fibrosis. *Biomolecules*, *11*(8), 1095. https://doi.org/10.3390/biom11081095

Takamura, N., & Yamaguchi, Y. (2022). Involvement of caveolin-1 in skin diseases. *Frontiers in Immunology*, *13*, 1035451. https://doi.org/10.3389/fimmu.2022.1035451

Tenbrock, L., Wolf, J., Boneva, S., Schlecht, A., Agostini, H., Wieghofer, P., Schlunck, G., & Lange, C. (2022). Subretinal fibrosis in neovascular age-related macular degeneration: Current concepts, therapeutic avenues, and future perspectives. *Cell and Tissue Research*, *387*(3), 361–375. https://doi.org/10.1007/s00441-021-03514-8

Teves, M. E., Sundaresan, G., Cohen, D. J., Hyzy, S. L., Kajan, I., Maczis, M., Zhang, Z., Costanzo, R. M., Zweit, J., Schwartz, Z., Boyan, B. D., & Strauss, J. F. (2015). Spag17 Deficiency Results in Skeletal Malformations and Bone Abnormalities. *PLOS ONE*, *10*(5), e0125936. https://doi.org/10.1371/journal.pone.0125936

Teves, M. E., Zhang, Z., Costanzo, R. M., Henderson, S. C., Corwin, F. D., Zweit, J., Sundaresan, G., Subler, M., Salloum, F. N., Rubin, B. K., & Strauss, J. F. (2013). Sperm-Associated Antigen–17 Gene Is Essential for Motile Cilia Function and Neonatal Survival. *American Journal of Respiratory Cell and Molecular Biology*, *48*(6), 765–772. https://doi.org/10.1165/rcmb.2012-0362OC

Thoma, C. R., Frew, I. J., Hoerner, C. R., Montani, M., Moch, H., & Krek, W. (2007). pVHL and GSK3β are components of a primary cilium-maintenance signalling network. *Nature Cell Biology*, *9*(5), 588–595. https://doi.org/10.1038/ncb1579

Thorpe, S. D., Gambassi, S., Thompson, C. L., Chandrakumar, C., Santucci, A., & Knight, M. M. (2017). Reduced primary cilia length and altered Arl13b expression are associated with deregulated chondrocyte Hedgehog signaling in alkaptonuria. *Journal of Cellular Physiology*, *232*(9), 2407–2417. https://doi.org/10.1002/jcp.25839

Tomoshige, S., Kobayashi, Y., Hosoba, K., Hamamoto, A., Miyamoto, T., & Saito, Y. (2017). Cytoskeleton-related regulation of primary cilia shortening mediated by

melanin-concentrating hormone receptor 1. *General and Comparative Endocrinology*, *253*, 44–52. https://doi.org/10.1016/j.ygcen.2017.08.021

Tourkina, E., Richard, M., Gööz, P., Bonner, M., Pannu, J., Harley, R., Bernatchez, P. N., Sessa, W. C., Silver, R. M., & Hoffman, S. (2008). Antifibrotic properties of caveolin-1 scaffolding domain in vitro and in vivo. *American Journal of Physiology-Lung Cellular and Molecular Physiology*, *294*(5), 843–861. https://doi.org/10.1152/ajplung.00295.2007

Tözser, J., Earwood, R., Kato, A., Brown, J., Tanaka, K., Didier, R., Megraw, T. L., Blum, M., & Kato, Y. (2015). TGF-β Signaling Regulates the Differentiation of Motile Cilia. *Cell Reports*, *11*(7), 1000–1007. https://doi.org/10.1016/j.celrep.2015.04.025

Truong, M. E., Bilekova, S., Choksi, S. P., Li, W., Bugaj, L. J., Xu, K., & Reiter, J. F. (2021). Vertebrate cells differentially interpret ciliary and extraciliary cAMP. *Cell*, *184*(11), 2911-2926.e18. https://doi.org/10.1016/j.cell.2021.04.002

Tuson, M., He, M., & Anderson, K. V. (2011). Protein kinase A acts at the basal body of the primary cilium to prevent Gli2 activation and ventralization of the mouse neural tube. *Development*, *138*(22), 4921–4930. https://doi.org/10.1242/dev.070805

Uhl, M., Aulwurm, S., Wischhusen, J., Weiler, M., Ma, J. Y., Almirez, R., Mangadu, R., Liu, Y.-W., Platten, M., Herrlinger, U., Murphy, A., Wong, D. H., Wick, W., Higgins, L. S., & Weller, M. (2004). SD-208, a Novel Transforming Growth Factor B Receptor I Kinase Inhibitor, Inhibits Growth and Invasiveness and Enhances Immunogenicity of Murine and Human Glioma Cells In vitro and In vivo. *Cancer Research*, *64*, 7954–7961.

Van Caam, A., Vonk, M., Van Den Hoogen, F., Van Lent, P., & Van Der Kraan, P. (2018). Unraveling SSc Pathophysiology; The Myofibroblast. *Frontiers in Immunology*, *9*, 2452. https://doi.org/10.3389/fimmu.2018.02452

van den Hoogen, F., Khanna, D., Fransen, J., Johnson, S. R., Baron, M., Tyndall, A., Matucci-Cerinic, M., Naden, R. P., Medsger, T. A., Carreira, P. E., Riemekasten, G., Clements, P. J., Denton, C. P., Distler, O., Allanore, Y., Furst, D. E., Gabrielli, A., Mayes, M. D., van Laar, J. M., … Pope, J. E. (2013). 2013 Classification Criteria for Systemic Sclerosis: An American College of

Rheumatology/European League Against Rheumatism Collaborative Initiative. *Arthritis & Rheumatism*, *65*(11), 2737–2747. https://doi.org/10.1002/art.38098

Varga, J., & Abraham, D. (2007). Systemic sclerosis: A prototypic multisystem fibrotic disorder. *Journal of Clinical Investigation*, *117*(3), 557–567. https://doi.org/10.1172/JCI31139

Varshney, N., Kebede, A. A., Owusu-Dapaah, H., Lather, J., Kaushik, M., & Bhullar, J. S. (2017). A Review of Von Hippel-Lindau Syndrome. *Journal of Kidney Cancer and VHL*, *4*(3), 20–29. https://doi.org/10.15586/jkcvhl.2017.88

Veland, I. R., Awan, A., Pedersen, L. B., Yoder, B. K., & Christensen, S. T. (2009). Primary Cilia and Signaling Pathways in Mammalian Development, Health and Disease. *Nephron Physiology*, *111*(3), p39–p53. https://doi.org/10.1159/000208212

Verbruggen, S. W., Nolan, J., Duffy, M. P., Pearce, O. M. T., Jacobs, C. R., & Knight, M. M. (2024). A Novel Primary Cilium-Mediated Mechanism Through which Osteocytes Regulate Metastatic Behavior of Both Breast and Prostate Cancer Cells. *Advanced Science*, *11*(2), 2305842. https://doi.org/10.1002/advs.202305842

Verma, P., Yalavarthi, B., Bhattacharyya, S., Khanna, D., Gudjonsson, J. E., Tsoi, L. C., Wells, R., Ross, R. L., Galdo, N. R.-D., Galdo, F. D., Fortier, S. M., Teves, M. E., Varga, J., & Bhattacharyya, D. (2024). *Morphological Reprogramming of Primary Cilia Length Mitigates the Fibrotic Phenotype in Fibroblasts Across Diverse Fibrotic Conditions*. bioRxiv. https://doi.org/10.1101/2024.01.06.574461

Vestergaard, M. L., Awan, A., Warzecha, C. B., Christensen, S. T., & Andersen, C. Y. (2016). Immunofluorescence microscopy and mRNA analysis of human embryonic stem cells (hESCs) including primary cilia associated signaling pathways. *Methods in Molecular Biology*, *1307*, 123–140. https://doi.org/10.1007/978-1-4939-2668-8

Vorobyeva, A. G., & Saunders, A. J. (2018). Amyloid-β interrupts canonical Sonic hedgehog signaling by distorting primary cilia structure. *Cilia*, *7*(1). https://doi.org/10.1186/s13630-018-0059-y

Walia, V., Cuenca, A., Vetter, M., Insinna, C., Perera, S., Lu, Q., Ritt, D. A., Semler, E., Specht, S., Stauffer, J., Morrison, D. K., Lorentzen, E., & Westlake, C. J. (2019). Akt Regulates a Rab11-Effector Switch Required for Ciliogenesis.

Developmental Cell, *50*(2), 229–246. https://doi.org/10.1016/j.devcel.2019.05.022

Walter, A. O., Seghezzi, W., Korver, W., Sheung, J., & Lees, E. (2000). The mitotic serine/threonine kinase Aurora2/AIK is regulated by phosphorylation and degradation. *Oncogene*, *19*(42), 4906–4916. https://doi.org/10.1038/sj.onc.1203847

Wang, E. X., Turner, J. S., Brautigan, D. L., & Fu, Z. (2022). Modulation of Primary Cilia by Alvocidib Inhibition of CILK1. *International Journal of Molecular Sciences*, *23*(15), 8121. https://doi.org/10.3390/ijms23158121

Wang, Q., Peng, Z., Long, H., Deng, X., & Huang, K. (2019). Polyubiquitylation of α-tubulin at K304 is required for flagellar disassembly in *Chlamydomonas*. *Journal of Cell Science*, *132*(6), jcs229047. https://doi.org/10.1242/jcs.229047

Wang, W., Jack, B. M., Wang, H. H., Kavanaugh, M. A., Maser, R. L., & Tran, P. V. (2021). Intraflagellar Transport Proteins as Regulators of Primary Cilia Length. *Frontiers in Cell and Developmental Biology*, *9*, 661350. https://doi.org/10.3389/fcell.2021.661350

Wang, X. M., Zhang, Y., Kim, H. P., Zhou, Z., Feghali-Bostwick, C. A., Liu, F., Ifedigbo, E., Xu, X., Oury, T. D., Kaminski, N., & Choi, A. M. K. (2006). Caveolin-1: A critical regulator of lung fibrosis in idiopathic pulmonary fibrosis. *The Journal of Experimental Medicine*, *203*(13), 2895–2906. https://doi.org/10.1084/jem.20061536

Wasson, C. W., Abignano, G., Hermes, H., Malaab, M., Ross, R. L., Jimenez, S. A., Chang, H. Y., Feghali-Bostwick, C. A., & Del Galdo, F. (2020). Long non-coding RNA HOTAIR drives EZH2-dependent myofibroblast activation in systemic sclerosis through miRNA 34a-dependent activation of NOTCH. *Annals of the Rheumatic Diseases*, *79*(4), 507–517. https://doi.org/10.1136/annrheumdis-2019-216542

Wasson, C. W., Ross, R. L., Wells, R., Corinaldesi, C., Georgiou, I. Ch., Riobo-Del Galdo, N. A., & Del Galdo, F. (2020). Long non-coding RNA HOTAIR induces GLI2 expression through Notch signalling in systemic sclerosis dermal fibroblasts. *Arthritis Research & Therapy*, *22*(1), 286. https://doi.org/10.1186/s13075-020-02376-9

Wei, J., Fang, F., Lam, A. P., Sargent, J. L., Hamburg, E., Hinchcliff, M. E., Gottardi, C. J., Atit, R., Whitfield, M. L., & Varga, J. (2012). Wnt/β-catenin signaling is hyperactivated in systemic sclerosis and induces Smad-dependent fibrotic responses in mesenchymal cells. *Arthritis & Rheumatism*, *64*(8), 2734–2745. https://doi.org/10.1002/art.34424

Wei, J., Melichian, D., Komura, K., Hinchcliff, M., Lam, A. P., Lafyatis, R., Gottardi, C. J., MacDougald, O. A., & Varga, J. (2011). Canonical Wnt signaling induces skin fibrosis and subcutaneous lipoatrophy: A novel mouse model for scleroderma? *Arthritis & Rheumatism*, *63*(6), 1707–1717. https://doi.org/10.1002/art.30312

Wheatley, D. N. (2005). Landmarks in the first hundred years of primary (9+0) cilium research. *Cell Biology International*, *29*(5), 333–339. https://doi.org/10.1016/j.cellbi.2005.03.001

Wheway, G., Abdelhamed, Z., Natarajan, S., Toomes, C., Inglehearn, C., & Johnson, C. A. (2013). Aberrant Wnt signalling and cellular over-proliferation in a novel mouse model of Meckel–Gruber syndrome. *Developmental Biology*, *377*(1), 55–66. https://doi.org/10.1016/j.ydbio.2013.02.015

Wheway, G., Nazlamova, L., & Hancock, J. T. (2018). Signaling through the Primary Cilium. *Frontiers in Cell and Developmental Biology*, *6*, 8. https://doi.org/10.3389/fcell.2018.00008

Wiegering, A., Dildrop, R., Kalfhues, L., Spychala, A., Kuschel, S., Lier, J. M., Zobel, T., Dahmen, S., Leu, T., Struchtrup, A., Legendre, F., Vesque, C., Schneider-Maunoury, S., Saunier, S., Rüther, U., & Gerhardt, C. (2018). Cell type-specific regulation of ciliary transition zone assembly in vertebrates. *The EMBO Journal*, *37*(10), e97791. https://doi.org/10.15252/embj.201797791

Woodman, S. E., Ashton, A. W., Schubert, W., Lee, H., Williams, T. M., Medina, F. A., Wyckoff, J. B., Combs, T. P., & Lisanti, M. P. (2003). Caveolin-1 Knockout Mice Show an Impaired Angiogenic Response to Exogenous Stimuli. *The American Journal of Pathology*, *162*(6), 2059–2068. https://doi.org/10.1016/S0002-9440(10)64337-4

Yamakawa, D., Katoh, D., Kasahara, K., Shiromizu, T., Matsuyama, M., Matsuda, C., Maeno, Y., Watanabe, M., Nishimura, Y., & Inagaki, M. (2021). Primary cilia-

dependent lipid raft/caveolin dynamics regulate adipogenesis. *Cell Reports*, *34*(10), 108817. https://doi.org/10.1016/j.celrep.2021.108817

Yang, T., Su, J., Wang, W.-J., Craige, B., Witman, G. B., Bryan Tsou, M.-F., & Liao, J.-C. (2015). Superresolution Pattern Recognition Reveals the Architectural Map of the Ciliary Transition Zone. *Scientific Reports*, *5*(1), 14096. https://doi.org/10.1038/srep14096

Yeyati, P. L., Schiller, R., Mali, G., Kasioulis, I., Kawamura, A., Adams, I. R., Playfoot, C., Gilbert, N., Van Heyningen, V., Wills, J., Von Kriegsheim, A., Finch, A., Sakai, J., Schofield, C. J., Jackson, I. J., & Mill, P. (2017). KDM3A coordinates actin dynamics with intraflagellar transport to regulate cilia stability. *Journal of Cell Biology*, *216*(4), 999–1013. https://doi.org/10.1083/jcb.201607032

Yilmaz, N., Olgun, S., Ahiskali, R., Karakurt, S., & Yavuz, S. (2014). Decreased sputum caveolin-1 ıs assocıated wıth systemic sclerosis related lung disease. *Sarcoidosis Vasc. Diffuse Lung Dis.*, *31*(1), 55–61.

Yin, F., Chen, Q., Shi, Y., Xu, H., Huang, J., Qing, M., Zhong, L., Li, J., Xie, L., & Zeng, X. (2022). Activation of EGFR-Aurora A induces loss of primary cilia in oral squamous cell carcinoma. *Oral Diseases*, *28*(3), 621–630. https://doi.org/10.1111/odi.13791

Yin, F., Wei, Z., Chen, F., Xin, C., & Chen, Q. (2022). Molecular targets of primary cilia defects in cancer (Review). *International Journal of Oncology*, *61*(2), 98. https://doi.org/10.3892/ijo.2022.5388

Younesi, F. S., Miller, A. E., Barker, T. H., Rossi, F. M. V., & Hinz, B. (2024). Fibroblast and myofibroblast activation in normal tissue repair and fibrosis. *Nature Reviews Molecular Cell Biology*, *25*(8), 617–638. https://doi.org/10.1038/s41580-024-00716-0

Zhang, B., Zhang, T., Wang, G., Wang, G., Chi, W., Jiang, Q., & Zhang, C. (2015). GSK3β-Dzip1-Rab8 Cascade Regulates Ciliogenesis after Mitosis. *PLOS Biology*, *13*(4), e1002129. https://doi.org/10.1371/journal.pbio.1002129

Zhang, G.-Y., Yu, Q., Cheng, T., Liao, T., Nie, C.-L., Wang, A.-Y., Zheng, X., Xie, X.-G., Albers, A. E., & Gao, W.-Y. (2011). Role of caveolin-1 in the pathogenesis of tissue fibrosis by keloid-derived fibroblasts in vitro: Decreased caveolin-1 in keloid. *British Journal of Dermatology*, *164*, 623–627. https://doi.org/10.1111/j.1365-2133.2010.10111.x

Zhang, Y., & Beachy, P. A. (2023). Cellular and molecular mechanisms of Hedgehog signalling. *Nature Reviews Molecular Cell Biology*, *24*(9), 668–687. https://doi.org/10.1038/s41580-023-00591-1

Zhang, Z., Jones, B. H., Tang, W., Moss, S. B., Wei, Z., Ho, C., Pollack, M., Horowitz, E., Bennett, J., Baker, M. E., & Strauss, J. F. (2005). Dissecting the Axoneme Interactome. *Molecular & Cellular Proteomics*, *4*(7), 914–923. https://doi.org/10.1074/mcp.M400177-MCP200

Zhang, Z., Zariwala, M. A., Mahadevan, M. M., Caballero-Campo, P., Shen, X., Escudier, E., Duriez, B., Bridoux, A.-M., Leigh, M., Gerton, G. L., Kennedy, M., Amselem, S., Knowles, M. R., & Strauss, J. F. (2007). A Heterozygous Mutation Disrupting the SPAG16 Gene Results in Biochemical Instability of Central Apparatus Components of the Human Sperm Axoneme1. *Biology of Reproduction*, *77*(5), 864–871. https://doi.org/10.1095/biolreprod.107.063206

Zhu, H., Luo, H., Li, Y., Zhou, Y., Jiang, Y., Chai, J., Xiao, X., You, Y., & Zuo, X. (2013). MicroRNA-21 in Scleroderma Fibrosis and its Function in TGF-β-Regulated Fibrosis-Related Genes Expression. *Journal of Clinical Immunology*, *33*(6), 1100–1109. https://doi.org/10.1007/s10875-013-9896-z

Zhu, H., Luo, H., Skaug, B., Tabib, T., Li, Y.-N., Tao, Y., Matei, A.-E., Lyons, M. A., Schett, G., Lafyatis, R., Assassi, S., & Distler, J. H. W. (2024). Fibroblast Subpopulations in Systemic Sclerosis: Functional Implications of Individual Subpopulations and Correlations with Clinical Features. *Journal of Investigative Dermatology*, *144*(6), 1251-1261.e13. https://doi.org/10.1016/j.jid.2023.09.288

Zimmerman, K. A., Song, C. J., Gonzalez-Mize, N., Li, Z., & Yoder, B. K. (2018). Primary cilia disruption differentially affects the infiltrating and resident macrophage compartment in the liver. *American Journal of Physiology-Gastrointestinal and Liver Physiology*, *314*(6), G677–G689. https://doi.org/10.1152/ajpgi.00381.2017

Zingg, D., Debbache, J., Peña-Hernández, R., Antunes, A. T., Schaefer, S. M., Cheng, P. F., Zimmerli, D., Haeusel, J., Calçada, R. R., Tuncer, E., Zhang, Y., Bossart, R., Wong, K.-K., Basler, K., Dummer, R., Santoro, R., Levesque, M. P., & Sommer, L. (2018). EZH2-Mediated Primary Cilium Deconstruction Drives Metastatic Melanoma Formation. *Cancer Cell*, *34*(1), 69-84.e14. https://doi.org/10.1016/j.ccell.2018.06.001